NAVAL RESEARCH LABORATORY

WASHINGTON. DC 20375

2009

NRL REVIEW

showcasing the Navy's corporate laboratory

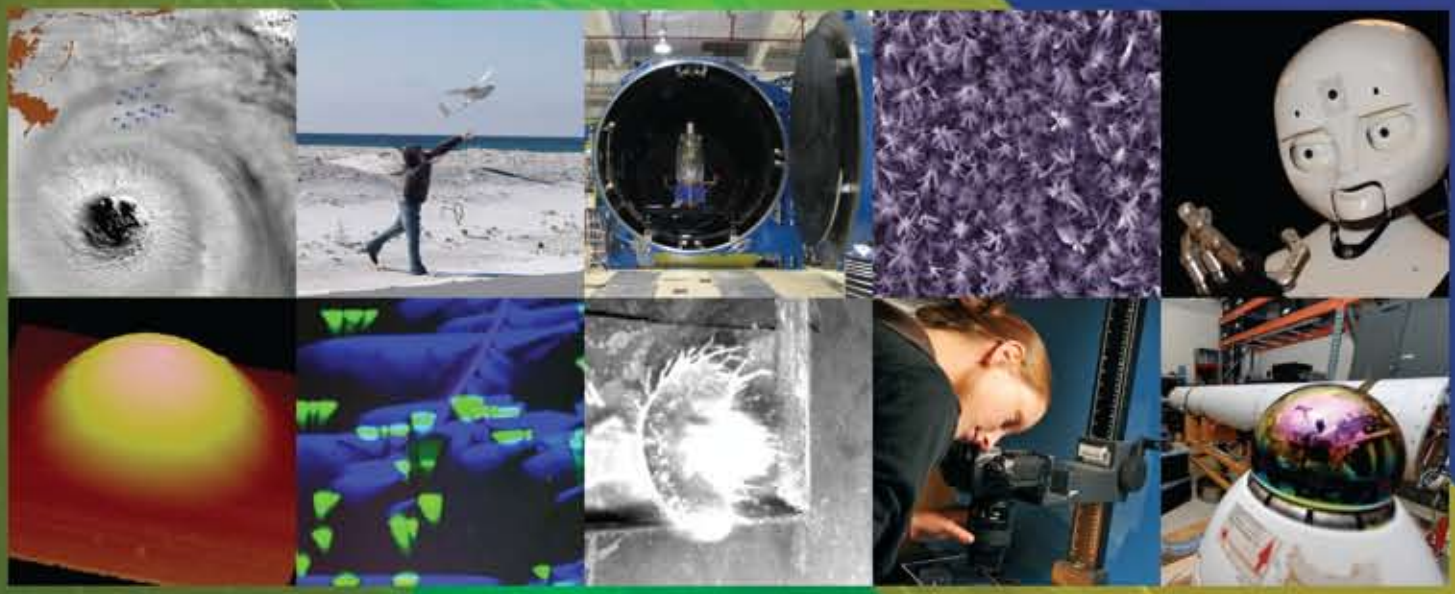

www.nrl.navy.mil

Report Documentation Page

Form Approved
OMB No. 0704-0188

Public reporting burden for the collection of information is estimated to average 1 hour per response, including the time for reviewing instructions, searching existing data sources, gathering and maintaining the data needed, and completing and reviewing the collection of information. Send comments regarding this burden estimate or any other aspect of this collection of information, including suggestions for reducing this burden, to Washington Headquarters Services, Directorate for Information Operations and Reports, 1215 Jefferson Davis Highway, Suite 1204, Arlington VA 22202-4302. Respondents should be aware that notwithstanding any other provision of law, no person shall be subject to a penalty for failing to comply with a collection of information if it does not display a currently valid OMB control number.

1. REPORT DATE	2. REPORT TYPE	3. DATES COVERED
2009		**00-00-2009 to 00-00-2009**

4. TITLE AND SUBTITLE	5a. CONTRACT NUMBER
NRL Review - 2009	5b. GRANT NUMBER
	5c. PROGRAM ELEMENT NUMBER
6. AUTHOR(S)	5d. PROJECT NUMBER
	5e. TASK NUMBER
	5f. WORK UNIT NUMBER
7. PERFORMING ORGANIZATION NAME(S) AND ADDRESS(ES) **Naval Research Laboratory,4555 Overlook Avenue SW,Washington,DC,20375**	8. PERFORMING ORGANIZATION REPORT NUMBER
9. SPONSORING/MONITORING AGENCY NAME(S) AND ADDRESS(ES)	10. SPONSOR/MONITOR'S ACRONYM(S)
	11. SPONSOR/MONITOR'S REPORT NUMBER(S)

12. DISTRIBUTION/AVAILABILITY STATEMENT
Approved for public release; distribution unlimited

13. SUPPLEMENTARY NOTES

14. ABSTRACT

15. SUBJECT TERMS

16. SECURITY CLASSIFICATION OF:			17. LIMITATION OF ABSTRACT	18. NUMBER OF PAGES	19a. NAME OF RESPONSIBLE PERSON
a. REPORT	b. ABSTRACT	c. THIS PAGE			
unclassified	**unclassified**	**unclassified**	**Same as Report (SAR)**	**255**	

General information on the research described in this *NRL Review* can be obtained from the Public Affairs Office, Code 1030, (202) 767-2541. Information concerning Technology Transfer is available from the Technology Transfer Office, Code 1004, (202) 767-7230. Sources of information on the various educational programs at NRL are listed in the *NRL Review* chapter entitled "Programs for Professional Development."

For additional information about NRL, the *NRL Fact Book* lists the organizations and key personnel for each division. It contains information about Laboratory funding, programs, and field sites. The *Fact Book* can be obtained from the Technical Information Services Branch, Code 3430, (202) 404-4963. The web-based *NRL Major Facilities* publication, which describes each NRL facility in detail, can be accessed at http://www.nrl.navy.mil.

Approved for public release; distribution is unlimited.

NRL REVIEW STAFF

SENIOR SCIENCE EDITOR
John D. Bultman

COORDINATOR
Jonna Atkinson

CONSULTANT
Kathy Parrish

DESIGN, LAYOUT, AND GRAPHIC SUPPORT
Jonna Atkinson and Donna Gloystein

EDITORIAL ASSISTANCE
Saul Oresky, Kathy Parrish, and Claire Peachey

PHOTOGRAPHIC PRODUCTION
Jamie Baker, Gayle Fullerton, and Jon Smallwood

COMMANDING OFFICER
CAPT Paul C. Stewart, USN

DIRECTOR OF RESEARCH
Dr. John A. Montgomery

REVIEWED AND APPROVED
NRL/PU/3430--09-515
RN: 10-1226-0273
March 2010

Paul C. Stewart, Captain, USN
Commanding Officer

MISSION

To conduct a broadly based multidisciplinary program of scientific research and advanced technological development directed toward maritime applications of new and improved materials, techniques, equipment, systems, and ocean, atmospheric, and space sciences and related technologies.

The Naval Research Laboratory provides primary in-house research for the physical, engineering, space, and environmental sciences; broadly based applied research and advanced technology development programs in response to identified and anticipated Navy and Marine Corps needs; broad multidisciplinary support to the Naval Warfare Centers; and space and space systems technology, development, and support.

contents

FEATURES

3
OUR PEOPLE ARE MAKING A DIFFERENCE

8
NAVY NAMES SHIP AFTER HOWARD O. LORENZEN

14
AUTONOMOUS SYSTEMS RESEARCH LABORATORY – FORGING THE TECHNOLOGY OF TOMORROW

16
NRL'S PETER WILHELM MARKS 50 YEARS OF GOVERNMENT SERVICE

18
DRS. JEROME AND ISABELLA KARLE RETIRE FROM NRL AFTER SIX DECADES OF SERVICE

2009 NRL REVIEW

THE NAVAL RESEARCH LABORATORY

27 NRL – Our Heritage
28 Highlights of NRL Research in 2008
35 NRL Today

FEATURED RESEARCH

59 Pointman
A Novel User Interface Controller for Dismounted Infantry Training
67 HiEx Foam
High Expansion Foam for Protecting Large Volume Mission Critical Shipboard Spaces
75 Using Our Heads to Save those of the **Warfighters**
Sensor Systems for Measuring Helmet-Head-Brain Response to Blast
87 CMG: Expanding Graphene Through Chemistry
Chemically Modified Graphene for Sensing and Nanomechanical Applications
97 Causality Bubbles to the Surface
Investigating Acoustic Causality in Highly Dispersive Bubbly Liquids
105 The Gamma Ray Sky as Seen by *Fermi*
Opening a New Window on the High Energy Space Environment
113 Keeping COMMx Cool
Design and Analysis of the Thermal Control System for the TacSat-4 Spacecraft COMMx Payload

RESEARCH ARTICLES

acoustics

127 Reconstruction of Acoustic Exposure on Orcas in Haro Strait
130 Operational Acoustic Transmission Loss Uncertainty Characterization

atmospheric science and technology

135 Operational Radar Performance Surfaces for RIMPAC 2008
138 The Atmospheric Neutral Density Experiment (ANDE)
142 Observing Guidance for Tropical Cyclones

contents

chemical/biochemical research

147 Guided Terahertz Waves for Characterizing Explosives
149 Innovative Foldamers: Engineering Heterochiral Peptides
152 A Multiwavelength Microflow Cytometer

electronics and electromagnetics

157 The Multifunction Electronic Warfare (MFEW) Advanced Development Model
160 Transportable Electronic Warfare Module (TEWM)
162 Laser Decoy System for Small Ground Platforms

information technology and communications

167 Free-Space Optical Link to an Explosive Ordnance Disposal (EOD) Robot
169 A Maritime Information Exchange Model (MIEM) for Sharing Actionable Intelligence
171 Tiled Image Archival and Distribution for Seafloor and Terrestrial Imagery
172 Cross-Domain Payload Migration

materials science and technology

177 Tunable Filter and Multiplexer for Improved Transmitter Electromagnetic Compatibility
180 Risk Mitigation for High Temperature Superconducting Generators
182 CT-Analyst Integration in Chemical/Biological/Radiological (CBR) Analysis Applications
185 Multifunctional Structure-Battery Composites for Marine Applications

nanoscience technology

189 Charge Transfer Between Quantum Dots and Peptide-Coupled Redox Complexes
192 Making the Most of a Scarce Metal
194 Optical Pulse Control of Electron and Nuclear Spins in Quantum Dots

ocean science and technology

199 A Thinning Arctic Ice Cap as Simulated by the Polar Ice Prediction System (PIPS): 2000–2008
202 Predicting "Ocean Weather" Using the HYbrid Coordinate Ocean Model (HYCOM)
206 Littoral Battlespace Characterization Using Small Unmanned Aerial Systems
208 The Environmental Post-Mission Analysis System: Through-The-Sensor to the Warfighter

optical sciences

213 Project CHLOE: High Altitude Defense Against Anti-Aircraft Missiles
215 Transparent Spinel Ceramic
217 Lightning Strike Sensing System for the Space Shuttle Launch Pad

remote sensing

221 Polarimetric Radar Imaging of the Ocean Surface
223 Airborne Remote Sensing of Trafficability in the Coastal Zone
228 Impulsive Noise Suppression via Adaptive Filtering

simulation, computing, and modeling

235 The DIME/PMESII Model Suite Requirements Project
239 Simulation of Supersonic Military Aircraft Jet Noise
241 Numerical Modeling of Plasmas Using the TurboWAVE Framework

space research and satellite technology

247 Laboratory Investigation of Near-Earth Space Plasma Processes
249 A New Class of Radio Halo
250 Integration and Testing Challenges of the Operationally Responsive Space (ORS) Phase III Bus Standards Prototype

SPECIAL AWARDS AND RECOGNITION

257 Special Awards & Recognition
270 Alan Berman Research Publication and NRL Edison (Patent) Awards
273 NRC/ASEE Postdoctoral Research Publication Awards

PROGRAMS FOR PROFESSIONAL DEVELOPMENT

277 Programs for NRL Employees — Graduate Programs, Continuing Education, Professional Development, Equal Employment Opportunity (EEO) Programs, and Other Activities
279 Programs for Non-NRL Employees — Recent Ph.D., Faculty Member, and College Graduate Programs, Professional Appointments, and College and High School Student Programs

GENERAL INFORMATION

283 Technical Output
284 Key Personnel
285 Contributions by Divisions, Laboratories, and Departments
288 Subject Index
292 Author Index
293 Employment Opportunities

nrl's involved!

3
Our People Are Making a Difference

8
Navy Names Ship After Howard O. Lorenzen

14
Autonomous Systems Research Laboratory – Forging the Technology of Tomorrow

16
NRL's Peter Wilhelm Marks 50 Years of Government Service

18
Drs. Jerome and Isabella Karle Retire from NRL After Six Decades of Service

NAVY NAMES SHIP AFTER

HOWARD O. LORENZEN

"Father of Electronic Warfare"

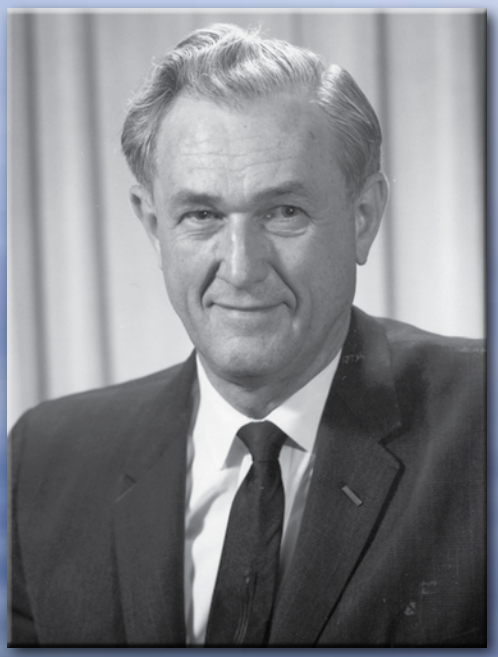

Howard O. Lorenzen

The Navy announced on October 10, 2008, that the name of the next missile range instrumentation ship will be USNS *Howard O. Lorenzen*. Designated T-AGM 25, the ship will honor the late NRL electrical engineer who was instrumental in the creation of our nation's electronic intelligence capabilities. Considered by many to be the "Father of Electronic Warfare," Lorenzen's accomplishments include developments in radar, electronic countermeasures systems, and intelligence satellite designs.

Lorenzen led the Galactic Radiation and Background (GRAB) program, the earliest successful U.S. reconnaissance satellite program and the first electronic intelligence satellite. NRL began the classified GRAB program shortly after the U-2 incident of 1960 to obtain information on Soviet air defense radars that could not be observed by U.S. military aircraft.

USNS *Howard O. Lorenzen* will be 12,575 tons, 534 feet in length, and have a beam of 89 feet. Manned by a combined crew of 88 sailors and civilian mariners, the ship will host embarked military and civilian technicians from other U.S. government agencies. The construction contract for T-AGM 25 was awarded to VT Halter Marine Inc., in Pascagoula, Mississippi.

Missile range instrumentation ships provide platforms for monitoring missile launches and collecting data that can be used to improve missile efficiency and accuracy. Like the Navy's two current missile range instrumentation ships, USNS *Observation Island* and USNS *Invincible*, T-AGM 25 will be owned and operated by Military Sealift Command and conduct missions sponsored by the Air Force.

– U.S. Department of Defense

(Illustration Naval Sea Systems Command)

No: T-AGM 25
Builders: VT Halter Marine, Inc.
Laid Down: 13 August 2008
Launched: 2009
Commissioned: June 2010
Displacement tons: 12,575 standard
Dimensions (feet): 534.1 x 88.6
Main machinery: Diesel-electric; 4 diesel generators; 2 motors; 20,115 hp (15 MW); 2 shafts
Speed (knots): 20
Range, in miles: 12,000 at 12 kt
Complement: 30 + 30 technicians + 16 spare
Radars, navigation: TBA

— Howard Otto Lorenzen —

June 24, 1912 – February 23, 2000

– Written by Ronald L. Potts in 2000
Reprinted from *Labstracts*, November 24, 2008

In the early 1940s, two decades before electronic warfare emerged as an ethereal form of combat with no obvious subordination to land, naval, or air warfare — a military science that mattered equally to soldiers, sailors, and airmen — Howard O. Lorenzen thought of it as radio countermeasures. After World War II, during his years of investigating captured German and Japanese electronic equipment, he began to think of it as electronic countermeasures, a discipline that detected and either interfered with or exploited for intelligence purposes any electromagnetic energy that an enemy might transmit for military purposes.

During the Korean War, when some of his colleagues started thinking of their art as electronics intelligence (ELINT), he deemed their view too narrow and refused to adopt the term to describe his activities. He even stuck with the concept of ECM when he led the way in the late 1950s to its first successful application in outer space — an ECM satellite. In 1965, when the Cold War got hot in Southeast Asia and U.S. aviators were first brought down over North Vietnam by Guideline missiles that had to be thwarted, he fired up his project engineers by requiring them to think from now on in terms of electronic warfare. EW remained his central focus thereafter, even when the Vietnam War wound down and he was called upon to lead space engineering for the Navy.

In his retirement, after thirty-three years of public service to the Navy and the Nation, Howard Lorenzen relived his career by reading between the lines of histories of WW II, Korea, Vietnam, and the Cold War. Articles and books he enjoyed most were ones written by his former colleagues, electronic warfare experts on both sides of the Atlantic Ocean. He never wrote a book himself. He had a mania about security, and he was so renowned among those who lived the early history of EW that he felt no need to stake any claims. He satisfied his natural urge to communicate with his peers by means of letters and amateur radio, a lifelong hobby and one he shared with most EW pioneers (who got their start in radio in their teens, by building their own antennas, receivers, and transmitters).

Howard O. Lorenzen died of pneumonia in a hospital in Redmond, Washington, on February 23, 2000, at age 87. As the word spread in today's EW community, some of its graybeards (like William E. W. Howe, James H. Trexler, Reid D. Mayo, Charles T. Christman, Lynwood A. Cosby) reflected on Howard's contributions and thought that the next generation might profit from hearing about them. Hence, this tribute to the father of U.S. Electronic Warfare.

WAR YEARS

In July 1940, after five years of designing commercial radios and components for Colonial Radio and Zenith Radio, 28-year-old Howard Otto Lorenzen started his career at the Naval Research Laboratory in Southwest Washington, working under the radar pioneers: A. Hoyt Taylor, Robert M. Page, Louis A. Gebhard, Robert C. Guthrie, John P. Hagen, and Edwin A. Speakman. They had already partnered with RCA to get air search radar (200 MHz, 15 kW) installed on selected battleships, aircraft carriers, heavy and light cruisers, and one seaplane tender. Lorenzen built a high-gain receiver, including an antijam capability, for a lightweight version, successfully demonstrated on the destroyer USS *Semmes* in July 1941, then manufactured by RCA and General Electric for Navy destroyers and smaller ships. Radio Superintendent "Doc" Taylor and Assistant Lou Gebhard looked the other way when Howard got a lathe and welding equipment and set up his own machine shop to manufacture engineering models, and they gave him new tasks and more two- and three-man groups of engineers and technicians to supervise.

NRL invented and developed the first U.S. radar (1922–1939).

Before the U.S. entered World War II, Lorenzen participated in NRL technical interchange with British scientists fighting the air war over Great Britain. After the Japanese struck the Pacific Fleet at Pearl Harbor, his radar work continued in receivers, cathode ray tube displays, transmitters, and motors — for naval shore installations, ships, and aircraft. He consulted to MIT Radiation Laboratory engineers who developed microwave radar sets for the U.S. Army Air Forces under Division 14, National Defense Research Committee (NDRC). As the war progressed, Lorenzen gradually expanded to radio countermeasures against enemy systems, most notably, the air-launched guided bomb. He developed a system installed on two destroyer escorts to intercept, record magnetically on steel wire, and analyze German aircraft radio signals that controlled the glide bombs built to sink allied warships in the Mediterranean Sea. The knowledge helped NRL's Special Projects Section develop intercept-jammers that defeated the Henschel 293 system, and the unwitting Luftwaffe engineers concluded that RF energy was too fickle or pilots too inept to make the intricate control mechanism work as designed. Howard's friendship with Louis W. Tordella (future Deputy Director, NSA) started when the Navy lieutenant came to his laboratory to learn how the successful intercept system had worked.

To thwart enemy jamming and eavesdropping, Lorenzen engineered a selectable 880-channel UHF voice receiving and transmitting system. He coordinated U.S./British UHF efforts and became well acquainted with the men who focused on radio and radar in the British Admiralty's Signal and Radar Establishment in Portsmouth, England, and their counterparts in the Royal Air Force and Royal Army. (His UHF transceiver transitioned to Raytheon, AN/URC-3, and was later mass-produced as the AN/ARC-27 for use during the Korean War by U.S. and Allied forces.)

By war's end, Howard Lorenzen supervised 11 small groups working in different areas of radio engineering. He was a key member of a countermeasures partnership between NRL and the Office of Naval Intelligence (ONI) in the Pentagon, which interfaced with NDRC Division 14 (Countermeasures) and industry. Sponsorship for NRL's intercept, direction finding, radar jamming, and decoy systems came from the Navy Bureaus of Ships and Yards & Docks, which also shepherded transition to industry for systems produced in quantity.

POST WAR

After the war, when many Navy scientists and engineers returned to their civilian occupations, Howard Lorenzen and some key members of his groups remained government employees and concentrated on captured electronic equipment sent to the United States from Europe and Asia. He and Jim Trexler arranged to permanently borrow certain other gems that fell into British hands, such as the Athos crystal video receiver and the Wullenweber goniometer. The WW II NDRC evolved to the Office of Scientific Research and Development (later Joint Research and Development Board), and Lorenzen maintained his military and industrial contacts. He represented the Navy to Joint and Allied committees and working groups with interests in countermeasures, particularly in the U.S., Canada, and Great Britain. He underwent nuclear orientation at facilities in New Mexico in 1948 and became an ECCM consultant to NATO's Mutual Weapons Development Program.

When the Soviet Union emerged as a new threat, Ed Speakman and Howard Lorenzen organized NRL's Countermeasures Branch and initially focused on Russian adaptations of western lend-lease equipment. Lorenzen's prior investigations of German equipment and documents soon paid off, for Soviet adaptations of German technology and techniques began to appear. The Branch developed intercept and DF systems for deployment to Navy ships, shore stations, and aircraft. A collaboration with Airborne Instruments Laboratory (Dr. Hector R. Skifter) yielded the first tunable airborne microwave intercept receiver (later AN/APR-9), which was integrated at NRL with James E. Gall's ECM signal display and analysis equipment, including multi-gun CRTs. The new capabilities enabled the outfitting of Naval landbased ferret probes along the periphery of the Sino-Soviet Bloc. Their first airborne systems were installed on P4M-1Q Mercators, PB4Y-2 Privateers, and P2V Neptunes. Other versions were tailored to surface ships and submarines. To get operational feedback on the UHF signal environment and the systems' usefulness and shortcomings, Lorenzen undertook an unofficial program to analyze intercept operators' logs at NRL. Initially, most of this analytical work was performed by himself and Robert D. Misner. By 1949, in cooperation with the Stromberg-Carlson Company, they had created the first U.S. magnetic tape recorder for intercept work, the Radio-Countermeasures Sound Recorder-Reproducer IC/VRT-7.

NATIONAL ELINT PROGRAM

To broaden participation in NRL's log analysis effort, Lorenzen promoted in ONI and helped organize a Countermeasures Intercept Analysis Group with sponsorship from the Joint Communication and Electronics Committee (JCEC) of the JRDB. Participating organizations were ONI, NRL, Naval Security Group (NSG), Army Signal Corps, and Air

Technical Intelligence Center (ATIC). He chaired the JCEC analysis working group during the Korean War, until it evolved in 1953 to the Army-Navy Electronic Evaluation Group (ANEEG), collocated with NSG Headquarters at 3801 Nebraska Avenue in Northwest Washington. By then, his branch had added drum recorders to the arsenal of intercept equipment, and second-echelon analysis of raw data tapes had become a practical objective.

During the 1950s, ECM technology advanced by Lorenzen's engineers included electronic signals intercept, direction finding, jamming, and deception techniques. Howard Lorenzen and John C. Link supported BUAER and the Air Force Tactical ECM Wing in Biloxi, Mississippi, with new forward-launch dispensers and lightweight chaff that worked. Lorenzen's team provided equipment (antennas, receivers, recorders, and analysis devices), technical support, and technology transfer for various surveillance and reconnaissance platforms via the Navy Bureaus of Ships and Aeronautics, the Army Signal Corps (ELINT vans), the CIA Office of ELINT (U-2 aircraft, crash boats, and agent devices), and ONI (covert installations and equipment loan to friendly foreign navies). Equipments were regularly upgraded to exploit new technology and keep pace with the threat signal environment as it spread into higher regions of the RF spectrum.

NRL developed the key transmitter and receiver technologies that allowed effective communication through a passive Moon circuit.

A National ELINT Program was established in 1955 under Air Force Secretary Donald A. Quarles, who had previously chaired the JCEC. ANEEG was reorganized as the National Technical Processing Center (NTPC). Soldiers, sailors, and civilian technicians, including some from CIA, were joined by an influx of airmen and civilians from ATIC at Wright Patterson AFB, Dayton, Ohio. NTSC's primary mission was to inform the Strategic Air Command (SAC) about Soviet air defense radar that SAC's B-47 and B-52 bombers would encounter in the event of nuclear war. Lorenzen's Countermeasures Branch participated in and supported the National ELINT Program by serving on technical committees; developing intercept equipment; collaborating with Army Signal Corps Signals Research and Development Laboratory in Fort Monmouth, New Jersey, and Air Development Centers in Rome, New York, and Dayton, Ohio; and evaluating data acquired from ECM configurations. NTPC was headed by an Air Force lieutenant colonel, and continuity was provided by senior civilian engineers like John E. Libbert and Henry F. (Hank) DeCourt. Lorenzen continued to chair the steering committee of the Navy's Technical ELINT Panel, which supported NTPC.

Jim Trexler was Lorenzen's project engineer for PAMOR (PAssive MOon Relay, a.k.a. "Moon Bounce"), which collected interior Soviet electronics and communication signals reflected from the Moon. It was Trexler who first started calling Howard, "Father," and he also led the way to Communications Moon Relay, which established operational communication circuits between Washington and Hawaii in the mid-1950s and set the stage for communication satellites in the 1960s. Charles W. Price, the Branch's chief mechanical engineer, designed the mechanical structures employed in several generations of Trexler's massive Moon Bounce antennas.

When ELINT was assimilated under the charter of the National Security Agency in March 1959, Lorenzen provided technical and engineering support to the Advanced Signals Analysis Division of NSA's Office of Collection and Signals Analysis and successor offices (C-1 and K-4), headed by John Libbert and, in the latter 1960s, by Raymond B. Potts. GCHQ mathematician Sylvester Stanley Strong worked there, too, and Stan was a Lorenzen friend from the post-WW II years.

Communications and radar intercept systems on aircraft, ships, submarines, and shore stations captured signals near the periphery of the Soviet Union and Communist China. Project Boresight created a global Navy network of HFDF stations to intercept and fix the source of radio transmissions from Soviet surface ships and submarines. Boresight successor Bullseye's huge circularly disposed antenna arrays included up to two rings of dipole antennas and two reflector screens and grew to an effective diameter of 800 feet. The first of the CDAA arrays, installed at the Hybla Valley Coast Guard Station, Alexandria, Virginia, in 1957, was used to track the Soviet Sputnik's 20 MHz signal and determine its orbit. Mack J. Sheets was Lorenzen's antenna engineer for Boresight and Bullseye; Bob Misner, signal processing.

SERVING OPERATIONAL NEEDS

Typical of the way Howard Lorenzen operated was the overnight revolution in the way his branch supported the silent service. Starting with the USS *Pike* in July 1944, all of NRL's submarine intercept and DF systems had located the intercept antennas on the conning tower, necessitating exposure and attendant risk when collecting signals. In December 1957, Rear Admiral Elton W. Grenfell, a submariner and mechanical engineer, came in from the Pacific Fleet, where he commanded U.S. submarine forces, and complained to Howard Lorenzen that he had written his last memorandum to BUSHIPS. He wanted hardware — now!

Lorenzen summoned several engineers and technicians to a brainstorming session in his office. Submariner Grenfell accepted Ralph A. Carpenter's proposed communications intercept configuration (15 kHz–265 MHz) and Reid Mayo's ELINT amplifier and crystal video detector (2.5–12 GHz), but rejected all of his ELINT antenna offerings as too large and grotesque — which stimulated William Edgar Withrow's design of a double-armed spiral antenna, not much bigger than a silver dollar, to fit inside a periscope.

A month later, following integration and testing at Kolmorgen Optical, Inc. in North Hampton, Massachusetts, Kolmorgen's modified periscope (type 8A) and NRL's intercept equipment were installed on the USS *Dogfish* in New London, Connecticut, to support its mid-January deployment to the Barents Sea. Reid Mayo and Ed Withrow observed the installation, tested the ECM system, participated in sea trials, and trained operators. They did the same in February for a second system on the USS *Wahoo* in Yokusaka, Japan. Wahoo would operate in the western Pacific. The full-production system (AN/BLR-6) transitioned to industry in June, just six months after Rear Admiral Grenfell pounded the table.

GRAB

When Russian Sputniks and Lunas, Army Explorers, and Navy Vanguards began

orbiting the Earth a dozen or so times daily, Lorenzen was already so renowned in ECM that the Director of Naval Intelligence, Rear Admiral Laurence H. Frost, forbade him from attending the launch of GRAB 1 or follow-on missions, for fear his presence would give away their ELINT mission.

Lorenzen's vision for a low-cost ELINT satellite was first published late in 1957, a section of the NRL's secret proposal for a U.S. satellite and space vehicle program beyond Vanguard. The space agenda, proposed by Navy to the Armed Forces Policy Council, defined military and scientific objectives that would later be parceled out, respectively, to DoD's Advanced Research Projects Agency (ARPA), when it was formed February 1958, and to the NASA, which became operational October 1958 and assimilated NRL's Vanguard team.

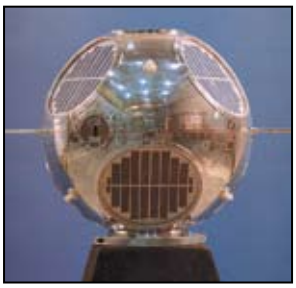

GRAB was America's first operational intelligence satellite. The GRAB project provided proof-of-concept for satellite-collected electronic intelligence.

Lorenzen hoped for, but could not count on, DoD to promptly approve and fund his proposal. So he persuaded BUAER to task NRL for an intercept system, subminiaturized and lightweight, to be installed on "supersonic vehicles, manned or unmanned" and to automatically retransmit intercepted data to existing naval receiving stations on the periphery of the Communist Bloc. The task was on NRL's books before ARPA's new bureaucrats could find their way around the Pentagon, and Lorenzen's first quarterly engineering progress report was submitted to BUAER in July 1958. If anyone objected, then the supersonic vehicle was a high-performance jet aircraft; otherwise, a satellite.

Enough Vanguard veterans stayed with the NRL to build the GRAB satellite and, later, form a new Satellite Techniques Branch under Martin J. Votaw. Lorenzen's own Countermeasures Branch designed the ELINT payload, ground electronics, and transportable equipment shelters for ELINT stations overseas. Beyond imparting the vision and addressing technical problems raised to his level, he entrusted design and engineering to a loosely coupled team of engineers and technicians supporting project engineer Reid Mayo. "Don't worry about money," he told Mayo, "I'll get you the money. Just don't let me down."

While their work progressed, Lorenzen led a parallel campaign to get the project approved and fully funded. Starting with ONI in July 1958, using large briefing boards mounted on a pedestal, Project Tattletale was sold at the Pentagon, Main Navy on Constitution Avenue, CIA Headquarters, NASA, and Capitol Hill. Congressmen were delighted to be briefed on a project "not costing tens of millions." In the spring of 1959, DNI Laurence Frost, ARPA Director Roy W. Johnson, and OSD's Graves B. Erskine (Special Operations) agreed that Tattletale was too visible, though. ARPA officially killed it and established Project Canes as a top secret security control system. Oaths were signed by those authorized for indoctrination, under 200 people altogether, with President Dwight D. Eisenhower heading the list.

The President approved Project Canes on August 24, 1959. On May 5, 1960, just four days after a CIA high-altitude U-2 reconnaissance aircraft was brought down over the Soviet Union (by an SA-2 Guideline missile, according to Soviet claims), he approved launch of the first Canes-controlled satellite. Known operationally as GRAB (Galactic RAdiation and Background), the ELINT satellite was launched successfully from Cape Canaveral, Florida, on June 22, 1960 and tested by NRL in Hawaii on July 5–8. Howard Lorenzen, Reid Mayo, Ed Withrow, Edgar L. Dix, and Vincent S. Rose were the first to hear the medley of radar signals detectable by a wide-open receiver in outer space. On the recommendation of State, Defense, and CIA, President Eisenhower authorized NRL to "trigger Project Canes on 12-15 passes over the Soviet Union during the course of a two- to four-weeks period of time," subject to a final phone-check with State, CIA, and the White House chief of staff before each turn-on. The Canes/GRAB ELINT tapes soon saturated U.S. analytical capabilities. On October 18, 1960, President Eisenhower approved the request from State, Defense, and CIA for more Navy ELINT satellites.

Bob Misner led the way to machine processing of the GRAB take, and Howard Lorenzen collaborated with Lou Tordella on a joint NRL/NSA effort to automate ELINT data processing. Intelligence derived from GRAB satellites, processed by the NSA and SAC, marked a turning point in U.S. strategic doctrine. The Soviet air defense system was too robust for penetration by SAC's high and medium altitude bombers, which were succeeded by low-altitude bombers and ballistic missiles, sea and land versions. (An air-launched version, Skybolt, was scrapped in the mid sixties.) GRAB also yielded the first intercept of a signal associated with the developmental Soviet Galosh anti-ballistic missile system.

GRAB was launched successfully from Cape Canaveral, Florida, on June 22, 1960.

While the National Reconnaissance Office (NRO) was being formed, Bill Howe looked out for Navy interests on behalf of ONI. He had high level help from the Director of NSA, Vice Admiral Laurence Frost, who wanted to continue the Navy ELINT satellites in the National Reconnaissance Program. (Lorenzen was then busy helping to save the Navy aircraft carrier by deception techniques that foiled U.S. Air Force simulated air attacks while President Kennedy monitored the exercise.) Project GRAB was assimilated in the NRO in July 1962.

EW DIVISION

Lorenzen became NRL's first Superintendent of Electronic Warfare when his branch was upgraded to division status in September 1966. He typically managed upwards of a hundred scientists, engineers, and technicians, who were kept busy pushing the state of the art, sharing their technology and ideas with cleared firms, and harvesting any useful components produced by industry. Their achievements, under his leadership, spanned the entire breadth of EW. During the late 1960s, his highest priority was the development of equipment for naval aircraft, particularly for defense against guided missiles, which he considered the

Laboratory's most vital support to U.S. Navy aviators at war in Vietnam. When the battleship USS *New Jersey* was refitted in 1968 to shell enemy supply routes inland, Lorenzen's EW Division equipped her with every device in their arsenal that could foil attack from North Vietnamese MIGs, missiles, or fast attack boats. He so overweighted his defensive EW branch that it emerged as a separate division under Lyn Cosby within a few years.

Lorenzen had the status of a presidential appointee (under Public Law 313), and he was as comfortable in acquisition management and operations circles as in science, engineering, and manufacture. When need be, he explained his projects on Capitol Hill, the Pentagon, the United States Intelligence Board, the President's Scientific Advisory Committee, the Bureau of the Budget, the General Services Administration, and the intelligence agencies (CIA, DIA, NSA, and NRO). Throughout the 1960s, he helped represent the United States at NATO and SEATO EW conferences and served as an advisor to the Joint Chiefs of Staff and the Secretary of Defense. When he was written up for an award, someone went through his personnel record and figured that he had spent nearly ten percent of his career since WW II abroad, 78 trips to 17 different foreign countries.

On February 11, 1970, the interagency ELINT RDT&E Coordinating Group met at NRL. NSA's David Wolfand chaired the ERG, but Howard Lorenzen was recognized as leader by most of the members. These captains of ELINT included Army Security Agency Chief Scientist Ed Speakman, Army ACSI Senior Technical Adviser Bill Howe, CNO Development Technical Director Stirling Thrift, NSA R&D Directorate's Robert J. Hermann, Air Force Colonel John B. Marks, NSA's Art Thom, Army Missile Intelligence Directorate's Mel Bachman, and representatives from CIA and DIA. Lorenzen's scientists and engineers displayed and discussed their latest technologies for every sort of platform: surface ships, submarines, early warning (VQ) and long range patrol (VP) aircraft, transportable equipment vans (land and sea), SIGINT stations, satellites, and even human beings (e.g., crystal video receivers appearing to be eye glasses and hearing aids). It was a most productive session and reunion of old friends and pioneers in ELINT. No one guessed that Howard Lorenzen would soon embark on a new mission.

SPACE SYSTEMS DIVISION

In September 1970, Deputy Defense Secretary David Packard aligned space systems acquisition responsibilities with those for weapon systems acquisition and authorized the military departments to pursue departmental need for space systems, including "unique surveillance (i.e., ocean or battlefield) needs" (DoDD 5160.32, Development of Space Systems). The Navy established a Navy Space Project Office (PM-16) in the Naval Material Command as a successor to NAVAIR's Astronautics Division (Air 538). NRL had been Air 538's prime space engineering asset. SOLRAD supported NASA's Apollo Program by monitoring solar radiation and predicting Sun activity that could interfere with communications during Moon missions. TIMATION (forerunner of GPS) provided time transfer and navigation data, via satellite, to mobile platforms. SURCAL calibrated the Navy Space Surveillance (NAVSPASUR) CW fence across and above the southern United States. CALSPHERE calibrated the Navy's Bullseye HFDF system. A classified program supported national capabilities. Wanted were Navy space systems for communications, ocean surveillance, and global positioning. At NRL, the satellite platform now seemed to eclipse the electronic warfare mission and would become the basis for a new, first-echelon Space Science and Technology area.

The SOLRAD program conducted long-term monitoring of the Sun's emissions and the disturbances they cause on Earth.

NRL turned to Howard Lorenzen to repeat in space what he had accomplished in EW: design total systems for military operational support. In February 1971, Lorenzen was appointed Superintendent of Space Systems and organized a new division that consolidated Moon relay SIGINT and most of NRL's ongoing space projects, including fabrication of lightweight satellite platforms by Peter G. Wilhelm's Satellite Techniques Branch and development of payload electronics and ground readout systems for communications, ELINT, time and navigation, ocean surveillance, and scientific experiments. Some of the former EW branches became a new Tactical EW Division under Lyn Cosby, specializing in systems for Navy ships and aircraft. Those specializing in HFDF systems at naval shore stations joined an expanded Communications Sciences Division, soon assigned to Bruce Wald.

NRL conceived of TIMATION as a way to provide accurate position and time data using synchronized clocks.

Presiding over the southeast end of NRL's main mall, near the front gate, Howard stayed in touch with his EW and SIGINT colleagues in buildings across the street, even as he concentrated on tactical applications of space technology. His advocacy of space systems was motivated, not only by cost-effectiveness, but by Navy losses, since 1950, of seventy-eight killed or missing and eight wounded crewmen by Sino-Soviet destruction of eight naval reconnaissance aircraft, most of which had been outfitted by his team. Within two years, NRL's major space R&D projects were destined for operational systems development and management by Navy or Air Force systems commands as joint or national programs. (The Space Systems Division underwent several transformations and expansions in the next three decades and is now the Naval Center for Space Technology, directed by Peter Wilhelm.)

His missions accomplished, Lorenzen retired in June 1973, and moved to Bellevue, Washington, in 1976, to be near family. There, he enjoyed family and new friends; built the amateur radio station of his dreams; welcomed visits from old friends from back East; and gardened some. Physical infirmities prevented Howard from participating in NRL's Diamond Jubilee in June 1998 and the initial public disclosure of Project GRAB by DNRO Keith R. Hall, but he enjoyed video tapes of those proceedings attended by GRAB alumni. His legacy survives with dozens of electronic warfare and space systems he pushed into operational use, many of them still classified, that have evolved and will continue to support the nation in the years to come.

NAVAL RESEARCH LABORATORY'S

Autonomous Systems Research Laboratory

forging the technology of tomorrow ...

RESEARCH LABORATORIES

Power and Energy

Sensors

Aerosol

Intelligent Autonomy

Mechanical and Electronics Prototyping

The **Autonomous Systems Research Laboratory** will become:

- the nerve center for basic research that supports autonomous systems research for the Navy and Marine Corps.
- a magnet for recruiting and maintaining a premier workforce.
- an adaptable testbed for system demonstration and validation prior to field testing.

The **Autonomous Systems Research Laboratory** will integrate S&T components into research prototype systems. These S&T components will include: modeling/simulation, sensors, power systems, networking/ communications, human-systems interactions, and mobility/robotics. The building will provide new simulated environments (littoral, desert, tropical, upland forest) and reconfigurable high bay spaces for initial systems testing.

SIMULATED ENVIRONMENTS

Desert

Littoral

Tropical

Upland Forest

Reconfigurable Prototyping

KEY S&T AREAS

- POWER AND ENERGY
- SENSORS
- AUTONOMY
- PLATFORMS
- NETWORKING
- COMMUNICATIONS
- MATERIALS
- MODELING AND SIMULATION

Open for business in 2012

NRL's Peter Wilhelm Marks *50 Years* of Government Service

Peter G. Wilhelm celebrated 50 years of government service on March 30, 2009. As Director of NRL's Naval Center for Space Technology (NCST), Mr. Wilhelm is responsible for the technical and managerial leadership of the NCST's mission, which is to preserve and enhance a strong space technology base and provide expert assistance in the development and acquisition of space systems which support naval missions. During Mr. Wilhelm's tenure, the space program at NRL has grown from a Branch to a Division and now to a Center.

Mr. Wilhelm, who has directed the NCST since its inception in 1986, has been with NRL since March 1959. Under his direction, NCST and the Navy have achieved numerous successes and "firsts" in space including the first Global Positioning System (GPS) satellite and the highly successful Clementine Deep Space Mission, which demonstrated the capability of, and has become the model for low-cost, high-value space exploration. Mr. Wilhelm's achievements include contributions to the design, development, and operation of 95 scientific and fleet-support satellites.

TIMELINE

1957 – began his career as an electrical engineer with Stewart Warner Electronics where he was assigned to a project to redesign the UPM-70, a Navy radar test set
Mar 1959 – joined NRL as an electronics engineer in the Electronics Division
Dec 1959 – joined the Satellite Techniques Branch
1961 – became head of the Satellite Instrument Section
1965 – became head of the Satellite Techniques Branch
1974 – became head of the Spacecraft Technology Center
1981 – named superintendent of the Space Systems and Technology Division
1986 – appointed director of the newly established Naval Center for Space Technology

HONORS AND AWARDS

Pioneer of National Reconnaissance, 2000
Presidential Distinguished Rank Award, 1999
AIAA Goddard Astronautics Award, 1999
The Secretary of the Navy Career Service Award, 1999
DoD Distinguished Civilian Service Award, 1998
NRL Lifetime Achievement Award, 1998
National Academy of Engineering, 1997
NRL's Roger L. Easton Award for Engineering, 1997
Rotary National "Award for Space Achievement" Foundation's Stellar Award for Program Management, 1993
Robert J. Collier Award (Team Award), 1992
Elected a Fellow of AIAA, 1989
Presidential Rank Award Meritorious Executive, 1988
CAPT Robert Dexter Conrad Medal (Navy's highest award for scientific achievement), 1987
Navy's Space Systems Program Achievement Award, 1985
E.O. Hulburt Award (NRL's highest award for science — first and only engineer to win this award), 1983
Federal SES Performance Awards, 1983, 1984, 1985, 1986, and 1994
IEEE Aerospace and Electronic Systems Group "Man-of-the-Year Award," 1981
Navy Meritorious Unit Commendation for Development, Acquisition, and Operation of Space Systems, 1977 to 1981
Navy Award of Merit and Special Achievement, 1976
Navy Unit Commendation for Exceptional Meritorious Service, 1974 to 1976
Elected Fellow of Washington Academy of Science, 1971
Navy Distinguished Civilian Service Award, 1971
Navy Meritorious Civilian Service Award, 1962

OTHER ACHIEVEMENTS

Lecture on NRL's Space Program at U.S. Space Foundation's Annual Conference – Plenary Session, 1996
Chairman of NASA's Origins External Review Board (OERB), 1996 and 1997
Lecture on Hybrid Assisted Reusable Launch VEhicle (HARVE) design at Joint Conference on Reducing Cost of Space Systems, 1995
Served on NRC Study on Reusable Launch Vehicle, 1995
Chairman of American Astronautical Society (AAS) Guidance and Control Conference, 1995
Served on Congressionally mandated "Launch Mobilization Study" – determined U.S. policy on launch issues, 1994
Member of the Mars Observer Failure Review Board, 1993
Member of the National Academy of Engineering, a Fellow of the American Institute of Aeronautics and Astronautics (AIAA), and the Washington Academy of Science

50 Years of Service

Drs. Jerome and Isabella Karle Retire from NRL After Six Decades of Service

Drs. Isabella and Jerome Karle

Dr. Jerome Karle and Dr. Isabella Karle retired from the Naval Research Laboratory on July 31, 2009, after a combined 127 years of Federal service. NRL celebrated their retirement at a fine ceremony on July 21, at which they were each awarded the Department of the Navy Distinguished Civilian Service Award, and were presented with letters of congratulation from the Secretary of Defense and the Chief of Naval Operations.

Jerome Karle began working for NRL in 1944 on a project at the University of Michigan; he retired as the Chair of Science and Chief Scientist of NRL's Laboratory for the Structure of Matter. Isabella Karle joined NRL in 1946, when both Karles came to Washington, DC; she retired as the Sr. Scientist for Structural Chemistry in the Laboratory for the Structure of Matter.

The ceremony was attended by The Honorable Ray Mabus, Secretary of the Navy, RADM Nevin Carr, Chief of Naval Research, and many other distinguished guests. In recognizing the Karles, Secretary Mabus said, "I have met a lot of people who have contributed to this country and to humankind. I'm absolutely certain I have never met anyone who has done so with more distinction, with more intensity over a longer period of time and with greater results than Dr. Isabella Karle and Dr. Jerome Karle." When Secretary Mabus presented the Navy Distinguished Civilian Service Award to the Karles, he said, "in a very real sense we do not have the capacity to honor you, you honor us. You honor us by your service, you honor us by the things you have done, not just for the Navy, not just for America, but for humankind."

Dr. Bhakta Rath, Associate Director of Research for Materials Science and Component Technology, spoke about the significance of the Karles' careers, saying, "The departure of Jerry and Isabella from our midst at NRL marks the end of an era. Through their persistent and dedicated research, they opened the doors to our understanding of the complexities of atomic arrangements in large biological and organic molecules. Their theoretical and experimental research, which is now commonly known as the direct method for solving the multivariable complex functions extracted from X-ray diffraction data, has made immeasurable contribution to our understanding of the structure and function of biomolecules and consequently to the development of various pharmaceutical products. Through their continued research, they created new areas known as quantum crystallography and the kernel method. Researchers the world over can solve structures of molecules containing tens of thousands of atoms in a matter of hours, which otherwise would have taken careers to solve.

I distinctly remember the day in 1985 when the announcement reached the lab that Jerry had received the Nobel Prize in chemistry. I was in Toronto, chairing a session at an international conference when someone came and whispered to me the news. Expressing my exuberance and taking the privilege of the chairman's prerogative, I announced the news to the attending scientists and declared a fifteen-minute break for celebration.

The combined length of service of Jerry and Isabella at NRL, extending over 127 years, beginning since the Manhattan project, will be long cherished and remembered as a historic event for the laboratory, the U.S. Navy, the nation, and the world."

NRL Establishes the Jerome and Isabella Karle Distinguished Scholar Fellowship

On June 18, 2008, NRL established a 1-year research fellowship in honor of Drs. Jerome and Isabella Karle.

The announcement of the scholarship (NRL Notice 12300) states, "Drs. Jerome and Isabella Karle have dedicated their entire professional lives to new and innovative advancements in science and technology. These two iconic scientists embody the intensity and fervor that NRL wishes to foster and harbor in the workforce of the future. To this end, effective 18 June 2008, on the occasion of Dr. Jerome Karle's 90th birthday, NRL established the Karles' fellowship."

The fellowship will be open to all new appointments at NRL (all sites) whose primary function is to perform research. Fellows will be selected by the Director of Research based on recommendation by the Division Superintendent at the time of recruitment. The scholastic achievement of the appointee must be a cumulative 3.5 or higher GPA.

NRL Prepares the Karle Room Exhibit

To celebrate the scientific achievements of Drs. Jerome and Isabella Karle, and to recognize their long service to the Naval Research Laboratory and Department of Defense, NRL has created a Karle Room in Building 226. The room was dedicated with a ribbon-cutting ceremony on June 24, 2008. Preparation of exhibits to fill the room is now under way.

The Technical Information Services Branch is writing and designing the exhibits, which consist of several museum-style panels. The main "history" panel will chronicle the path of the Karles' scientific research: their early years in electron diffraction, the development of their theories and procedures, the application to X-ray crystallography, and the winning of the Nobel Prize by Jerome Karle and Herbert Hauptman. Other panels will highlight some of the most important applications of the Karles' structure-determining methodologies – identification of toxins, antimalarials, peptides, energetic materials, and more. A final panel will exhibit some of the numerous awards the Karles have received.

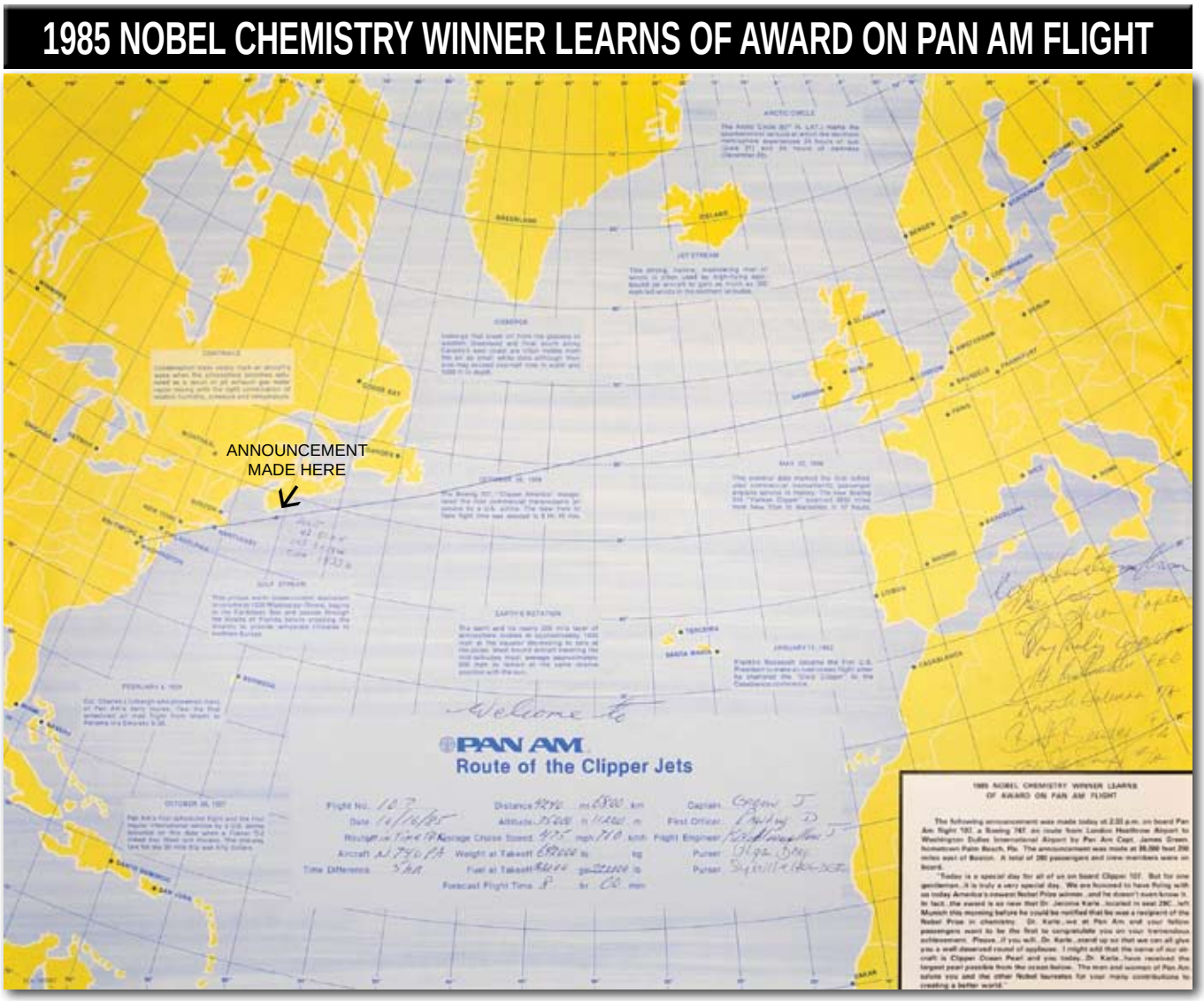

The Karles were presented with this signed map by the crew of Pan Am flight 107 of October 16, 1985. The citation at lower right reads: The following announcement was made today at 2:33 p.m. on board Pan Am flight 107, a Boeing 747, en route from London Heathrow Airport to Washington Dulles International Airport by Pan Am Capt. James Green, hometown Palm Beach, FL. The announcement was made at 39,000 feet 200 miles east of Boston. A total of 280 passengers and crew members were on board. "Today is a special day for all of us on board Clipper 107. But for one gentleman…it is truly a very special day. We are honored to have flying with us today America's newest Nobel Prize winner…and he doesn't even know it. In fact…the award is so new that Dr. Jerome Karle…located in seat 29C…left Munich this morning before he could be notified that he was a recipient of the Nobel Prize in chemistry. Dr. Karle…we at Pan Am and your fellow passengers want to be the first to congratulate you on your tremendous achievement. Please…if you will…Dr. Karle…stand up so that we can all give you a well deserved round of applause. I might add that the name of our aircraft is Clipper Ocean Pearl and you today…Dr. Karle…have received the largest pearl possible from the ocean below. The men and women of Pan Am salute you and the other Nobel laureates for your many contributions to creating a better world."

Drs. Jerome and Isabella Karle came to the Naval Research Laboratory together in 1946 and retired together in 2009. They have devoted their distinguished careers to the study of the structure of materials, and in so doing have made seminal contributions to many fields of science. Their work in electron and X-ray diffraction led them to develop theories and techniques to directly determine complex molecular structures, accomplishing in the 1950s and 1960s what most had thought was impossibly difficult. This work has been recognized with dozens of awards, including the Nobel Prize in Chemistry for Jerome, and the National Medal of Science and Bower Award for Isabella. Their structure determination techniques became standard laboratory practice and made the Naval Research Laboratory a center of structural research.

NRL's Laboratory for the Structure of Matter, established in 1968 with Jerome as its Chief Scientist and Isabella as head of the X-ray Diffraction Section, has been the site of many landmark discoveries and fruitful collaborations. The laboratory has identified, synthesized, or optimized the design of antimalarials, antinarcotics, frog toxins, nanotubes, peptides, energetic materials, and many other organic and inorganic substances, for the great benefit of the Navy, the nation, and the world.

Jerome and Isabella Karle have been partners in life and in science since they met. They have raised a family, mentored students and colleagues, and grown along with NRL over the decades. Upon their retirement, we wish them fair winds and following seas.

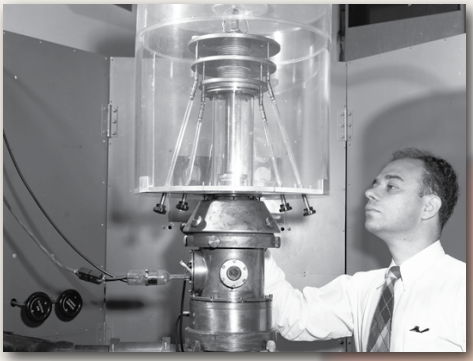

Drs. Isabella and Jerome Karle at the NRL electron diffraction apparatus, 1949.

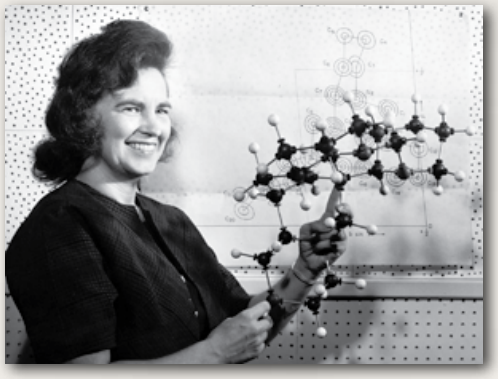

Isabella holding a ball-and-stick model of a molecule, with an electron density map in the background.

These help us see into the molecules!

Dr. Jerome Karle, Dr. Bhakta Rath, and RADM Marc Y.E. Pelaez, at the ceremony honoring Dr. Isabella Karle's receipt of the 1993 Bower Award.

Drs. Richard Gilardi, Jerome Karle, Walter Sperling, and Isabella Karle study the structure of the retinal photochemical sensor that Dr. Sperling had recently synthesized (1971).

Dr. Jerome Karle and Dr. Bhakta Rath.

Jerome, Isabella, and two of their three daughters.

MEDALS and AWARDS

NRL Celebrated the Karles' Retirement with a Ceremony on July 21, 2009

The Karles, surrounded by some of the distinguished guests who attended the ceremony, from left to right: Mr. Zachary Lemnios, Director of Defense Research and Engineering; Dr. Walter Jones, Technical Director, Office of Naval Research; Dr. Dave Skatrud, Army Research Laboratory; Mr. Tony Torres Ramos, Director, Senior Executive Management Program Office, Office of Civilian Human Resources; RADM Nevin Carr, Chief of Naval Research; Mr. Douglas Lundberg, Director of Human Resources Policy and Programs, Department of the Navy; The Honorable Ray Mabus, Secretary of the Navy; CAPT Paul Stewart, NRL Commanding Officer; Mr. James Thomsen, Principal Civilian Deputy Assistant Secretary of the Navy for Research, Development and Acquisition; Dr. John Montgomery, NRL Director of Research; and Ms. Patricia Adams, Deputy Assistant Secretary of the Navy for Civilian Human Resources.

The Honorable Ray Mabus, Secretary of the Navy, congratulates the Karles.

The Karle family.

Dr. Bhakta Rath, Associate Director of Research for Materials Science and Component Technology.

The Karles with NRL military personnel.

Ms. Patricia Adams, Deputy Assistant Secretary of the Navy for Civilian Human Resources, congratulating Drs. Jerome and Isabella Karle.

Dr. Walter Jones, Technical Director, Office of Naval Research; Dr. Gerry Borsuk, Associate Director of Research, Systems Directorate; Dr. Bhakta Rath, Associate Director of Research, Materials Science and Component Technology Directorate; and CAPT Douglas Rau (Ret.), former NRL Commanding Officer.

the naval research laboratory

27
NRL – Our Heritage

28
Highlights of NRL Research in 2008

35
NRL Today

NRL — OUR HERITAGE

The Naval Research Laboratory's early 20th-century founders knew the importance of science and technology in building naval power and protecting national security. They equally knew that success depended on taking the long view, focusing on the long-term needs of the Navy through fundamental research. NRL began operations on July 2, 1923, as the United States Navy's first modern research institution.

Thomas Edison's Vision: The first step came in May 1915, a time when Americans were deeply worried about the great European war. Thomas Edison, when asked by a *New York Times* correspondent to comment on the conflict, argued that the Nation should look to science. "The Government," he proposed in a published interview, "should maintain a great research laboratory....In this could be developed...all the technique of military and naval progression without any vast expense." Secretary of the Navy Josephus Daniels seized the opportunity created by Edison's public comments to enlist Edison's support. He agreed to serve as the head of a new body of civilian experts — the Naval Consulting Board — to advise the Navy on science and technology. The Board's most ambitious plan was the creation of a modern research facility for the Navy. Congress allocated $1.5 million for the institution in 1916, but wartime delays and disagreements within the Naval Consulting Board postponed construction until 1920.

The Laboratory's two original divisions — Radio and Sound — pioneered in the fields of high-frequency radio and underwater sound propagation. They produced communications equipment, direction-finding devices, sonar sets, and perhaps most significant of all, the first practical radar equipment built in this country. They also performed basic research, participating, for example, in the discovery and early exploration of the ionosphere. Moreover, the Laboratory was able to work gradually toward its goal of becoming a broadly based research facility. By the beginning of World War II, five new divisions had been added: Physical Optics, Chemistry, Metallurgy, Mechanics and Electricity, and Internal Communications.

World War II Years and Growth: Total employment at the Laboratory jumped from 396 in 1941 to 4400 in 1946, expenditures from $1.7 million to $13.7 million, the number of buildings from 23 to 67, and the number of projects from 200 to about 900. During WWII, scientific activities necessarily were concentrated almost entirely on applied research. New electronics equipment — radio, radar, sonar — was developed. Countermeasures were devised. New lubricants were produced, as were antifouling paints, luminous identification tapes, and a sea marker to help save survivors of disasters at sea. A thermal diffusion process was conceived and used to supply some of the ^{235}U isotope needed for one of the first atomic bombs. Also, many new devices that developed from booming wartime industry were type tested and then certified as reliable for the Fleet.

Post-WWII Reorganization: The United States emerged into the postwar era determined to consolidate its significant wartime gains in science and technology and to preserve the working relationship between its armed forces and the scientific community. While the Navy was establishing its Office of Naval Research (ONR) as a liaison with and supporter of basic and applied scientific research, it was also encouraging NRL to broaden its scope and become, in effect, its corporate research laboratory. There was a transfer of NRL to the administrative oversight of ONR and a parallel shift of the Laboratory's research emphasis to one of long-range basic and applied investigation in a broad range of the physical sciences.

However, rapid expansion during WWII had left NRL improperly structured to address long-term Navy requirements. One major task — neither easily nor rapidly accomplished — was that of reshaping and coordinating research. This was achieved by transforming a group of largely autonomous scientific divisions into a unified institution with a clear mission and a fully coordinated research program. The first attempt at reorganization vested power in an executive committee composed of all the division superintendents. This committee was impracticably large, so in 1949, a civilian director of research was named and given full authority over the program. Positions for associate directors were added in 1954, and the laboratory's 13 divisions were grouped into three directorates: Electronics, Materials, and Nucleonics.

The Breadth of NRL: During the years since World War II, the Laboratory has conducted basic and applied research pertaining to the Navy's environments of Earth, sea, sky, space, and cyberspace. Investigations have ranged widely — from monitoring the Sun's

behavior, to analyzing marine atmospheric conditions, to measuring parameters of the deep oceans. Detection and communication capabilities have benefitted by research that has exploited new portions of the electromagnetic spectrum, extended ranges to outer space, and provided a means of transferring information reliably and securely, even through massive jamming. Submarine habitability, lubricants, shipbuilding materials, firefighting, and the study of sound in the sea have remained steadfast concerns, to which have been added recent explorations within the fields of virtual reality, superconductivity, biomolecular science and engineering, and nanotechnology.

The Laboratory has pioneered naval research into space — from atmospheric probes with captured V-2 rockets, through direction of the Vanguard project (America's first satellite program), to inventing and developing the first satellite prototypes of the Global Positioning System (GPS). Today, NRL is the Navy's lead laboratory in space systems research, as well as in fire research, tactical electronic warfare, microelectronic devices, and artificial intelligence.

The consolidation of NRL and the Naval Oceanographic and Atmospheric Research Laboratory, with centers at Bay St. Louis, Mississippi, and Monterey, California, added critical new strengths to the Laboratory. NRL now is additionally the lead Navy center for research in ocean and atmospheric sciences, with special strengths in physical oceanography, marine geosciences, ocean acoustics, marine meteorology, and remote oceanic and atmospheric sensing.

The Twenty-First Century: The Laboratory is focusing its research efforts on new Navy strategic interests in the 21st century, a period marked by global terrorism, shifting power balances, and irregular and asymmetric warfare. NRL scientists and engineers are working to give the Navy the special knowledge, capabilities, and flexibility to succeed in this dynamic environment. While continuing its programs of basic research that help the Navy anticipate and meet future needs, NRL also moves technology rapidly from concept to operational use when high-priority, short-term needs arise — for pathogen detection, lightweight body armor, contaminant transport modeling, and communications interoperability, for example. The interdisciplinary and wide-ranging nature of NRL's work keeps this "great research laboratory" at the forefront of discovery and innovation, solving naval challenges and benefiting the nation as a whole.

HIGHLIGHTS OF NRL RESEARCH IN 2008

The scientific community at NRL conducts innovative research across a wide spectrum of technical areas, much of it detailed in the *NRL Review* chapters ahead. The following is a selection of the many projects pursued during 2008.

Launch and Commissioning of NASA's Fermi Gamma-ray Space Telescope: The Fermi Gamma-ray Space Telescope (formerly GLAST), NASA's newest observatory, has begun its mission of exploring the high-energy space environment in gamma rays. Launched from Florida on 11 June 2008, the spacecraft and its instruments passed their orbital checkout and commissioning with flying colors. Fermi's primary instrument, the Large Area Telescope (LAT), is now surveying the gamma-ray sky at energies from tens of millions to hundreds of billions of times greater than those we see with our eyes. With its unprecedented sensitivity and sky-survey viewing, the LAT is revolutionizing our understanding of the near-Earth environment and distant universe in energetic gamma rays, the most penetrating type of electromagnetic radiation. NRL scientists designed and built the LAT calorimeter, which measures the energies of the gamma rays, and led the commissioning of the LAT on orbit. NRL also provided facilities and technical support for the environmental testing of the instrument and observatory.

Launch of NASA's Fermi Gamma-ray Space Telescope from Cape Canaveral Air Force Station. Inset: The Fermi spacecraft during installation on the Delta IIH rocket. The LAT instrument is the large silver rectangular instrument on top of the spacecraft.

The TTCP Anti-ship Missile Project Arrangement (TAPA) Electronic Warfare Experiment: The TAPA II Electronic Warfare (EW) coalition experiment was planned and successfully conducted in 2008, with NRL as the overall manager. This large, multi-day experiment focused on R&D and Fleet EW systems for ship defense against airborne surveillance and targeting radars and RF anti-ship missile simulators. Key data was obtained to improve digital radio frequency memory (DRFM)-based systems and EW coalition techniques and tactics.

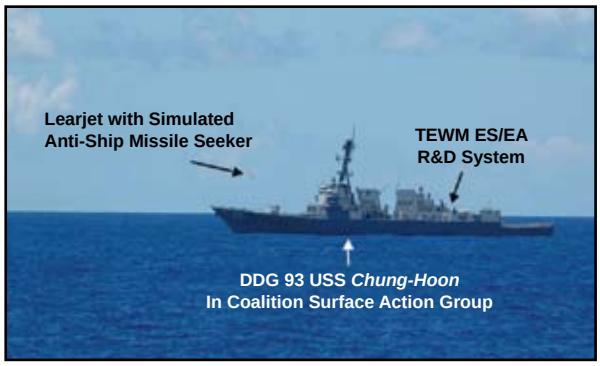

TAPA EW Experiment: EW R&D systems working against simulated anti-ship missile (ASM) engagements.

Multifunction Electronic Warfare (MFEW) above- and below-deck trailers and receive array installed on USS *Comstock*.

Successful Demonstration of the Multifunction Electronic Warfare (MFEW) Advanced Development Model (ADM): The Multifunction Electronic Warfare Advanced Development Model completed successful testing at the NRL Chesapeake Bay Detachment in 2008. The system then underwent at-sea testing aboard USS *Comstock* (LSD 45) during the TAPA II EW testing event, part of the RIMPAC 08 multinational fleet exercise. The at-sea testing involved the successful detection, classification, and tracking of multiple threat emitters aboard several aircraft simulating an attack. The MFEW ADM demonstrated a critical new EW capability for the Navy.

High Pressure EOF Micropump Integrated into HPLC-on-a-Chip for Explosives Separation: NRL has designed an electro-osmotic flow (EOF)-based micropump on a planar quartz substrate by densely packing a short microchannel with 800-nm silica particles. At a modest applied electric field strength of 200 V/cm, the EOF micropump generates a maximum pressure of >1000 psi (~7 MPa) and a maximum flow rate of 282 nL/min when aqueous CHES buffer (10 mM, pH 9.0) is used as the pumping fluid. The EOF micropump has been integrated onto a portable quartz microchip with a cross-T injection design, a downstream, sol–gel packed separation column, and a 2D spectral UV absorbance detection system for successful separation of six nitroaromatic and nitramine explosives and their degradation products via high performance liquid chromatography (HPLC).

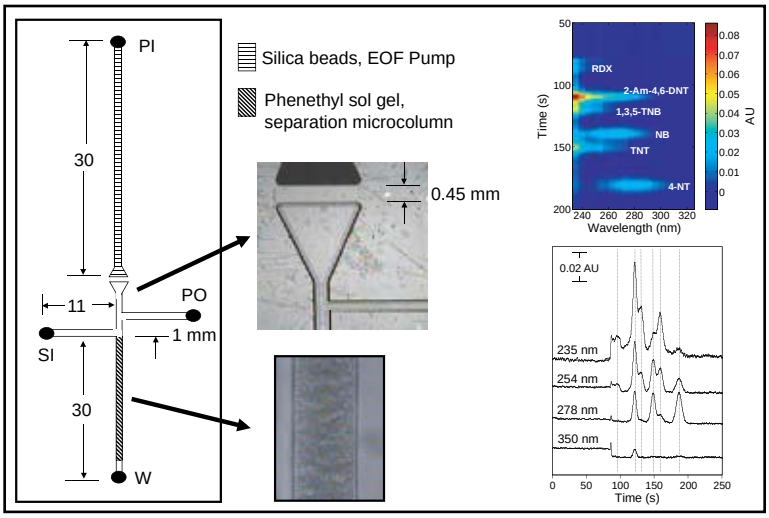

Quartz substrate (left) integrating EOF pump (top, middle) with sol-gel separation microcolumn (bottom, middle) enables the separation of six explosives and degradation products as shown in a two-dimensional spectral absorbance plot (upper right) and from select wavelength slices (lower right).

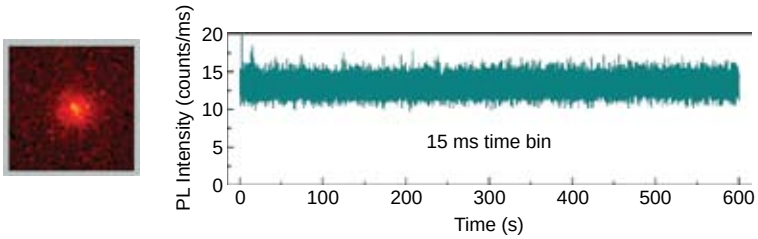

Photoluminescence image and time dependent photoluminescence intensity traces from a single CdZnSe nanocrystal.

Creation of Non-Blinking Semiconductor Nanocrystals: Photoluminescence "blinking" in semiconductor nanocrystals severely limits the usefulness of nanocrystals in applications requiring a continuous output of single photons. NRL and several collaborators have eliminated the blinking by engineering a radially graded alloy core-shell structure with a soft confinement potential. These non-blinking nanocrystals may enable substantial advances in a variety of nanoscale applications, including in biology, quantum optics, and optoelectronics.

Hyperspectral Imager for the Coastal Ocean (HICO): The NRL Hyperspectral Imager for the Coastal Ocean will be the first spaceborne hyperspectral imager optimized for environmental characterization of the coastal zone. In orbit, HICO will demonstrate the retrieval of products of value to naval forces including bathymetry, bottom type, in-water visibility, and onshore terrain, vegetation, and traffficability maps, for diverse coastal types worldwide. HICO is manifested for launch to the International Space Station in 2009.

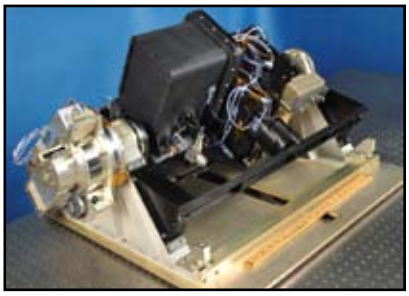

The Hyperspectral Imager for the Coastal Ocean (HICO).

AUV used in the Low Frequency Broadband Mine Identification program.

Low Frequency Broadband Mine Hunting: In the Low Frequency Broadband Mine Identification program, NRL has demonstrated structural acoustic–based mine identification using broadband very low frequency sonar mounted on an autonomous underwater vehicle (AUV). Highly successful blind tests were carried out in medium-grained sand and mud and silt environments. This work is now transitioning to PMS-403, the Navy's Unmanned Undersea Vehicles Program Office.

Photoinduced Electron Transfer at Bioinorganic Interfaces: NRL is developing ultra-lightweight, high power density, self-assembling biophotovoltaic devices based on photosynthetic proteins. The proposed devices will integrate photosynthetic reaction center (RC) proteins into solid-state carbon surfaces and nanotube arrays and use the same protein for assisted formation of the second (gold) electrode. Utilization of genetically engineered RC proteins, specifically synthesized organic linkers, and precisely fabricated inorganic electrodes will make desired connections to overcome the energy barrier between the protein and the electrodes at the macroscopic and nano scales. At the same time, this allows for using the same protein as a nanometer scale insulator. Potential applications include ultra-lightweight power sources, distributed autonomous sensors, and nanosize field effect transistors and logic gates. Another advantage of the proposed devices is their biocompatibility and the possibility of their integration into the human body.

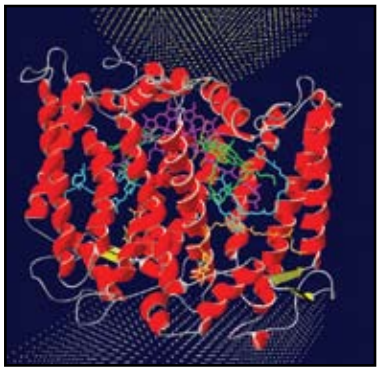

Photosynthetic photovoltaic module for highly efficient light energy conversion.

High-power solid-state ytterbium laser with zero quantum defect.

Kilowatt-Scale Radiation-Balanced Laser: The most serious design concern for high-power solid-state lasers is managing the heat balance in the lasing materials to retain beam quality. NRL has demonstrated the first solid-state laser to operate at high power without detrimental bulk heating. By incorporating the principle of fluorescence cooling into the laser medium, the radiation-balanced laser reduces thermal loading 100-fold compared to the previous state of the art.

Military Aircraft Jet Noise Simulations: In a study to characterize the noise generated by high-performance military aircraft engines, NRL has conducted monotonically integrated large eddy simulations (MILES) of the flow fields and acoustics of supersonic jet flows, and compared them to experimental data. A finite-element flow solver using unstructured grids allows modeling the jet exhaust nozzle geometry accurately, and the MILES approach directly computes the large-scale turbulent flow structures. No explicit subgrid scale model is used and the modeling of the subgrid scales is implicitly provided by the embedded flux limiter. MILES for several total pressure ratios under non-ideally expanded flow conditions were simulated and compared to experimental data. The agreement between the predictions and the experimental data is very good, validating the computational methodology and paving the way for follow-on work on noise reduction techniques.

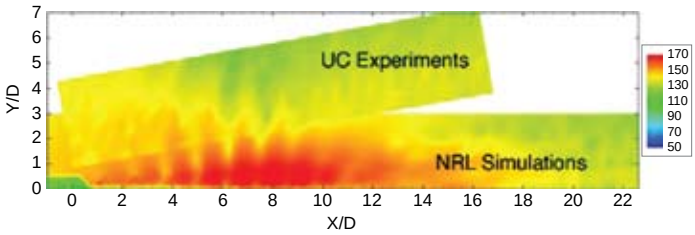

The computed sound pressure level in the exhaust of supersonic military jet aircraft is compared to experimental data from the University of Cincinnati (UC). The agreement is excellent, indicating that the numerical simulations are very realistic.

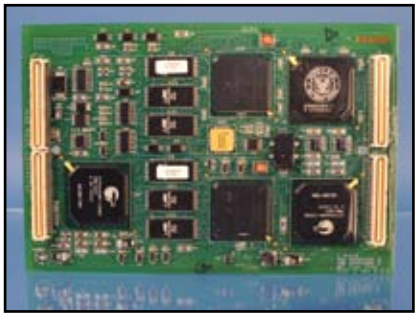

The PEIP-II multi-channel software programmable MILS (multiple independent levels of security) cryptographic module.

Programmable Embeddable INFOSEC Product – Phase II (PEIP-II): The PEIP-II programmable cryptographic engine developed by NRL for the National Security Agency (NSA) is recognized as an enabling technology for the DoD Cryptographic Modernization program. NSA security certification activities were completed for PEIP-II and PEIP-II+ (the airborne qualified and environmentally hardened version), and PEIP-II has now been embedded for use in modernized cryptographic devices: the KG-334 developed by SPAWAR, and the KG-333/KGV-361 by Rockwell Collins. It is currently being integrated in the Modular Integrated Link Electronics System (MILES), Highband Network Radio, and other similar programs to support their cryptographic requirements.

Field-testing the explosives detection system at Yuma Proving Ground, with the sample tripod at about 10 meters standoff. The red arrow illustrates the path of the invisible IR beam.

Standoff Detection of Trace Explosives Residues Using Infrared Photothermal Imaging: Developing technology that can detect explosives without the need for swabbing surfaces is a major thrust for the DoD and Department of Homeland Security. The ultimate goal is for real-time detection from a significant standoff distance using techniques safe for people and non-damaging to objects. NRL has developed and tested a technique that can meet these goals. An eye-safe infrared laser is directed to a surface of interest, which is viewed using a thermal imager. Resonant absorption by the analyte at specific infrared wavelengths selectively heats the analyte, providing a thermal contrast with the substrate. The technique has been demonstrated to detect TNT and RDX explosives residues from several meters away.

Chemically Modified Graphene: A Benchtop Approach to Graphene-based Sensors: NRL has developed a process to form large-area, ultra-thin, chemically modified graphene (CMG) films, and from these, create state-of-the-art chemical sensors and nanomechanical resonators. By tuning the chemistry of CMG films, the sensitivity and level of 1/f noise in conductance-based chemical sensors can be controlled. These sensors are capable of detecting 10-second exposures to simulants of the three main classes of chemical-warfare agents and an explosive, at parts-per-billion concentrations. The films also have outstanding mechanical properties and can be used to fabricate high Young's modulus (<E> = 185 GPa), ultra-low-mass nanomechanical resonators. We have demonstrated radio frequency resonators with quality factors and figures of merit well exceeding those of pure graphene resonators and comparable to diamond films.

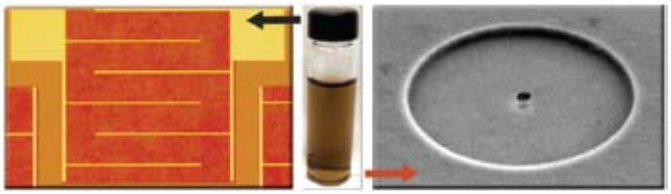

Graphene, a single atomic sheet of graphite, has extraordinary physical properties, but its extreme thinness poses challenges in forming and manipulating it. In this work, we take advantage of a water soluble form of graphene in which oxygen functional groups are attached to the graphene basal plane.

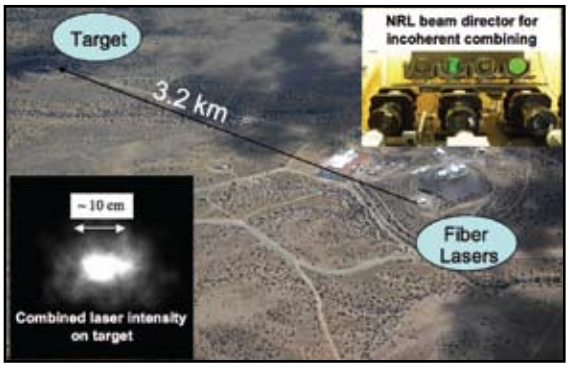

Field tests of the NRL incoherent beam combining architecture (Starfire Optical Range, NM, 2008). Four kilowatts of continuous laser power was transmitted 3.2 kilometers at 90% efficiency.

Incoherent Combining of High-Power Fiber Lasers for Long-Range Directed Energy Applications: NRL's high-energy fiber laser program is developing a robust, compact, highly efficient, long-range laser weapon system for near-term Navy applications. The system is based on incoherently combining high-power fiber lasers. The unique characteristics of this laser system make it ideal for operation aboard an all-electric ship. Experiments to evaluate laser beam control, propagation, and lethality have been completed; the agreement between experimental results and modeling is excellent.

Afghanistan Integrated Airborne Geospatial Study: NRL conducted its second airborne multisensor geospatial survey of Afghanistan in 2008. Objectives of the project were to develop new techniques in combined sensor collections, improve data processing and analysis techniques, begin building next-generation data basing and dissemination for large geospatial data sets, and obtain data in support of counternarcotics operations and troop support. The sensor suite included a digital photogrammetric camera, hyperspectral imager, thermal imaging camera, gravimeter, magnetometer, and high-altitude scanning topographic lidar system. The multiple systems enable a more complete characterization of terrain and features by utilizing various portions of the optical spectrum. Derived products were rapidly pushed to planners and warfighters in Afghanistan.

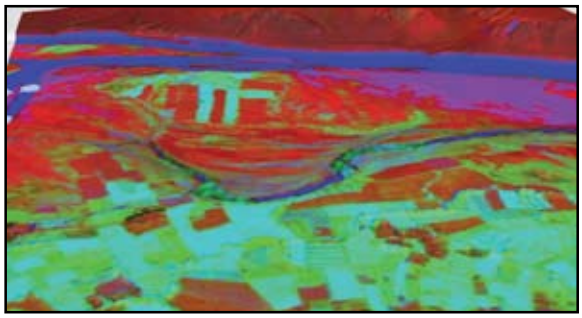

One example of the imagery collected over Afghanistan: false-color image produced by a hyperspectral camera.

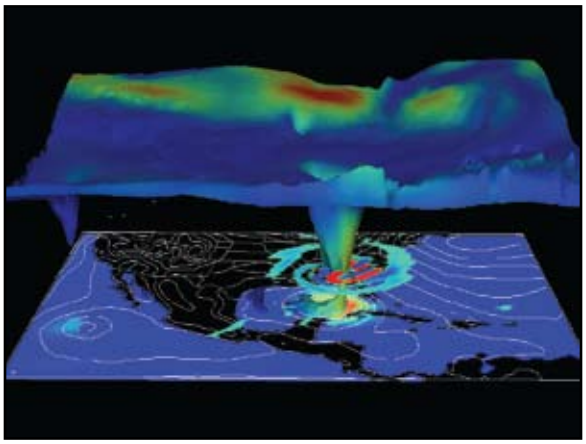

COAMPS-TC three-dimensional depiction of hurricane Katrina (valid at 00 UTC 29 August 2005), which includes the 340K equivalent potential temperature isosurface, sea-level pressure (white), 10-m wind speed (color), and the 2.5-km adjoint sensitivity.

Development and Demonstration of COAMPS®-TC: Prediction of the formation and intensity of tropical cyclones by numerical models is a formidable forecast problem. NRL has developed a new version of the Navy's high-resolution operational mesoscale model specifically for tropical cyclone prediction, called COAMPS®-TC, and tested it in real time during a field campaign in the western Pacific. This new version of the model exhibited considerable promise in providing skillful intensity forecasts, while also providing guidance for storm track that was superior to current operational mesoscale guidance. NRL also developed a mathematical tool for this modeling system for guiding research aircraft to optimal areas for deploying dropsondes for measuring and forecasting tropical cyclones in the formation stage. This is the first such systematic targeting endeavor for tropical cyclone genesis ever conducted.

FREND Autonomous Robotic Grapple of Simulated Spacecraft: NRL and DARPA have successfully developed and ground-demonstrated critical space robotic technology needed for autonomous, unaided servicing of legacy spacecraft not pre-designed for servicing. This effort, the Front-end Robotic Enabling Near-term Demonstration (FREND), successfully accomplished full-scale hardware simulations of spacecraft docking via robotic grapple with a mock geosynchronous spacecraft under simulated orbital lighting and dynamics conditions. These simulations were performed with spaceflight-prototype and spaceflight-ready robotics, machine vision sensors, and control algorithms.

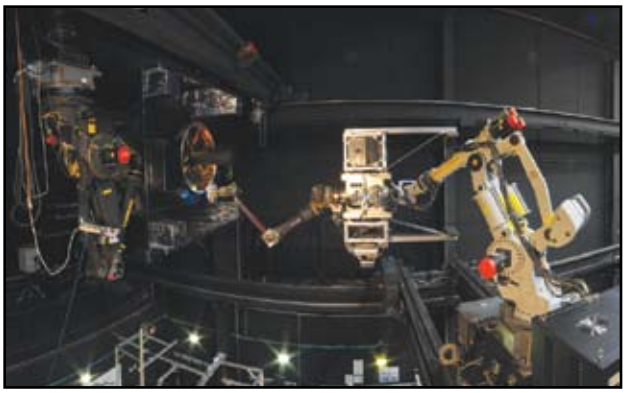

Full-scale spacecraft rendezvous and docking testing in NRL's Proximity Operations Laboratory against a simulated geosynchronous communication satellite (left). Spaceflight-ready two-meter robot arm (center).

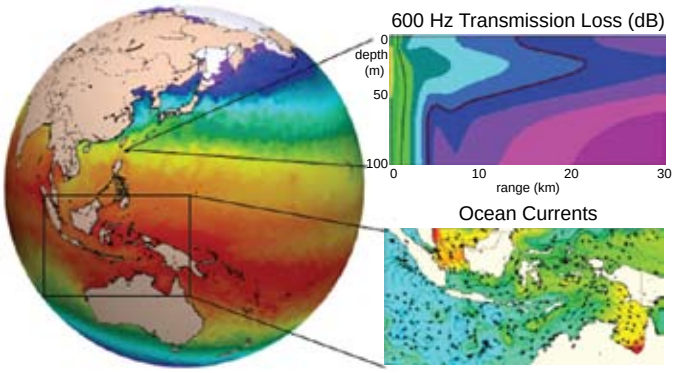

Transmission loss section from NOSSP using GOFS 2.6.

Transition of the NRL Global Ocean Nowcast/Forecast System v2.6: In August 2008, NRL's Global Ocean Forecast System (GOFS) version 2.6 was declared operational by the Naval Oceanographic Office (NAVOCEANO) as a source of currents and boundary conditions for nested ocean models. GOFS 2.6 advances beyond prior capabilities by adding assimilation of in situ observations, using mixed-layer depth forecasts to modify projected synthetic profiles, and coupling with the Los Alamos Community Ice CodE (CICE) for the first two-way coupling of Navy ice and global ocean models in the Arctic. These capabilities enable GOFS 2.6 and higher-resolution nested Navy Coastal Ocean Models (NCOM) to form a new Navy Ocean Sound Speed Prediction (NOSSP) capability for NAVOCEANO. NOSSP will provide more accurate estimates of acoustic transmission loss to enable improved resource allocation, search effectiveness, and risk assessment in antisubmarine warfare. NCOM-based NOSSP using GOFS 2.6 was declared operational in November 2008.

Maritime Automated Supertrack Enhanced Reporting (MASTER) Joint Capability Technology Demonstration (JCTD): Presidential directives for maritime security, maritime domain awareness, and global maritime intelligence integration mandate a significant improvement in national capabilities to provide timely dissemination of quality, actionable maritime situational awareness. The MASTER JCTD, for which NRL serves as Technical Manager, is developing and demonstrating maturing maritime domain awareness technologies and operational concepts to provide the following capabilities: ability to achieve and maintain maritime situational awareness of vessels, cargo, people, and infrastructure; ability to automatically generate, update, and rapidly disseminate high quality ship tracks; ability to aggregate maritime tracks from multiple intelligence sources at multiple levels of security to provide past and current ship movement; and ability to generate and display automated rule-based maritime alert notifications.

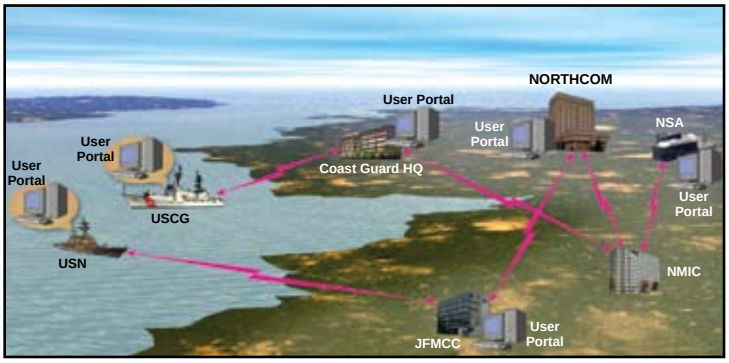

A typical example of MASTER node dispersion and operation.

NRL TODAY

ORGANIZATION AND ADMINISTRATION

The Naval Research Laboratory is a field command under the Chief of Naval Research, who reports to the Secretary of the Navy via the Assistant Secretary of the Navy for Research, Development and Acquisition.

Heading the Laboratory with joint responsibilities are CAPT Paul C. Stewart, USN, Commanding Officer, and Dr. John A. Montgomery, Director of Research. Line authority passes from the Commanding Officer and the Director of Research to three Associate Directors of Research, the Director of the Naval Center for Space Technology, and the Associate Director for Business Operations. Research divisions are organized under the following functional directorates:

- Systems
- Materials Science and Component Technology
- Ocean and Atmospheric Science and. Technology
- Naval Center for Space Technology.

The *NRL Fact Book*, published every two years, contains information on the structure and functions of the directorates and divisions.

NRL operates as a Navy Working Capital Fund (NWCF) Activity. All costs, including overhead, are charged to various research projects. Funding in FY08 came from the Chief of Naval Research, the Naval Systems Commands, and other Navy sources; government agencies such as the U.S. Air Force, the Defense Advanced Research Projects Agency, the Department of Energy, and the National Aeronautics and Space Administration; and several nongovernment activities.

PERSONNEL DEVELOPMENT

At the end of FY08, NRL employed 2559 persons — 35 officers, 76 enlisted, and 2448 civilians. In the research staff, there are 761 employees with doctorate degrees, 302 with master's degrees, and 440 with bachelor's degrees. The support staff assists the research staff by providing administrative support, computer-aided design, machining, fabrication, electronic construction, publication and imaging, personnel development, information retrieval, large mainframe computer support, and contracting and supply management services.

Opportunities for higher education and other professional training for NRL employees are available through several programs offered by the Employee Relations Branch. These programs provide for graduate work leading to advanced degrees, advanced training, college course work, short courses, continuing education, and career counseling. Graduate students, in certain cases, may use their NRL research for thesis material.

For non-NRL employees, several postdoctoral research programs exist. There are also agreements with several universities for student opportunities under the Student Career Experience Program (formerly known as Cooperative Education), as well as summer and part-time employment programs. Summer and interchange programs for college faculty members, professional consultants, and employees of other government agencies are also available. These programs are described in the *NRL Review* chapter "Programs for Professional Development."

NRL has active chapters of Women in Science and Engineering (WISE), Sigma Xi, Toastmasters International, and the Federal Executive and Professional Association. An amateur radio club, a drama group, and several sports clubs are also active. NRL has a Recreation Club that provides sports leagues and swim, whirlpool bath, gymnasium, and weight-room facilities. NRL also has an award-winning Community Outreach Program. See "Programs for Professional Development" for details on all these programs and activities.

NRL has its very own credit union. Established in 1946, NRL Federal Credit Union (NRLFCU) is a sound financial institution that serves about 20,000 NRL employees, contractors, select employee groups, and their families. Focusing on its mission of *Trusted Partners for Life*, NRLFCU provides many free and low cost products and services including free bill payer, great rates on deposits, credit cards, auto loans, mortgages and more. It offers direct deposit, online access, three local branches (one of them located in Bldg. 222) and nationwide access via the National Shared Branching Network. NRLFCU also offers full-service investment and brokerage services. For more information, call 301-839-8400 or log onto www.nrlfcu.org.

Public transportation to NRL is provided by Metrobus. Metrorail service is three miles away.

SITES AND FACILITIES

NRL's main campus in Washington, DC, consists of 87 main buildings on about 130 acres. NRL also maintains 11 other research sites, including a vessel for fire research and a Flight Support Detachment. The many diverse scientific and technological research and support facilities are described here.

RESEARCH FACILITIES

Institute for Nanoscience

The revolutionary opportunities available in nanoscience/nanotechnology have led to a National Nanotechnology Initiative. NRL has been a major contributor to the science of nanostructures and is making a commitment to expand that effort. The NRL Institute for Nanoscience was established in 2001 with a current annual budget of $11 million in core research funds. The mission of the Institute for Nanoscience is to conduct highly innovative, interdisciplinary research at the intersections of the fields of materials, electronics, and biology in the nanometer size domain. The Institute exploits the broad multidisciplinary character of the Naval Research Laboratory to bring together scientists with disparate training and backgrounds to pursue common goals at the intersection of their respective fields in systems at this length scale. The objectives of the Institute's programs are to provide the Navy and DoD with scientific leadership in this complex, emerging area and to identify opportunities for advances in future defense technology. Its current research program emphasizes multidisciplinary, cross-division efforts in nanomaterials, nanoelectronics, and nanosensors/devices.

The Institute for Nanoscience building opened in January 2004. It has 5000 ft^2 of Class 100 clean room space for device fabrication, 4000 ft^2 of "quiet" space with temperature controlled to 0.5 °C, acoustic isolation at the NC35 standard (35 dB at 1 kHz), floor vibration isolation to <150 μm/s rms at 10 to 100 Hz and <0.3 mOe magnetic noise at 60 Hz. There are also 1000 ft^2 of "ultra-quiet" space with temperature controlled to 0.1 °C and acoustic isolation at the NC25 standard (25 dB at 1 kHz).

Radar

NRL has gained worldwide renown as the "birthplace of radar," and for more than half a century has maintained its reputation as a leading center for radar-related research and development. A number of facilities managed by NRL's Radar Division continue to contribute to this reputation.

A widely used major facility is the Compact Antenna Range (operated jointly with the Space Systems Development Department) for antenna design and development and radar cross section measurements. The range is capable of simulating far-field conditions from 1 to 110 GHz, with a quiet zone approximately 7 ft in diameter and 8 ft in length. Instrumentation covers from 1 to 95 GHz. Another strong division capability is in the Computational Electromagnetics (CEM) Facility, which has capabilities for complex electromagnetic modeling, including radar target and antenna structures. The Radar Signature Calculation Facility within this group produces detailed computations of radar cross sections of various targets, primarily ships. The CEM facility includes multiple-CPU supercomputers that are also used to design phased array radar antennas. The tremendous synergism between the CEM group and the Compact Antenna Range Facility provides the ability to design in the CEM environment, to test in the compact range, and to have immediate feedback between the theoretical and experimental aspects to shorten the development cycle for new designs.

In connection with airborne radar, the division operates a supercomputer-based Radar Imaging Facility and an inverse synthetic aperture radar (ISAR) deployed either in the air, on the ground, or aboard ship for radar imaging data collection. A P-3 aircraft equipped with the AN/APS-145 radar and cooperative engagement capability is also available for mounting experiments.

In connection with ship-based radar, the division operates the Radar Testbed Facility at the Chesapeake Bay Detachment (CBD), Randle Cliffs, Maryland. The site has radars for long-range air search and surface search functions and features the newly developed W-band Advanced Radar for Low Observable Control (WARLOC), a fully operational high-power coherent millimeter-wave radar operating at 94 GHz. The WARLOC transmitter is capable of producing 10 kW average power with a variety of waveforms suitable for precision tracking and imaging of targets at long range. Waveforms with a bandwidth of 600 MHz can be transmitted at full power. A 6-ft Cassegrain antenna is mounted on a precision pedestal and achieves 62 dB of gain.

The Advanced Multifunction Radio Frequency Concept (AMRFC) testbed is a new installation at CBD, operated by the Radar Division, with joint participation of several other NRL divisions as well. The goal of the AMRFC program is to demonstrate the integration of many sorts of shipboard RF functions, including radar, electronic warfare (EW), and communications, by utilizing a common set of broadband array antennas, signal and data processing, and signal generation and display hardware. The testbed consists of separate active transmit and receive arrays that operate over the 6 to 18 GHz band (nominally). Current functionality of the testbed includes a multimode navigation/surface surveillance Doppler radar, multiple communication links (line-of-sight and satellite), and passive and active EW capabilities. Testbed electronics are housed in seven converted 20-ft shipping containers and trailers. The arrays are mounted on a 15° tilt-back in the ends of two of the trailers overlooking the Chesapeake Bay, simulating a possible shipboard installation.

The AMRFC testbed, located at NRL's CBD, was developed as a proof-of-principle demonstration system that is capable of simultaneously transmitting and receiving multiple beams from common transmit and receive array antennas for radar, electronic warfare, and communications. These RF functions are controlled by common resource allocation manager (RAM) software over a real-time control network. New RF functionality may be readily added to the testbed as required for further demonstrations.

The division also has access to other radar systems: the Microwave Microscope (MWM); the Navy's relocatable over-the-horizon radar (AN/TPS-71); and an experimental Cooperative Aircraft Identification system. The internally developed MWM has a high-resolution (2 cm) ultrawideband capability that is used to investigate backscatter from surface and volumetric clutter, has through-wall detection capability, and characterizes the impulse responses of scattering objects. With respect to the AN/TPS-71, the division provides direct technical support and has direct access to data. The Cooperative Aircraft Identification system is used to explore system concepts and engineering developments in connection with target identification.

Information Technology

NRL's Information Technology Division (ITD) conducts basic research, exploratory development, and advanced technology demonstrations in the collection, transmission, processing, dissemination, and presentation of information. ITD's research program spans the areas of artificial intelligence, autonomous systems, high assurance systems, computer networks, modeling and simulation, virtual and augmented reality, human/computer interaction, communication systems, transmission technology, and high performance computing.

A Voice Communication Laboratory supports the development of tactical voice technology, and a Wireless Networking Testbed supports the development of Mobile Ad Hoc Networking (MANET) technology. A Freespace Laser Communications Laboratory supports the design and development of prototype technical solutions for Naval laser communications requirements. ITD research networks connect internal NRL networks via high-speed links to the Defense Research and Engineering Network (DREN) and to an all-optical network that forms the DoD's Global Information Grid Evaluation Facility (GIG-EF). ITD's High Performance Computing Facilities and the Laboratory for Large Data provide a OC-192c based environment for experimentation and proof-of-concept development in high performance networking and the use and sharing of extremely large (petabytes and larger) data sets.

The Cryptographic Technology Laboratory supports the development of certifiable Communications Security (COMSEC) and Information Security (INFOSEC) products, including programmable cryptographic devices, cryptographic applications, and high assurance cross-domain solutions. The Naval Key Management Laboratory investigates electronic key management and networked key distribution technologies for the Navy and DoD. The Cyber Defense Development Laboratory provides direct support to the Fleet in the areas of computer network defense and visualization, cross-domain solutions, and reverse code analysis.

The Robotics and Autonomous Systems Laboratory provides the ability to develop and evaluate intelligent software and interfaces for autonomous vehicles. The Immersive Simulation Laboratory utilizes a collection of COTS and specially developed components to support R&D in interfaces for virtual simulators, ranging from fully immersive to desktop simulations. The Warfighter Human System Integration Laboratory maintains a range of Virtual Environment interface technologies as well as wearable, wi-fi physiological monitors and associated real-time processing algorithms for use in adaptive operational and training support technologies. The Audio Laboratory has facilities for rendering and analyzing complex sound for military applications, and the 3D Virtual and Mixed Environments Laboratory (3DVMEL) explores methods by which 3D computer graphics assists in the collection, interpretation, and dissemination of information for both operational and training purposes. The Behavioral Detection Laboratory supports the development of algorithms, processes, and sensor suites associated with behavioral indicators of deception.

The Navy Center for Applied Research in Artificial Intelligence is investigating learning and adaptation within teams of autonomous robots. Recent work has focused on a team of robots performing force protection.

Optical Sciences

The Optical Sciences Division has a broad program of basic and applied research in optics and electro-optics. Areas of concentration include fiber optics and fiber optic sensing, materials and sensors in the visible and infrared, integrated optical devices, signal processing, optical information processing, panchromatic and hyperspectral imaging for surveillance and reconnaissance, and laser development.

The division occupies some of the most modern optical facilities in the country. The newest facility in Optical Sciences is the Surface Characterization Facility, which includes instrumentation for ultraviolet and X-ray photoemission spectroscopy, atomic force and scanning tunneling microscopy (STM), and STM-induced light emission measurements. Other facilities include several fiber-optic facilities including preform fabrication, draw towers, optical fiber coaters, fiber splicers, and fiber-optic sensor testing stations such as an acoustic test cell and a three-axis magnetic sensor test cell. There is also an Ultralow-loss Infrared (IR) Fiber-Optic Waveguide Facility using high-temperature IR glass technology. The facilities for ceramic optical materials includes powder preparation, vacuum presses, and a 50-ton hot press for sintering. The Focal Plane Array Evaluation Facility allows measurement of the optical and electrical characteristics of infrared focal plane arrays being developed for advanced Navy sensors. The IR Missile-Seeker Evaluation Facility performs open-loop measurements of the susceptibilities of IR tracking sensors to optical countermeasures. A UHV multi-chamber deposition apparatus is used for fabrication of electro-optical devices and can be interlocked with the Surface Characterization Facility. Other scanning probe facilities are equipped with atomic

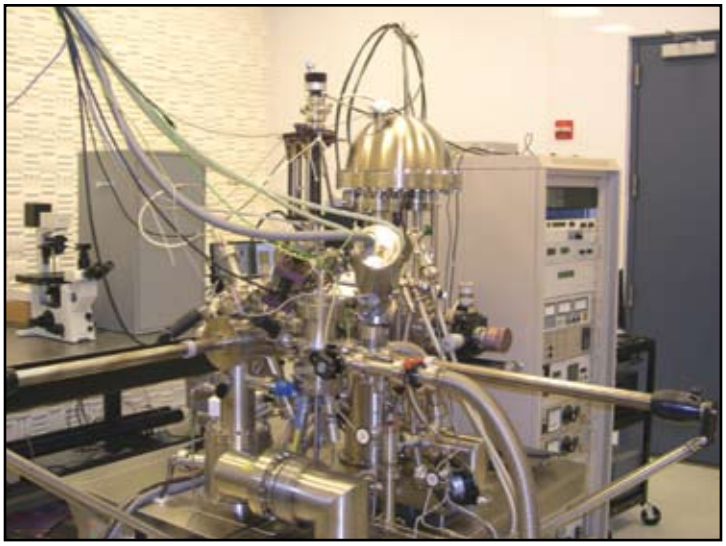

The Optical Sciences Surface Characterization Facility includes instrumentation for ultraviolet and X-ray photoemission spectroscopy (UPS and XPS), atomic force and scanning tunneling microscopy (AFM and STM), and STM-induced light emission (STM-LE) measurements.

force and magnetic force microscopes. Another material growth facility is a molecular beam epitaxial growth system dedicated to quantum confined GaSb/InAs/AlSb structures. An extensive set of laboratories exists to develop and test new laser and nonlinear frequency conversion concepts and to evaluate nondestructive test and evaluation techniques.

Electronic Warfare

The Tactical Electronic Warfare (TEW) Division's program for electronic warfare (EW) research and development covers the entire electromagnetic spectrum. The program includes basic technology research and advanced developments and their applicability to producing EW products. The range of ongoing activities includes components, techniques, and subsystems development as well as system conceptualization, design, and effectiveness evaluation. The focus of the research activities extends across the entire breadth of the battlespace. These activities emphasize providing the methods and means to counter enemy hostile actions — from the beginning, when enemy forces are being mobilized for an attack, through to the final stages of the engagement. In conducting this program, the TEW Division has an extensive array of special research and development laboratories, anechoic chambers, and modern computer systems for modeling and simulation work. Dedicated field sites, an NP-3D EW flying laboratory, and Learjets allow for the conduct of field experiments and operational trials. This assemblage of scientists, engineers, and specialized facilities also supports the innovative use of all Fleet defensive and offensive EW resources now available to operational forces.

Laboratory for the Structure of Matter

This laboratory investigates the atomic arrangements in materials to improve them or facilitate the development of new substances. Various diffraction methodologies are used to make these investigations. Subjects of interest include the structural and functional aspects of energy conversion, ion transport, device materials, and physiologically active substances such as drugs, antibiotics, and antiviral agents. Theoretical chemistry calculations are used to complement the structural research. Computer graphics aid in modeling and molecular dynamics studies. The facilities include two state-of-the-art X-ray diffraction units.

Chemistry

NRL has been a major center for chemical research in support of naval operational requirements since the late 1920s. The Chemistry Division continues this tradition. The Chemistry Division conducts basic research, applied research, and development studies in the broad fields of diagnostics, dynamics, synthesis, materials, surface/interfaces, environment, combustion, and fuels. Specialized programs currently within these fields include the synthesis and characterization of organic and inorganic materials, coatings, composites, nondestructive evaluation, surface/interface modification and characterization, nanometer structure science/technology, chemical vapor processing, tribology, solution and electrochemistry, mechanisms and kinetics of chemical processes, analytical chemistry, theoretical chemistry, decoy materials, radar-absorbing materials/radar-absorbing structures (RAM/RAS) technology, chemical/biological warfare defense, atmo-

Learjet with simulators overflies USS *Chung-Hoon* (DDG 93) during RIMPAC 08 exercises.

Recently remodeled facilities at Key West. Left: Marine Coatings Facility. Right: Marine Corrosion Facility.

sphere analysis and control, environmental remediation and protection, personnel protection, and safety and survivability. The division has several research facilities.

Chemical analysis facilities include a wide range of modern photonic, phononic, magnetic, electronic, and ionic based spectroscopic/microscopic techniques for bulk and surface analysis.

The Magnetic Resonance Facility includes advanced high-resolution solid-state nuclear magnetic resonance (NMR) spectroscopy techniques to observe nuclei across much of the periodic table and provides detailed structural and dynamical information.

The Synchrotron Radiation Facility has intense, monochromatic X-ray photon beams tunable from 10 eV to 35 KeV available from four beam lines developed by NRL at the National Synchrotron Light Source at the Brookhaven National Laboratory.

The Nanometer Characterization/Manipulation Facility includes fabrication and characterization capability based on scanning tunneling microscopy/spectroscopy, atomic force microscopy, and related techniques.

The Materials Synthesis/Property Measurement Facility has special emphasis on polymers, surface-film processing, and directed self-assembly.

The Chemical Vapor and Plasma Deposition Facility is designed to study and fabricate materials such as diamond using in situ diagnostics, laser machining, and plasma deposition reactors.

The Navy Fuel Research Facility performs basic and applied research to understand the underlying chemistry that impacts the use, handling, and storage of current and future Navy mobility fuels.

Fire research facilities include a 11,400 ft^3 fire-research chamber (Fire I) and the 457-ft ex–USS *Shadwell* (LSD 15) advanced fire research ship. Commensurate support has been devoted to survivability of the new classes of ships, DDX, LPD 17, and LHA(R).

The Marine Corrosion and Marine Coatings Facilities located on Fleming Key at Key West, Florida, offer an ocean-air environment and unpolluted, flowing seawater for studies of environmental effects on materials. Equipment is available for experiments involving weathering, general corrosion, fouling, and electrochemical phenomena, as well as coatings, cathodic protection devices, ballast water treatment, and other means to combat environmental degradation.

The Chemistry Division has focused on force protection/homeland defense (FP/HD) since September 11, 2001, especially on the development of improved detection techniques for chemical, biological, and explosive threats. As part of a multidivisional program to develop new technology systems, the Chemistry Division is a major contributor to the NRL Institute for Nanoscience. Nanoscience complements FP/HD in that nanoscience is expected to provide dramatic improvements to chemical/biological detection, protection, and neutralization. Chemistry will approach the nanoscale from the bottom up — building smaller atoms and molecules into nanostructures with new properties and developing the directed assembly of nanostructures into hierarchical systems. The NRL Nanoscience building is linked directly into the Chemistry building to provide controlled access and auxiliary space for work not requiring a "low noise" environment.

Materials Science and Technology

The Materials Science and Technology Division at NRL conducts materials research using seven major division facilities.

The Magnetoelectronics Fabrication Facility consists of a Class 1000 clean room equipped with tools

The Magnetoelectronics Fabrication Facility consists of a Class 1000 clean room equipped with tools for lithographic construction of magnetoelectronic and spintronic devices.

for lithographic construction of magnetoelectronic and spintronic devices. It provides pattern definition, metallization, dielectric layer deposition, and both reactive and Ar^+ ion etching of wafers and small pieces.

The Electrical, Magnetic, and Optical Measurement Facility contains several complementary instruments that allow for the magnetic, electrical, optical, and heat capacity characterization of materials and devices. SQUID (superconducting quantum interference device) magnetometry and vibrating sample magnetometry are used to determine important properties of superconducting, paramagnetic, diamagnetic, and ferromagnetic materials. The transport properties of materials, namely the temperature- and magnetic-field-dependent resistivity combined with heat-capacity measurements, allow for a fundamental physical understanding of electronic properties.

The Materials Processing Facility includes apparatuses for powder production by fluid atomization, thermal evaporation, and arc erosion, and a physical vapor deposition system designed to produce and coat submicron powders in situ. Facilities to process powder into bulk specimens by hot and cold isostatic pressing permit a variety of consolidation possibilities. The isothermal heat treatment facility and quenching dilatometer permit alloy synthesis and single crystal growth. Bulk alloys can be prepared by induction melting, while rapid solidified metals of thin cross section can be made by splat quenching and melt spinning. Ceramic and ceramic-matrix composites processing facilities include a wide variety of conventional, controlled atmospheric furnaces, hot presses, a ball milling apparatus, particle size determination capability, and sol-gel and organometallic coating processing capabilities.

The Mechanical Characterization Facility consists of various testing systems, many with automated computer control and data acquisition, for determining the mechanical response of materials under controlled loading/deformation and environmental conditions. Basic capabilities include quasistatic tensile and fracture testing, dynamic storage and loss moduli as a function of frequency and temperature, cyclic fatigue crack growth and corrosion fatigue testing, and stress-corrosion cracking testing.

The Thin-Film Materials Synthesis and Processing Facility provides users a wide variety of techniques for growth and processing of thin films (thickness 1 μm or less). Sputter deposition offers a versatile method of depositing metallic and dielectric films and is a primary tool of this facility. Thermal evaporation of metals is implemented in both high-vacuum and ultrahigh-vacuum systems. Pulsed laser deposition (PLD) with variable stage temperature and controlled atmosphere allows growth of oxides. Electrolytic deposition offers efficient growth of gold and silver films. Laser direct-write ablation and deposition processes provide unique methods for imposing CAD-defined features via ablation of a substrate film and ablative mass transfer to a substrate.

The 3-MV Tandem Pelletron Accelerator Facility uses two "pelletron" charging chains to produce a terminal voltage up to 3 MV in the accelerator. Negative ions are injected at 10 to 70 keV, accelerated up to the terminal where they undergo collisions with a stripper gas or a carbon stripper foil and lose electrons, then are accelerated as positive ions back to ground potential. Protons can be accelerated up to 6 MeV, He up to 9 MeV, and highly stripped Au (+12) up to 39 MeV. The lower limit of beam energy is about 400 keV. On the analysis beam line, the sample of interest is located at the end of the beam line, and a signal generated by scattering of incident high-energy ions indicates the

composition of the sample. Incident high-energy ions can also be used to damage the surface of a sample of interest, or to introduce a dopant.

The Micro/Nanostructure Characterization Facility is capable of performing transmission electron microscopy (TEM), scanning transmission electron microscopy (STEM), atomic resolution transmission electron microscopy (ARTEM), electron energy loss spectroscopy (EELS), Z-contrast imaging, and spectral imaging through the use of a JEOL 2010F transmission electron microscope, a Phillips CM30 transmission electron microscope, and a Leo scanning electron microscope. Other standard microstructure characterization instruments are also available.

Laboratory for Computational Physics and Fluid Dynamics

The Laboratory for Computational Physics and Fluid Dynamics maintains a very powerful collection of computer systems applied to a broad range of research. There are currently 192 shared memory Itanium processors, 1824 clustered ×86 cores, and their associated support systems. In addition, there are more than 50 Macintoshes in the group, most of which are capable of large calculations both independently and in parallel ad hoc clusters.

The shared memory computer systems are comprised of three 64 core Itanium 2 SGI Altix machines. There are four 64-bit ×86 multi-core distributed memory clusters, each well coupled with Infiniband high speed switched interconnect or Myrinet.

Each system has on the order of 14 terabytes of disk for storage during a simulation, and at least 1 gigabyte of memory per processor core. All unclassified systems share a common disk space for home directories as well 1.4 terabytes of AFS space which can be used from any AFS-capable system throughout the allowed Internet.

The AFS capability also allows access to other storage systems including NRL's multi-resident AFS (MRAFS) system which automatically handles archiving to a multi-terabyte tape archival system.

Plasma Physics

The Plasma Physics Division is the major center for in-house Navy and DoD plasma physics research. The division conducts a broad program in laboratory and space plasma physics and related disciplines, which include high power lasers, pulsed-power sources, intense particle beams, advanced radiation sources, materials processing, and nonlinear dynamics.

The two largest of the division's lasers, Nike and Electra, are krypton fluoride (KrF) lasers operating at 0.25-micron wavelengths and are used for inertial confinement fusion (ICF) energy studies. Nike provides a single, 3-kilojoule pulse and is used primarily for ICF target physics. Electra is used to develop repetitively-pulsed KrF technology. The 1-kilojoule Pharos III glass laser is used for laboratory simulation of space plasmas and nuclear weapons effects. Two ultrashort-pulse, high-intensity lasers, the Table-Top Terawatt (T3) laser and the Ti:Sapphire Femtosecond Laser (TFL), investigate intense laser-target interactions, laser-driven accelerators, and laser propagation in air, plasmas, and water. The High Energy Laser Laboratory includes four multi-kilowatt, continuous-wave (CW) fiber lasers and investigates laser propagation in the atmosphere and incoherent beam combining for directed energy applications.

The Division also has a number of pulsed-power, microwave, and laboratory plasma facilities. The Railgun Materials Testing Facility railgun focuses on materials issues for a major Navy effort to develop a long-range, electromagnetic launcher for a future electric ship. Two large, high-voltage, pulsed-power

NRL's Materials Testing Facility railgun. The 6-m-long railgun is capable of launching 0.5-kG projectiles at 2.5 km/s using an 11 MJ capacitive energy store. This system is designed to perform experiments on bore materials under high-power launch conditions.

devices, Gamble II and Mercury, are used to produce intense electron and ion beams, flash X-ray sources, and high-density plasmas. The microwave materials processing laboratory includes a 20-kW, CW, 83-GHz gyrotron. Laboratory plasma experiments include the Space Plasma Simulation Chamber (SPSC), an 11 m^3 space chamber capable of reproducing the near-Earth space plasma environment, and the Large Area Plasma Processing System (LAPPS), designed to study modification of polymers and other sensitive materials.

Electronics Science and Technology

The Electronics Science and Technology Division conducts a multidisciplinary basic and applied research program in solid-state electronics; electronic materials including growth, theory and characterization of semiconductors and heterostructures; surface and interface science; microwave and millimeter-wave components and techniques; microelectronic device research and fabrication; nanoelectronics science and technologies; vacuum electronics; power electronics; and process modeling and simulation.

The Division operates seven major facilities: the Compound Semiconductor Processing Facility (CSPF), the Laboratory for Advanced Materials Synthesis (LAMS), the Ultrafast Laser Facility (ULF), the Epicenter, the Advanced Silicon Carbide Epitaxial Research Laboratory (ASCERL), the Space Solar Cell Characterization Facility (SSCCF), and the Millimeter-Wave Vacuum Electronics Synthesis Facility (MWVESF).

The CSPF processes compound semiconductor structures on a service basis, especially if advanced fabrication equipment such as electron beam lithography or reactive ion etching is required. But most fabrication can be hands-on by NRL scientists to assure personal process control and history. The LAMS uses metal-lorganic chemical vapor deposition to synthesize a wide range of thin films, particularly wide bandgap semiconductors such as Gallium Nitride (GaN) and related alloys. The Epicenter (a joint activity of the Electronics Science and Technology, Materials Science and Technology, Optical Sciences, and Chemistry divisions) is dedicated to the growth of multilayer nanostructures by molecular beam epitaxy (MBE). Current research involves the growth and etching of conventional III-V semiconductors, ferromagnetic semiconductor materials, 6.1Å II-V semiconductors and II-VI semiconductors. The structures grown in this facility are analyzed via in situ scanning tunneling microscopy and angle resolved electron microscopy.

The ASCERL is the focal point of NRL efforts to develop thin film heterostructure materials needed for high-voltage, high-power silicon carbide (SiC) power electronic components in future naval systems. ASCERL employs an EPIGRESS reactor capable of growing thick, low-defect, ultra high purity SiC epitaxial layers. The SSCCF studies the effects of particle irradiation on new and emerging solar cell technologies for space applications. The ULF is optimized for the characterization of photophysical and photochemical processes on a timescale of tens of femtoseconds. It includes a synchronously pumped dye laser system for simulating the effects of charge deposited in semiconductors characteristic of space radiation.

The MWVESF contains a computer numerically controlled (CNC) milling machine and a CNC precision lathe capable of fabricating intricate millimeter-wave vacuum electronic components and a wire electric discharge machining (EDM) tool for fabrication of submillimeter-wave components that can not be fabricated by conventional rotary cutting tools. EDM offers a non-contact process for both hard and soft metals as well as SiC and doped silicon.

The Electronics Science and Technology Division's Advanced Silicon Carbide Epitaxial Research Laboratory (ASCERL).

Bio/Molecular Science and Engineering

The Center for Bio/Molecular Science and Engineering conducts research and development using biotechnological approaches to support the Navy, DoD, and the nation at large. Studies involve biomaterial development for chemical/biological warfare defense, structural and functional applications, and environmental quality/cleanup. Program areas include optical biosensors, nanoscale manipulations, genomics and proteomics, bio/molecular and cellular arrays, surface modification, energy harvesting, viral particles as scaffolds, and bio-organic materials from selfassembly.

The staff of the Center is an interdisciplinary team with expertise in biochemistry, surface chemistry, biophysics, molecular and cell biology, organic synthesis, and materials science and engineering. The Center also collaborates throughout NRL, and with other government laboratories, universities, and industry.

The Center's modern facilities include laboratories for research in chemistry, biochemistry, molecular biology, and physics. Specialized areas include an electron microscope facility, a scanning probe microscope laboratory, instrument rooms with access to a variety of spectrophotometers, and an optical microscope facility including polarization, fluorescence, and confocal microscopes. Additional laboratories accommodate an NMR, a liquid chromatograph–mass spectrometer (LCMS), and equipment for biosensor programs, including a plastic micro-fabrication facility to enable fabrication of microfluidic and micro-optical systems in polymers. In 2008 the Center upgraded the X-ray diffraction system to a state-of-the-art MicroSTAR-H X-ray generator. In combination with new detectors and components, the system is ideal for data collection on proteins or very small single crystals of organic compounds and is also capable of collecting data on films and powders.

The Center's facilities have been used to demonstrate the capabilities of a microarray system developed at NRL for broad-spectrum pathogen surveillance. The system detected multiple infectious and bioterrorism agents in a demonstration involving NRL staff, Air Force medical personnel, and contractors. A smaller-scale version of the genomicsbased molecular diagnostic array was developed in the Center and is currently being validated in field trials.

Acoustics

The Acoustics Division conducts a broad research and development program in underwater acoustics, atmospheric acoustics, and physical acoustics requiring laboratory and at-sea measurements.

Laboratory Facilities: The division has three integrated structural acoustic facilities — two pools (one with a sandy bottom) and a large in-air, semi-anechoic laboratory. These facilities support research in areas including mine detection and identification, antisubmarine warfare, and detection of improvised explosive devices (IEDs). These facilities have a number of measurement capabilities including compact range scattering, nearfield holography, and scanning laser Doppler vibrometry (LDV). The major pool facility is cylindrical (17 m dia. × 15 m deep) and filled with approximately 1 million gallons of deionized water. Features include vibration and temperature control and anechoic interior walls to reduce reverberation.

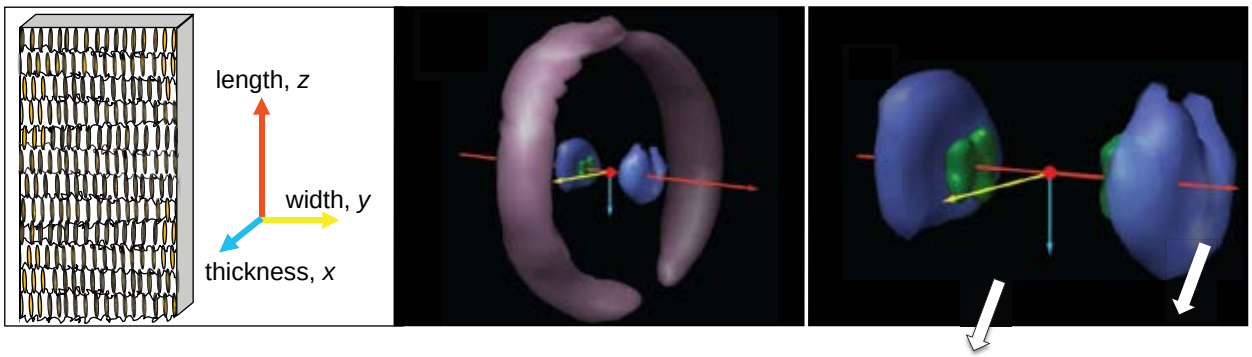

X-ray modeling of a novel liquid crystal–based elastomer (LCE) actuator. The Center for Bio/Molecular Science and Engineering facilities were used to develop this electrically driven, soft actuator, which has potential for applications ranging from soft robotics to shape-changing membranes, shown schematically in the left panel. Insight into the molecular packing and reorientation of this smectic elastomer in three different states (unstressed, under mechanical load, and in the presence of electric fields) has been obtained. A 3D diffraction pattern of an unstressed LCE, shown in the center and right panels, offers insight into the molecular packing of the material and the mechanism of actuation upon application of an applied field. Splitting of the smectic layer-related diffraction bands (white arrows) revealed two molecular domains with the elastomer, each preferentially aligned with the polarity of an applied field and associated with alignment of the permanent dipole of the liquid crystal molecules. From these data, a comprehensive model was developed in collaboration with the Laboratory for the Structure of Matter to account for both the molecular packing and reorientation. Axis colors correspond to the colors of the coordinate system in the left panel.

The Salt Water Tank Facility provides a controlled environment for studying complex ocean processes under saline conditions, especially the acoustics of bubbly media. This 6 × 6 × 3 m pool facility has large plexiglass windows on all four sides to permit imaging of processes inside the tank. Instrumentation includes acoustic sources, amplifiers, hydrophones, environmental sensors, a Digital Holographic Imaging System, high-speed digital cameras, and a LabVIEW-based data acquisition system.

The Geoacoustic Model Fabrication Laboratory enables fabrication of rough topographical surfaces in various materials (usually plastics) for acoustic scattering and propagation measurements in the tank facilities. The facility consists of a three-axis computer controlled milling machine capable of cutting with 100-μm accuracy over a 1.37 × 1.27 m region.

The SOnoMAgnetic LABoratory (SOMALAB) is used to study magnetic fields produced by acoustic motions in electrically conducting media, such as seawater. Two nested skins of HY-80 steel plate magnetically shield this facility. Inside is a 3 × 6 × 3 ft plexiglass experimental water tank on a vibration-insulating optical table equipped with three sets of mutually perpendicular Helmholtz coils to control the magnetic field. The tank is instrumented with a three-axis magnetometer, and acoustic signals are generated from an external transducer.

The division also operates laboratories to study the structural dynamics and performance of high-Q oscillators and other micro-mechanical and nano-mechanical systems. A super-resolution nearfield scanning optical microscope (NSOM) permits spatial mapping of the complex vibratory motion at resolutions of 100 nm. These laboratories can also measure the mechanical and electrical properties of micro-oscillators, and thin films applied to them.

At-Sea Research: The division operates several systems to generate and receive sound in at-sea experiments. Sound sources include two XF-4 units, one ITC 2077 source with tow body, two battery-operated organ-pipes that can project single tones from off-board moorings, and a towable, vertically directional source array consisting of 10 individually controllable elements at frequencies of 1.5 to 9.5 kHz. In addition, the division has several battery-operated, rubidium-clock controlled, programmable sound source moorings that can transmit sounds with arbitrary waveforms. The division has a 64-channel broadband source-receiver array with time reversal mirror functionality operating over 500–3500 Hz. The division operates high frequency (up to 600 kHz) measurement systems to obtain scattering, target strength and propagation data using bottom moored instrumentation towers and a remotely operated vehicle.

The division performs research to relate acoustic array gain variability to fluid dynamic variability and bottom heterogeneity in the littorals. Measurements are made with an autonomous acoustic data acquisition suite. Three independent autonomous 32-channel vertical arrays receive and store 24-bit data at 4 kHz for 22 days. Two autonomous sources operate at center frequencies of 300 and 500 Hz and generate programmable waveforms at 50% duty cycle for 22 days. The division also has unique, self-recording digital acquisition buoy systems (DABS) used to obtain multichannel

A 21-inch-diameter AUV is used for detection and classification in mine hunting and anti-submarine warfare applications.

(up to 128) acoustic data from 10 Hz to 5 kHz. These systems provide up to 250 Gbytes of data storage.

Narrow beam 200 and 350 kHz acoustic backscattering (flow visualization) systems are used to study fine structure, internal wave and larger-scale fluid dynamic perturbation of the density and sound speed field in the ocean. A 25 kW radar system is used in conjunction with the flow visualization system to record the surface expression of internal waves.

The division conducts research addressing the channel capacity of multi-node underwater acoustic communications networks. Two 8-channel acoustic communications data acquisition systems or modems, which can be moored or towed and remotely controlled, provide measurements in the 2–5 kHz, 6–14 kHz, and 10–14 kHz frequency bands.

NRL is developing and deploying AUV- and rail-based systems for acquiring signature data at sea. The rail-based system has a 100-meter horizontal robotic scanner used to collect synthetic aperture (SA) scattering data from proud and buried targets. The receiver system is used in conjunction with impulsive broadband projectors mounted on the scanner. The AUV-based system uses acoustic SA techniques to recover high-fidelity, quantitative broadband data over a large range of target aspect angles.

Remote Sensing

The Remote Sensing Division is the Navy's center of excellence for remote sensing research and development, conducting a broad program of basic and applied research across the full electromagnetic spectrum using active and passive techniques from ground-, air-, and space-based platforms. The Division includes both remote sensing technology and phenomenological expertise within the same organization. Current applications include earth, ocean, atmospheric, astronomy, astrometry, and astrophysical science, and surveillance/reconnaissance activities including maritime domain awareness, anti-submarine warfare, and mine warfare. Special emphasis is given to developing space-based platforms and exploiting existing space systems.

Research in ocean and earth science includes maritime hyperspectral imaging, radar measurements of the ocean surface for the remote sensing of waves and currents, model and laboratory-based hydrodynamics, and land-based trafficability studies.

The Remote Sensing Division conducts airborne hyperspectral data collections for characterization of the littoral environment. Current sensors include two visible/near IR systems: the airborne Portable Hyperspectral Imager for Low-Light Spectroscopy (PHILLS) system (built in house from COTS parts), and the commercial Compact Airborne Spectrographic Imager (CASI-1500) hyperspectral imager. Both sensors are specifically designed for use over maritime areas. The Division also has a long- and mid-wave IR thermal camera and an airborne short-wave IR hysperspectral instrument.

Proper interpretation of the hyperspectral data requires both radiometric and spectral calibration of the sensor. The Remote Sensing Division operates an Optical Calibration Facility that includes a NIST-traceable integrating sphere and a set of gas emission standards for wavelength calibration.

To validate the results of airborne hyperspectral sensing, and to support interpretation of the physical processes they reveal, the Division has developed a Profiling Optics Package. This system measures the inherent optical properties of water (absorption, attenuation, and scattering), and collects water samples for various laboratory measurements.

The Division is beginning a two-phase, rapid-development program for maritime hyperspectral imaging from space. The first phase, now under way, is to develop a PHILLS airborne imager for use in space. This sensor, Hyperspectral Imager for the Coastal Ocean (HICO), is manifested for a September 2009 launch aboard the International Space Station. The second phase will be to build and launch the fully space-qualified Coastal Ocean Imaging Spectrometer (COIS) with significantly improved performance and operational capability.

The NRL Focused Phased Array Imaging Radar (NRL FOPAIR) is an X-band, polarimetric radar capable of producing time-sequences of radar images at a per-polarization frame rate approaching 400 fps. The system was designed for basic research into the relationship between ocean surface waves and the radar backscatter that they create.

The NRL Interferometric Synthetic Aperture Radar (NRL INSAR) is an X-band, 2-channel system designed for operation on a light aircraft. To date, the system has been operated in both polarimetric and along-track interferometric modes in support of basic and applied Navy research projects.

To support the ocean remote sensing research program, the Division has developed the Free-Surface Hydrodynamics Laboratory (FSHL), which consists of a 10 m wave tank equipped with a high-precision, computer-controlled wave generator capable of generating breaking waves 0.2 to 1.2 m in length. Diagnostic tools include an IR thermal camera, a Langmuir film balance to measure the properties of surface films, hot-wire and laser-Doppler anemometry, and the new quantitative flow techniques of laser speckle, particle tracking, and particle image velocimetry. The Division also conducts a wide range of numerical and analytical research dealing with the physics of the ocean's

free surface. Lab experiments conducted in the FSHL are used to test and validate the numerical results and analytical theories. Both the modeling and lab-based research are used to aid in the interpretation of remote sensing field measurements.

Current atmospheric science research areas include the remote sensing of aerosols (and supporting modeling studies), measurement of ocean surface winds, and middle atmospheric research.

The Remote Sensing Division has developed a unique eye-safe volume-imaging lidar system to remotely characterize aerosol backscatter variations in coastal boundary layers, and to map those variations over hundreds of meters. Unlike Doppler lidar systems that can measure only radial wind speeds, the NRL lidar uses correlation methods and measures the wind vector (speed and direction) and turbulence.

WindSat, developed and built by NRL and launched in January 2003 and still operational, is the first spaceborne polarimetric microwave radiometer. Its primary mission is to demonstrate the capability to remotely sense the ocean surface wind vector with a passive system. WindSat, the primary payload on the DoD Space Test Program Coriolis mission, provides major risk reduction for development of the microwave imager for the NPOESS next-generation weather satellite system. Although WindSat wind vector retrieval algorithm development is still an important R&D effort in the Remote Sensing Division, WindSat wind vectors are processed in real time at the Navy Fleet Numerical Meteorology and Oceanography Center (FNMOC), and operationally assimilated into the Navy global weather model, NOGAPS. In addition, the Remote Sensing Division is exploiting WindSat's unique data set to develop retrievals for other environmental parameters such as sea surface temperature, soil moisture, and sea ice concentration.

The Airborne Polarimetric Microwave Imaging Radiometer (APMIR) is a multichannel microwave radiometer system designed and built by the Remote Sensing Division. APMIR was built primarily to provide extensive airborne calibration and validation of spaceborne remote sensing assets: the NRL WindSat mission, the Defense Meteorology Space Program Special Sensor Microwave Imager/Sounder (SSMIS) mission, and the future Microwave Imager Sounder (MIS) instruments to fly on the converged NPOESS mission.

The NRL Polar Ozone and Aerosol Measurement (POAM II and III) missions operated from 1998 through 2005. POAM measured ozone and other important constituents of the polar stratosphere using the uv/visible solar occultation technique. POAM provided the first space-based ozone profile measurements in the Antarctic ozone hole, and was a very important part of the national ozone monitoring effort. To date, more than 60 scientific paper have been published on POAM data, and analysis is ongoing.

The Water Vapor Millimeter-wave Spectrometer (WVMS) is a ground-based instrument designed to measure water vapor in the middle atmosphere using ground-based mm-wave spectroscopy. Primarily under NASA sponsorship, the instrument has been transitioned to operations as part of the ground-based Network for Detection of Atmospheric Change (NDAC). Three instruments have been built and are now operational in the field: Lauder, NZ, Mauna Loa, HI, and Table Mountain, CA.

The Remote Sensing Division has several active research programs in astronomy and astrophysics ranging, in wavelength, from the optical to long-wave radio.

The Navy Prototype Optical Interferometer (NPOI) is an optical interferometer located on Anderson Mesa near Flagstaff, AZ, that is used for optical astrometry, to investigate unfilled aperture imaging technologies, and to conduct astrophysical research. It is a joint project between the U.S. Naval Observatory and the NRL Remote Sensing Division. The instrument has a six-input beam combiner. Current maximum baseline is 80 m, and when completed, the maximum baseline will be 250 m, making it the highest resolution ground-based optical telescope in the world.

The Remote Sensing Division also has a strong program in radio astronomy, with emphasis on low-frequency (< 100 MHz) observations. The Division has developed and installed 74-MHz receivers on the National Radio Astronomy Observatory's (NRAO) Very Large Array (VLA), thereby producing the world's highest-angular-resolution and most sensitive astronomical interferometric array operating below 150 MHz. The VLA's maximum baseline is 35 km; all previous astronomical interferometers operating below 150 MHz had baselines of less than 5 km because of the decorrelation effects of ionospheric structure, and consequent corruption of interferometric imaging, at larger baselines. However, work in the Remote Sensing Division has shown that radio astronomical techniques can now remove the ionospheric phase variations, at least at VLA baselines. As a result, the low-frequency VLA system has become an important science instrument not only for NRL, but for the entire radio astronomy community. The success of the NRL/NRAO 74-MHz system indicates that it is possible to open a new, high-resolution, high-sensitivity astronomical window by going to even larger, more sensitive systems. The NRL Long Wavelength Demonstrator Array (LWDA), a 16-element phased array deployed as a technology and scientific testbed station and pathfinder for the next-generation low-frequency RF phased array imaging systems, is in operation near Socorro, New Mexico.

Oceanography

The Oceanography Division is the major center for in-house Navy research and development in oceanography. It is known nationally and internationally for its unique combination of theoretical, numerical, experimental, and remotely sensed approaches to oceanographic problems. The division's modeling focus is on a truly integrated global-to-coastal modeling strategy, from deep water up to the coast including straits, harbors, bays, and inlets. This requires emphasis on both ocean circulation and wave/surf prediction, with additional emphasis on coupling the ocean models to biological, optical, and sediment models. This modeling is conducted on the Navy's and DoD's most powerful vector and parallel processing machines. The division has an in-house Ocean Dynamics and Prediction Computational Network Facility that provides computer services to scientists for program development, graphics, data processing, storage, and backup. To study the results of this intense modeling effort, the division operates a number of highly sophisticated graphic systems to visualize ocean and coastal dynamic processes.

The seagoing experimental programs of the division range worldwide. Unique measurement systems include a wave measurement system to acquire in situ spatial properties of water waves; a salinity mapper that acquires images of spatial and temporal sea surface salinity variabilities in littoral regions; an integrated absorption cavity, optical profiler system, and towed optical hyperspectral array for studying ocean optical characteristics; self-contained bottom-mounted upward-looking acoustic Doppler current profilers (ADCPs) for measuring ocean variability; and an in situ volume scattering function measurement system to support remote sensing and in-water optical programs. NRL is working jointly with the NATO Undersea Research Center (NURC) for development and deployment of the SEPTR instrument, a trawl-resistant, bottom-mounted ADCP system that includes a pop-up profiling float for real-time observation and reporting.

The Oceanography Division has acquired new capabilities for sensing the littoral environment. These include a Vertical Microstructure Profiler (VMP), a Scanfish, and four Slocum Gliders. The turbulent dissipation rate can be quickly obtained with very high accuracy from measurements collected by the VMP. The Scanfish allows efficient and rapid three-dimensional mapping of mesoscale oceanic features. The Gliders rely on a low-powered battery-induced change of buoyancy to glide autonomously through the coastal ocean collecting both physical and optical data that are uplinked to satellite and then relayed to the laboratory or ship in near real time.

In the laboratory, the division operates an environmental scanning electron microscope for detailed studies of biocorrosion in naval materials. The division's remote sensing capabilities include the ability to analyze and process multi/hyperspectral, infrared, syn-

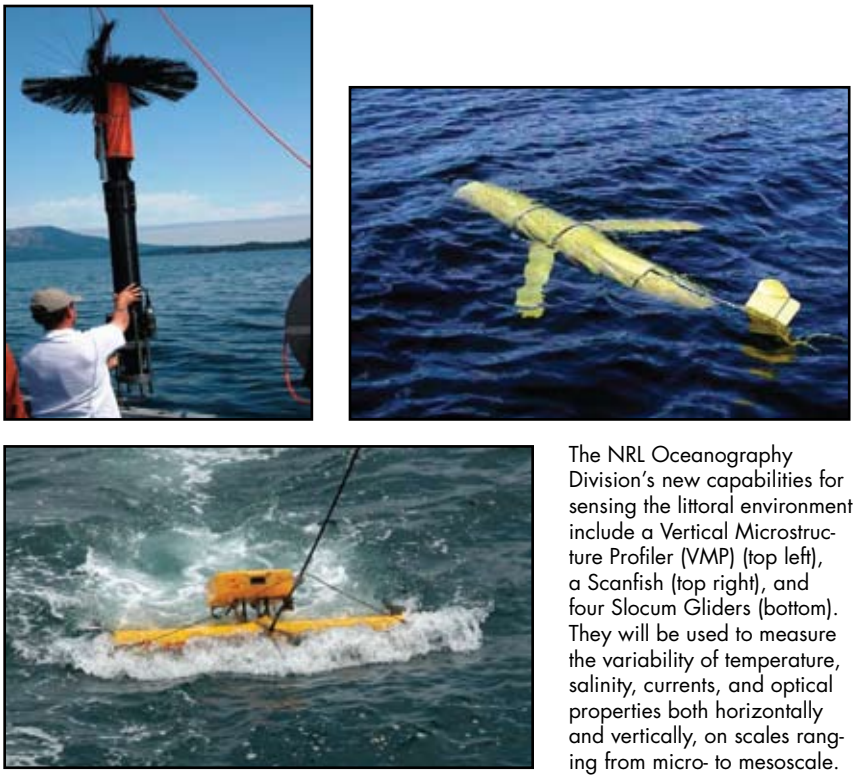

The NRL Oceanography Division's new capabilities for sensing the littoral environment include a Vertical Microstructure Profiler (VMP) (top left), a Scanfish (top right), and four Slocum Gliders (bottom). They will be used to measure the variability of temperature, salinity, currents, and optical properties both horizontally and vertically, on scales ranging from micro- to mesoscale.

thetic aperture radar, and other satellite data sources. The Ocean Optics section has added the capability to download Moderate Resolution Imaging Spectroradiometer (MODIS) data directly using the new X-band receiving system. The division is a national leader in the development and analysis of MODIS ocean color data for oceanographic processes and naval applications in littoral areas.

Marine Geosciences

The Marine Geosciences Division is the major Navy in-house center for research and development in marine geology, geophysics, geodesy, geoacoustics, geotechnology, and geospatial information and systems.

Instrumentation used in the field is deployable from aircraft, ships, submarines, remotely operated and unmanned vehicles, undersea platforms, and by divers. Instrumentation includes an integrated airborne geophysical sensor suite with gravity, magnetic, and sea/ice/land topographic profiling sensors, all based on cm-level KGPS aircraft positioning. Seafloor and subseafloor research uses the Deep-Towed Acoustics/Geophysics System (220 to 1000 Hz); a chirp sub-bottom profiler; high-resolution sidescan sonars (100 and 500 kHz); the Acoustic Seafloor Characterization System (15, 30, and 50 kHz); the In Situ Sediment Acoustic Measurement System, measuring compressional and shear wave velocities and attenuation; a heat flow probe system; and underwater stereo photography and nearshore video imaging systems. Five instrumented, 8-ft-long, 2220-lb, mine-like cylinders are used to gather impact burial data (one system) and scour and sand wave burial data (four systems) for testing and validation of mine burial prediction models.

Laboratory facilities allow measurement of sediment physical, geochemical, and geotechnical properties. Equipment includes a photon correlation spectrometer and a laser Doppler velocimeter to measure size and electrostatic properties of submicrometer-size sediment particles. The Transmission Electron Microscopy Facility includes a 300 kVa transmission electron microscope with environmental cell enabling real-time observations of hydrated and gaseous experiments for research in microscale biological, chemical, and geological processes. A high-resolution industrial computed-tomography scanner provides capability for investigating volumetric heterogeneity of sediments.

The Moving Map Composer Facility is used to design and write mission-specific map coverages for F/A-18 and AV-8B tactical aircraft onto militarized optical disks. The Geospatial Information Data Base capability provides Internet access to the Digital Nautical Chart data, mapping data, imagery, and other data types such as video and pictures used for planning, training, and operations.

Marine Meteorology

The Marine Meteorology Division's research facilities support basic research as well as the development of systems and products for operational applications. The Mobile Atmospheric Aerosol and Radiation Characterization Observatory (MAARCO) is a set of climate-controlled containers with integrated suites of meteorological, aerosol, gas, and radiation instruments that can be rapidly deployed to operate in strategic areas around the globe, including remote regions, overseas locales, and onboard ships at sea. The instruments can also be removed and mounted on aircraft for added flexibility in field data collection, and are used to investigate boundary layer meteorology, aerosol microphysics, and electro-optical propagation.

A state-of-the-art Satellite Data Processing Laboratory allows direct downlink of real-time NOAA geostationary data and data relays from three other geostationary satellites. Data from numerous polar orbiting platforms is also received in near-real-time; some data is received directly and some is provided through various inter-agency agreements. In total,

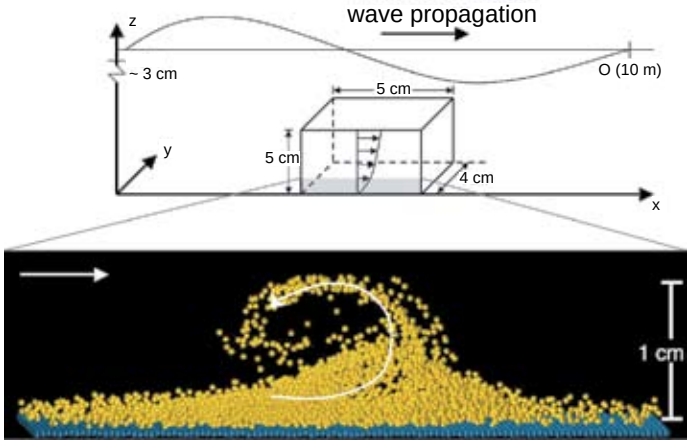

In the Marine Geosciences Division, a detailed two-phase flow model for the wave bottom boundary layer is being developed to study fluid-sediment turbulent interactions at the seafloor. The upper image is a schematic of a horizontally periodic domain under a progressive gravity wave. The lower image is a snapshot of particles simulated using the discrete element method that are coupled to a three-dimensional direct numerical simulation of the turbulent fluid flow. Here the particles (yellow) are near neutrally buoyant (S = 1.03), and are interacting with the fluid, with each other, and with the rough bottom (blue). The image is taken right after the fourth flow reversal of a sinusoidal wave and the formation of a turbulent eddy about 1 cm in diameter is evident.

NRL's Marine Meteorology Division has a direct downlink capability for real-time geostationary data from NOAA's GOES-E and GOES-W satellites.

NRL Monterey processes satellite data from 33 low-earth orbit sensors and 5 geostationary platforms and uses that data to conduct research and development of multisensory data fusion products to support a variety of DoD operations. These activities range from monitoring and analyzing tropical cyclone characteristics to providing enhanced imagery in support of combat operations in Southwest Asia.

The Division's Atmospheric Prediction System Development Laboratory is built around two LINUX clusters (with 176 and 44 processors), supported by a 200 TB RAID storage system and a 1000 TB tape library, as well as several smaller LINUX clusters, including a 22-processor cluster with SIPRNET connectivity. These systems enable the division to efficiently develop, improve, and transition numerical weather analysis and prediction systems and coupled air/ocean systems to operational use, producing guidance which is used by Fleet forces around the globe. These systems also support basic research in atmospheric processes such as air-sea interaction, atmospheric dynamics, and cloud/aerosol physics.

Space Science

The Space Science Division conducts a broad-spectrum RDT&E program in solar-terrestrial physics, astrophysics, upper/middle atmospheric science, and astronomy. Division researchers conceive, plan, and execute scientific research and development programs on instruments to be flown on satellites, sounding rockets and balloons, ground-based facilities and mathematical models, and transition the results to operational use. Division major research thrusts include remote sensing of the upper and middle atmospheres, studies of solar activity and effects on the Earth's ionosphere, and studies of high-energy natural radiation and particles for applications ranging from astrophysics through force protection.

The division's Vacuum Ultraviolet Solar Instrument Test (SIT) facility is an ultra-clean solar instrument test facility designed to satisfy the rigorous contamination requirements of state-of-the-art solar spaceflight instruments. The facility has a 400 ft2 Class 10 clean room and a large Solar Coronagraph Optical Test Chamber (SCOTCH). The SIT clean room is ideally suited for assembly and test of contamination-sensitive space-flight instrumentation. It contains a large vibration-isolated optical bench and a 1-ton capacity overhead crane. The SCOTCH consists of a large vacuum tank and a precision instrument-pointing table. The division also maintains extensive facilities for supporting ultraviolet (UV) spectroscopy sounding rocket programs. These facilities include a dedicated Class 1000 instrument clean room, and a gray room area for assembling and testing the rocket payloads that incorporates all of the fixtures required for safe handling of payloads. The division rocket facilities also include a large UV optical test chamber that is additionally equipped with a large vibration- and

The VERIS payload is being loaded for testing into the Space Science Division solar rocket laboratory UV optical test chamber.

thermal- isolated optical bench for telescope testing, which allows the laboratory area to be turned into a reasonable quality Schlieren facility.

The division has a wide range of new rocket, space, and ground-based instruments under development, including HERSCHEL (HElium Resonant Scattering in the Corona and HELiosphere), a sounding rocket scheduled for launch in early 2009; VERIS (VEry high angular Resolution Imaging Spectrometer), a sounding rocket scheduled for launch in late 2009; CPEX (Coronal Physics Explorer) a NASA Small Explorer Mission currently in Phase A with an anticipated follow-on selection in mid-2009; and the NRL-led Department of Homeland Security MISTI (Mobile Imaging and Spectroscopic Threat Identification) to demonstrate standoff detection of radiation/nuclear weapons of mass destruction in urban environments, for FY09 delivery.

Division scientists, using the division network of computers and workstations and other connected high performance computing assets, develop and maintain physical models in support of their research, among them: NOGAPS-ALPHA, the Advanced Level Physics High Altitude middle atmosphere extension of the Navy Operational Global Atmospheric Prediction System; and GAIM (Global Assimilation of Ionospheric Measurements), a physics based assimilative model of the ionosphere now operational at the Air Force Weather Agency.

Space Technology

In its role as a center of excellence for space systems research, the Naval Center for Space Technology (NCST) designs, builds, analyzes, tests, and operates spacecraft and identifies and conducts promising research to improve spacecraft and their support systems. NCST facilities that support this work include large and small anechoic radio frequency chambers, clean rooms, shock and vibration facilities, an acoustic reverberation chamber, large and small thermal/vacuum test chambers, a heat pipe integration and test facility, a spacecraft robotics engineering and control system interaction laboratory, satellite command and control ground stations, a fuels test facility, and modal analysis test facilities. Also, the Center maintains and operates a number of electrical and electronic development laboratories and fabrication facilities for space and airborne payloads, radio frequency equipment, spacecraft power systems, telemetry, and command and control systems, and includes an electromagnetic interference–electromagnetic compatibility test chamber. NCST has a facility for long-term testing of satellite clock time/frequency standards under thermal/vacuum conditions linked to the Naval Observatory; a 5-m optical bench laser laboratory; and an electro-optical communication research laboratory to conduct research in support of the development of space systems.

RESEARCH SUPPORT FACILITIES

Technology Transfer Office

The NRL Technology Transfer Office (TTO) is responsible for NRL's implementation of the Federal Technology Transfer Act. It facilitates the transfer of NRL's innovative technologies for public benefit by marketing NRL technologies, and by negotiating patent license agreements and Cooperative Research and Development Agreements (CRADAs).

TTO markets NRL technologies through its website, by the preparation of Fact Sheets to be distributed at trade shows and scientific conferences, and through DOD contracted Partnership Intermediaries such as TechLink.

A license grants a company the right to make, use, and sell NRL technologies commercially in exchange for equitable licensing fees and royalties. Revenue is distributed among the inventors and NRL's general fund. Prior to granting a license, TTO reviews the commercialization plan submitted by the licensee in support of its application for license. The plan must provide information on the licensee's capabilities, proposed development expenditures, milestones, a time line to commercialization, and an assessment of the intended market.

A license may be exclusive, partially exclusive (exclusive for a particular field of use or geographic area), or non-exclusive. Once a license is executed, TTO monitors the licensee for timely payments and for its diligence in commercializing the licensed invention.

TTO also negotiates Government Purpose Licenses to transition NRL technologies for manufacture and sale solely for Navy and other U.S. Government purposes.

CRADAs provide a vehicle for NRL scientists and engineers to collaborate with their counterparts in industry, academia, and state and local governments. Under a CRADA, a company may provide funding for collaborative work between it and NRL and is granted an exclusive option to license technologies developed under that CRADA's Statement of Work (SOW). TTO works with the NRL scientist to develop a SOW that has sufficient detail to define the scope of the CRADA partner's rights.

Technical Information Services

The Technical Information Services (TIS) Branch combines publication, graphics, photographic, multimedia, exhibit, and video services into an integrated

organization. Publication services include writing, editing, composition, publications consultation and production, and printing management. Quick turnaround digital black-and-white and color copying/printing services are provided. TIS uses digital publishing technology to produce scientific and technical reports that can be used for either print or Web. Graphics support includes technical and scientific illustrations, computer graphics, design services, photographic composites, display posters, and framing. The HP Designjet 5500ps wide format printer offers exceptional color print quality up to 600 dpi and produces indoor posters and signs with 56 inches being the limitation on one side. Lamination and mounting are available. Photographic services include digital still camera coverage for data documentation, both at NRL and in the field. Photographic images are captured with state-of-the-art digital cameras and can be output to a variety of archival media. Photofinishing services provide custom printing and quick service color prints from digital files. Video services include producing video reports and presentations of scientific and technical programs. TIS digital video editing equipment allows in-studio and on-location editing. The video production, "A Tour of NRL," won four international awards: the Crystal, the Gold Aurora, and two Bronze Tellys. The head of the Exhibits Program works with NRL's scientists and engineers to develop exhibits that best represent a broad spectrum of NRL's technologies, and promotes these technologies to scientific and nonscientific communities throughout the United States.

Administrative Services

The Administrative Services Branch is responsible for collecting and preserving the documents that comprise NRL's corporate memory. Archival documents include personal papers and correspondence, laboratory notebooks, and work project files — documents that are appraised for their historical or informational value and considered to be permanently valuable. The Branch provides records management services, training, and support for the maintenance of active records, including electronic records, as an important information resource. The Branch is responsible for processing NRL's incoming and outgoing correspondence and provides training and support on correct correspondence formats and practices. The Branch is responsible for NRL's Forms and Reports Management Programs (including designing electronic forms and maintaining a Web site for Lab-wide use of electronic forms), compiles and publishes the NRL Code Directory and Organizational Index, and is responsible for providing NRL postal mail services for first class and accountable mail and for mail pickup and delivery throughout NRL. The Branch also provides NRL Locator Service.

Employees of the Administrative Services Branch working in the mail room.

Ruth H. Hooker Research Library

NRL's Ruth H. Hooker Research Library continues to support NRL and ONR scientists in conducting their research by making a comprehensive collection of the most relevant scholarly information available and useable; by providing direct reference and research support; by capturing and organizing the NRL research portfolio; and by creating, customizing, and deploying a state-of-the-art digital library.

Traditional library resources include extensive technical report, book, and journal collections dating back to the 1800s housed within a centrally located research facility that is staffed by subject specialists and information professionals. The collections include 44,000 books; 80,000 bound historical journal volumes; 3,500 current journal subscriptions; and nearly 2 million technical reports in paper, microfiche, or digital format (classified and unclassified). Research Library staff members provide advanced information consulting; literature searches against all major online databases including classified databases; circulation of materials from the collection including classified literature up to the SECRET level; and retrieval of articles, reports, proceedings, or documents from almost any source around the world. Staff members provide scheduled and on-demand training to help researchers improve productivity through effective use of the library's resources and services.

The Research Library staff has developed and is continuing to expand the NRL Digital Library. The Digital Library currently provides desktop access to thousands of journals, books, and reference sources to NRL-DC; NRL-Stennis; NRL-Monterey; and the Office of Naval Research.

Library systems provide immediate access to scholarly information, including current issues of journals and conference proceedings that are fully searchable at the researcher's desktop (nearly 3,500 titles). Extensive

journal archives from all the major scientific publishers and scholarly societies are now available online. The breadth and depth of content available through TORPEDO Ultra, NRL's locally-loaded digital repository, continues to grow and provides a single point of access to scholarly information by providing full text search against journals, books, conference proceedings and technical reports from 20 publishers (11.1million items by the close of 2008). The NRL Online Bibliography, a Web-based publications information system, is ensuring that the entire research portfolio of written knowledge from all NRL scientists and engineers since the 1920s will be captured, retained, measured, and shared with current and future generations.

FIELD STATIONS

NRL has acquired or made arrangements over the years to use a number of major sites and facilities for research. The largest facility is located at the Stennis Space Center (NRL-SSC) in Bay St. Louis, Mississippi. Others include a facility at the Naval Postgraduate School in Monterey, California (NRL-MRY), and the Chesapeake Bay Detachment (CBD) and Scientific Development Squadron One (VXS-1) in Maryland. Additional sites are located in Virginia, Alabama, and Florida.

Stennis Space Center (NRL-SSC)

The NRL Detachment at Stennis Space Center, Mississippi (NRL-SSC), consists of NRL's Oceanography Division and portions of the Acoustics and Marine Geosciences divisions. NRL-SSC, a tenant activity at NASA's John C. Stennis Space Center (SSC), is located in the southwest corner of Mississippi, about 50 miles northeast of New Orleans, Louisiana, and 20 miles from the Mississippi Gulf Coast. Other Navy tenants at SSC include the Naval Meteorology and Oceanography Command, the Naval Oceanographic Office, the Navy Small Craft Instruction and Training Center, the Special Boat Team-Twenty-two, and the Human Resources Service Center Southeast. Other Federal and State agencies at SSC involved in marine-related science and technology are the National Coastal Data Development Center, the National Data Buoy Center, the U.S. Geological Survey, the Environmental Protection Agency's Gulf of Mexico Program and Environmental Chemistry Laboratory, the Center for Higher Learning, University of Southern Mississippi, and Mississippi State University.

The Naval Meteorology and Oceanography Command and the Naval Oceanographic Office are major operational users of the oceanographic, acoustic, and geosciences technology developed by NRL researchers. The Naval Oceanographic Office operates the Major Shared Resource Center (MSRC), one of the nation's High Performance Computing Centers, which provides operational support to the warfighter and access to NRL for ocean and atmospheric science and technology.

The Acoustics, Marine Geosciences, and Oceanography divisions occupy more than 175,000 ft^2 of research, computation, laboratory, administrative, and warehouse space. Facilities include the sediment core laboratory, transmission electron microscope, moving-map composer facility, underwater navigation control laboratory, computed tomography scanning laboratory, visualization laboratory, ocean color data receipt and processing facility, environmental microscopy facility, maintenance and calibration systems, environmental modeling and simulation high-speed network, and numerous laboratories for acoustic, geosciences, and oceanographic computation, instrumentation, analysis, and testing. Special areas are available for constructing, staging, refurbishing, and storing seagoing equipment.

Monterey (NRL-MRY)

NRL's Marine Meteorology Division (NRL-MRY) is located in Monterey, California, on a 5-acre campus about 1 mile from the Naval Postgraduate School (NPS) campus. This group has occupied this site since the early 1970s, when the U.S. Navy decided to collocate the meteorological research facility with the operational center, now known as Fleet Numerical Meteorology and Oceanography Center (FNMOC). FNMOC was stood up in Monterey around 1960 to be able to share resources and expertise with NPS. This collocation of research, education, and operations continues to be a winning formula, as FNMOC remains the primary customer for the numerical weather prediction and satellite product systems developed by NRL-MRY. NRL scientists have direct access to FNMOC's large classified supercomputers, allowing advanced development to take place using the real-time on-site global atmospheric and oceanographic databases, set in the same computational environment as operations. Such access offers unique advantages for successfully implementing new systems and system upgrades, and allows for rapid integration of new research results into the operational systems. Proximity to NPS also offers unique opportunities for collaborative research, as well as educational and teaching/mentoring opportunities for NRL staff.

Today, the NRL/FNMOC compound is comprised of four primary buildings — one dedicated to FNMOC supercomputer operations; two large shared buildings dedicated to NRL-MRY and FNMOC office spaces, computer laboratories, and conference facilities; and a fourth building now occupied by NOAA's local National Weather Service Forecast Office, which

offers additional opportunities for interagency collaboration and data sharing. In addition to the main buildings, NRL-MRY also occupies two modular office buildings and a warehouse on the campus. Altogether, NRL-MRY occupies approximately 1500 ft^2 of storage space and 26,500 ft^2 of office/laboratory/conference space, which includes a research library, a computer center that supports the Atmospheric Prediction System Development Laboratory and the Satellite Data Processing Laboratory, and a small classified processing facility.

Chesapeake Bay Detachment (CBD)

NRL's Chesapeake Bay Detachment (CBD) occupies a 168-acre site at Randle Cliffs, Maryland, and provides facilities and support services for research in radar, electronic warfare, optical devices, materials, communications, and fire research. A ship-motion simulator (SMS) is used to test and evaluate radar, satellite communications, and line-of-sight RF communications systems under dynamic conditions (various sea states). The SMS can handle up to 12,000 lb of electronic systems. A roll motion of up to 30° (15° to port and 15° to starboard) can be applied to this axis. The pitch axis has a fixed motion of 10° (5° to stern and 5° to bow). Periods along both axes, pitch and roll, are variable—from a slow 32-s to a brisk 4-s rate. Variable azimuth motion can also be added to the pitch and roll action. Synchronized positioning information (×1 and ×36) is available for each of the three axes of the SMS.

Because of its location high above the western shore of the Chesapeake Bay, unique experiments can be performed in conjunction with the Tilghman Island site, 16 km across the bay from CBD. Some of these experiments include low-clutter and generally low-background radar measurements. By using CBD's support vessels, experiments are performed that involve dispensing chaff over water and characterizing aircraft and ship radar targets. Basic research is also conducted in radar antenna properties, testing of radar remote sensing concepts, use of radar to sense ocean waves, and laser propagation. CBD also hosts facilities of the Navy Technology Center for Safety and Survivability, which conducts fire research on simulated carrier, surface, and submarine platforms.

Scientific Development Squadron One (VXS-1)

Scientific Development Squadron ONE located at Naval Air Station, Patuxent River, Maryland, is manned by approximately 14 officers, 80 enlisted, and 9 civilians. VXS-1 is currently responsible for the maintenance, operations, and security of three uniquely configured NP-3D Orion aircraft and two RC-12 Beech King Air research aircraft. The squadron conducts numerous worldwide detachments in support of a wide range of scientific research projects.

In FY08, VXS-1 provided flight support for several diverse research programs: Operation Rampant Lion II consisted of exploration, reconstruction, counter-narcotics, and security efforts in Afghanistan, and provided airborne support to an emerging riverine mission set in Iraq; THORPEX Pacific-Asian Regional Campaign (T-PARC) was a multinational endeavor collecting data directly from one tropical storm and three typhoons to increase the predictability of tropical cyclones in the Western Pacific region; Operation Rampant Lion III was a presidential priority mission in support of ongoing MIA recovery efforts, including data collection in the search to find the remains of CAPT Speicher lost in 1991 and a crew lost in a 1942 search and recovery effort; and Missile Defense Agency (MDA) testing and experimentation vital to the success of global defense efforts included multinational land- and surface-based missile tracking and interceptor tests. VXS-1 surpassed 46 years and over 68,000 hours of Class "A" mishap-free operations in FY08.

Midway Research Center

The Midway Research Center (MRC) is located on a 162-acre site in Stafford County, Virginia. Located adjacent to the Quantico Marine Corps' Combat Development Command, the MRC has 16,000 ft^2 of operations and administration area. Instruments include three precision 18.5-m-diameter parabolic antennas housed in 100-ft radomes, a fast-tracking 1-m telescope currently used for satellite laser ranging, and a transportable 16-inch telescope capable of passive optical tracking and laser communications. The MRC, under the auspices of the Space Systems Development Department, provides NRL with state-of-the-art facilities dedicated solely to space-related applications in naval communications, navigation, and basic research.

Research Platforms

Mobile research platforms contribute greatly to NRL's research. These include six P-3 Orion turboprop aircraft and one ship, the ex–USS *Shadwell* (LSD 15), berthed in Mobile Bay, Alabama. The ex–USS *Shadwell* is used for research on aboard-ship fire suppression techniques.

Marine Corrosion Facility

The Chemistry Division's Marine Corrosion Facility, described above in the Chemistry section, is located in Key West, Florida.

THE CORPORATE FACILITIES INVESTMENT PLAN (CFIP)

To conduct preeminent research for tomorrow's Navy, NRL must maintain and upgrade its scientific and technological equipment and provide modern research facilities. The physical plant to house this equipment must also be state of the art. NRL has embarked on a Corporate Facilities Investment Plan (CFIP) to accomplish these goals.

The CFIP is a capital investment plan that uses both Congressionally approved military construction (MILCON) funds and Laboratory overhead funds to provide modern, up-to-date laboratory facilities for NRL. Planning for future MILCON projects includes an Autonomous Systems Research Lab in the FY09 time frame, a Space Systems Technology Lab (FY11), an Electronics Research Lab (FY12), and the Marine Meteorology Center (FY12).

To complement these efforts, overhead funds are being used to renovate and upgrade laboratory and support areas in several existing buildings.

featured research

59
Pointman
A Novel User Interface Controller for Dismounted Infantry Training
J.N. Templeman, L.E. Sibert, R.C. Page, and P.S. Denbrook

67
HiEx Foam
High Expansion Foam for Protecting Large Volume Mission Critical Shipboard Spaces
J.P. Farley and F.W. Williams

75
Using Our Heads to Save those of the Warfighters
Sensor Systems for Measuring Helmet-Head-Brain Response to Blast
K.E. Simmonds, A. Bagchi, A.C. Leung, W.R. Pogue III, P. Matic, J.M. Byers, G.K. Hubler, D.R. Mott, D.A. Schwer, R.D. Corsaro, and B.H. Houston

87
CMG: Expanding Graphene Through Chemistry
Chemically Modified Graphene for Sensing and Nanomechanical Applications
J.T. Robinson, F.K. Perkins, E. Snow, M. Zalalutidinov, B.H. Houston, J.W. Baldwin, Z. Wei, and P.E. Sheehan

97
Causality Bubbles to the Surface
Investigating Acoustic Causality in Highly Dispersive Bubbly Liquids
G.J. Orris, M. Nicholas, and D.K. Dacol

105
The Gamma Ray Sky as Seen by *Fermi*
Opening a New Window on the High Energy Space Environment
J.E. Grove and W.N. Johnson

113
Keeping COMMx Cool
Design and Analysis of the Thermal Control System for the TacSat-4 Spacecraft COMMx Payload
R.W. Baldauff, W.J. Armiger, and T.T. Hoang

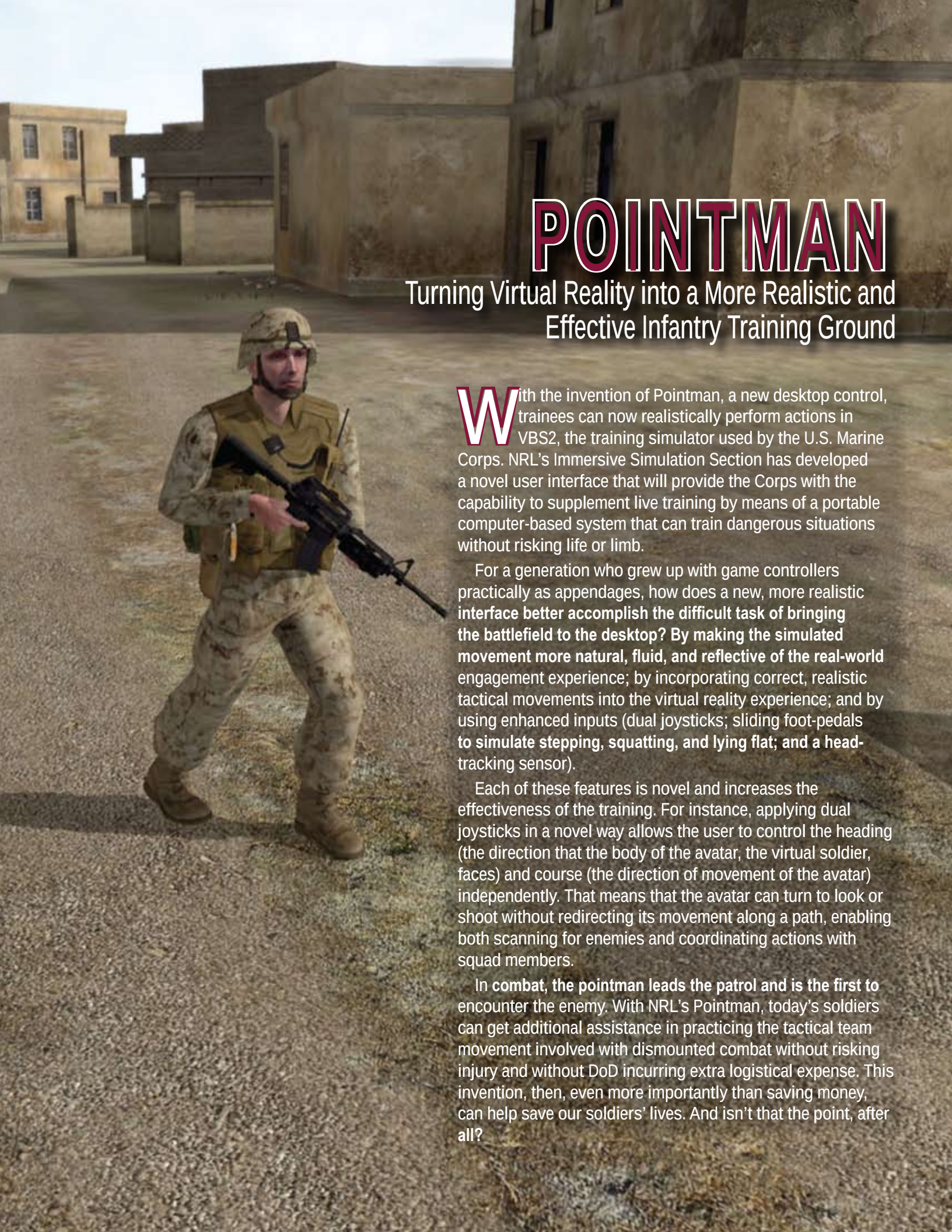

POINTMAN

Turning Virtual Reality into a More Realistic and Effective Infantry Training Ground

With the invention of Pointman, a new desktop control, trainees can now realistically perform actions in VBS2, the training simulator used by the U.S. Marine Corps. NRL's Immersive Simulation Section has developed a novel user interface that will provide the Corps with the capability to supplement live training by means of a portable computer-based system that can train dangerous situations without risking life or limb.

For a generation who grew up with game controllers practically as appendages, how does a new, more realistic **interface better accomplish the difficult task of bringing the battlefield to the desktop? By making the simulated movement more natural, fluid, and reflective of the real-world** engagement experience; by incorporating correct, realistic tactical movements into the virtual reality experience; and by using enhanced inputs (dual joysticks; sliding foot-pedals **to simulate stepping, squatting, and lying flat; and a head-**tracking sensor).

Each of these features is novel and increases the effectiveness of the training. For instance, applying dual joysticks in a novel way allows the user to control the heading (the direction that the body of the avatar, the virtual soldier, faces) and course (the direction of movement of the avatar) independently. That means that the avatar can turn to look or shoot without redirecting its movement along a path, enabling both scanning for enemies and coordinating actions with squad members.

In **combat, the pointman leads the patrol and is the first to** encounter the enemy. With NRL's Pointman, today's soldiers can get additional assistance in practicing the tactical team movement involved with dismounted combat without risking injury and without DoD incurring extra logistical expense. This invention, then, even more importantly than saving money, can help save our soldiers' lives. And isn't that the point, after **all?**

A Novel User Interface Controller for Dismounted Infantry Training

J.N. Templeman, L.E. Sibert, and R.C. Page
Information Technology Division

P.S. Denbrook
Denbrook Computing Services

For more than a decade, the Immersive Simulation Section has developed novel user interfaces for U.S. Marine Corps (USMC) infantry training simulators that let users interact in the 3D virtual world with close to the same abilities and constraints people have in the real world, in terms of moving through the environment and coordinating with teammates. Pointman is a new desktop control interface that combines a dual-joystick gamepad, head tracking, and sliding foot-pedals (inexpensive rudder pedals used with flight simulator games) that, for the first time, gives users the capability to apply correct tactical infantry movements using a desktop system. The USMC has adopted VBS2 (Virtual BattleSpace-2), an infantry and combined arms desktop training simulator to supplement live training. VBS2 is a product of Bohemia Interactive and will be used within the framework of the USMC's Deployable Virtual Training Environment (DVTE). Training simulators present dangerous situations without risking injury or accidents. They can represent any location that has been modeled, have a small footprint, and are deployable. They are less costly because they do not require travel to physical training sites and do not use consumables. The USMC recognizes the advantages of Pointman for increasing training effectiveness and has endorsed Pointman's integration with VBS2 through the Office of Naval Research's Rapid Technology Transition (RTT) Program and in cooperation with the USMC Program Manager Training Systems office (PMTRASYS) in Orlando, Florida.

INTRODUCTION

Desktop training simulators have the potential to provide training anytime and anywhere. A multiplayer training simulator can engage a whole squad in one action. A missing component in today's desktop simulators is a user interface controller that allows trainees to execute realistic military tactics, techniques, and procedures. Tactical movement relies heavily on the ability to look around (scan) while moving along any chosen path. Figure 1 illustrates the characteristics of tactical movement for moving around a corner in a high-threat environment. The objective is to clear the corner while minimizing the person's exposure to a threat. The action requires incrementally "pie-ing" the corner, turning the upper body and rifle together as a unit to face the corner, while moving down the hallway and focusing attention on the area just past the corner's edge.

The ideal user interface would enable the user to fully control the movement of the user's avatar (virtual body) in the virtual world. This movement is characterized by the avatar's heading (the direction in which the avatar's body faces) and course (the direction in which the avatar moves). Current dual-joystick gamepad con-

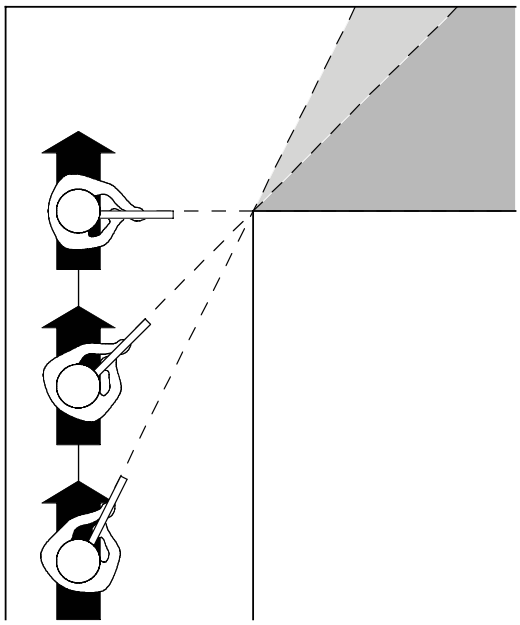

FIGURE 1
Turning the heading toward a corner while maintaining a straight course is a tactically correct way to clear a corner (referred to as *pie-ing* a corner). Direction of movement is represented by the arrow and heading coincides with the direction of aim.

trollers for first-person shooting games make it difficult to execute tactical movements because of limitations in the control mapping, which conflate the control over the avatar's heading and course. The problem is that the joystick used to turn the heading also redirects the course. The right joystick is a rate control that turns the heading and course together, while the left is a directional control that changes the course relative to the heading. Tactics for first-person shooter games reflect this control deficiency by emphasizing artificial strafing motions: moving sideways and spiraling toward or away from the target.

From its inception, the goal in developing Pointman was to create an interface that allows the user to move his or her avatar in a tactically correct manner. We learned a great deal about control over natural and tactical movement in developing Gaiter, a full-body immersive interface that uses a head-mounted display to surround the user in the virtual world and tracks the user's body segments in six degrees of freedom to provide direct interaction.[1] With Gaiter, the user steps in place to move the avatar through the virtual world and physically turns to rotate. The ability to turn naturally is central to Gaiter because it allows the user to turn immediately toward or away from any sight or sound.

The design goal for both Gaiter and Pointman is for tasks in the virtual world to be performed at the same rate, accuracy, and effort as they are in the real world to maintain timing and scale.[2] Having close to the same capability in the virtual world as a person has in the real world makes it more likely that skills developed in one will transfer to the other. For example, the cadence set when stepping in place with Gaiter or using Pointman's sliding foot-pedals is mapped to a real-world walking or running cadence on a moment-by-moment basis to give the user a realistic sense of distance traveled.

OVERVIEW OF POINTMAN

The Pointman user interface consists of a conventional dual-joystick gamepad for directing motion and weapons handling; sliding foot-pedals to control stepping; head tracking for directing the view and aim; and a desktop display (Fig. 2). The components combine to allow the user to control the actions of the user's avatar in a natural manner.

Unlike conventional gamepad controls, both joysticks on the gamepad are applied as directional controls. The user simply points the joystick in the direction the avatar should move or turn. Figure 3 shows the mapping of Pointman's dual-joystick gamepad. To turn smoothly, the right joystick is pushed forward and slid against the circular outer rim to continuously redirect the heading. To turn quickly in a known direction, the joystick is pushed in the desired direction from the neutral centered position. The user's avatar then turns at the maximum rate a person can physically turn in that situation. The left joystick controls the stepping direction (forward, backwards, sideways, or in any diagonal direction). The length of the avatar's stride and stepping cadence are expressed via sliding foot-pedals, which mimic a person's reciprocal foot motion when walking or running. Pointman lets users directly sense how far their avatar has turned or traveled, even with their eyes closed: users feel their avatars' alignment through the position of the joysticks and perceive how far they have traveled by the amount they have stepped.

Using the right joystick alone while operating the sliding foot-pedals advances the avatar in a forward direction relative to the current heading. People spend most of their time walking along paths in this way (for example, down a hall) and the design of Pointman makes such common acts easy to do. Using the left joystick alone while operating the foot-pedals translates the avatar along the indicated course while keeping the avatar's heading constant.

The real power of Pointman comes when the joysticks are jointly engaged. Working together, they provide independent control over heading and course: the right joystick turns the avatar (for example, to face a target) while the left sets the avatar's direction of movement. This independent control over heading and course is what lets the user scan while moving along a path.

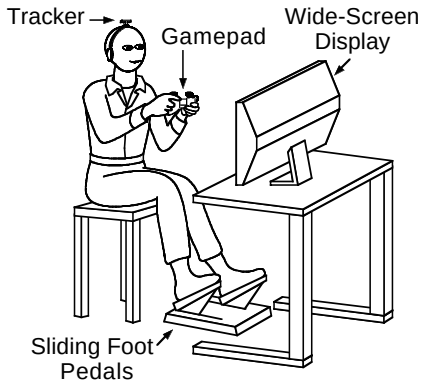

FIGURE 2
Pointman user interface with dual joystick gamepad, head tracking, and sliding foot-pedals.

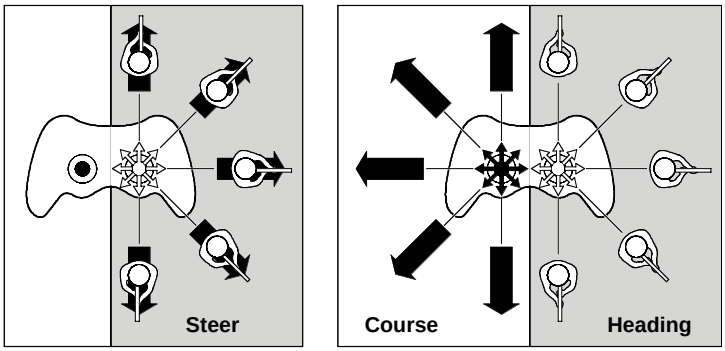

FIGURE 3
Mapping of Pointman's dual joystick gamepad to control the avatar's movement.

Weapons handling is accomplished through button presses on the gamepad. One button is the trigger and another cycles through the different ways of carrying the rifle: slung, carry, ready, and aim. A change in posture is also indicated through a button press, cycling through standing, prone, seated. Tilting the foot-pedals (similar to an accelerator pedal) adjusts the height of a posture; for example, with standing, pushing the pedals down moves the avatar from an upright posture to a crouch.

A three-degree-of-freedom (orientation only) tracker or a six-degree-of-freedom (orientation and translation) tracker worn on the user's head provides control over viewing and aiming. Head tracking controls the yaw (turning about the vertical axis), pitch (tilting up and down), and roll (tilting left and right) of the avatar's head and aim relative to the joystick-directed heading. The yaw derived from the head tracking data is added to the current heading to turn the view an additional amount (limited by how far the user can turn his or her head while seated in front of the desktop display). Since the degree to which the user can pitch his or her head up and down while viewing the desktop display is limited, the pitch derived from the head tracking data is amplified to allow the avatar to look directly up or down in the virtual world. If the tracker provides six degrees of freedom, the user can direct the avatar's upper body to lean forward, backward, and side-to-side independently of how the head is oriented, further increasing the realism. The direction of aim is, therefore, linked to both the heading set by the joystick and the direction of view, allowing the head, upper body, and rifle to be rotated as a unit to maintain an indexed shooting posture as is done in the real world. With six-degree-of-freedom tracking, users can also lean to shoot from behind cover.

USER'S AVATAR

The Immersive Simulation Section has pioneered the use of a fully articulated user avatar continuously driven in real time either by the user's own body motion or through control actions. An articulated avatar is used with both Gaiter and Pointman. A central part of the integration effort is to add an articulated avatar to VBS2.

Traditionally, avatars in first-person shooter games, including VBS2, use prerecorded animation sequences to portray the user's actions. A user indicates that the avatar should move forward by deflecting a joystick or pushing a button, and an animation sequence of a walking or running avatar is played. In contrast, Pointman lets the user directly control his or her avatar. The sliding foot-pedals control the avatar's stepping motion, course and heading are controlled with the dual joysticks, and because the user's head is tracked, the user's avatar turns to look in the same direction that the user's head turns. In other words, with Pointman, the avatar moves in correspondence with the user's actions to an unprecedented degree for a desktop control.

Users operate in first person and see the virtual world out of their avatars' eyes. The avatar is fully rendered so the user sees his or her avatar's arms, legs, and feet. Users also see their teammates as fully articulated avatars acting in the virtual world. The challenge is to realistically portray the actions performed by the user's avatar under direct, continuous control. Being able to act in a realistic manner in the virtual world gives the user a sense of perspective, relative distance, and presence in the environment. Watching the actions of teammates' avatars gives a better sense of their intent. Having a finer level of control in the virtual world leads to a fuller range of expression, greater situational awareness, better communication among immersed teammates, and support for cooperative action.

INTEGRATION WITH VIRTUAL BATTLESPACE-2

VBS2 currently uses a keyboard and mouse interface or conventional gamepad with thumbsticks and buttons, and prerecorded animations for avatar movement. Enabling users to execute correct tactical methods in the virtual world requires the integration

of both the Pointman user interface and an articulated avatar continuously directed in real time. NRL's Immersive Simulation Section has developed a detailed VBS2-Pointman Interface Specification that allows Pointman to direct the user's avatar in VBS2. The goal is to create a Pointman-enhanced version of the VBS2 training simulator, adding more realistic interaction while minimizing latency and communication overload. Figure 4 shows the user's avatar as controlled by Pointman and rendered in VBS2.

The VBS2 integration coincides with new research to extend the range of behaviors supported by Pointman to meet the demands of military action in urban terrain. The user's avatar needs to not only stand but also crouch and sit while handling a rifle. We have conducted research in fluid control over the avatar's body posture and engagement stance so that the avatar can transition between poses with the same timing and constraint people use in the real world. Figure 5 shows the design for accomplishing a smooth transition

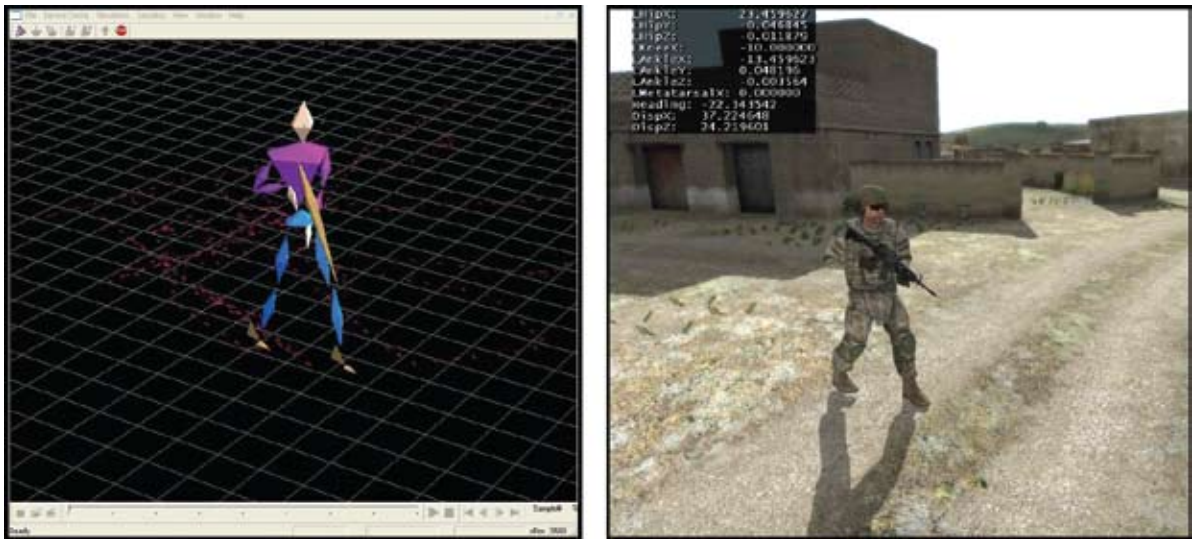

FIGURE 4
Integration of Pointman with Virtual BattleSpace-2. The left panel shows the user's avatar as controlled by Pointman; the right panel is the avatar as rendered in VBS2.

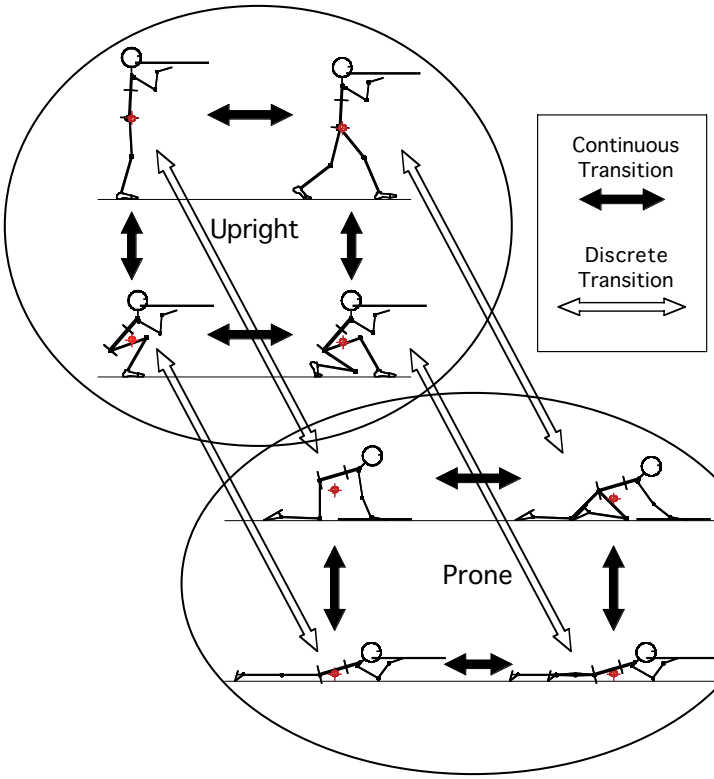

FIGURE 5
Design of the smooth transition between a high and low stance in upright and prone postures.

between a high and low stance in upright and prone postures. The challenge has been to make the different means of controlling the avatar's stance and movement work together to express the user's intent in a natural manner.

CONCLUSIONS

Pointman is a new user interface that gives users the ability to execute realistic tactical infantry movements in a desktop environment. The military has a growing interest in using desktop simulators for training because they are portable, relatively inexpensive, and can support a large number of users. Four U.S. Marine Corps Generals who visited our lab recognized Pointman's advantages. While Pointman's independent control over moving and looking remains the core of the user interface, a key effort has been researching how to make the transition between avatar postures and stances more fluid and natural. The final result will be a desktop training simulator that provides realistic control over action to support teaching the full range of tactics, techniques, and procedures used in infantry operations.

[Sponsored by the NRL Base Program]

ACKNOWLEDGMENTS

We thank the USMC Program Manager Training Systems office (PMTRASYS) for their support of this effort, especially Mr. Jeffery Moss, who is the Program Manager for the ONR RTT. Pointman has been developed and is being extended under support from the NRL Base Program.

References

[1] J.N. Templeman, P.S. Denbrook, and L.E. Sibert, "Virtual Locomotion: Walking In Place Through Virtual Environments," *Presence* **8**, 598–617 (1999).

[2] J.N. Templeman, L.E. Sibert, R.C. Page, and P.S. Denbrook, "Designing User Interfaces for Training Dismounted Infantry," in D. Nicholson, D. Schmorrow, and J. Cohn (eds.), *The PSI Handbook of Virtual Environments for Training and Education* (Westport, CT, Greenwood Publishing Group, 2008).

HiEx Foam

The Ultimate Fire Fighter Goes Where No Foam Has Gone Before

NRL's Navy Technology Center for Safety and Survivability is running full-scale fire tests on high expansion (HiEx) foam for shipboard firefighting to protect large volume mission-critical spaces. HiEx foam is 3D capable; that is, it expands to fill up the volume of flammable spaces in minutes, flowing around obstructions that previously mandated manual firefighting in order to completely extinguish fires. And it does so with less liquid solution, meaning less water damage and less resulting clean-up. NRL researchers solved the critical problem of traditional HiEx systems requiring fresh air, a rare commodity in shipboard spaces that are already aflame, by focusing on the use of fire compartment air. Because of NRL's research, HiEx foam is a strong candidate for inclusion into future (and safer) ship design.

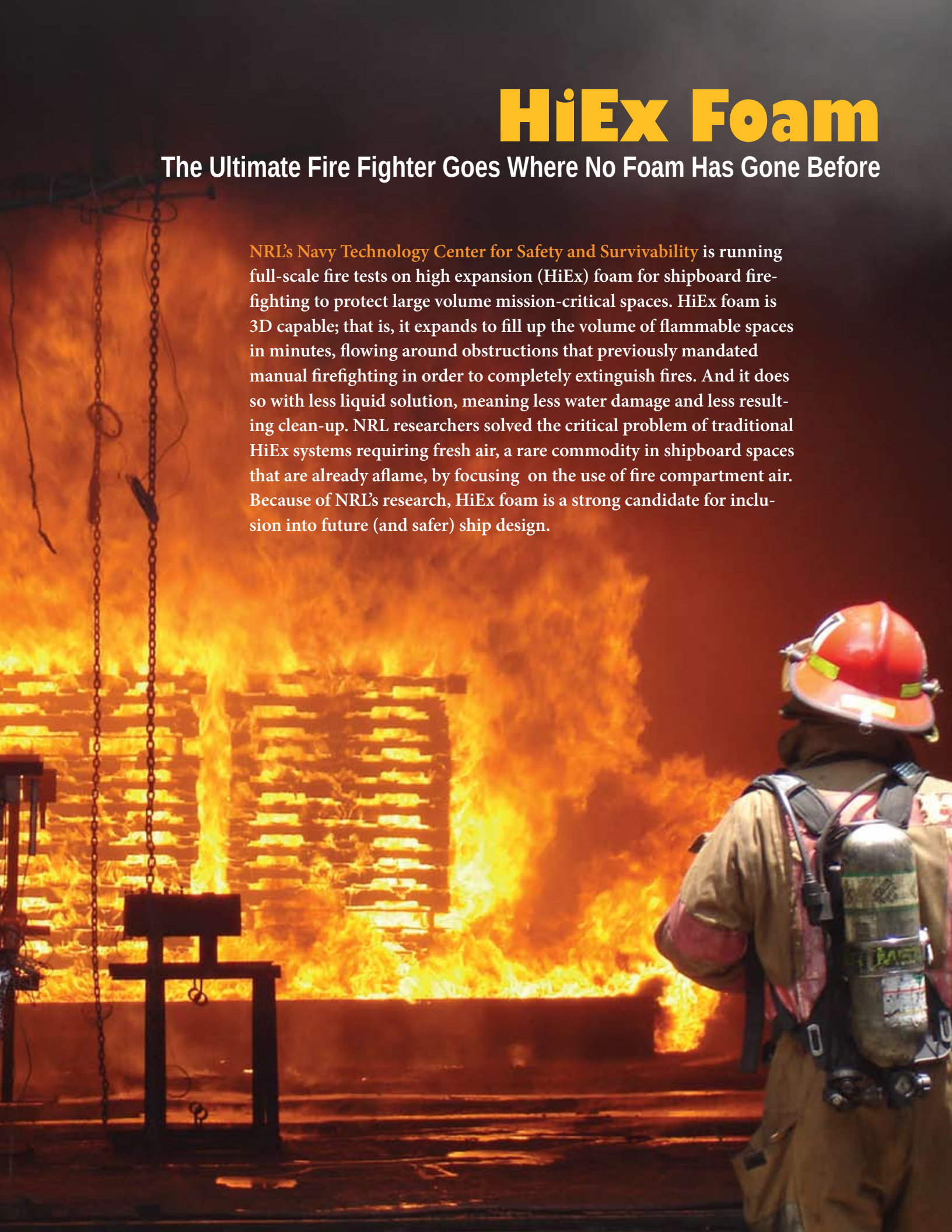

High Expansion Foam for Protecting Large Volume Mission Critical Shipboard Spaces

J.P. Farley and F.W. Williams
Chemistry Division

NRL's Navy Technology Center for Safety and Survivability recently initiated a full-scale fire test series to demonstrate the efficacy of high expansion foam for protecting large volume shipboard spaces. High expansion foam was pursued because of its inherent ability to travel around obstructions, fill the volume in minutes, and provide a three-dimensional firefighting capability that would not depend on a manual firefighting attack to complete final extinguishment. In addition, it can accomplish all this by using only a small quantity of liquid solution, which results in reduced water damage and minimal clean-up after its use. The demonstrated success of this NRL fire test series has helped to generate considerable interest within the Navy's ship design community for incorporating high expansion foam systems into future surface ship designs.

INTRODUCTION

Large volume shipboard spaces can include multiple Class A (combustible solids) and Class B (flammable liquids) fire threats. Prior testing conducted onboard the NRL full-scale fire test ship, ex-USS *Shadwell*, has identified the limitations in protecting these large-volume spaces using aqueous film-forming foam (AFFF) sprinklers designed only to combat Class B two-dimensional pool fires.[1] The consequence of these noted limitations necessitates a manual attack when tightly stacked Class A materials or three-dimensional Class B running fuel fires are present. This requisite manual attack also introduces additional hardships when considering the degree of clutter and heavy smoke conditions that will be present, which adversely affects firefighting performance and personnel safety.

To address this, NRL recognized the tremendous capabilities of high expansion foam and developed an experimental fire test protocol to examine the possibility of incorporating it into a ship's firefighting system design. NRL further recognized that employing a traditional high expansion foam generator would impact shipboard applicability since it requires a fresh air supply (outside air) and an internal fan for suitable foam generation. For fixed high expansion foam systems aboard future ships, it would be advantageous, from a point of view of installation and cost, to have foam generators that do not require external duct work or moving parts, and simply use the fire compartment air (inside air) to generate the high expansion foam. This concept would also allow application well within the confines of the ship where immediate access to fresh air sources may be problematic. Historically, the use of inside air (i.e., hot air contaminated with combustion products) has presented a challenge.[2] Therefore, due to the potential economies that could be realized, NRL focused this experimental study to assess the efficacy of a new type of high expansion foam generator that has been specifically designed to work with inside air.

FOAM GENERATOR TECHNOLOGY

A manually activated, total flooding, high expansion foam system was selected for this experimental study. Manufactured by Svenska Skum AB, Kungalv, Sweden, it is called HotFoam. The system consists of a uniformly spaced overhead grid of small, unconventional generators (Fig. 1). Air is entrained by a spray nozzle within the generator to make the foam, rather than by a fan drawing outside air. The foam concentrate used was Meteor P+ synthetic foam concentrate, designed to be proportioned at 2 percent. The HotFoam Meteor P+ concentrate has been formulated to be suitable for use with fresh, sea, or brackish water and is environmentally acceptable.

FIRE TEST PROTOCOL

The full-scale fire tests were conducted onboard the NRL fire test ship, ex-USS *Shadwell*, located in Mobile, Alabama, in the Well Deck fire test area (Fig. 2). The dimensions of this area were 21.3 m (70 ft) long, by 13.4 m (44 ft) wide, with an 8.5 m (28 ft) high overhead. The total deck area was 285 m^2 (3080 ft^2).

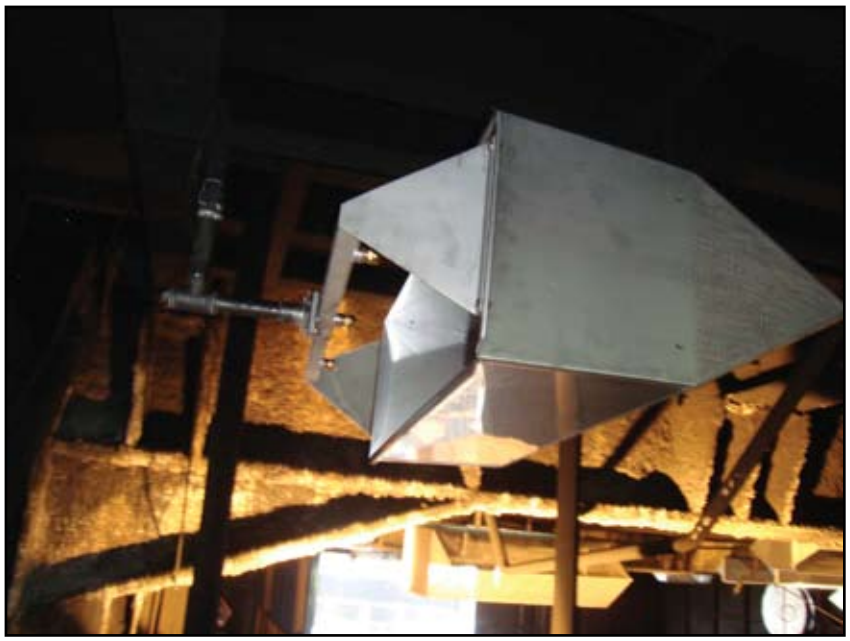

FIGURE 1
HotFoam HG-25 generator mounted in the overhead grid system.

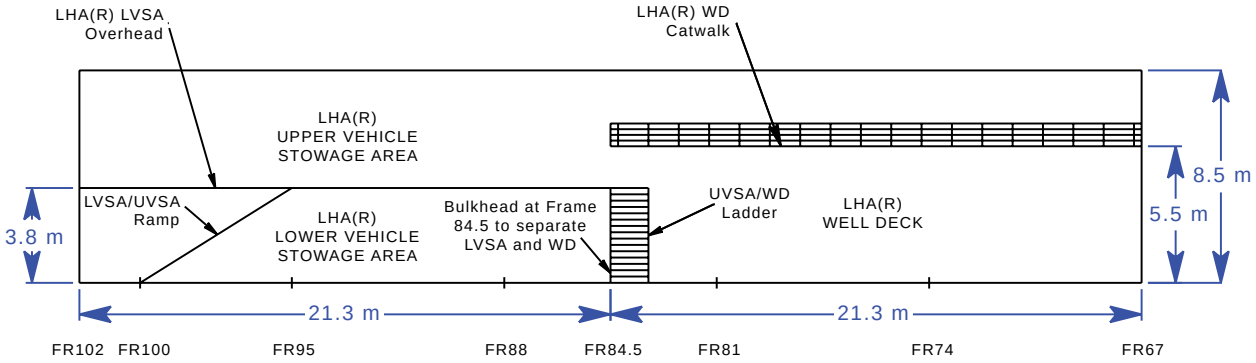

FIGURE 2
Ex-USS *Shadwell* test area, section view.

A quadruple fire threat consisting of Class A and B test materials was developed to simulate an actual fire casualty (Fig. 3). The Class A fuel package, which provided a repeatable fire test surrogate for Class A vehicle fires, consisted of six 1.8-m (6-ft) high stacks consisting of 15 standard size oak pallets. This Class A fuel package created a 30 megawatt (MW) fire when all were fully involved. The two Class B (marine diesel) spill fire scenarios included a two-dimensional pool fire in a test pan measuring 4.6 m by 6.1 m (15 ft by 20 ft) and a three-dimensional running fuel fire using a 0.9-m (3.0-ft) by 0.6-m (2-ft) by 1.8-m (6-ft) high steel structure metered to flow fuel at a rate of 13.6 Lpm (3.6 gpm). The calculated heat release rates for these two Class B fire threats were 60 MW and 8 MW, respectively. An additional, shielded Class B-initiated small wood crib was located in an adjacent compartment that opened into the Well Deck test area. This setup simulated a vehicle in the Well Deck that had an obstructed area such as an open vehicle door, tailgate, or window. Figure 4 provides a picture of the developed quadruple fire threat prior to fire suppression system activation.

Five full-scale tests were conducted to assess the efficacy of the inside air-generated high expansion foam system. The fire test scenarios were developed and selected to enable a direct comparison to previously conducted AFFF and outside air high expansion foam fire test findings.[3,4] The determined tests can be categorized as follows:

1. Cold Discharge test. This test was conducted to establish and verify the system pressure flow, concentration characteristics, and submergence (fill)/dissipation times.

2. Fire test with the Class B pool, Class A pallets, and Class A adjacent space fire, but without the Class B cascade running fuel fire.
3. Fire tests that included the "3D" cascade running fuel fire in addition to the other fire threats. This was the "quadruple" 98 MW fire test scenario.

All tests were conducted with the after-test area door partially open, resulting in a vent opening of approximately 27 m^2 (286 ft^2) in the test area. Measures of fire control and extinguishment were derived by visual observation and by thermocouple data.

RESULTS

The following definitions were used to conduct the tests and analyze the data:

1. Pre-burn Time – the time from ignition of the Class B pool or cascade running fuel fire.
2. Knockdown – the time when very rapid cooling occurred within the pallets.
3. Extinguishment – the time when:
   a. By visual or video observation, no flaming combustion was observed; or
   b. By data, the time at which the last thermocouple reached 230 °C (446 °F) for Class A fires (i.e., approximately the piloted ignition temperature of wood or paper) or approximately 50 °C (122 °F) above the pool or cascade (i.e., below the flash point of marine diesel).
4. Submergence (fill) Time – the time from system activation to the time for foam to reach various heights in the Well Deck.
5. Foam Dissipation (breakdown) Time – the time the system was secured until the foam drained to reach a certain level in the Well Deck.

The cold discharge test was conducted with 23 overhead HotFoam generators. The adjacent compartment was open to the Well Deck volume, making the total floodable volume 1173 m^3 (41,328 ft^3). The temperature in the space was 31 to 32 °C (87.8 to 89.6 °F). The foam filled the desired volume within the Well Deck test area in 1 minute 44 seconds, which was in good agreement with the pre-test calculation of 1 minute 30 seconds (Fig. 5). The calculated average fill rate was 2.2 m/minute (7.2 ft/minute) and the calculated expansion ratio was 375:1. After holding the foam for a period of 60 minutes, the overhead generator system was again activated with water only to note its potential foam knockdown capability, which could be used for future high expansion foam firefighting doctrine development. It was observed that this tactic was able to dissipate the foam blanket to within 0.6 to 0.9 m (2 to 3 ft) of the deck in 120 seconds, which would enable adequate access for post-fire investigation activities and a reasonably quick unmanned process for space reclamation efforts following a shipboard fire event.

The first fire test included the Class B pool, Class A pallet, and the Class A adjacent space fire threats. After activating the HotFoam system, there was rapid extinguishment of the pool fire (36 seconds) and pallet fires (76 seconds). The adjacent space fire was extinguished in 2 minutes 12 seconds. The time to fill the Well Deck test area to the desired level was 4 minutes 38 seconds. Fluctuations in oxygen concentration measured low in the space, and the total heat flux measured approximately 6 m (20 ft) away from the test pan area indicated some level of steam production effects during the fire suppression process.

The next three fire tests included the Class B cascade running fuel fire in addition to the other fire threats and a delayed activation time to further challenge the foam generation process using inside air within a post-flashover thermal layer environment. For fire test two, extinguishment of the Class B pool fire occurred at 43 seconds, the Class A pallets at 90 seconds, the Class B cascade at 96 seconds, and the Class A adjacent space fire at 10 minutes 16 seconds. The time to fill the Well Deck to the desired level was 10 minutes 12 seconds. It was apparent that the increase in heat load affected the build-up of foam and there was also a notable increase in steam production.

For fire tests 3 and 4, the solution flow rate and configuration/location of the foam generators were adjusted to further investigate the potential impact these changes may have on inside air-generated foam expansion. In fire test 3, 18 generators were kept in the overhead and 12 generators were located approximately mid-level in the Well Deck compartment to lessen their exposure to the upper hot thermal layer. In this arrangement, the HotFoam system extinguished the Class B pool in 12 seconds, the Class A pallet fires in 36 seconds, the Class B cascade running fuel fire in 36 seconds, and the Class A adjacent space fire in 4 minutes 42 seconds. The time to fill the Well Deck to the desired level was 5 minutes 45 seconds. Foam expansion improved and steam production was notably less in comparison to fire test 2. For fire test 4, 30 generators were located in the overhead, resulting in the Class B pool fire extinguishment in 36 seconds, the Class A pallet fires in 48 seconds, the Class B cascade running fuel fire in 66 seconds, and the Class A adjacent space fire in 2 minutes 6 seconds. The HotFoam system was secured at about 2 minutes of activation due to a ruptured pipe casualty to the system. Although all fires were quickly extinguished, there was very little visible foam on the deck (Fig. 6). This indicates that all extinguishment action was done either by water

FIGURE 3
(a) Well Deck Mixed Class A and Class B Fuel Package. (b) Class A fuel package for the adjacent space fire.

FIGURE 4
Quadruple 98 MW test fire prior to HotFoam activation.

FIGURE 5
HotFoam cold discharge test.

cooling or steam smothering. Water conversion to steam and localized oxygen depletion is postulated as the primary mechanism of suppression as opposed to direct surface wetting. The suppression of the Class B cascade and adjacent space Class A fires (where there was no direct water application) supports this theory.

SUMMARY AND CONCLUSIONS

There was concern that the HotFoam system would be ineffective on large fires due to injection of heat and smoke into the generators. This might prevent generators located inside the affected space from generating good quality foam. The system tested was effective on all fire scenarios, including the quadruple fire threat and delayed activation scenarios. The HotFoam system, at lower comparable solution flow rates, 2040 to 2600 Lpm (538–684 gpm), was as effective or more effective than the previously tested outside air-generated high expansion foam flowing at 3100 Lpm (820 gpm). The outside air high expansion foam appears to have relied more on cooling and fuel surface oxygen displacement. The HotFoam system, particularly for the high heat threat, delayed activation scenario, relied on steam conversion and associated steam smothering. Although the steam generation phenomenon associated with the HotFoam system was an unforeseen finding that requires further study, it did provide important insight into some additional capabilities that a HotFoam system may possess. This noted steam generation phenomenon may also open up other avenues of opportunity for developing an alternative overhead AFFF nozzle design that is better suited to combating mixed Class A and Class B fire threats. These additional fire suppression research efforts will help to ensure that future ship classes with large volume mission critical spaces are adequately protected against any fire threat that may be present.

[Sponsored by NAVSEA 05P14]

REFERENCES

[1] A.C. Lures, M.A. Harrison, H.V. Pham, J.A. Lynch, J.L. Scheffey, J.P. Farley, F.W. Williams, and M.P. Hunstad, "Test Report for Well Deck and Vehicle Stowage Area Vulnerability and Fire Model Validation Tests, Series 1 – An Evaluation of Aqueous Film Foaming Foam (AFFF) Suppression Systems for Protection of LHA(R) Well Deck and Vehicle Stowage Areas," NRL Ltr Rpt 6180/0369, Naval Research Laboratory, Washington, DC, October 26, 2004.

[2] I. Wilder, "High Expansion Foam for Shipboard Fire Fighting," Naval Applied Science Laboratory, 72nd Annual Meeting of the National Fire Protection Association, Atlanta GA, May 20, 1968.

[3] J.L. Scheffey, J.P. Farley, and F.W. Williams, "Summary Report – AFFF Overhead Sprinkler Suppression Systems Used to Combat a Hangar Bay, Well Deck, or Vehicle Storage Fire Threat," NRL Ltr Rpt 6180/0171, Naval Research Laboratory, Washington, DC, July 23, 2008.

[4] J.L. Scheffey, J.P. Farley, H.V. Pham, and F.W. Williams, "Summary Report – High Expansion Foam Suppression Systems Used to Combat a Hangar Bay, Well Deck, or Vehicle Storage Fire Threat," NRL Ltr Rpt 6180/0196, Naval Research Laboratory, Washington, DC, September 22, 2008.

FIGURE 6
Fire test 4, immediately after fire suppression due to steam smothering.

Using Our Heads to Save those of the Warfighters

NRL Studies the Helmet-Skull-Brain Response to Prevent TBI

Is today's helmet good enough?

No existing helmet protects all warfighters in all scenarios. Traumatic brain injury (TBI) accounts for a shocking 19 percent of all injuries seen in our soldiers returning from the wars in Iraq and Afghanistan. In an effort to prevent TBI, NRL is studying the dynamics of brain injury. Building on its previous successes with the GelMan surrogate model of the human torso and the QuadGard (arm and leg protection) already deployed and saving lives, the Lab's Materials Science and Technology Division, in conjunction with the Laboratory's Acoustics Division and Laboratory for Computational Physics and Fluid Dynamics, has now taken on the challenge of a system of even greater complexity: the head.

The ultimate goal of their research is to lay the foundation for designing and building a helmet that will protect the warfighter in various theaters of operation and also be mobile, lightweight, and comfortable. What is not known is precisely how the shock waves associated with blasts, ballistic impacts, and vehicular accidents affect the brain to cause mild, moderate, or severe TBI as based on medical diagnosis. Finding the answers involves modeling the response of the brain to blast and analyzing medical data from open literature to correlate biomechanical data with the dynamics of TBI.

The key is to accurately characterize the helmet-skull-brain interaction, and NRL is exploring that interaction through two parallel efforts:

- an instrumented helmet-skull-brain system, which has the capability of measuring strain and pressure to identify regions in the brain with a high potential for damage, and

- an environmental helmet sensor, which can measure and catalog real-time signatures of dynamic events during a blast or ballistic impact, relating to post-injury diagnosis.

Both of these efforts yield data on brain acceleration and consequent brain damage that bio-engineers and medical practitioners can use to interpret and better understand causes of TBI. This is just further proof that NRL researchers are using their heads to save those of others.

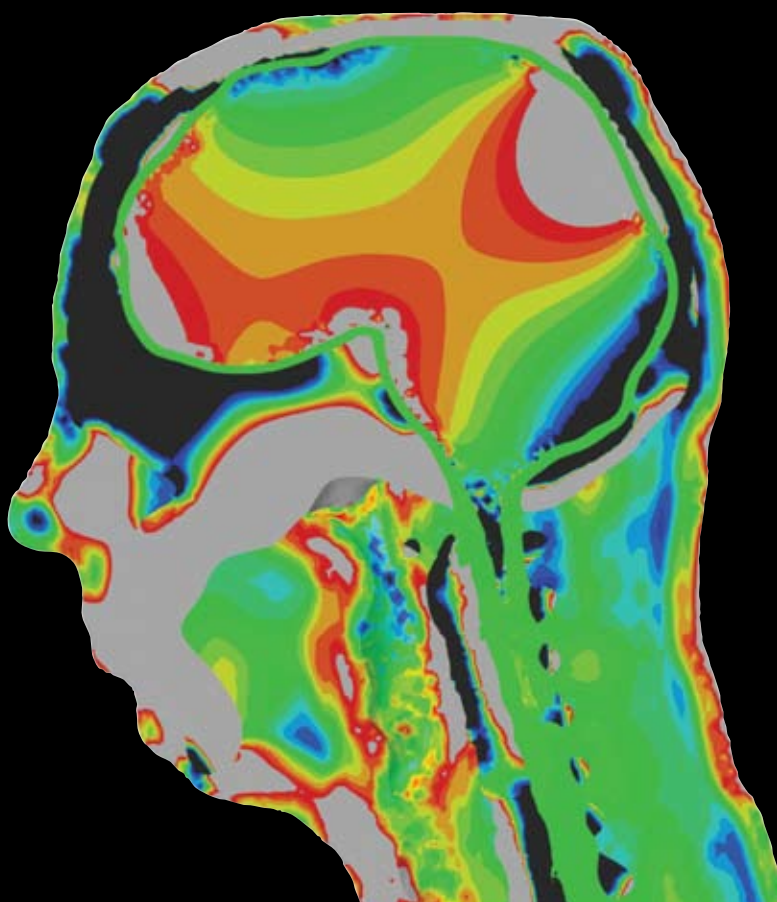

Sensor Systems for Measuring Helmet-Head-Brain Response to Blast

K.E. Simmonds, A. Bagchi, A.C. Leung, W.R. Pogue III, P. Matic, J.M. Byers, and G.K. Hubler
Materials Science and Technology Division

D.R. Mott and D.A. Schwer
Laboratory for Computational Physics and Fluid Dynamics

R.D. Corsaro and B.H. Houston
Acoustics Division

From World War I (WWI) to the war in Iraq, helmets have transitioned from steel to Kevlar composite materials. Just prior to WWI, helmets were non-existent because mobility and weight requirements took precedence over protection. Today mobility, weight, comfort, and protection factor into helmet design based on current threats from various ammunition, fragmentation threats, and operational environments. Inside the helmet, liners have evolved from leather to plastic suspension to sophisticated energy-absorbing padded liners, and new prototype suspensions are being tested every year to improve comfort and increase protection. Because of recent medical advances, it is apparent that experimental methods, measurement devices, and newer classes of helmets are necessary to provide warfighters with the best personal protection equipment for combating traumatic brain injuries (TBI).

TWO APPROACHES TO RESEARCHING BRAIN INJURIES

Traumatic brain injuries (TBI) are classified as mild, moderate, and severe in warfighters subjected to blasts or ballistic impacts, and in vehicular accidents. In each category, certain physical and mental impairments are associated with various parts of the brain. In open literature, most physical and visual evidence of TBI is vascular damage (detected by magnetic resonance imaging (MRI)) and brain swelling. The more subtle cases are chemical and neuronal stress that leads to cell death. As discussed in open literature, causes of TBI are not well understood by medical personnel who can only diagnose symptoms as they surface either physically or behaviorally as post-traumatic stress disorders, often months after a warfighter has returned from an assignment.

The Materials Science and Technology Division at NRL is developing research tools and measurement devices to document events that are likely to cause significant brain injuries to warfighters in battlefield environments. This paper addresses two parallel efforts for understanding shockwave interaction with the head and induced blunt force trauma to the brain. The first approach is the use of an instrumented GelMan skull-brain surrogate with an instrumented helmet. The second approach is a helmet-mounted sensor such as the newly designed NRL and Allen-Vanguard environmental helmet sensor capable of measuring and cataloging real-time signatures of warfighters subjected to dynamic events during a blast, a ballistic impact, or both. In both approaches, the data are analyzed and interpreted to measure brain acceleration to establish a fundamental understanding of brain damage. The outcome of this research can be used by bio-engineers and medical practitioners to understand and interpret causes of brain damage and TBI.

This paper has three sections. The first section describes an instrumented helmet-skull-brain system (HSB), computational results, and experimental results. The second section covers the NRL and Allen-Vanguard environmental helmet sensor system (EHS), simulation results, and experimental testing. The last section summarizes the impact of NRL's research in helmet-performance characterization.

INSTRUMENTED HELMET-SKULL-BRAIN SYSTEM

A commercial finite-element analysis tool is used to investigate the response of a head model subjected to a blast pressure from a C4 explosive charge detonated 2.44 m away from the surrogate head model. The model is comprised of a representative brain, cerebral spinal fluid, the skull with cervical vertebrae, and generalized tissue (Fig. 1(a)), and constrained at the

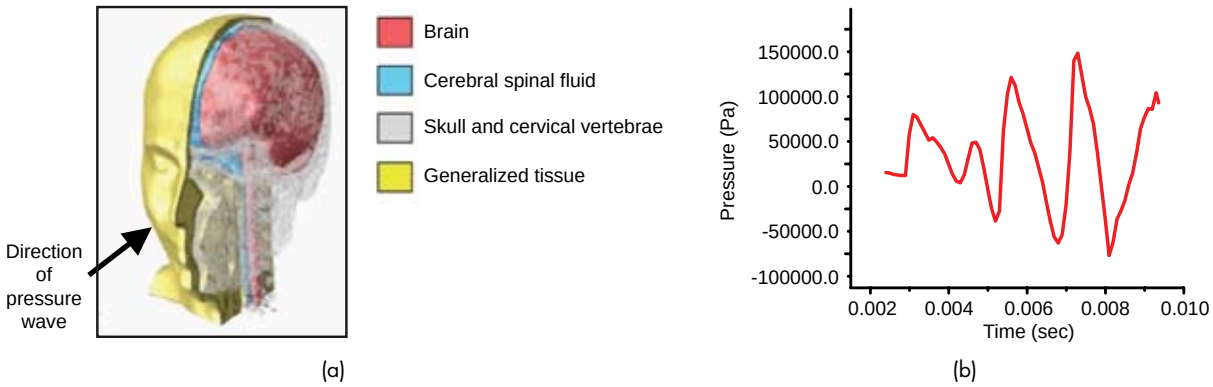

FIGURE 1
(a) Finite element mesh of head. (b) Pressure profile on the face of the head from a 0.45 kg C4 charge exploded at 2.44 m from the head.

shoulder. The blast pressure impacting the head model is shown in Fig. 1(b). The three-dimensional finite-element mesh of the head with neck and shoulders is constructed from an MRI scan of a 50th percentile male. The brain tissue and skull properties are from open literature. The brain is modeled as viscoelastic, the cerebral spinal fluid as a hyperelastic material with a low shear stress and a high bulk modulus, and the skull with cervical vertebrae and the generalized tissue are considered to be linear elastic materials.

Figure 2 shows the pressure contours in the head as a result of the applied blast pressure wave. Immediately following the blast (time = 3.30 ms and 3.77 ms), the stresses develop primarily in the stiffer modulus material, the skull. Tensile and compressive stresses in the direction of the wave propagation then begin to increase near the surface of both frontal and occipital lobes. At later times (between 4.47 ms and 5.00 ms), oscillating compressive and tensile stresses are observed that travel along the surface of the frontal lobe, the parietal lobe, the occipital lobe, and the cerebellum. As the blast pressure increases further (more than 5.00 ms), tensile and compressive stresses increase briefly at the surface of the frontal and occipital lobes of the brain in the direction of the propagating wave. After 6.17 ms, shear and longitudinal stress waves develop, with varying levels of stresses evident in all lobes. This analysis of the blast wave impacting the skull-brain system clearly shows the significant internal stress variation due to a blast wave.

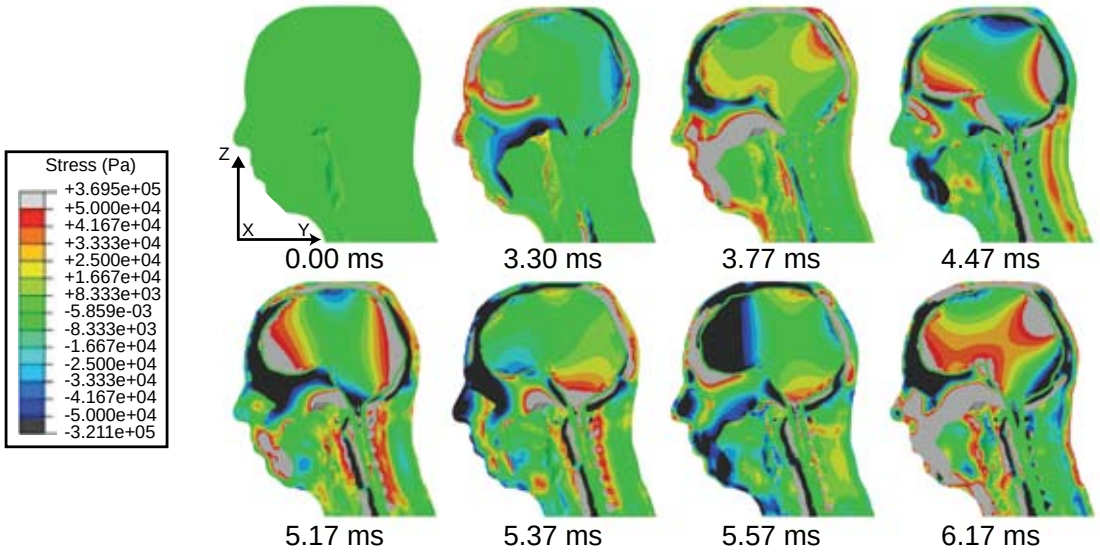

FIGURE 2
Pressure contours in the head at the sagittal plane.

In general, the brain has a separate response in pressure from the other components (skull and generalized tissue) due to differences in wave speeds. The highest pressures observed occur primarily within the brain and mouth region. In addition, as a result of the irregular shape of the brain, there is a translational (in the Y and negative Z direction) and a rotational motion that occurs about the brain stem.

The HSB as a system consists of three basic components: instrumented helmet, skull, and brain surrogate. The main component of this system is an anatomically shaped brain of generalized tissue simulant encased in a polymer skull. The brain is fabricated by molding a transparent pliable thermoplastic polymeric material with miniature piezo-electric accelerometers and pressure sensors strategically placed in each major lobe. Two instrumented surrogate brains were fabricated, one with 11 pressure sensors and one accelerometer, and the other with 11 accelerometers and one pressure sensor, thus allowing calculation of both pressure and strain transfer functions.

The HSB is mounted on a Hybrid III neck and stand, placed in an enclosed structure, and blast-tested using C4 explosive (Fig. 3(a)). The HSB is subjected to an initial shockwave traveling at speeds greater than Mach-1 (speed of sound in air), multiple shockwave reflections, blast winds approaching hurricane wind speeds, and flames traveling at much lower speeds. From high-speed videos we are able to visualize multiple reflections of the shockwave that combine into more complex wave shapes that produce complicated brain strains further in time. Although the flames from the blast (Fig. 3(b)) engulf the HSB, the exposure time is not long enough to ignite any of the materials or contribute to the brain response.

From accelerometers located within the various brain lobes, meaningful data such as displacements are calculated from measured acceleration time histories. In order to quantify brain response in engineering terms, average strains (Fig. 4) between sensor locations are calculated (i.e., between the lobes in the brain). The strains show the relative influence of charge weight, external motion, helmet-liner system, and distance from blast. The HSB system provides a baseline for understanding possible injury mechanisms and establishing new metrics for testing new designs of helmets and helmet liners.

(a)

(b)

FIGURE 3
(a) HSB in blast chamber. (b) High-speed video frame showing the blast wave and the flame front approaching the HSB during blast testing.

ENVIRONMENTAL HELMET SENSOR

In the battlefield, one of the common threats to the head is the effect of blast pressure fronts on the face and infiltration through the gap between the skull and the helmet. These pressures are commonly believed by the medical community to be a major contributor to brain damage and traumatic brain injury. To understand the effect of such pressure infiltration, NRL conducted blast tests with an instrumented head-helmet system and complemented it with computer simulations for a better representation of the sequence of events in a blast.

Allen-Vanguard and NRL used two mannequins wearing Marine Corps lightweight helmets with current production pads and face shields, and placed them in close proximity to a blast of a commercial explosive, such as C4. The mannequins were instrumented with pressure sensors at F3 on the forehead, over the ear, and at R2 on the back of the head (see Fig. 5(a)). Computational fluid dynamic simulations were carried out for a planar shock wave approaching the helmet and head, with a gap between the head and the helmet, but no helmet liner.

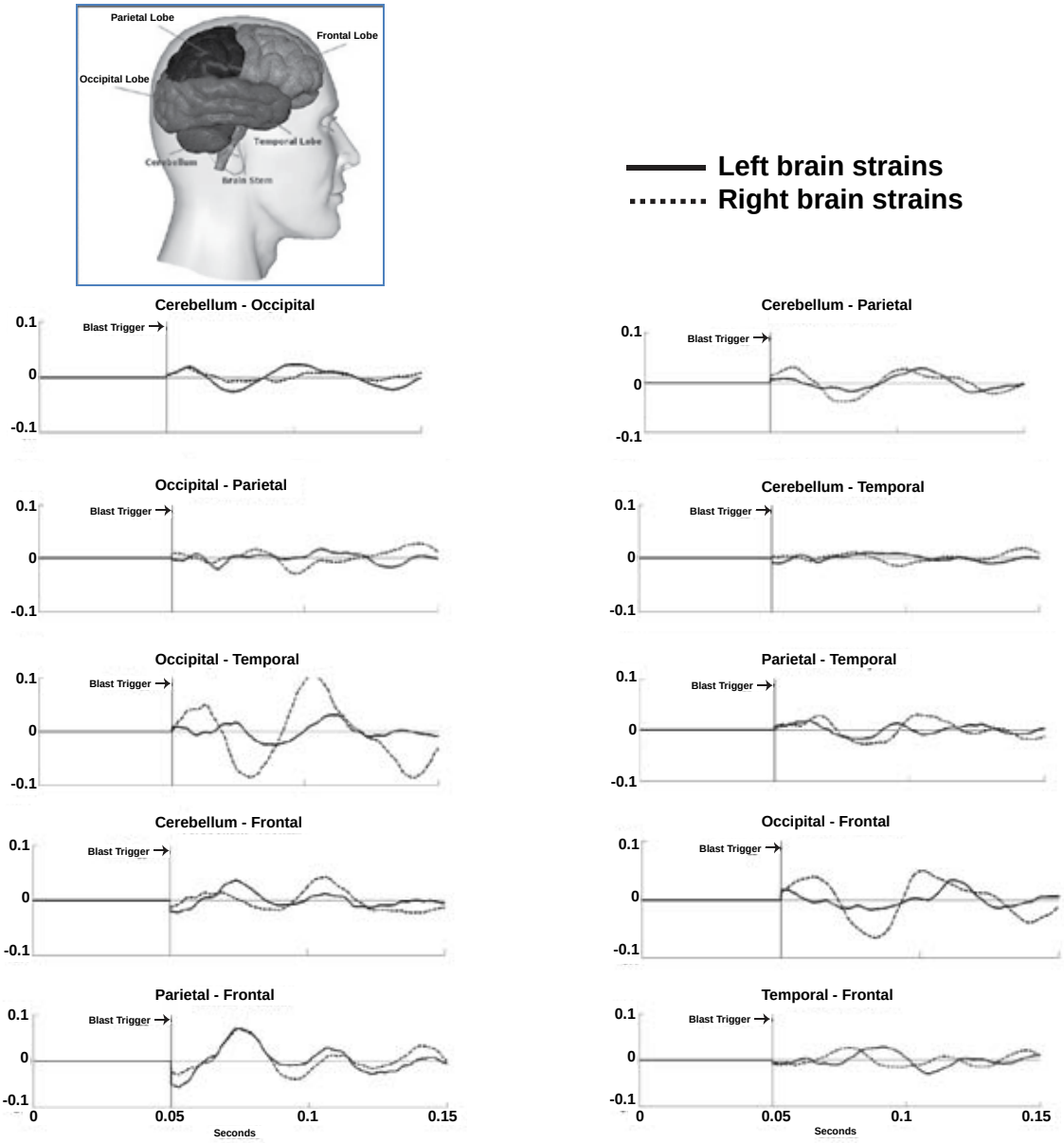

FIGURE 4
Calculated strain response from accelerometers in the brain from a C4 charge exploded at distance of 2.44 m from HSB.

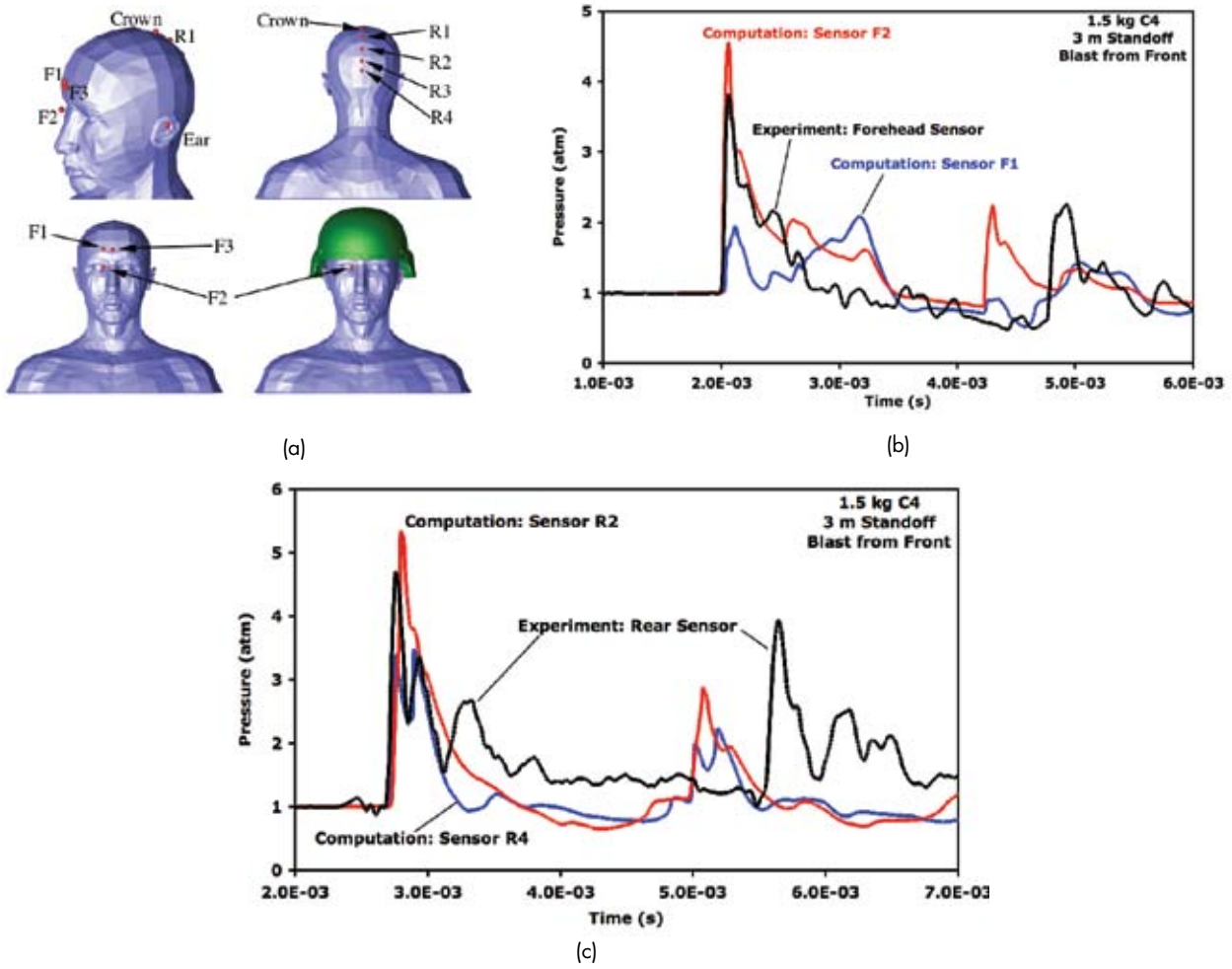

FIGURE 5
(a) Sensor locations for the computational data. (b) Forehead pressure traces for the forward blast scenario. (c) Rear pressure traces for the forward blast scenario.

Pressure histories on the front of the face are compared in Fig. 5(b). Two computational points — F1 just under the helmet and F2 just outside the helmet — are compared with the experimental data collected from the blast at F3, adjacent to F1. Computational results show that at F1 there is a considerable reduction of peak pressure compared with that at F2, exposed to the blast. Also, the experimental data at F3 seems to compare reasonably well with the computational data from F2. This suggests that there is a significant pressure infiltration between the helmet and the head.

Figure 5(c) shows the pressure histories at the back of the head, and an expanded view of the initial peaks for both experimental and computational data. Both the experimental and simulation results show a double peak at the onset followed by a third broader and shorter peak. This double peak occurs when two pressure waves, approaching from two directions, arrive at slightly different times. The computational analysis predicts a double peak formation at R4 from waves propagating around the sides of the helmet. At R2 (the experimental measurement point), the two waves traveling around the head arrive simultaneously, producing a significantly higher peak pressure at R2 than at R4. This is confirmed by computational and experimental data for R2, the point of highest pressure behind the head.

Based on these results and discussions with the Navy medical community and the Marine Corps, NRL developed an environmental helmet sensor (EHS). The EHS is designed to document the events such as blasts, impacts, and drops that occur on the battlefield. The goal is to be able to provide documented evidence for the medical community to correlate with brain damage.

NRL developed the first prototype EHS using a three-axis accelerometer, a triggering circuit, and new control algorithms. The EHS was designed to be mounted on the back of the helmet. NRL sent the prototype to Allen-Vanguard, a major manufacturer of explosives demolition protective suits, for further enhancements. Allen-Vanguard redesigned and rug-

gedized the EHS to survive battlefield conditions, and added a pressure sensor and software to download data for 500 events. The EHS is designed to measure acceleration up to 4000 g in three directions, ambient temperature, and peak pressure up to 17 atmospheres. It also distinguishes between blast and blunt trauma events, and has batteries and electronics designed for seven months continuous operation. Figure 6(a) shows the EHS mounted on a Marine Corps lightweight helmet (LWH).

Allen-Vanguard extensively blast-tested the EHS (see Fig. 6(b)). A three-axis accelerometer was mounted inside the Hybrid III head to record head acceleration. The experimental data from blasts and other tests were used to calculate equivalent integrated head acceleration as a TBI injury criterion, similar to Head Injury Criterion used by the automotive industry to measure severity of injury in a crash. This integrated head acceleration is a first approximation to quantify brain response for blast and other threats in terms of direction of the blast and its intensity based on helmet-mounted sensors such as the EHS.

Figure 7 shows the variation of integrated head acceleration with peak acceleration for blast tests, dropped helmets, ballistic hits, and various weapon firings. Nearly all non-blast events are well below the blast data, except the data for helmets dropped on concrete, which partially overlap the lower intensity blast data. The data clearly show the ability of the EHS to make the distinction between the different types of events — blast and non-blast types — and thus provide a valuable tool to the medical community to non-intrusively collect helmet acceleration and pressure data.

Thirteen months after the inception of the program, the EHS was transitioned to a viable product by NRL and Allen-Vanguard. The U.S. Army and Marine Corps have purchased thousands of EHS units, most of which are deployed in Iraq and Afghanistan.

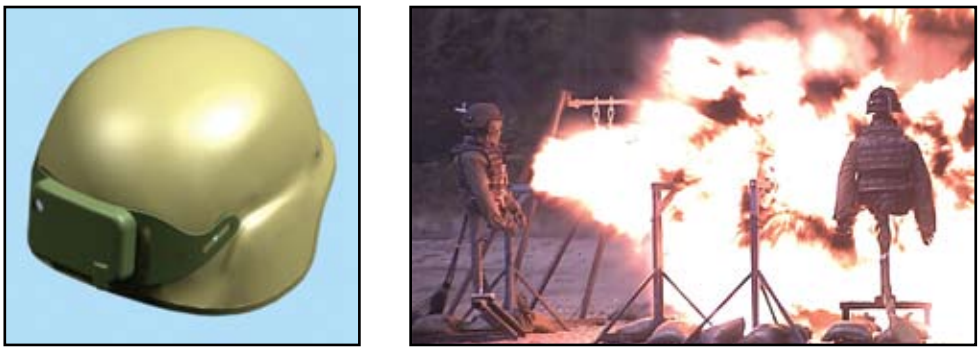

(a) (b)

FIGURE 6
(a) View of the helmet mounted system attached to a Marine LWH. (b) Blast testing of EHS mounted on LWH.

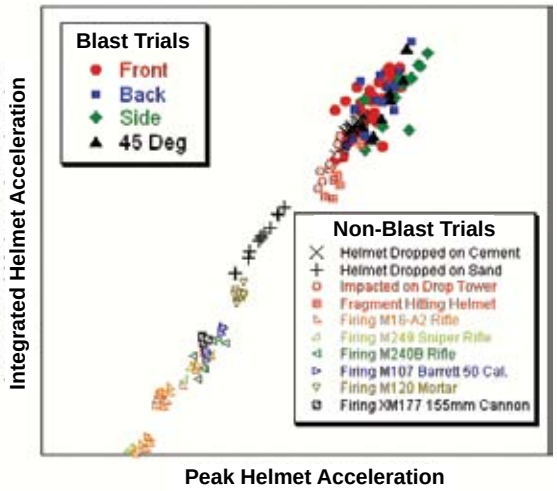

FIGURE 7
Variation of Helmet HIC with Peak Helmet Acceleration for different events in the theater.

The goal is for the correlation of data from these fielded units with cataloged injury reports to lead to validation of the helmet-mounted system while providing valuable data to help the medical community understand the cause(s) of TBI. Simultaneously, NRL and Allen-Vanguard have started development of a more compact second-generation EHS one-third of the weight of the first-generation EHS and mounted inside the helmet.

SUMMARY

This review presented two parallel efforts at NRL aimed at collecting battlefield data. The HSB is able to derive displacements and engineering strains from measured accelerations for the first time. The EHS, on the other hand, provides battlefield and other types of acceleration and pressure data non-intrusively. The combination of these data will augment the medical understanding of brain injury and provide a baseline for understanding and treating these types of injuries. The data will also be valuable in evaluating new energy mitigating materials and designs of helmet and liner systems.

ACKNOWLEDGMENTS

The authors thank J.P. Dionne, Jeff Levine, and Aris Makris from Allen-Vanguard; David Horner, John Gauvin, and Dirk Van Der Loo from Honeywell; Theodore R. Young of the NRL Laboratory for Computational Physics and Fluid Dynamics; Richard Pitre of Robtre Research LLC; Matthew Ford and Kevin Tores, summer student interns; and Doug Bueley and Terry Rohachuk from Allen-Vanguard. The authors appreciate the financial support from the Marine Corps Systems Command, the Office of Naval Research, and NRL. Our appreciation also goes to Rick Guilbeault, Don Wilson, Dean Newfer, and Brian Beard of the Canadian Explosives Research Laboratory.

[Sponsored by NRL and the Marine Corps Systems Command]

CMG:

Expanding Graphene Through Chemistry

Carbon used to be so plain, so ordinary, so common. In its two atomic forms based on chemical bonding, graphite (sp^2) and diamond (sp^3), it certainly has its charms, but it was largely ignored in its unalloyed states for high-tech applications until the discovery of stable, nanoscale structures starting with buckyballs (C_{60}) in 1985. However, how to cheaply mass produce C_{60}, also known as fullerene, remained a mystery. Then, when another even more usable form, nanotubes, was discovered in 1991, interest began to pick up again as the phenomenal properties of these atomic forms of carbon became apparent. Researchers began to speculate that if 1D layers of graphite appeared in balls and tubes, then a flat layer, which they dubbed graphene, must also be attainable. This was achieved in 2004, and since then, the race has been on to produce graphene in quantity at costs that would make it economically feasible for industrial applications. Chemically modified graphene (CMG) has emerged as a new form of graphene that can be manipulated to display some remarkable qualities previously unattainable in pure graphene. NRL researchers have developed a way to cheaply produce large-area, ultra-thin CMG films through which they can test its properties and also produce prototype electrical and mechanical devices. CMG can be fine-tuned to its specific application and has been used to produce sensors of extraordinary sensitivity, illustrating its potential as a key material for tomorrow's commercial and defense-oriented marvels.

Chemically Modified Graphene for Sensing and Nanomechanical Applications

J.T. Robinson, F.K. Perkins, and E. Snow
Electronics Science and Technology Division

M. Zalalutidinov, B.H. Houston, and J.W. Baldwin
Acoustics Division

Z. Wei and P.E. Sheehan
Chemistry Division

Chemically modified graphene (CMG) has emerged as a new material whose many attractive properties complement those of pure graphene. Graphene, a single atomic sheet of carbon bonded in a honeycomb lattice, has remarkable physical properties ranging from near-ballistic electron conduction to extremely high mechanical stiffness (more than five times that of steel). Such extreme properties motivate researchers to investigate these materials for use in applications ranging from high-frequency, low-power electronics, to flexible displays, chemical/biological sensors, and high-frequency electromechanical devices. We have developed a process to form large-area, ultra-thin CMG films that enable us to investigate CMG properties and to explore prototype devices. Using these films we have fabricated state-of-the-art chemical sensors and nanomechanical resonators. For chemical sensors, we have increased the sensitivity and reduced the level of noise by tuning the CMG film chemistry. These optimized sensors are capable of real-time detection of explosives and the three main classes of chemical-warfare agents at parts-per-billion concentrations. For nanomechanics, we have utilized chemical modification to produce suspended films under high tension. These high-stiffness, low-mass resonators display quality factors (up to 4000) and figures of merit well exceeding those of pure graphene resonators and are comparable to diamond thin films. Together, these results demonstrate that CMG is an inexpensive, high-performance material that will find application in a wide range of defense and commercial applications.

INTRODUCTION

Atomic carbon forms two primary structures, which are based upon sp^3 (diamond) or sp^2 (graphite) chemical bonding (Fig. 1). Of these, diamond is the less stable form and will transform into graphite when heated (Fig. 1(b)). The sp^2-graphitic structure currently dominates the world of carbon nanomaterials as it forms the full spectrum of low-dimensional geometries. For example, in its most compact stable form, sp^2-carbon arranges into a zero-dimensional (0D) structure known as a buckyball (Fig. 1(e)). By inserting rows of atoms around the equator of this buckyball, a one-dimensional (1D) carbon nanotube emerges (Fig. 1(d)). Finally, if this carbon nanotube is "unzipped" along its length, we have a flat, two-dimensional (2D) sheet known as graphene (Fig. 1(c)).

Interest in these low-dimensional carbon sheets began around 1985 with the discovery of buckyballs, but became mainstream after carbon nanotubes debuted in 1991. The newest member, graphene, created a resurgence of both scientific and technological interest after its discovery in 2004.[1] Electrons in graphene possess a unique "photon-like" dispersion relationship whereby they behave as massless particles. This phenomenon has led to the observation of unique electron transport phenomena, and has enabled researchers to use graphene as a laboratory for exotic quantum physics experiments. In addition, graphene's unique atomic structure, near-perfect electronic conduction, and extreme mechanical stiffness offer promise for a wide range of technological advances in the areas of electronics, electro-optics, sensors, and electromechanical devices.

Graphene Formation

For decades it was theorized that 2D solids were unstable and would melt at any temperature. This notion was disproved in 2004 when the first atomically thin graphene sheet was successfully isolated and studied.[2] In the few short years since then, a modern gold rush has transpired as researchers quest for a low-cost, high-yield production method. The simplest and most ubiquitous technique mechanically exfoliates graphene from bulk graphite, whereby graphite is rubbed across

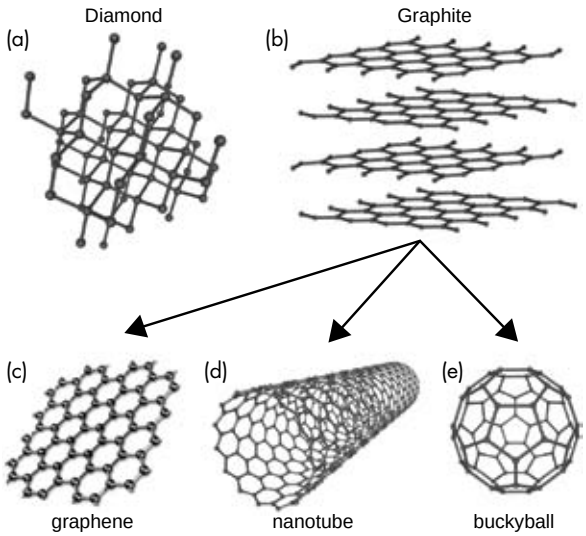

FIGURE 1
The two major allotropes of carbon are (a) sp^3-bonded diamond and (b) sp^2-bonded graphite. The sp^2-bonded allotrope is formable into three low-dimensional structures: (c) 2D sheets known as graphene, (d) 1D nanotubes, or (e) 0D buckyballs.

a flat substrate leaving behind small flakes, some of which are a monolayer thick. This random, low-yield approach precludes its use for large-scale production, though it continues to enable many interesting physics experiments. A second approach forms graphene epitaxially by heating SiC to >1400 °C in vacuum. At elevated temperatures, Si preferentially desorbs from the SiC surface, leaving behind carbon-rich layers that rearrange into thin graphene films. Technologically opposite from mechanical exfoliation, epitaxial graphene on SiC is large-area but expensive due to the high cost of SiC substrates.

A third approach, and that employed in this work, is chemical exfoliation of graphene from graphite. By attaching oxygen-rich functional groups to graphite's individual atomic planes, the planes become hydrophilic.[3] When immersed in water, H_2O molecules diffuse between these hydrophilic layers and completely exfoliate the graphene sheets (Fig. 2(a) and (b)). These oxidized platelets of graphene can be

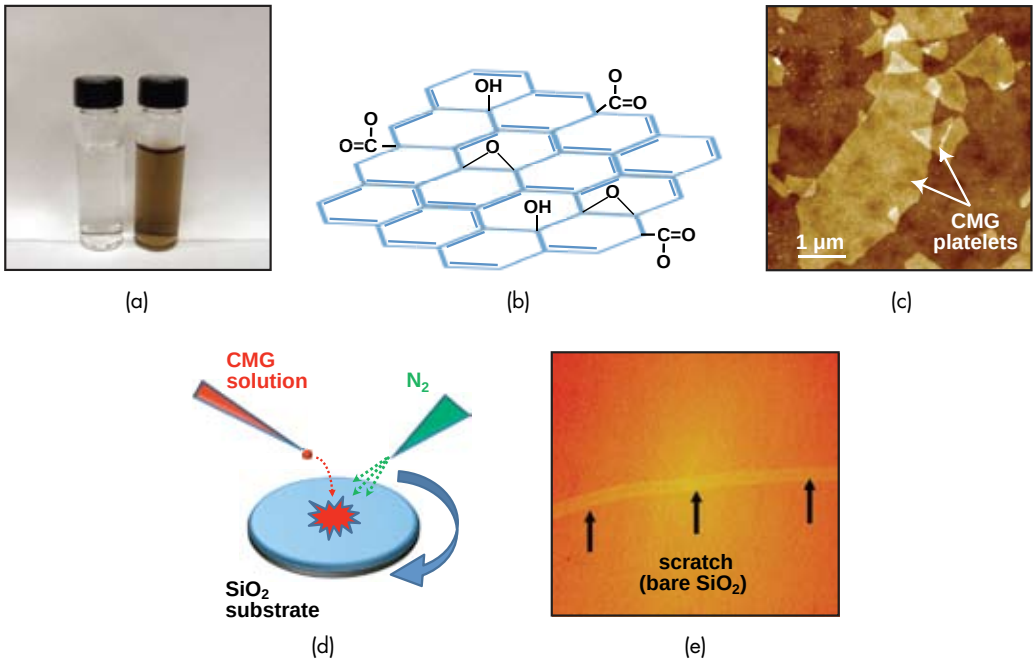

FIGURE 2
(a) Photograph showing a vial of pure water (left) and a mixture of exfoliated chemically modified graphene (CMG) platelets and water (right). (b) Cartoon showing oxygen functional groups on a CMG sheet, which include carboxyls, alcohols, and epoxides. (c) Atomic force microscope image of CMG platelets on a glass substrate. The platelets are approximately 1 to 1.5 nm thick. (d) Modified spin-casting technique developed at NRL for the large-area deposition of ultra-thin CMG films. (e) Optical microscope image (20x) of a continuous 2-nm-thick film. A scratch across the center reveals a slight color contrast between the substrate and film.

deposited onto almost any surface using a variety of benchtop techniques. The deposited oxidized graphene can subsequently be chemically reduced back toward graphene using chemical or thermal treatments to form stable films of chemically modified graphene (CMG). We have shown that the chemical modification alters graphene's electronic and mechanical properties in useful ways.[4] Figure 2(c) shows an atomic force microscope (AFM) image of deposited CMG platelets, which typically measure a few microns laterally and ~ 1 nanometer thick. At NRL we have developed a spin-casting technique to form continuous, ultra-thin, large-area CMG films at low cost (Fig. 2(d,e)). We have begun to investigate and develop these films for several DoD-relevant applications.

CARBON – THE ULTIMATE SENSOR MATERIAL

The detection of low-concentration, toxic, and explosive chemical vapors and gases is critical for the DoD and for homeland security. Due to their unique structure, in which every atom is a surface atom, sp^2-bonded carbon nanomaterials represent the ultimate sensor material. We previously developed single-walled carbon nanotube (SWNT) sensors capable of detecting chemical vapors at parts-per-billion concentrations,[5] although these sensors require somewhat sophisticated electronics to realize their full potential. We have found that CMG films can also serve as an extremely sensitive active material while requiring much simpler detection electronics.

Research into the sensing properties of carbon nanomaterials reveals that the transduction mechanisms by which molecular adsorption events are converted into electrical signals are often dominated by interaction with defects in the sp^2-bonded atomic structure. For many classes of molecules, the interaction with defect sites is often much stronger than with the relatively chemically inert sp^2-bonded carbon. Thus, controlling the number and type of defects can greatly enhance both sensitivity and specificity.[6] The optimal defect density will balance the gains in sensitivity against the rapid degradation in conductivity and increase in noise caused by the defects. In this regard, CMG is an ideal material for balancing these effects since it contains a variety of functional sites whose density is controllable.

An Atomically Thin Sensor

Figure 3(a) shows a typical experiment for testing the sensitivity of chemically modified graphene. We start with CMG thin films that consist of 1-nm-thick overlapping platelets. Using standard photolithography, we create interdigitated arrays of Ti/Au electrodes. Importantly, the oxygen functional groups on CMG are reduced chemically (e.g., with hydrazine, N_2H_4) or thermally (e.g., by annealing in H_2), providing a knob with which to tune the sensor response. These devices are then exposed to pulses of chemical vapors, and the resulting change in material conductance is measured.

Two important parameters are used to consider chemical sensor performance: (1) the level of low-frequency noise (which is generally dominated by $1/f$ noise) and (2) the sensitivity of the conductance response to molecular adsorbates. In general, the $1/f$ noise arises from fluctuations in carrier mobility or carrier density and is ubiquitous in solid-state devices. In the case of SWNTs, such fluctuations can arise from impurity charges in the substrate or the presence of defects within individual tubes. Here, the 2D planar geometry of graphene provides an inherent advantage over SWNTs. When two or more layers are present, the $1/f$ noise in graphene is strongly suppressed due to an effective screening of fluctuating charges in the substrate. Increasing the CMG film thickness to ~ 4 nm lowers the noise below background thermal limits (Fig. 3(b)). Figure 3(c)compares the responses of an SWNT device and a CMG device to doses of 500 parts-per-trillion DNT, a simulant for the explosive TNT. The low-noise response of the CMG device permits lower detection limits than a comparable SWNT device.

Interestingly, the chemical sensitivities of SWNT and CMG devices are complementary. Figure 3(d) compares the minimum detectable levels (MDLs) of SWNT and CMG devices for hydrogen cyanide (HCN) and simulants for mustard gas (CEES), sarin (DMMP), and TNT (DNT). These results highlight how different classes of molecules can distinctly interact with different surface sites — HCN weakly interacts with nominally pristine sp^2-bonded nanotubes while strongly interacting with remnant defects in CMG; the reverse is true for organophosphates (i.e., DMMP), and the responses to aromatics and alkane derivatives are similar (i.e., DNT and CEES, respectively). Enhancement of the specific oxygen functional group that interacts strongly with each simulant should allow even lower MDLs for CMG-based sensors and will enhance chemical selectivity.

CARBON – THE ULTIMATE ELECTROMECHANICAL MATERIAL

Nanoelectromechanical systems (NEMS) extend microelectromechanical systems (MEMS) to nanometer dimensions and are an exciting frontier for next-generation devices in sensing, RF technology, and computing. When NEMS resonators shrink below 100 nm, they achieve high operating frequencies (up to 10^9 Hz) with extreme sensitivities. Importantly, NEMS resonators already display extremely low mass sensitivities and are a viable route to parts-per-quadrillion

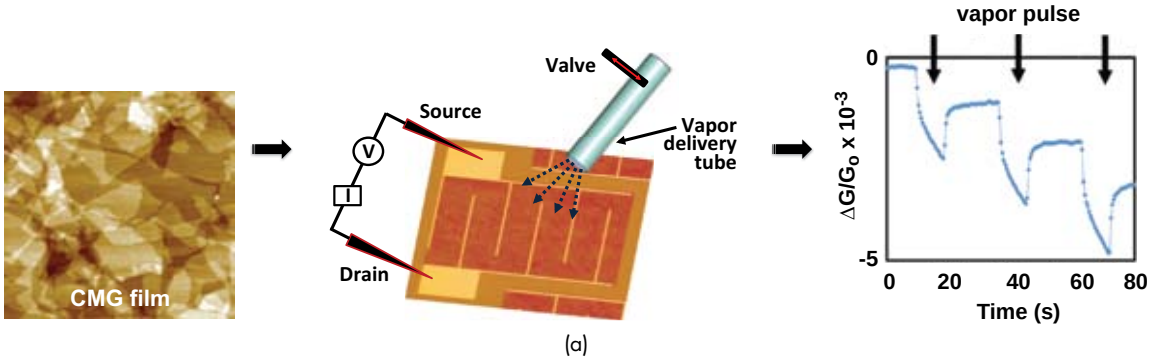

(a)

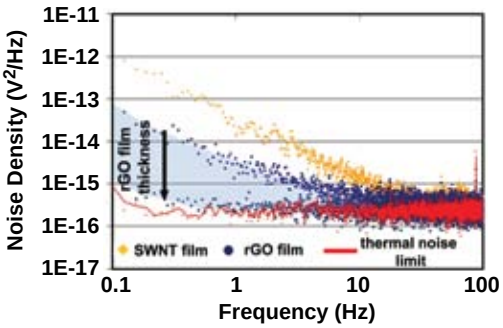

(b)

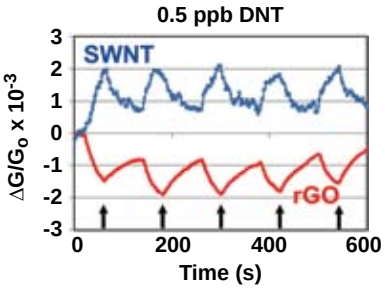

(c)

Simulant	SWNT: 10 s (ppb)	CMG: 10 s (ppb)	JCAD specifications ≤ 10 s (ppb)	CDC specifications (ppb)
HCN	>4,000	70	$2x10^6$	$5x10^4$ [a]
CEES	0.5	0.5	7,500	0.5 [b]
DMMP	0.1	5	170	17 [a]
DNT	0.1	0.1	——	——

[a] Immediately Dangerous to Life or Health (IDLH): ≤ 30 minutes does not cause death
[b] Threshold Limit Value (TLV): lifetime exposure without adverse health risk

(d)

FIGURE 3
(a) Approach for characterizing the sensing properties of CMG thin films. (b) Plot showing the noise density vs frequency spectrum for an SWNT device (orange diamonds) and two CMG (also known as rGO, reduced graphene oxide) devices with different film thicknesses (blue circles). (c) Response curves for an SWNT and a CMG (rGO) device to 0.5 parts per billion DNT. (d) Comparison of the minimum detectable level for an SWNT network sensor and a CMG network sensor to 10-second pulses of HCN, CEES, DMMP, and DNT, as well as the corresponding response to live agents using the target specifications for the Joint Chemical Agent Detector (JCAD) and exposure limits provided by the Centers for Disease Control (CDC).

chemical detection. For any NEMS system, the most important material properties are the Young's modulus, E, and density, ρ, which dictate the speed of sound in the material, c, and fundamental frequency, f_o, of the device, with $f_o \propto c = (E/\rho)^{1/2}$. Critically, of the many materials one might choose, carbon in the form of carbon nanotubes or graphene exhibits the highest E/ρ ratios.

One drawback to nanoscale resonators, however, is the tendency to lose mechanical energy at increasing rates, which results in low quality factors (Q) and diminished performance. For graphene-based systems, a reason behind this increased energy loss is poor adhesion of the resonator to its support structure. The sp^2-bonded carbon is fairly inert and adheres poorly to many substrates. Fortunately, chemically modified graphene offers a route to enhancing the performance of graphene-based NEMS since attached functional groups can better anchor the material to its surroundings.

An Atomically Thin Drumhead

To explore the incorporation of CMG materials into NEMS devices, we developed a process to transfer ultra-thin films (> ~4 nm) onto prepatterned substrates. Subsequent to film deposition as shown in Fig. 2, films are released intact from the substrate using a

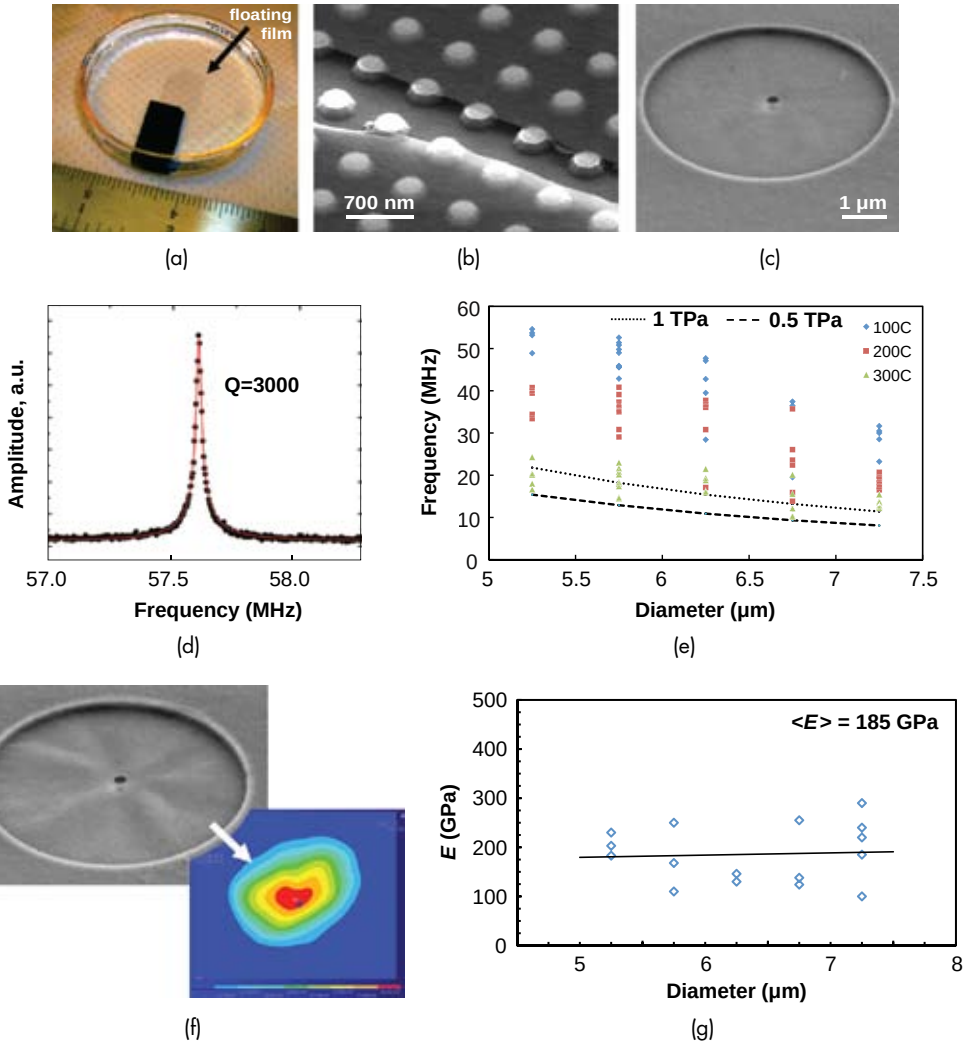

FIGURE 4
(a) Photograph showing an 8-nm-thick CMG film floating in water. The thin film measures approximately 1 × 0.5 inches. (b) Scanning electron microscope (SEM) image of a suspended CMG film after drying on a bed of pillars. (c) SEM image of a suspended CMG drum resonator with a small hole milled in its center. (d) Amplitude vs frequency plot of the fundamental mode, where the Q-value is 3000. (e) Plot of frequency vs drum diameter for a 15-nm-thick film. The resonators are annealed at successively higher temperatures to release tension. (f) Perspective SEM image of a buckled resonator after tension release and the expected frequency response determined from finite element modeling. (g) Plot showing the Young's modulus vs drum diameter for several drum resonators.

basic solution and transferred into water (Fig. 4(a)). These delaminated films are subsequently recaptured and dried on substrates prepatterned with pillars (Fig. 4(b)) or holes (Fig. 4(c)) to form suspended resonators. Importantly, the controlled deposition, delamination, and transfer of CMG films opens the door to numerous mechanical and nanoelectromechanical experiments.

To probe the elastic properties of these films, we use the well-established technique of laser interferometry to measure vibrations of the suspended drum resonators (Fig. 4(c)). A blue (412 nm) diode laser thermoelastically excites the CMG drums into resonance, while a red (633 nm) HeNe laser interferometrically measures the frequency of vibration in a Fabry-Pérot configuration. The fundamental frequency of vibration and overtone spacings depends on the tension (T) in the drums, which can act either as a plate ($T \approx 0$) or as a membrane ($T > 0$). Determination of Young's modulus (E) is straightforward when the drum responds in the plate mode. For a circular plate, the frequency modes are given by

$$f_{mn} = \frac{\pi h}{4 a^2} \sqrt{\frac{E}{3\rho (1 - s^2)}} (\beta_{mn})^2 \qquad (1)$$

where h is the film thickness, a is the drum radius, ρ is the material density, s is Poisson's ratio, and β_{mn} is the nth root of the mth-order Bessel function.

Unexpectedly, the measured f_o for all drum resonators is significantly higher than that expected from Eq. (1), which signifies the resonators are under tension. This built-in tension together with enhanced adhesion to the SiO_2 substrate from remnant oxygen groups notably improves the quality factors. Pure graphene resonators typically have Q-values of 10 to 200,[7] whereas our CMG resonators consistently show quality factors over 1500 (Fig. 4(d)), with 4000 the highest value measured to date. These values compare favorably with state-of-the-art diamond resonators, which typically have Q-values of ~3000 at room temperature. Combined with the extreme low mass of these resonators, we estimate their mass sensitivity at 10^{-18} grams.

Though the tension enhances the mechanical response of the resonators, extracting the Young's modulus requires removing the tension, which we accomplished through thermal annealing. Figure 4(e) shows f_o vs drum diameter for a 15-nm-thick film after annealing in argon at different temperatures. After annealing at 300 °C, the release of tension causes the originally flat drums to buckle, meaning the flat-plate approximation of Eq. (1) will not accurately describe the resonance response. To more accurately extract the Young's modulus, we use finite element modeling (FEM) instead (Fig. 4(f)). Figure 4(g) shows the FEM results after modeling 16 textured drums and reveals that the modulus averages 185 GPa, which is approximately the same as steel.

SUMMARY AND OUTLOOK

Our work with chemically modified graphene demonstrates the versatile nature of this material system. At NRL we have developed a low-cost, large-area deposition technique in which thin films are readily fashioned for both electronic- and mechanical-based devices. Not only do these films show promise as the active area of conductance-based chemical sensors, their large stiffness and low density make them feasible for use in nanomechanical systems also. For sensing applications, the relatively large number of chemically active groups affords the possibility of covalent chemical functionalization for increased chemical or biological selectivity. The nanomechanical experiments point to the exciting opportunities afforded by chemically modifying sp^2-bonded carbon to form hybrid sp^2–sp^3 interbonded materials that exhibit both strength and processability. Indeed, we foresee a bright future for graphene-based technologies.

ACKNOWLEDGMENTS

We thank Konrad Bussmann and Doe Park for advice and assistance with the drum resonator fabrication. This work was partially supported by the Office of Naval Research.

[Sponsored by NRL]

References

[1] A.K. Geim and K.S. Novoselov, "The Rise of Graphene," *Nature Materials* **6**(3), 183–191 (2007).

[2] K.S. Novoselov et al., "Electric Field Effect in Atomically Thin Carbon Films," *Science* **306**(5696), 666–669 (2004).

[3] S. Stankovich et al., "Synthesis of Graphene-based Nanosheets via Chemical Reduction of Exfoliated Graphite Oxide," *Carbon* **45**(7), 1558–1565 (2007).

[4] J.T. Robinson et al., "Reduced Graphene Oxide Molecular Sensors," *Nano Letters* **8**(10), 3137–3140 (2008); J.T. Robinson et al., "Wafer-scale Reduced Graphene Oxide Films for Nanomechanical Devices," *Nano Letters* **8**(10), 3441–3445 (2008).

[5] E.S. Snow et al., "Chemical Detection with a Single-Walled Carbon Nanotube Capacitor," *Science* **307**(5717), 1942–1945 (2005).

[6] J.A. Robinson et al., "Role of Defects in Single-Walled Carbon Nanotube Chemical Sensors," *Nano Letters* **6**(8), 1747–1751 (2006).

[7] J.S. Bunch et al. "Electromechanical Resonators from Graphene Sheets," *Science* **315**(5811), 490–493 (2007).

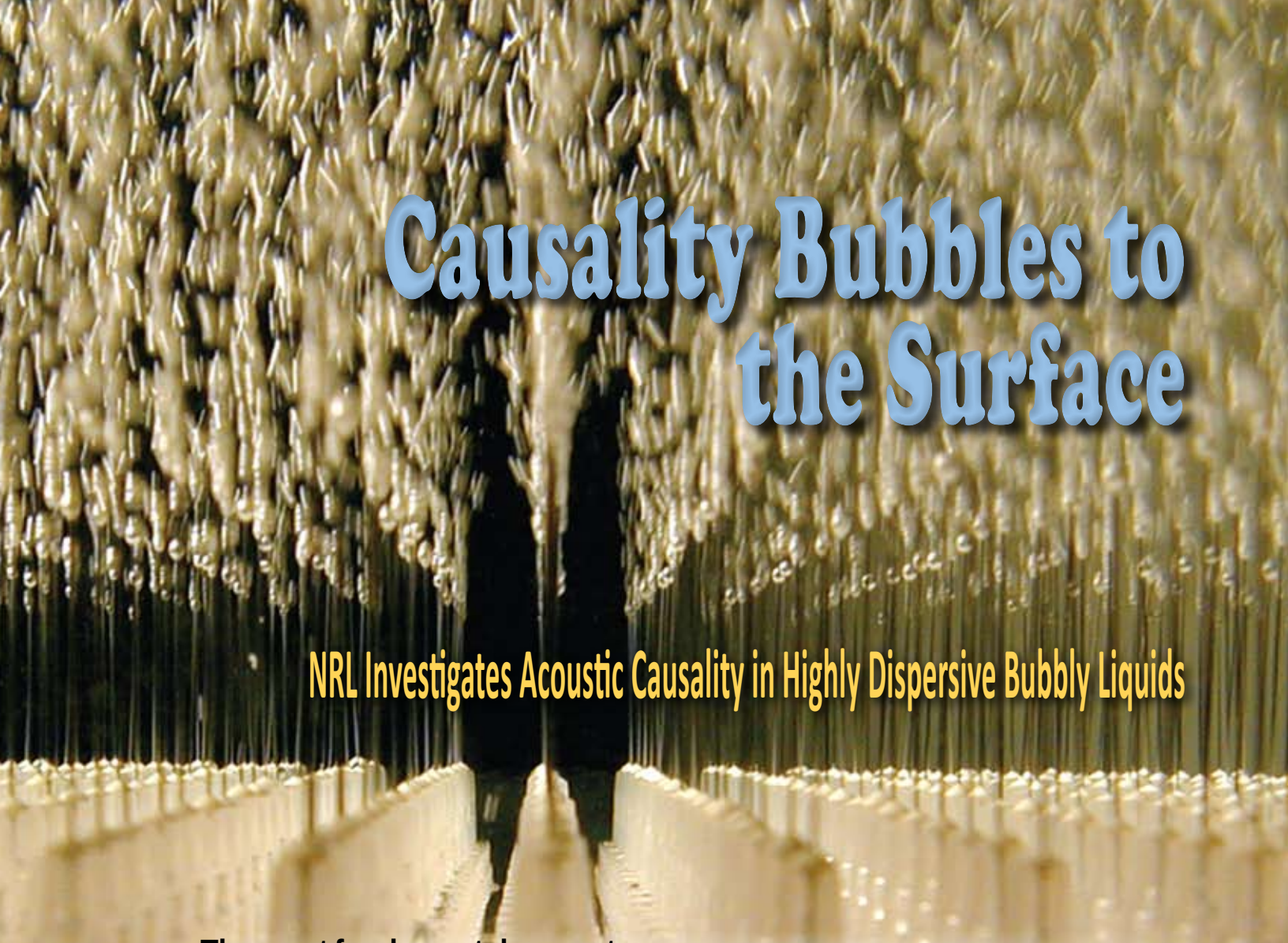

Causality Bubbles to the Surface

NRL Investigates Acoustic Causality in Highly Dispersive Bubbly Liquids

The most fundamental property exhibited by any physical system is causality: in essence, cause must precede effect. The modern interpretation of causality sprung forth from Albert Einstein's classic, yet at the time of its publication controversial, work on Special Relativity, wherein he postulated that the travel time of any signal cannot exceed the speed of light in a vacuum. The same underlying physical and mathematical principles pioneered by Arnold Sommerfeld and Léon Brillouin nearly a century ago that were used to quell Einstein's critics and prove his assertions continue to provide essential and intriguing insights into scientific phenomena of vital importance to the U.S. Navy: acoustic propagation through highly dispersive subsurface bubbles and bubble clouds in the ocean.

Since the commissioning of NRL's unique Salt Water Tank Facility in the late 1990s, NRL scientists have conducted many experiments designed to investigate different aspects of acoustic propagation in bubbly liquids. One of the major accomplishments of this facility in 2008 provided experimental verification of an important correction to contemporary theories of acoustic propagation in bubbly media. This correction has resulted in a causal self-consistent theory verified by both higher frequency data taken in the Salt Water Tank Facility and historical data. Further observations have elucidated some additional features that have significant implications upon acoustic signal propagation and suggest that despite many decades of scientific investigation, we have only begun to sketch out a comprehensive description of the physical phenomena surrounding acoustic propagation in the strongly scattering highly dispersive environment of bubbly media.

Investigating Acoustic Causality in Highly Dispersive Bubbly Liquids

G.J. Orris, M. Nicholas, and D.K. Dacol
Acoustics Division

Causality in nearly all physical systems has been a recurrent subject, often causing apparent paradoxes since before the 20th century. Linear acoustic propagation through subsurface bubble clouds in the ocean offers an especially challenging physical system within which to investigate issues of causality, and in the past has had several competing fundamental theories. Signal travel times and absorption in such a system exhibit enormous variations depending on the acoustic signal frequency, bubble size distribution, void fraction, and other ambient physical parameters. We have found a correction to some contemporary theories of acoustic propagation in bubbly media that has brought these theories into compliance with the physical law of causality. In doing so we have created a self-consistent theory that also matches higher-frequency data taken in the NRL Salt Water Tank Facility, as well as historical data. We have experimentally investigated this new theory and have observed some additional features that have significant implications upon acoustic signal propagation and suggest that we have only begun to scratch the surface of providing a comprehensive description of the physical phenomena surrounding acoustic propagation in the highly dispersive environment of bubbly media.

INTRODUCTION

Einstein's postulate that no physical process can travel faster than the speed of light was disputed by several leading physicists shortly after its publication. The main objection to the theory was based on studies of existing dispersive metal compounds with measured values for their phase velocities, where the derived group velocities were greater than the velocity of light in a vacuum.[1] The erroneous assumption in the argument against Einstein's postulate was based on the original work of Stokes that stated the group velocity, $\partial\omega/\partial k$, determined the velocity of propagation of wavelike signals in any medium. The argument used to object to Einstein's postulate neglected two important and omnipresent suppositions. The first supposition was that any signal that can send information is by necessity of finite length and, therefore, of infinite frequency extent. The second supposition was concerned with the experimental system, based on the interaction of electromagnetic waves with metals, which generated the data that were used to counter Einstein's postulate. This system had a significant degree of dispersion and a highly frequency-dependent dispersion function. This manifests itself within the model of electrons in metals, which at that time were considered to behave classically as damped harmonic oscillators.

These two points and their physical implications were pointed out in a now classic set of companion papers published in 1914 by Sommerfeld and Brillouin that laid the theoretical groundwork for countless developments in physics, information theory, and engineering throughout the 20th century.[2,3] Their resolution to the neglected suppositions was based on a detailed analysis of the definition of a wave pulse of finite length and the signal's frequency content for a wave travelling in a dispersive medium. Using the theory of complex analytic functions, they observed that the dispersion formula, and, hence, the Fourier integral defining the wave pulse at a future time and position separated from the origin of the pulse, could be shown to be analytic in the upper half complex frequency plane. Thus it could be demonstrated that all electromagnetic signals are undetectable until at least such a time $t = x/c_0$ has elapsed, where x is the distance from source to receiver, and c_0 is the velocity of light in a vacuum in the infinite frequency limit. Due to the nature of the medium, instrumentation of infinite precision might be needed to detect the incoming signal moving at that velocity for a given dispersive medium and pulse carrier frequency. This requirement of analyticity led Kramers and Krönig to separately derive their now famous relation between the real and imaginary parts of the dispersion formula.

From the standpoint of acoustic wave propagation in any fluid, bubbles represent one of the strongest, most ubiquitous, and complex extinction mechanisms. These mechanisms can be modeled in much the same

way as the semi-classical electrodynamics systems used to model the propagation of electromagnetic waves in metals. Thus we are naturally led to ask if there is an equivalent theory of causality, or in effect a "speed limit," of acoustic waves in a continuum mechanical system, e.g., dispersive bubbly media, to that of the electromagnetic case first investigated over 100 years ago. Understanding the complex dynamics of bubbles and the acoustic interaction with a bubble field is a necessary first step in trying to model and measure the propagation of an acoustic signal in or near a bubbly medium or when creating new acoustic devices using bubbles.

The ubiquity of bubbles in the ocean can be imagined by noting that a single plunging breaker at the ocean surface can generate hundreds of millions of bubbles. While many of these bubbles are relatively large and rise quickly to the surface where the bubble wall collapses and the bubble ceases to exist, a significant fraction of the bubbles are relatively small, with average radii typically between 20 and 50 μm. These small bubbles have a small buoyancy and can be mixed into the upper surface of the ocean to form larger clouds that can persist for many seconds and be forced down to depths of 20 m or more by circulation cells. The clouds typically have complex shapes and population densities with horizontal scales from 1 to 100 m.

We are thus left with the following complex picture of acoustic wave propagation in the upper ocean: the acoustic medium is itself a semi-regular collection of clouds with complex time-dependent spatial extent. Not only does each bubble interact with an incoming acoustic wave approximately as a damped harmonic oscillator, but the injection of a gas into the liquid fundamentally changes the compressibility of the medium in and near the bubble/bubble clouds. This changes the acoustic phase velocity in and near the clouds, causing them to become effective scatterers/resonators and in so doing, provide for a broader range of scattering scale sizes. Complicating the picture even further is the fact that the phase velocity and associated medium attenuation are highly dependent on the incident wave frequency in a nontrivial and nonlinear way that causes significant dispersion to occur. Thus it is imperative that the dispersion and the fundamental limits that causality places upon any theory of wave propagation in a dispersive bubbly acoustic medium be understood in full.

SINGLE BUBBLE OSCILLATIONS

Physically, a bubble exists because of the molecular/atomic effects of surface tension at an interface between two fluids. While large bubbles in water often exhibit large fluctuations in the shape of this interface as they are deformed due to nonuniform surface drag forces in their eventual rise towards the surface, the majority of oceanic bubbles (particularly those that persist) are small, and small radial pulsations about an equilibrium value are by far the most significant mode of oscillation of the bubble interface. Furthermore, it has been experimentally demonstrated that even extremely deformed bubbles radiate acoustic energy very much as though they were spherical, and undergoing a small radial oscillation. Thus, the acoustic signature and natural frequency of oceanic bubbles can be well approximated as small radial pulsations alone governed by the Rayleigh-Plessett equation,[4,5]

$$\left(1-\frac{1}{c_0}\frac{dR}{dt}\right) R\,\frac{d^2R}{dt^2}+\frac{3}{2}\left(1-\frac{1}{3c_0}\frac{dR}{dt}\right)\left(\frac{dR}{dt}\right)^2 = \frac{1}{\rho}\left(1+\frac{1}{c_0}\frac{dR}{dt}+\frac{R}{c_0}\frac{d}{dt}\right)(p_B-P)$$

where c_0 is the phase velocity of sound in a quiescent medium, $R(t)$ is the radius of the bubble as a function of time, p_B is the static equilibrium pressure inside the bubble given by the static quiescent pressure external to the bubble and the Laplace pressure $p_L = (2\sigma)/(R_0)$, and $P(t)$ is the driving external pressure (acoustic) field. Since the Laplace pressure is inversely proportional to the radius of the bubble, it can have a substantial impact on the dynamics of small bubbles. This added pressure also causes the smaller bubbles to dissolve into the solution at an ever-increasing rate, as the leakage of the entrapped gas into the liquid is a strong function of the internal bubble pressure. This causes the bubbles to become smaller yet, increasing the internal pressure even more, and hastening their dissolution. The second effect is that the bubble's natural frequency is modified as the bubble becomes effectively stiffer, effectively increasing the apparent resonance frequency. The Rayleigh-Plesset equation results in additional first-order terms in the radial deflection that are complex and thus result in energy dissipation.

The second dissipative effect on the acoustic field when it encounters a bubble is the liquid's viscosity. The forced oscillations of the bubble wall necessarily deform the liquid around the bubble wall. A volume element of liquid near the bubble wall will deform as the bubble expands and contracts, becoming thicker with less solid angle upon contraction and thinner with larger solid angle upon expansion. Energy in the process is not conserved, as all deformations of a volume element of a viscous liquid demand work. For general small radial oscillations, the associated dissipation can be shown to result in a damping term of the form $4\pi\mu$, where μ is the dynamic coefficient of viscosity of the liquid.[6]

The third dissipation mechanism of bubble dynamics is the thermodynamics of the heat generated as a byproduct of expansion and contraction of the gas trapped in the bubble volume. This heat is conducted from the internal vapor into the greater liquid thermal bath (ocean). Early bubble acoustics either assumed that the bubble oscillated in either an isothermal or adiabatic process depending on the frequency of ensonification. However, the actual heat transfer is significantly more complicated and has far-reaching consequences for acoustic propagation in a bubbly liquid. Since the heat conduction takes some time to travel to and from the bubble wall, there is a phase delay between the total pressure field and the bubble radius (or, equivalently, volume). If it is assumed that the internal bubble gas can be treated as a polytropic gas, then for small linear radial oscillations, the bubble radius can be considered to have a form of $R(t) = R_0\,(1 + X(t))$, where $X(t)$ is a dimensionless small harmonic perturbation. The pressure can then be given similarly as $P(t) = P_0\,(1 + \Phi X(t))$, where the factor Φ is a complex function of the frequency, the equilibrium bubble radius, the ratio of specific heats of the bubble gas, and the diffusivity of the bubble gas through[6,7]

$$\Phi(\omega, R_0) = \frac{3\gamma_g}{1+3(\gamma_g-1)i\chi(\omega,R_0)\left[\sqrt{1/i\chi(\omega,R_0)}\coth\left(\sqrt{1/i\chi(\omega,R_0)}\right)-1\right]},$$

$$\text{where } \chi(\omega,R_0)=\frac{D_g}{\omega R_0^2} \text{ and } D_g=\frac{(\gamma_g-1)\kappa_g T_g}{\gamma_g p_\infty},$$

where the subscripts "g" refer to the gas phase and p_∞ is the quiescent pressure minus surface tension effects.

FROM THE ACOUSTICS WITH A SINGLE BUBBLE TO THE ACOUSTICS OF A CLOUD

The transition from a single bubble to a collection of bubbles follows along that of the two-phase fluid. This results in a generalized wave equation for the pressure in the liquid phase with an added term involving the expansion and contraction of the bubbles, represented as a total change in macroscopic void fraction,[8]

$$\frac{1}{c^2}\frac{\partial^2 P}{\partial t^2}-\nabla^2 P=\rho\frac{\partial^2\beta}{\partial t^2},$$

where β is the void fraction of the gas in the liquid and ρ is the density of the liquid. When the bubble field can be regarded in an isotropic and homogeneous system, then $\partial^2\beta/\partial t^2$ can be determined from the linearization of the Rayleigh-Plesset equation with the added effects of viscosity, surface tension, and finite conductivity of the bubble gas. This effective medium approach presents itself as a modified dispersion formula relating the wavevector to all of the physical parameters, and is necessarily a complex function reflecting the dissipation,[9]

$$k_{cm}^2=\frac{\omega^2}{c_0^2}\left(1+4\pi c_0^2\int_0^\infty dR_0\,\frac{R_0\rho_{BSD}(R_0)}{\frac{p_0\Phi(\omega,R_0)}{\rho R_0^2}-\frac{2\sigma}{\rho R_0^3}-\frac{\omega^2}{1-i\frac{\omega R_0}{c_0}}-i\frac{4\omega\mu_0}{\rho R_0^2}}\right)$$

where ρ_{BSD} is the bubble size distribution and ω is the radial frequency of the driving acoustic wave. Here it is evident that there are a significant number of physical parameters that affect acoustic wave propagation in bubbly water and that even this theory represents only a linear approximation to the physical reality. How faithful this treatment of the problem is, whether the behavior that this theory predicts represents a true system that is causal, and what theoretical predictions can be detected in the laboratory have been the focus of research at NRL's Salt Water Tank Facility, shown in Figs. 1 through 3.

At very low frequencies, the system becomes isothermal and the effect of the injection of a gas into the liquid can be grossly regarded as a change in the system's mean compressibility and mean density that result in Wood's equation for the phase speed of the combined liquid. The air (gas) phase in the two-phase fluid has a high degree of compressibility compared to the liquid. In the case of water, this ratio is approximately 10^4. However, the mass density ratio is approximately 10^{-3} and thus is not changed significantly by the inclusion of small amounts of gas. This combination frequently results in an acoustic phase speed that can be significantly lower than that of the gas alone.

If the bubble size distribution is relatively sharply peaked, then there is a frequency regime that can be identified with the resonance of a sizable portion of the bubbles. This is manifest as a dip in the phase speed curve to values even lower than that given by Wood's equation in the low frequency limit. Because the bubbles are now responding via the Rayleigh-Plesset equation as a damped resonating harmonic oscillator, the bubble pulsations and, hence, the total radial deflections maximize. As this occurs, the volume fluctuations maximize and, hence, thermal dissipation becomes a significant loss mechanism.

Just above the resonance frequency we enter the anomalous absorption regime where all of the loss mechanisms, viscous, thermal, and radiative (scattering), are significant. This area is characterized by three

FIGURE 1
Exterior view of the Salt Water Tank, with a small bubbler test tank on the left. The main tank measures 6 m x 6 m x 4 m deep, although typical water depth is 3 m. The interior of the tank has 50 precision-controlled air-flow ports to allow for various air injection mechanisms to be arranged for each experiment. Barely visible at the far left is the salt mixing tank used to mix salt into the main tank to any desired level of salinity. Visible through the Plexiglas windows of the large tank is an ITC2010 acoustic source, used for much of the experimental data below 10 kHz.

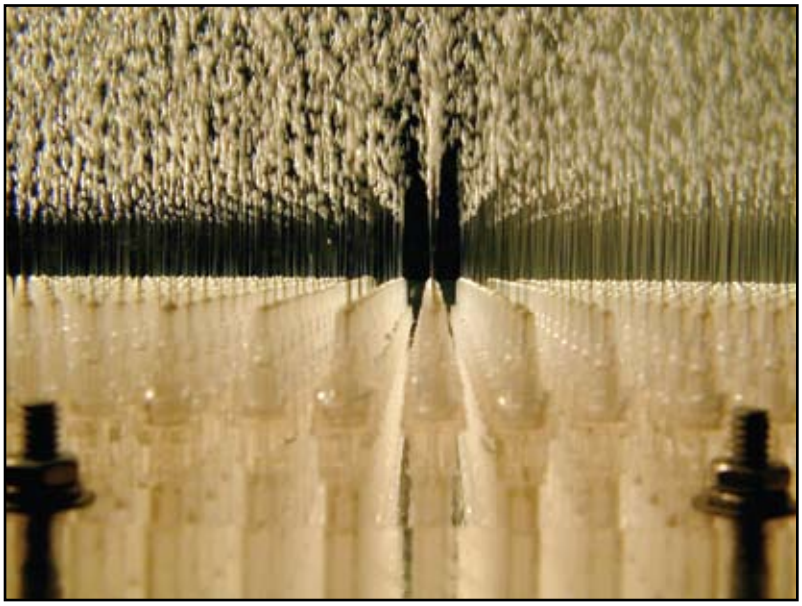

FIGURE 2
Precision bubbler. This bubbler consists of 3000 luer-lock square cut hypodermic needles glued into a 2.5-cm-thick Plexiglas sheet. This sheet is bolted over a plenum box weighted to be nearly neutrally buoyant. Since the pressure is nearly identical over all needles, the rate of bubble formation and size of bubbles is close to uniform.

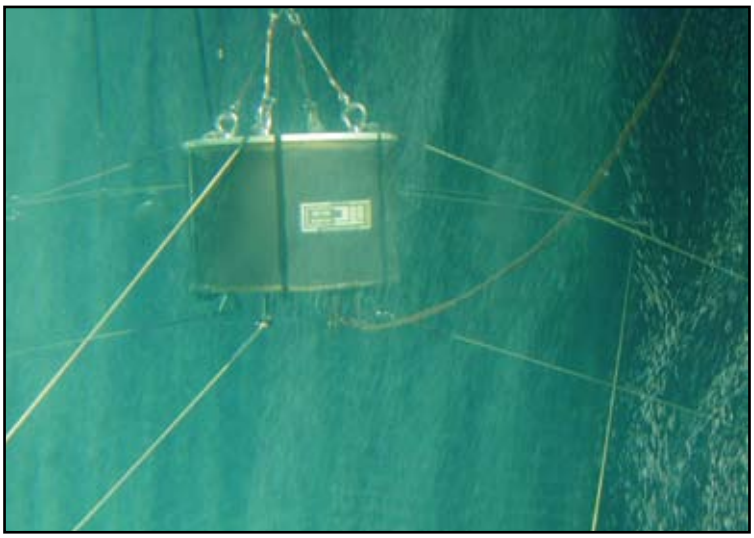

FIGURE 3
An ITC2010 acoustic source tethered in a bubble cloud produced by aeration tubes (which generate a log-normal bubble size distribution). Much of the data is collected under similar conditions to these. Here the void fraction is only 0.001 with a mean bubble radius of only 0.4 mm. Note that the ascent of so many bubbles drags enough fluid upwards to cause the source to move, and hence it is lashed to the side of the tank throughout our experiments: precise phase measurements can be made only when the source and receiver positions are well known. Typical data collection times can exceed a week for each set of physical parameters (temperature, salinity, void fraction, etc.).

dominant features. The first is the rise of the absorption to very high levels that can approach hundreds of dB/m for void fractions even as small as 10^{-4}. The second feature is a similar rise in the acoustic phase speed that can be tens of thousands of meters per second for similarly small void fractions (10^{-4}). This is due to the bubble's resonant frequency beginning to oscillate out of phase with the incident acoustic wave driving the small radial oscillations. As such, the medium stiffens considerably with respect to the phase speed. The third major feature is the significant departure of the acoustic signal velocity from the acoustic group velocity. The group velocity, as a quantity derived from behavior of the phase velocity, eventually passes through infinity to negative infinity and back: clearly the wave propagation velocity can no longer be approximated by the group velocity and we must rely on a complicated determination of the signal's velocity.

Far above resonance, the velocity of the signal asymptotes with both the group velocity and phase velocity to the quiescent medium's speed of sound. Furthermore, the attenuation becomes effectively constant with frequency, signifying the dominance of scattering as the loss mechanism at high frequencies. Here the wavelength of the incident acoustic field in the medium between the bubbles becomes significantly less than the size of the typical bubble.

CAUSALITY AND THE ACOUSTIC SIGNAL VELOCITY

If the dispersion formula as stated above is used directly to calculate the phase speed, attenuation, and group velocity of an acoustic pulse in a bubbly liquid, then the problems seen a century ago by Sommerfeld and Brillouin are essentially repeated, albeit with a significantly more complex dispersion formula. The bubbly liquid dispersion formula can be shown to be analytic in the upper half complex frequency plane. Thus, Cauchy's integral theorem trivially proves causality, as the Fourier integral describing the propagation of an acoustic pulse is zero for times less than x/c_0. To determine the behavior of the signal as a function of time for times equal to or greater than this, the behavior of the dispersion formula in the complex frequency plane must be determined in detail, and in general the saddle point method can be used to determine the propagation characteristics as a function of time. This is because the lower half complex plane contains several branch cuts that must be included in any calculation.

An example of a typical integration path using this method is shown in Fig. 4. As in the electromagnetic case, there are three different phases of an incident signal's arrival: the Sommerfeld precursor, the Brillouin precursor, and the signal. The first two are dependent upon the behavior of the dispersion function in the complex plane near the point at infinity and the origin, respectively, and hence are independent of the source characteristics (i.e., frequency).[2,3,9] The actual signal arrival is determined by the crossings of the saddle point integration path (which is a function of time, distance, and the physics of the propagation medium) with the abscissa. If a portion of the signal's spectrum exists at this crossing, then there will be a simple pole in the Fourier integral, requiring an altering of the integration path around the pole to exclude it from the integration region. The consequences of this are a dominating contribution to the integral at that point and the arrival of energy with that frequency.[9]

EXPERIMENTAL EFFORT IN THE SALT WATER TANK FACILITY

Since the surface tension of water is affected by the presence of salt, the bubble size distribution found in saline environments is different from that found in

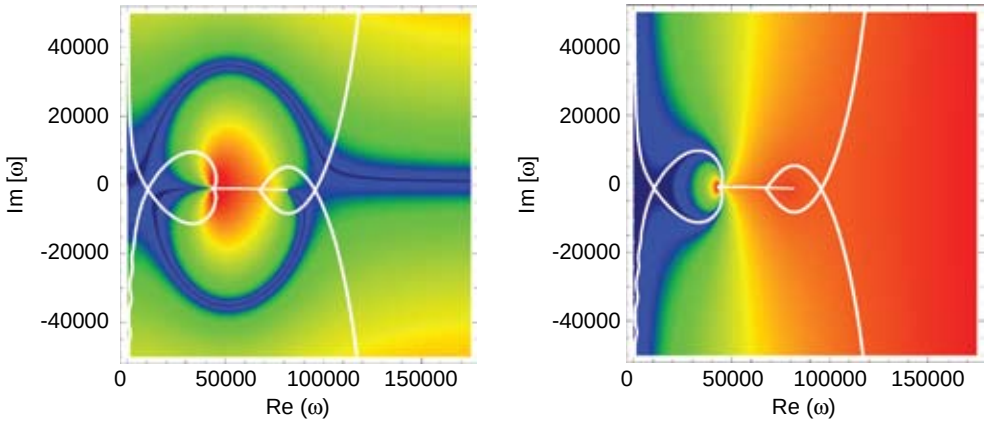

FIGURE 4
Real (left) and Imaginary (right) density plots of the complex phase function in the complex frequency domain. The Saddle Point Method of calculation of the Fourier integral defining the signal as it travels in time and space is determined by the shape and value of the functions shown here. The white loops around the branch cuts are the paths of integration for a specific time and distance from the source. Frequencies on the real axis that are intersected by the curves can have arrival times at distance x, thus defining the signal velocity of that frequency.

fresh water. However, the violent nature of the bubble entrainment mechanisms found in the open ocean tends to break up larger bubbles until the external turbulent forces no longer have sufficient force to overcome the surface tension. The Salt Water Tank Facility (SWTF) at NRL (see Figs. 1 through 3) was specifically constructed to test acoustic propagation in bubbly salt water to fully verify and validate theoretical predictions of acoustic wave propagation in bubbly water relevant to oceanic environmental conditions.

The SWTF consists of a vinyl-coated steel walled tank measuring 6 m × 6 m × 4 m deep, with 12 clear Plexiglas windows in the tank walls, each window being 3 m × 1-1/2 m × 10 cm thick. Within this tank, we used 50 fabric-coated aeration tubes, each one 5 m long, placed 10 cm apart on the tank floor and fed from both ends by a filtered compressed air supply. These tubes continuously injected bubbles of a wide size distribution into the water volume, which would then rise to fill almost the entire volume of the tank. Depending on the air overpressure applied to the aeration tubes, the tank would contain from 7 to 70 million bubbles, which translates into void fractions of between 0.0002 and 0.002. At the center of the water volume we then used acoustic transducers to transmit narrowband acoustic signals, which we would then detect on hydrophones positioned at precisely measured distances from the sources. The time of flight and received intensity were measured directly from a comparison of the data recorded at a monitoring hydrophone placed next to the source and those recorded at the various receivers. The absolute phase of the signal's carrier frequency at the receiver can be inferred from the data and the phase velocity thus determined. Comprehensive acoustic data sets were collected for several void fractions between 0.0002 and 0.002, multiple salinities, and covering frequencies from 1 kHz (which is far below bubble resonance) up to 100 kHz (which is far above bubble resonance) in 100 Hz increments. Coincidentally, an underwater camera was used to capture bubble images alongside a calibration scale, and these were later used to generate numbers for the bubble size distributions, and to verify the void fraction measurements made from air flow meter and bubble rise time measurements.

[Sponsored by ONR]

References

[1] A. Sommerfeld, "Ein Einwand gegen die Relativtheorie der Elektrodynamik und seine Beseitigung," *Physikalisehe Zeitschrift* **8**(21), 841 (1907).

[2] A. Sommerfeld, "Über die Fortpflanzung Des Lichtes in dispergierenden Medien," *Annalen der Physik* **44**(4), 177–202 (1914).

[3] L. Brillouin, "Über die Fortpflanzung Des Lichtes in dispergierenden Medien," *Annalen der Physik* **44**(4), 203–240 (1914).

[4] Lord Rayleigh, "On the Pressure Developed in a Liquid during the Collapse of a Spherical Cavity," *Philosophical Magazine* **34**(199-04), 94–98, Jul-Dec 1917.

[5] M. Plesset, "The Dynamics of Cavitation Bubbles," *Mechanics-Transactions of the ASME* **16**(3), 277–282 (1949).

[6] J.C. Devin, "Survey of Thermal Radiation and Viscous Damping of Pulsating Air Bubbles in Water," *J. Acoust. Soc. Am.* **31**(12), 1654–1667 (1959).

[7] A. Prosperetti, L. A. Crum, and K. W. Commander, "Nonlinear Bubble Dynamics," *J. Acoust. Soc. Am.* **83**(2), 502–14 (1988).

[8] K. W. Commander and A. Prosperetti, "Linear Pressure Waves in Bubbly Liquids: Comparison between Theory and Experiments," *J. Acoust. Soc. Am.* **85**(2), 732–746 (1989).

[9] G.J. Orris, D.K. Dacol, and M. Nicholas, "Causality and the Velocity of Acoustic Signals in Bubbly Liquids," *J. Acoust. Soc. Am.* **121**(6), 3349–3362 (2007).

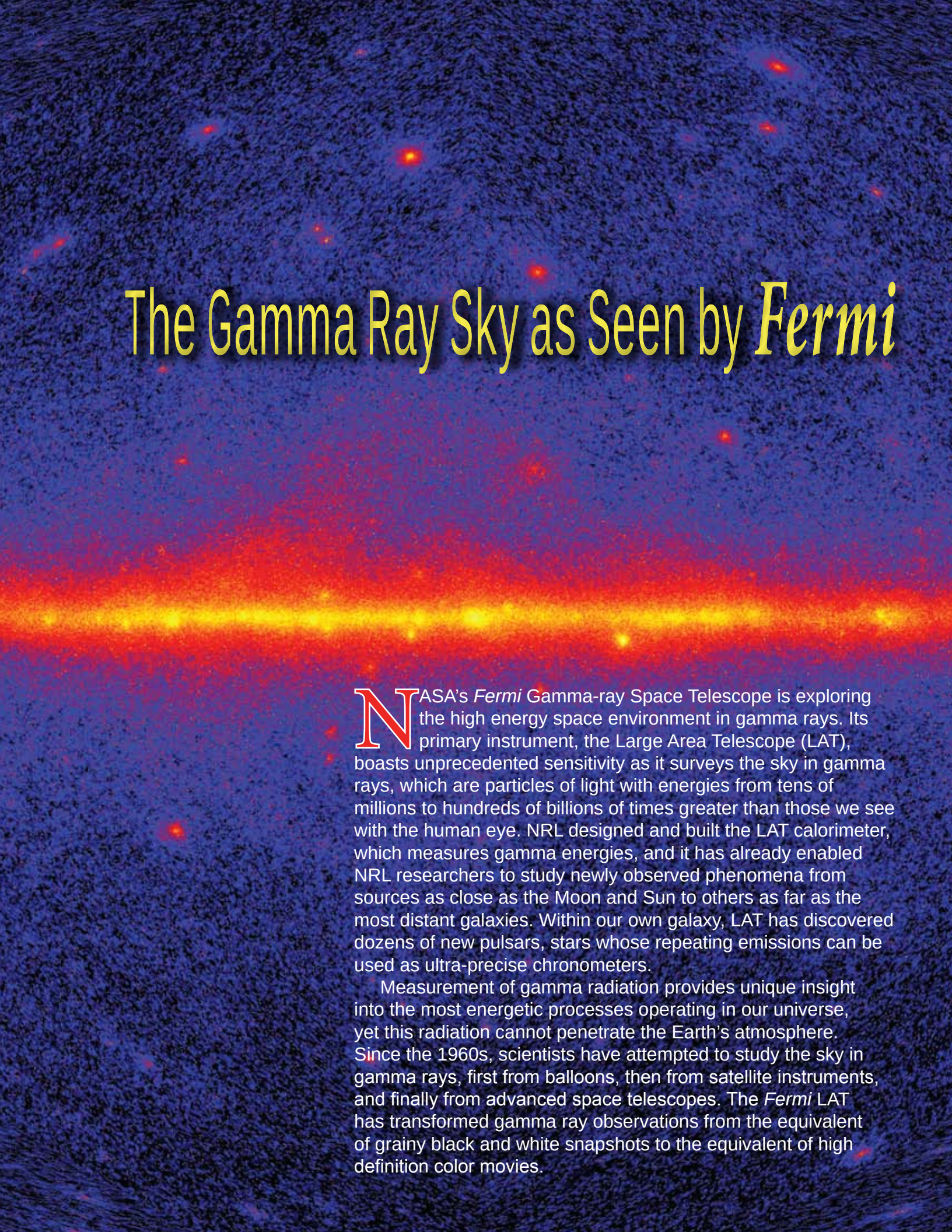

The Gamma Ray Sky as Seen by *Fermi*

NASA's *Fermi* Gamma-ray Space Telescope is exploring the high energy space environment in gamma rays. Its primary instrument, the Large Area Telescope (LAT), boasts unprecedented sensitivity as it surveys the sky in gamma rays, which are particles of light with energies from tens of millions to hundreds of billions of times greater than those we see with the human eye. NRL designed and built the LAT calorimeter, which measures gamma energies, and it has already enabled NRL researchers to study newly observed phenomena from sources as close as the Moon and Sun to others as far as the most distant galaxies. Within our own galaxy, LAT has discovered dozens of new pulsars, stars whose repeating emissions can be used as ultra-precise chronometers.

Measurement of gamma radiation provides unique insight into the most energetic processes operating in our universe, yet this radiation cannot penetrate the Earth's atmosphere. Since the 1960s, scientists have attempted to study the sky in gamma rays, first from balloons, then from satellite instruments, and finally from advanced space telescopes. The *Fermi* LAT has transformed gamma ray observations from the equivalent of grainy black and white snapshots to the equivalent of high definition color movies.

Opening a New Window on the High Energy Space Environment

J.E. Grove and W.N. Johnson
Space Science Division

The *Fermi* Gamma-ray Space Telescope, NASA's newest observatory, has begun its mission of exploring the high-energy space environment in gamma rays. Successfully launched from Florida on June 11, 2008, the spacecraft and its instruments passed their orbital checkout and commissioning with flying colors. *Fermi*'s primary instrument, the Large Area Telescope (LAT), is now surveying the gamma-ray sky at energies from tens of millions to hundreds of billions of times greater than those we see with our eyes. With its unprecedented sensitivity and sky-survey viewing, the LAT is revolutionizing our understanding of the near-Earth environment and distant universe in energetic gamma rays, the most penetrating type of electromagnetic radiation. NRL scientists designed and built the LAT calorimeter, which measures the energies of the gamma rays, and led the commissioning of the LAT on orbit. NRL also provided facilities and technical support for the environmental testing of the instrument and observatory.

WHY OBSERVE IN GAMMA RAYS?

For the last 400 years, astronomers have observed the sky using the latest technology to understand the fundamental processes that drive the Sun, the solar system, and the distant stars and galaxies. Observations from radio waves through X-rays have shown that the bulk of the emission from the Sun and stars is thermal radiation, but they have also revealed unexpected non-thermal processes associated with highly relativistic particles. Well above the thermal regime, gamma-ray observations are a direct probe of radiations from the most energetic, non-thermal processes operating throughout the universe — in our Sun, around highly magnetized neutron stars, in jets from black holes and exploding stars in our Milky Way galaxy, and in jets from distant galaxies.

Glimpses of the sky in gamma rays have come from pioneering balloon flights and the OSO-3 spacecraft in the 1960s, from SAS-2 and COS-B in the 1970s, and the EGRET telescope on the *Compton* Gamma Ray Observatory in the 1990s. In mapping the full sky, EGRET expanded the list of gamma-ray sources to a few hundred objects. However, because of the limited sensitivity and long exposures required to make those maps, we have only modest snapshots of the non-thermal engines that drive these objects. Now the technology is in place with the *Fermi* Large Area Telescope (LAT) to take what amounts to color movies of the most violent and extreme environments in the universe.

We can find an example of energetic, gamma-ray-producing processes close to home, in solar flares. Solar flares are explosions that occur in the atmosphere of the Sun, emitting radiation over the full range of the electromagnetic spectrum, from radio to gamma rays. The energy released in a solar flare in a few tens of seconds can be greater than 10^{32} ergs, enough to meet the energy demand of the United States for 100,000 years. At the Earth, the phenomena can disrupt radio communication, damage satellites and destabilize their orbits, cause failures in long-distance power lines, change the terrestrial magnetic field, and even endanger astronauts. The potential impact of such solar activity on DoD assets and enterprises is clear.

High-energy gamma-ray observations of solar flares will open a new, unexplored energy domain for flare science, possibly revealing new processes associated with ion acceleration, transport, and interaction in flares. It will certainly provide critical additional tests and constraints on our understanding of the flare process.

THE *FERMI* GAMMA-RAY SPACE TELESCOPE

Gamma rays are the most energetic and most penetrating type of electromagnetic radiation and have no trouble crossing the billions of light-years through most of the visible universe or passing through dust lanes and gas clouds that block X-rays and most lower-energy radiations from reaching us. Nevertheless, they cannot penetrate the dense atmosphere of our Earth. To see them, we have to launch specialized telescopes into space.

The *Fermi* Gamma-ray Space Telescope, known before launch as GLAST, the Gamma-ray Large Area Space Telescope, carries two scientific instruments cov-

ering more than a factor of 10 million in energy across the electromagnetic spectrum. It is the first gamma-ray observatory to survey the entire sky every day, and the first with high sensitivity. As such, it provides a unique opportunity to study the ever-changing universe at extreme energies. Figure 1 shows the *Fermi* telescope being prepared for launch, and Fig. 2 shows the June 11, 2008, launch of the Delta II rocket that bore the *Fermi* telescope.[1]

The primary instrument on *Fermi*, the Large Area Telescope, is a state-of-the-art, wide-field-of-view imaging spectrometer for high-energy gamma rays from approximately 20 million electron volts (MeV) to greater than 300 billion electron volts (GeV), to use the conventional units of energy in this regime. (For comparison, photons of visible light have energies of a few eV.) The LAT will collect more than 100 times the number of gamma rays of the previous-generation instrument, the *Compton* EGRET, more than 30 million every year. Its field of view (FOV) covers approximately 20 percent of the sky at a time — roughly the same as the human eye — and it surveys the entire sky approximately every 3 hours. This capability is extremely important, as one of the primary conclusions from EGRET was that the gamma-ray sky is extraordinarily variable. Every week, the LAT achieves the same source sensitivity that EGRET reached only after its entire nine-year lifetime.

The 3000-kg LAT was designed and manufactured by an international collaboration under the leadership of Stanford University. The Stanford Linear Accelerator Center (SLAC) managed the overall program and integrated the substantial hardware contributions from institutions in France, Italy, Japan, Sweden, and the United States.[2]

HOW THE INSTRUMENT WORKS

Far too energetic to be focused or captured using conventional optics, gamma rays require technology adapted from ground-based particle accelerator experiments and medical imaging systems. A high-energy gamma ray interacts with matter by converting some of its energy directly into a matter and anti-matter pair of charged particles, an electron and a positron. The remainder of the energy of the gamma ray becomes the kinetic energy of the electron-positron pair and carries the pair forward in the direction of the gamma ray at ultra-relativistic speeds. By tracking the electron-positron pair, we can therefore measure the direction of the incoming gamma ray. As the pair passes through more material, it multiplies and cascades into a family of charged particles and photons in an "electromagnetic shower," depositing its energy in a well-understood profile. By measuring the profile of energy deposition, we can measure the energy of the original gamma

FIGURE 1
The first half of the payload fairing is moved into place around the *Fermi* observatory as the vehicle is prepared for launch. (Credit: NASA – Jim Grossmann.)

FIGURE 2
Fermi Gamma-ray Space Telescope launches from the Cape Canaveral Air Force Station aboard a Delta II Heavy rocket on June 11, 2008. (Credit: United Launch Alliance – Carleton Bailie.)

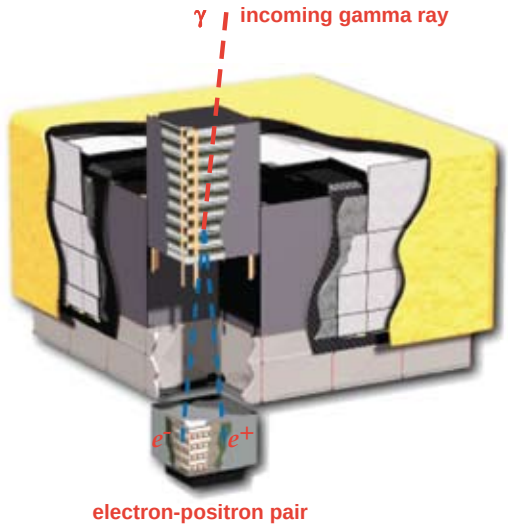

FIGURE 3
Artist's rendering of a gamma ray converting into an electron-positron pair within the Large Area Telescope tracker. Precise measurement of the direction of the pair in the tracker gives the direction of the incoming gamma ray. The pair propagates into the calorimeter and cascades in an electromagnetic shower (not shown) that deposits the energy of the gamma ray into the calorimeter. The tracker and calorimeter are modular assemblies of 16 identical towers.

ray. Celestial gamma ray sources are, unfortunately, not particularly bright objects, and their emissions are dwarfed by high fluxes of charged particles in low Earth orbit. Therefore, a gamma ray telescope must be extremely efficient at identifying and rejecting this charged-particle background.

Following on these concepts, the LAT (see Fig. 3) consists of three detector subsystems — a tracker to convert the gamma ray and image the electron-positron pair, a calorimeter to measure the energy and profile of the electromagnetic shower, and a covering anti-coincidence detector to help identify background charged particles. The tracker contains multiple layers of thin tungsten foil converters and silicon strip detectors to track the electron and positron. The calorimeter, which was developed and assembled at NRL, consists of multiple layers of scintillating cesium iodide crystals, which are dense enough to develop and contain most of the electromagnetic shower.

The shower of particles through the cesium iodide produces flashes of scintillation light proportional to the energy deposited in the crystals. This scintillation light is then converted by photodiodes bonded to each crystal into electrical signals that are digitized and recorded on board. The cesium iodide bars are arranged in two orthogonal directions (see Fig. 4) to image the development of the shower within the calorimeter — improving the energy measurement — and to help reject background particles, since their pattern of energy deposition is different from that of gamma rays.

The accuracy of the energy measurement is largely determined by the ability of the calorimeter to collect all the energy from the cascade of particles in the electromagnetic shower. The penetrating nature of these particles means that a massive detector is required to stop or capture them. The LAT calorimeter is assembled from more than 1500 thallium-doped cesium iodide, CsI(Tl), crystals totaling 1350 kg, about half of the weight of the entire LAT instrument.

Because the gamma-ray flux from celestial sources is small, gamma-ray telescopes must be very large: the square LAT "aperture" is 1.8 m on a side. Even in this large, state-of-the-art telescope, the brightest persistent celestial source registers only one photon every 4 minutes, and the total rate of celestial gamma rays in the LAT FOV is only about one per second! (Transient events such as solar flares and gamma ray bursts can, however, be orders of magnitude brighter.)

Digitized signals from the calorimeter, tracker, and anti-coincidence detector are processed by the LAT's three onboard computers. Conservative pattern-recognition algorithms developed from extensive

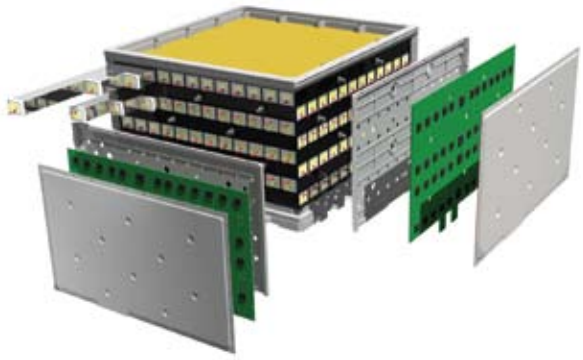

FIGURE 4
Exploded rendering of a calorimeter module containing an array of CsI(T1) scintillating crystals with electronic readout. The full calorimeter consists of 16 of these modules.

Monte Carlo simulations of gamma-ray and charged-particle interactions in the LAT then identify and reject approximately 90 percent of the background charged particles in the LAT data on board, reducing the bandwidth enough to allow the gamma ray data to be sent to the ground through the spacecraft's high-gain antenna. The remainder of background rejection is performed on the ground by much more sophisticated versions of those same algorithms.

NRL'S ROLE IN THE *FERMI* GLAST MISSION

The High Energy Space Environment Branch of NRL's Space Science Division (SSD) has played a leading role in the *Fermi* GLAST mission for more than 14 years, from when the early concepts for the LAT instrument were first designed and tested. The SSD led the team from U.S., French, and Swedish institutions in the design and manufacture of the LAT calorimeter. We assembled and tested the calorimeter hardware in the Spacecraft Engineering Department of the Naval Center for Space Technology (NCST) at NRL and completed delivery of the calorimeter detectors to the Stanford Linear Accelerator Center in May 2005, where they were subsequently integrated with other components into the LAT instrument.

In May 2006, the LAT instrument came to the NCST at NRL for environmental testing, subjecting it to dynamic, thermal, and vacuum environments exceeding those at launch and testing its electromagnetic emissions and susceptibility. The four-month test program was executed on schedule with great success. In August 2007, the LAT returned to NRL, now fully integrated into the *Fermi* GLAST observatory, for thermal-vacuum testing at the NCST.

After its successful launch in June 2008, the observatory underwent a 60-day on-orbit commissioning program and transitioned to normal science operations in early August 2008. A team of 14 NRL astrophysicists in the High Energy Space Environment Branch, including three NRC post-docs and a graduate student, are currently actively mining the LAT data.

EARLY SCIENTIFIC RESULTS

As a hint of the discoveries to come, here we show just a few of the early scientific results from the first three months of LAT operations.

The Gamma-ray Sky

Figure 5 shows an image of the full sky accumulated over the first three months of LAT science operations. Here the entire celestial sphere is shown split open and laid flat in an Aitoff projection, with the center of our Milky Way galaxy in the center of

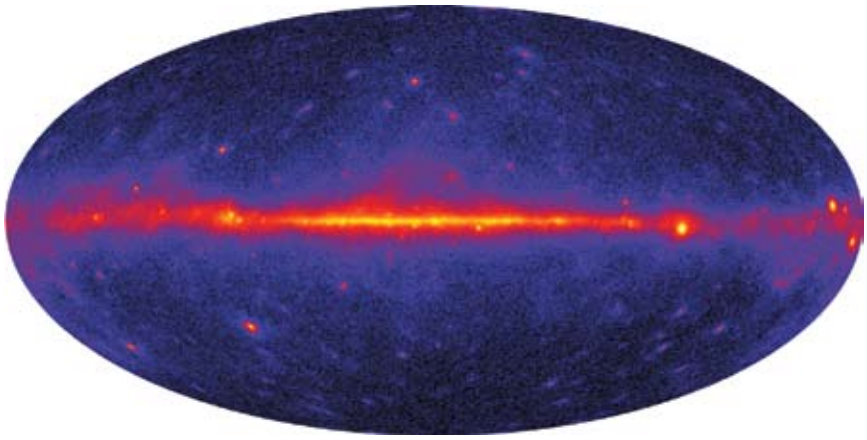

FIGURE 5
False-color image of the full sky in gamma rays created from three months of LAT data, shown as an Aitoff (equal-area) projection in galactic coordinates. The color indicates the intensity of the gamma-ray flux. The plane of our Milky Way galaxy is the bright horizontal band. Over 200 bright sources are detected in this image.

the image, and the galactic anti-center at the left-most and right-most edges of the projection. The bright band is the plane of our galaxy, which glows brightly in gamma rays as energetic cosmic ray charged particles collide with interstellar gas and dust. Shining out of that diffuse glow are a number of bright point sources, mostly gamma ray pulsars — rotating, magnetized neutron stars — as discussed below. The bright sources above and below the galactic plane are predominantly distant active galactic nuclei (AGN) called blazars, galaxies fueled by a central supermassive black hole and emitting a jet of relativistic particles that happens to point directly at us, along our line of sight.

This three-month image contains over 200 bright sources (sources detected at greater than 10σ significance) and hundreds more at lower statistical significance.[3] By comparison, in its nine-year lifetime, EGRET found fewer than 30 sources at this confidence level. Also faintly visible in the upper right quadrant is the track of the Sun. Although no major solar flares have occurred since the launch of *Fermi*, the LAT is able to detect persistent gamma-ray emission caused by cosmic rays striking the atmosphere of the Sun. Long-term studies of this quiescent emission will provide a unique diagnostic of the Sun's magnetic field.

Gamma-ray Bursts

The *Fermi* LAT has already made several important discoveries about gamma-ray bursts (GRBs), intense flashes of gamma-ray light observed about once per day from random locations on the sky. GRBs are thought to be produced when a black hole is formed from the collapse of a massive stellar core, or from the coalescence of compact objects such as neutron stars and white dwarfs. The GLAST Burst Monitor, the secondary instrument on *Fermi,* has already detected over 100 GRBs with energies ranging from several hundreds of keV to GeV energies and higher.

The most dramatic case is that of GRB 080916C, so named because it was the third GRB detected on September 16, 2008. In this instance, the 100 MeV to GeV radiation suddenly appeared about 5 seconds after the initial burst of radiation that triggered the Burst Monitor. Theorists are actively trying to understand the puzzle of the late-appearing GeV radiation, and whether it is related to a separate radiation component, possibly due to the acceleration of cosmic-ray protons following the more rapid, lower-energy signal formed by accelerated electrons.

Neutron Stars

Perhaps the most important early discoveries of Fermi have been from objects in our galaxy. The LAT has discovered 12 new pulsars that seem to be visible only in gamma rays and has detected gamma-ray pulses from at least 18 radio pulsars, including seven with rotational periods of only milliseconds.

A pulsar is a rapidly rotating and highly magnetized neutron star, the remnant core of a massive star that has gone supernova. Most of the 1800 known pulsars were discovered through their sharply pulsed radio emission, which is thought to be a narrow lighthouse beam originating from the star's magnetic poles. But this radio emission comprises only a few parts per million of the pulsar's total power output. For the half-dozen pulsars known prior to the *Fermi* mission to be gamma-ray emitters, those gamma rays, in contrast, carry more than 10 percent of the pulsar's power. The much larger population of LAT pulsars is now allowing us to see and understand the dynamo engine that powers these objects.

The supernova remnant CTA 1 has been known to astronomy since 1960 when it was discovered in a radio survey. Follow-up work in X-rays found the nebular remnant of the stellar explosion and a point source suggestive of a neutron star. It was logical to expect this point source to be a pulsar, but deep searches for pulsations in X-ray and radio were not successful. The LAT, however, quickly revealed the pulsar in data from the early checkout of the instrument. The age and energetics of this source are now understood, and it is recognized as a young pulsar and nebula similar in many ways to the Crab Pulsar and Nebula.[4] In one respect, however, CTA 1 is strikingly different: the pulses are seen in gamma rays alone, unlike the pulses of the Crab. The gamma-ray sensitivity provided by *Fermi* LAT is the only way this pulsar could have been found and understood. Eleven other pulsars previously unknown at other wavelengths have now been discovered by LAT.

Finally, the discovery of pulsed gamma rays from several radio pulsars with millisecond spin periods, previously suggested in just one such object by the EGRET instrument, is particularly intriguing. These stars spin so rapidly that the portion of the magnetosphere that co-rotates with the neutron star — the region where LAT data show the gamma rays originate — cannot be more than several stellar radii in size, or particles on those field lines would be forced to travel faster than the speed of light, in clear violation of Special Relativity. Deciphering the pattern of observed gamma rays will undoubtedly lead to new insight into the extreme environment surrounding these relativistic stars.

ACKNOWLEDGMENTS

The *Fermi* LAT collaboration acknowledges generous and ongoing support from a number of agencies and institutes that have supported the development

and operation of the LAT. These include NASA and the Department of Energy in the United States; the Commissariat a l'Energie Atomique (CEA) and the Centre National de la Recherche Scientifique (CNRS)/ Institut National de Physique Nucleaire et de Physique des Particules (IN2P3) in France; the Agenzia Spaziale Italiana (ASI), the Instituto Nazionale di Fisica Nucleare (INFN), and the Instituto Nazionale di Astrofisicia (INAF) in Italy; the Ministry of Education, Culture, Sports, Science and Technology (MEXT), the High Energy Accelerator Research Organization (KEK), and the Japan Aerospace Exploration Agency (JAXA) in Japan; and the K.A. Wallenberg Foundation and the Swedish National Space Board (SNSB) in Sweden.

[Sponsored by NASA)

References

[1] For more information, see the *Fermi* mission website at http://*Fermi*.gsfc.nasa.gov/.

[2] W.B. Atwood et al., "The Large Area Telescope on the *Fermi Gamma-Ray Space Telescope* Mission," *The Astrophysical Journal* **697**(2), 1071–1102 (2009).

[3] A. Abdo et al., "*Fermi*/Large Area Telescope Bright Gamma-Ray Source List," *The Astrophysical Journal Supplement Series* **183**(1), 46–66 (2009).

[4] A. Abdo et al., "The Fermi Gamma-Ray Space Telescope Discovers the Pulsar in the Young Galactic Supernova Remnant CTA 1," *Science* **322**, 1218–1221 (2008).

Keeping COMMx Cool

NRL Addresses a Hot TacSat-4 Challenge

Before the U.S. Navy's TacSat-4 satellite could provide crucial **communications, data exfiltration, and tracking functions, difficult thermal control** requirements for the onboard electronics had to be met. Using traditional methods of spacecraft thermal design, project **engineers could not find adequate heat** rejection space in the satellite design for its COMMx electronic payload without making the satellite too large and heavy. NRL researchers stepped in and were able to apply their Central Thermal Bus concept developed in the 1990s to redesign the thermal payload control system for the **most efficiency in terms of performance,** ease of integration, and, most importantly, mass/volume, without limiting payload performance or mission goals.

Design and Analysis of the Thermal Control System for the TacSat-4 Spacecraft COMMx Payload

R.W. Baldauff, W.J. Armiger, and T.T. Hoang
Spacecraft Engineering Department

The thermal requirements for the TacSat-4 payload electronics (COMMx) were difficult to meet with traditional methods of spacecraft thermal design. TacSat-4 is a U.S. Navy satellite intended to be launched into an elliptical orbit to provide relevant capabilities for communications, data exfiltration, and tracking. In a conventional passive thermal design, the electronics boxes are distributed around the spacecraft at suitable locations where heat rejection to space is available. This technique, while simple, can be inefficient with satellite real estate and so posed a real threat to COMMx payload implementation. Specifically, the spacecraft would become large and heavy due to inefficient packaging, requiring a larger and more expensive launch vehicle. The result of a trade study indicated that a Central Thermal Bus design, a concept first proposed by the U.S. Naval Research Laboratory in 1994 and the subject of a funded study in 1999, would yield the most efficient thermal control system for the TacSat-4 payload in terms of performance, ease of integration, and more importantly, mass/volume. The challenge facing NRL thermal engineers was to design the payload thermal control system to fit within the multitude of program constraints without limiting payload performance or mission goals.

INTRODUCTION

TacSat-4 is a Navy-led space program jointly sponsored by the Office of Naval Research (ONR), Office of the Secretary of Defense (OSD), and Department of Defense Operationally Responsive Space (ORS) Program Office to provide relevant capabilities for communications, data exfiltration, and tracking. Figure 1 illustrates the basic configuration of the TacSat-4 spacecraft. The satellite, comprising a separately developed bus and payload, will be launched into a 4-hour elliptical orbit, shown in Fig. 2, to provide maximum operation time over the geographical areas of interest. A 12-foot deployable ultra-high frequency (UHF) antenna and associated electronics payload are designated COMMx, with the electronics boxes housed inside a relatively small enclosure.

The challenges facing the COMMx Thermal Control System (TCS) were extensive. Extreme heat dissipation given the small size of the payload, some 600 W, while coping with significant periods of payload off-time made management of component temperatures difficult. The temperature limits of the electronics boxes are 0 °C to +40 °C during normal operations and –30 °C to +50 °C during the survival mode. Variable spacecraft orientation meant that the radiator sink could change from deep space to full Sun during payload operations. To prevent "back-loading" of absorbed solar heat to the payload, thermal diode (action) devices were required in the TCS design. Additionally, traditional limitations associated with a Class D space program, including high risk and limited funds, along with constraints on power, mass, and volume, converged to force a novel TCS architecture solution.

At the beginning of the development program, a trade study of various technologies and architectures was carried out. The result indicated that only one solution met the aforementioned requirements. It entailed the Central Thermal Bus (CTB) concept and the Loop Heat Pipe (LHP) technology in conjunction with an LHP temperature control method. The CTB architecture for a spacecraft TCS was first proposed by the Naval Center for Space Technology (NCST) at the U.S. Naval Research Laboratory (NRL) in 1994. It then became the subject of a funded experimental study in 1999.[1] The essence of the CTB approach is to package all heat-dissipating devices close together at a central location inside the spacecraft while using a cooling technology to (a) collect the waste heat, (b) transport it to the spacecraft radiators, and (c) reject it to space at a place where the heat removal is the most efficient (i.e., the coldest sink). The CTB offered many advantages over traditional TCS architectures. Among them are mass/volume savings of the TCS, ease of integration of the payloads, and optimal placement of the electronics inside the spacecraft to enhance radiation shielding. As presented below, the LHP technology played a crucial role in providing the heat transport for the CTB. Like conventional heat pipes, LHPs are two-phase heat

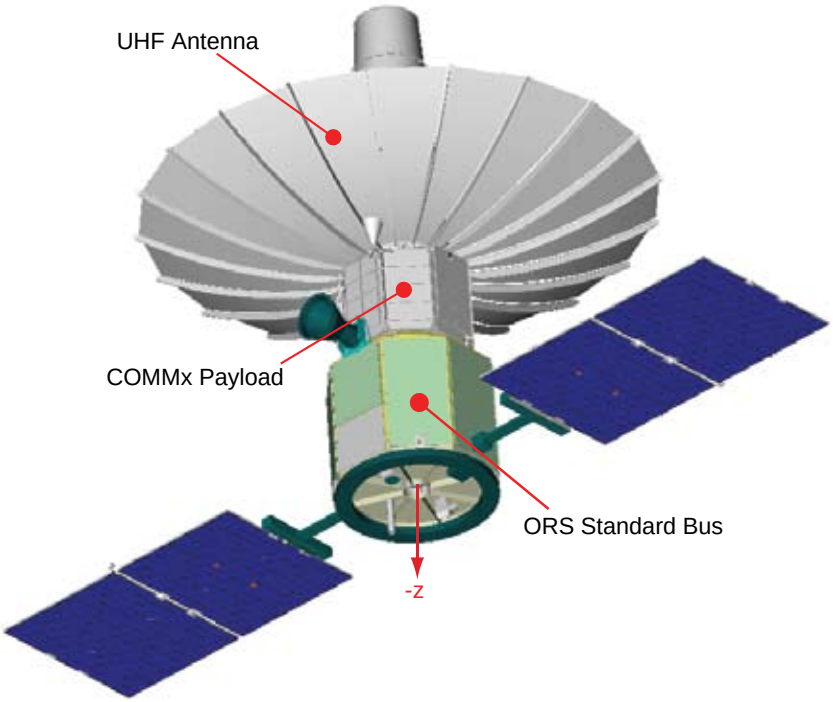

FIGURE 1
TacSat-4 spacecraft with deployed UHF antenna.

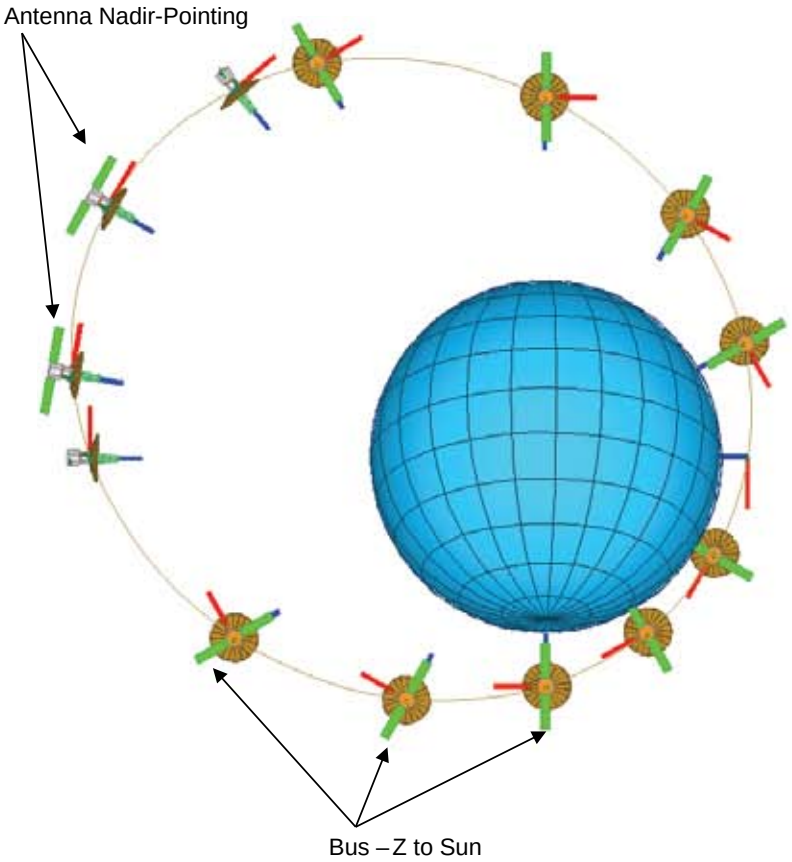

FIGURE 2
TacSat-4 elliptical orbit at a high beta angle, as viewed from the Sun.

transport mechanisms using only capillary action to circulate the working fluid in a closed loop. LHPs have no mechanical moving parts to wear out or require lubrication, resulting in tremendous operational reliability and long service life.

TACSAT-4 MISSION

The TacSat-4 mission provides operationally relevant capabilities and advancements in Operationally Responsive Space (ORS). The TacSat-4 payload (COMMx) consists of 10 UHF channels that will be used in any combination of communications, data exfiltration, or Blue Force tracking. The mission enables communications-on-the-move with legacy radios and provides a wideband Mobile User Objective System "MUOS-like" channel. The 4-hour elliptical orbit provides 1- to 2-hour dwells per pass that augment the geosynchronous communications by facilitating a near-global (but not continuous) coverage, including high latitudes. The TacSat-4 program advances key ORS interests such as spacecraft bus standards, long dwell orbits, dynamic tasking, and net-centric operations.

OVERVIEW OF THERMAL TECHNOLOGY

Fluid circulation in a closed loop is an effective way to transfer heat from one location (e.g., payload electronics) to another (e.g., space radiators). For space applications, in which high system reliability and long life are often required, the capillary pumped heat transport technologies such as Capillary Pumped Loop (CPL) and LHP are preferred for the TCS. In contrast to mechanically pumped systems, CPLs and LHPs contain no mechanical moving parts to wear out or break down. More importantly, they do not require internal lubrication that can contaminate the working fluid and lead to the generation of non-condensable gas.

The CPL and LHP were developed independently in the United States and in the former Soviet Union, respectively, in the 1980s. Recognizing the need for high-performance thermal management technologies for the Navy's next-generation spacecraft, NRL has been participating in the research and development of advanced two-phase heat transfer technology since 1992. NRL led a joint effort that began in 1996 to demonstrate the CPL multiple-evaporator operation in micro-gravity, culminating with the flight experiment CAPL-3 in 1999.[2] NRL was also a full participant in the flight experiment LHP-FX in 1998.[3] Even though CPL and LHP share many common characteristics, LHP is better suited for COMMx due to its higher heat transport capacity and transient environment tolerance.

Loop Heat Pipe

Figure 3(a) is a functional schematic of the LHP. The LHP consists of a capillary pump, condensers (for simplicity, Fig. 3(a) shows only one condenser), a reservoir (a.k.a. compensation chamber), vapor/liquid transport lines, and a thermoelectric cooler (TEC). An LHP operates as follows: (a) heat from the heat source conducts through the capillary pump casing to vaporize liquid on the outer surface of the wick, (b) the vapor travels along the vapor line to the condenser, where it rejects the heat to revert back to liquid, and finally (c) the liquid flows in the liquid line to the pump to complete the cycle. The LHP condenser is not used entirely for condensation. A portion of it needs to cool the exiting liquid below the saturation temperature that allows the system to overcome the environmental heating and heat leak from the evaporator. Note that there always exists both liquid and vapor (two-phase) in the reservoir such that its temperature and pressure control the saturation condition of the entire loop (i.e., changing the reservoir temperature will result in a corresponding change in the payload temperatures). A detailed description of the LHP and its applications can be found in Ref. 4.

Thermoelectric Cooler

A TEC is a small solid-state heat pump capable of removing 1 to 25 W and providing the heat source a maximum temperature lift of 60 °C. By applying a positive voltage across the TEC, heat is pumped from the cold side to the hot side of the TEC (refrigeration mode). If the voltage polarity is reversed, the heat flow changes direction, resulting in the heat pump mode. Increasing/decreasing the voltage will increase/decrease the amount of heat flow.[5]

Figure 3(a) illustrates the use of a TEC to regulate the heat flow in/out of the LHP reservoir. One side of the TEC is thermally strapped to the reservoir and the other side is strapped to the active portion of the capillary pump body. By regulating the TEC applied voltage, the LHP temperature can be maintained within ± 0.5 °C, keeping the payload at a desired temperature regardless of the operating conditions.

COMMx THERMAL DESIGN

Figure 3(b) presents the functional schematic of the COMMx TCS, and Figs. 4(a) through 4(c) illustrate the actual layout of the components. As seen in Fig. 4(a), the electronics boxes with the highest heat dissipation are mounted on both sides of the main deck. The remaining boxes, selected because of their relatively

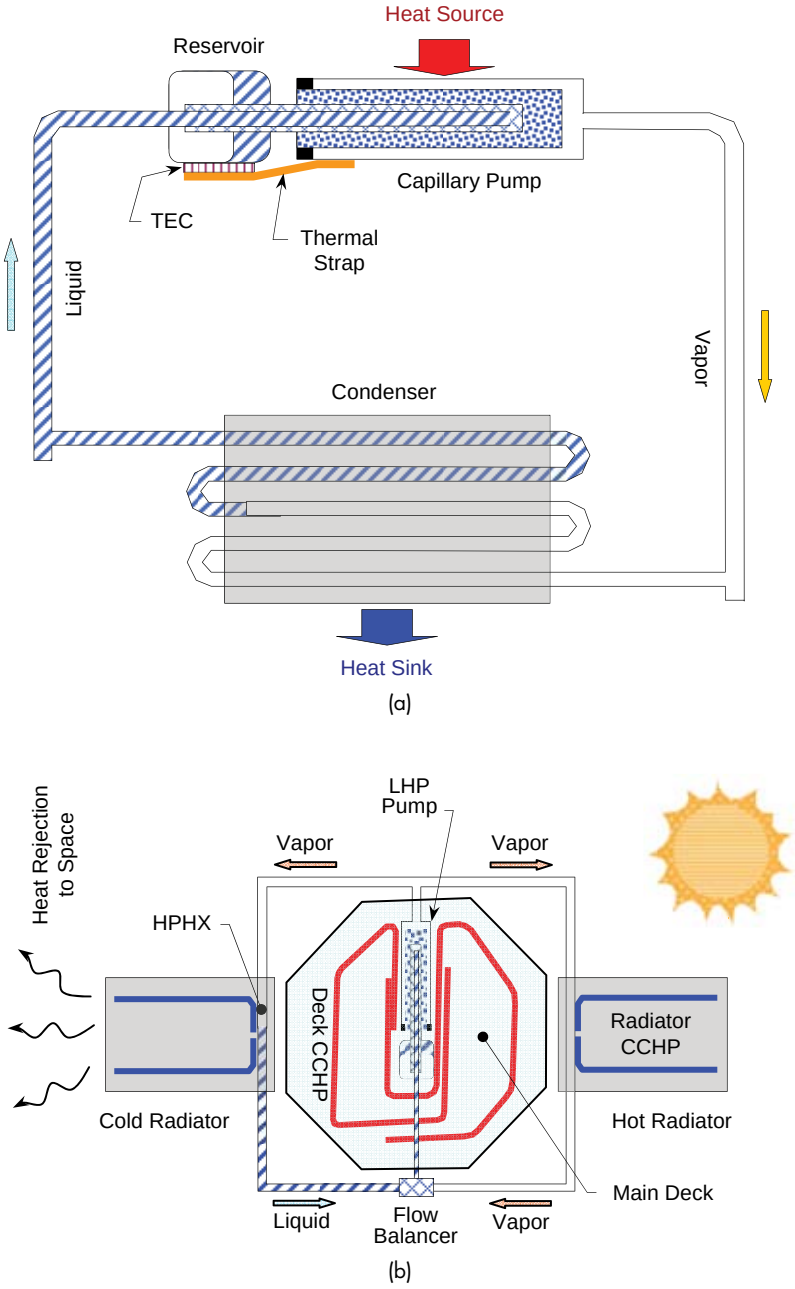

FIGURE 3
(a) Functional schematic of a loop heat pipe with a thermoelectric cooler. (b) Functional schematic of the Central Thermal Bus thermal control system implementation for COMMx.

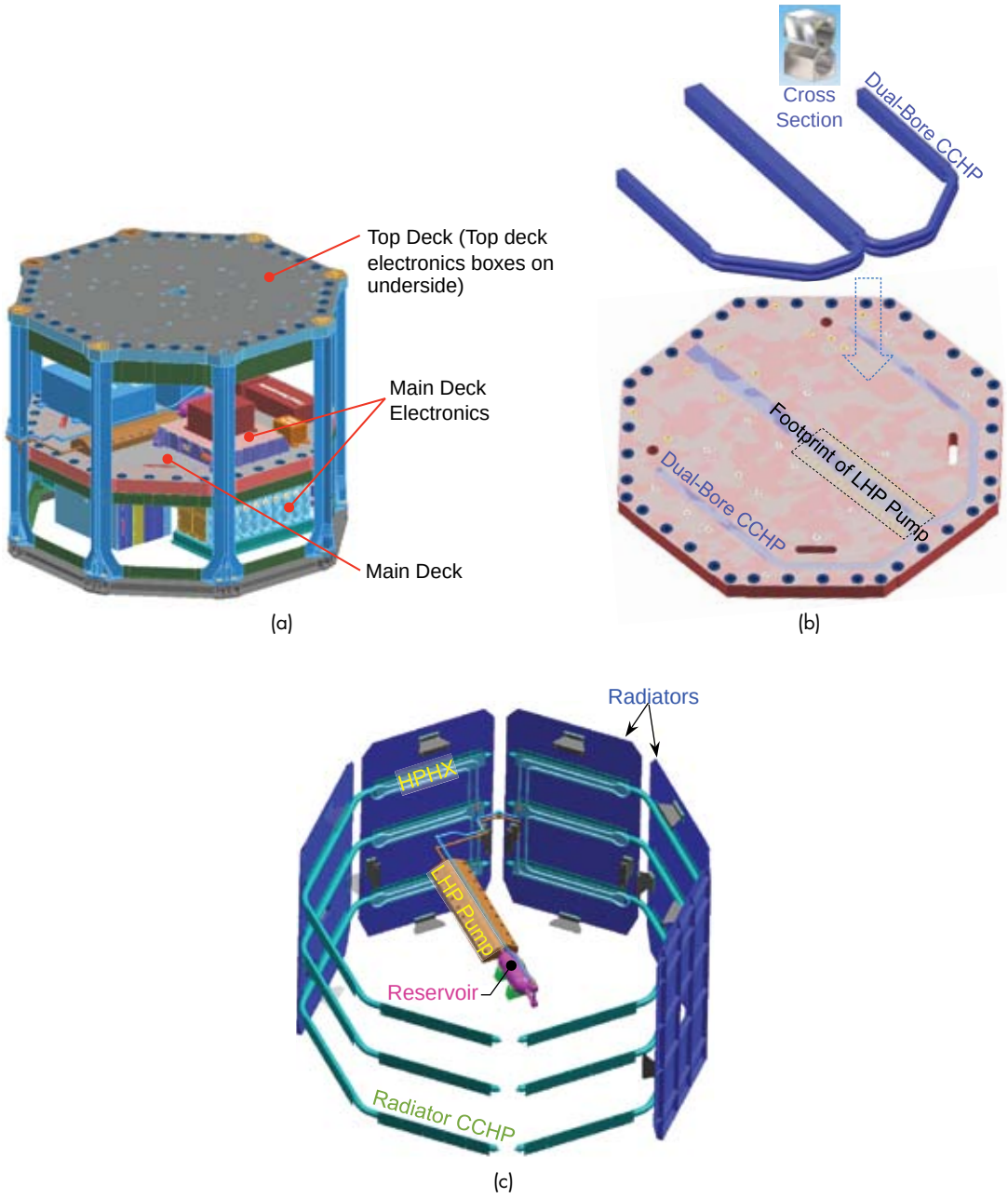

FIGURE 4
(a) Configuration of the COMMx electronics enclosure. (b) Four conjoined CCHPs embedded within the COMMx main deck. (c) Physical configuration of the COMMx TCS including the LHP and radiator CCHPs.

small dissipations, are bolted to the underside of the top deck. The COMMx enclosure is well insulated from the surrounding environment, making the LHP cooling system the sole heat path to the space sink. The cooling system picks up the waste heat from the main deck and transports it to eight radiator panels for rejection. The radiators are supported by, but thermally isolated from, the COMMx structure. Moreover, all interior surfaces of the COMMx enclosure, including the electronics, are provided with a high-emittance surface finish to facilitate radiative heat transfer from the top deck to the main deck where heat transport to the radiators takes place.

The main deck consists of a 1½-in.-thick honeycomb panel embedded with a pair of "dual-bore" constant conductance heat pipes (CCHPs), as shown in Fig. 4(b). The CCHPs efficiently collect the waste heat from the electronics boxes (including those on the top deck via radiation) and deliver it to the LHP evaporator. Since the Sun can illuminate any one side of the payload during the orbit, the eight radiator panels are provided in two separate, thermally coupled groups of four (see Fig. 4(c)). Both sets of radiators are sized to reject the entire heat load in the worst hot case (while one of the two sets faces the Sun). The LHP serves as the variable heat transport system between the deck and the two independent sets of radiators for removal.

Even though the design includes thermostatically controlled heaters to prevent the radiator temperatures from dropping below the ammonia freezing point (–77 °C) in the worst cold case, a decision was made to incorporate heat-pipe-heat-exchangers (HPHX) in the TCS. The HPHX, a 180-in.-long, S-shaped CCHP (see Fig. 4(c)), is the method by which each set of radiators is thermally coupled together. The thermal footprint between the radiator CCHPs and the LHP condensers is sufficiently small to allow the survival heaters to keep the ammonia in the LHP from freezing (even if the radiators are well below –77 °C). Note that CCHPs are freeze tolerant.[6] Finally, the LHP employs a capillary flow balancer to serve as a thermal diode to prevent heat flow from the "hot" radiators (e.g., the radiators illuminated by the Sun) back to the payload (see Ref. 4 for details on the capillary flow balancer).

To ensure that the LHP starts up successfully under any initial system condition, two 25-W "starter" heaters having a ½-in.^{2} surface area are attached to the capillary pump body (see Fig. 5). If the pump fails to start on its own, the starter heater will be activated by the onboard computer to facilitate the (nucleate) boiling process in the pump.[7] A 10-W Kapton film heater is bonded to the reservoir outer surface to serve two functions: (a) to raise the loop temperature for the payload temperature control operation, and (b) to shut down the loop when the payload becomes too cold. In addition, a Marlow TEC Model No. DT3-6 is used to thermally couple the reservoir to the capillary pump (see Fig. 5). The TEC is placed on the pump body with the hot side down. One end of the 6-in.-long by 1-in.-wide by ¼-in.-tall copper bar is secured to the top of the TEC, and the other end to the reservoir. In this application, the TEC functions only as a cooler allowing the loop to lower its temperature for payload temperature control.

To keep the electronics above the temperature limit in the worst cold case survival mode, additional film heaters with a combined power of 44 W are placed at various locations on the top deck (inner surface) and main deck. Likewise, two 40-W line heaters are strung along the LHP condenser lines and a 6-W survival heater is attached to the LHP reservoir to ensure shutdown. The survival heaters are sized with respect to the minimum bus voltage of 22 V.

Figure 6 shows the fully configured payload with the integrated TCS.

TACSAT-4 THERMAL MODEL

A detailed thermal analysis was carried out for the COMMx TCS to predict the on-orbit performance of the cooling system in accordance with the anticipated operating scenarios. A highly complex model of the payload and the cooling system was developed for this purpose. Specifically, the orbital simulations were intended to (a) determine the maximum operation time per orbit, (b) verify that the electronics temperatures meet the limits of 0 °C to +40 °C for normal operation and –30 °C to +55 °C in the survival mode, (c) size the survival heaters, (d) verify that all aspects of the LHP and CCHP operation are nominal (e.g., the wicks do not exceed their respective capillary limits, or the capillary flow balancer provides adequate diode

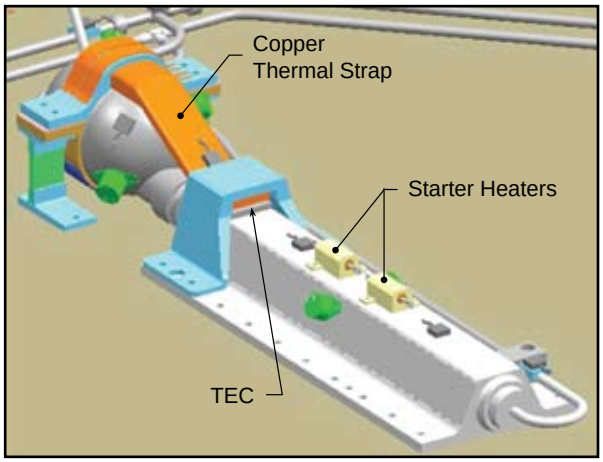

FIGURE 5
COMMx LHP pump-reservoir assembly.

FIGURE 6
Photograph of the fully configured COMMx payload with the integrated TCS.

action in the worst flow imbalance situation), and (e) ensure that the ammonia in the LHP condensers does not freeze in the worst cold case condition given the predicted amount of survival heater power.

Thermal Model Description

The TacSat-4 thermal model was developed with Thermal Desktop (TD) software. TD combines the user-defined Geometry Math Model (GMM) and Thermal Math Model (TMM) into a single platform. A Monte Carlo ray tracing method is used to calculate the radiative couplings (RADKs) for the GMM, while a SINDA-based solver is used to solve the TMM for the nodal temperatures. In addition, NRL incorporates an LHP transient code, developed by TTH Research and refined at NRL, into the subroutine library to advance the LHP temperatures for each time step in the TMM.[8]

As shown in Figs. 7(a) and 7(b), the spacecraft model consists of four major components: the UHF antenna, the COMMx payload, a simplified model representing the ORS Standard Bus and its solar arrays, and the LHP/CCHP cooling system. The TMM contains approximately 10,000 nodes. While SINDA has been the industry standard for spacecraft thermal analysis for the last 30 years, the LHP transient code is a recent development. In 2001, NASA Goddard Space Flight Center funded TTH Research to produce an efficient computer code to be used with SINDA that was capable of solving the transient behavior of LHPs. Following a period of verification processes, NASA and NRL engineers started using the computer code in 2004 for both ground- and space-based LHP systems.[9,10] In short, the LHP code simultaneously solves the equations governing the conservation laws of mass, momentum, and energy for fluid- and thermodynamics.

Model Results

Figure 8(a) presents the results of the maximum power simulation in the worst hot case. As predicted, the COMMx payload can operate for 2 hours per orbit at 600 W of power dissipation. At the end of the 2-hour dwell, the warmest electronics box is roughly 35 °C at the base plate. The boxes on the main deck are nearly isothermal due to the embedded CCHPs.

Figure 8(b) gives the results of the cold survival case electronics box temperatures. During the worst cold case orbit, with no operations and survival heater power only, the thermal model predicts that the electronics boxes remain above their survival temperature limits for both a stowed and deployed UHF antenna.

CONCLUSION

The maturity of the Loop Heat Pipe technology in the United States has enabled the Central Thermal Bus architecture to become a viable thermal control option for spacecraft. In the case of COMMx, the CTB design allows many more heat-intensive electronics to be packaged in a limited volume of the spacecraft than can be achieved otherwise. As a result, the TacSat-4 payload provides exceptional capability in its mission orbital arena. From a broader perspective, success of the space demonstration of the CTB architecture will certainly convince the next generation of spacecraft developers that an "increase in payload capability" does not necessarily equate to "increase the size of the spacecraft." If the satellite volume can be kept small, the more tangible advantage of CTB is perhaps that a mission will not require a larger fairing, or more importantly, a bigger and much more expensive (mission-prohibitive) launch vehicle. Based on these observations, the CTB concept is poised to enable significant improvements in Navy and U.S. space capability.

ACKNOWLEDGMENTS

We thank the ONR for continued program sponsorship, and Edge Space Systems for contributions to the analysis effort.

[Sponsored by ONR]

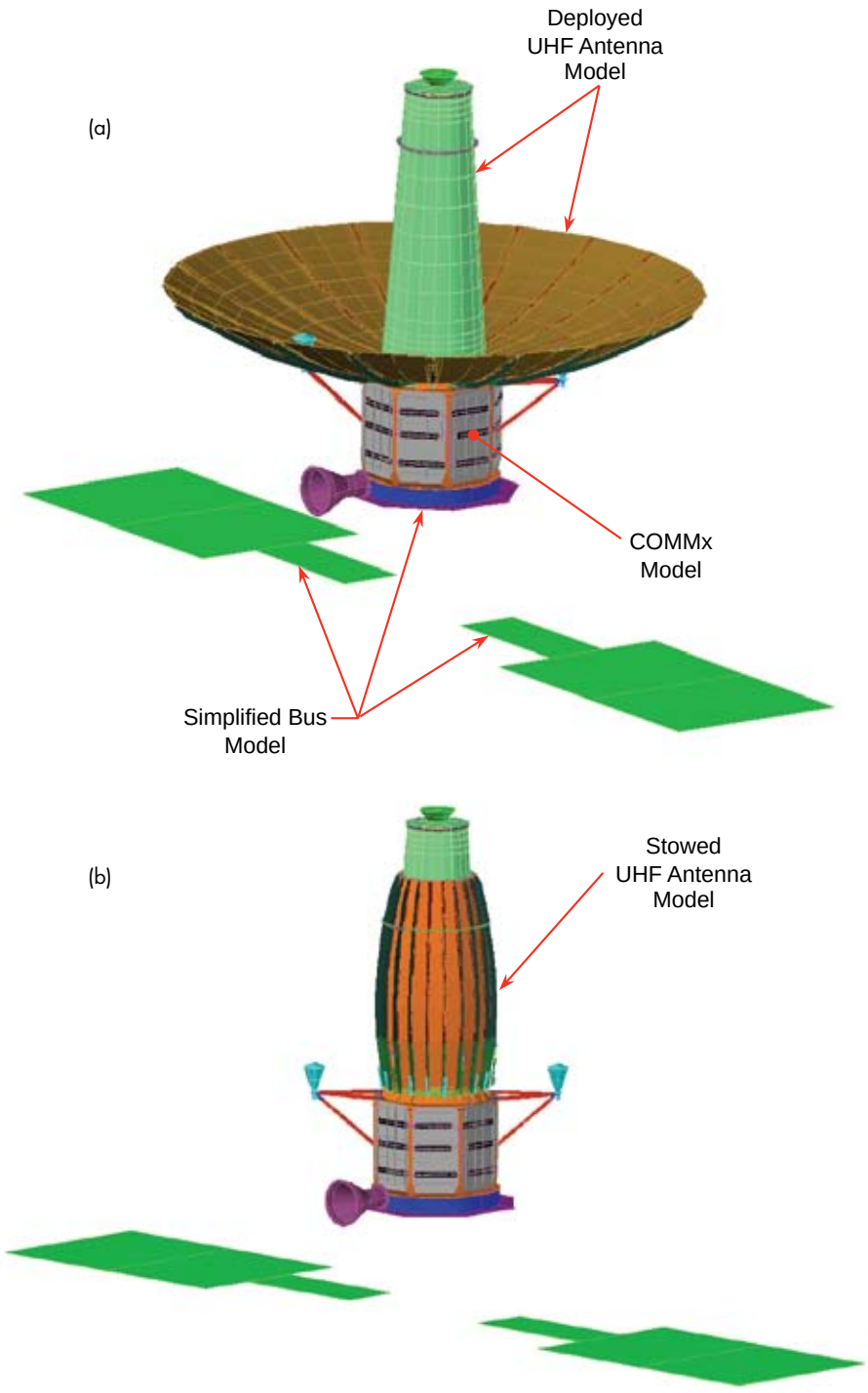

FIGURE 7
(a) COMMx thermal model with deployed UHF antenna. (b) COMMx thermal model with stowed UHF antenna.

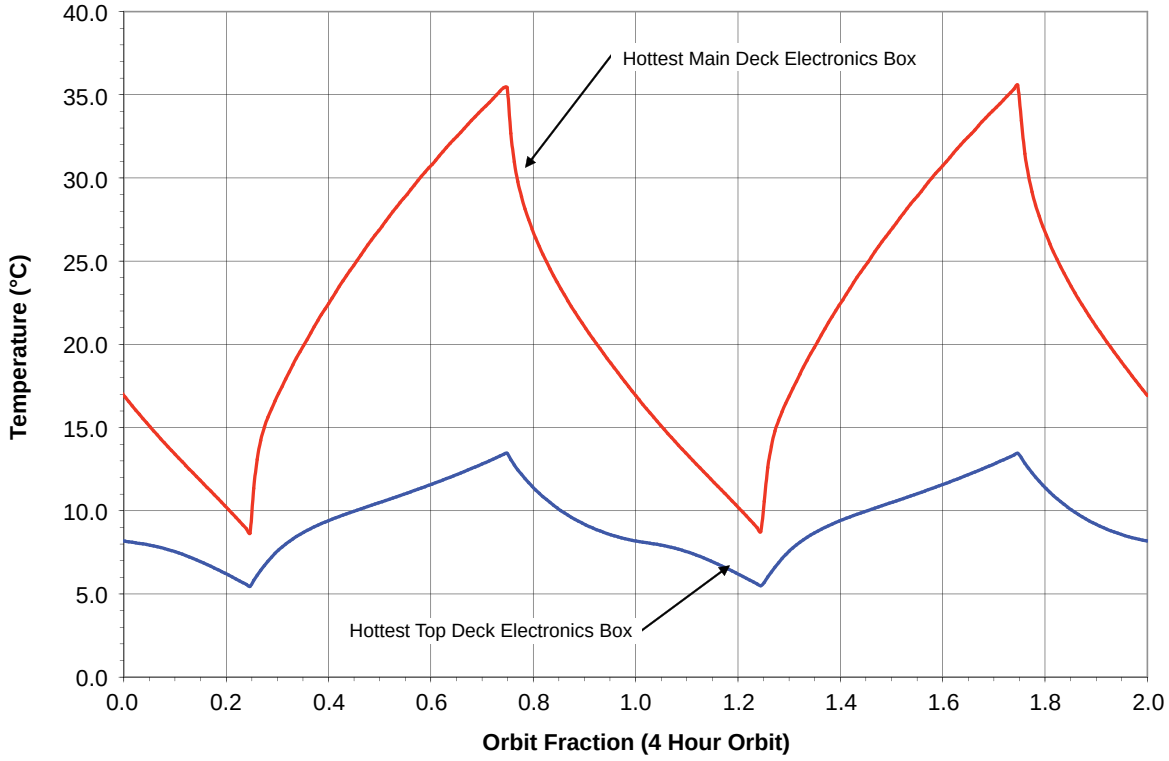

(a)

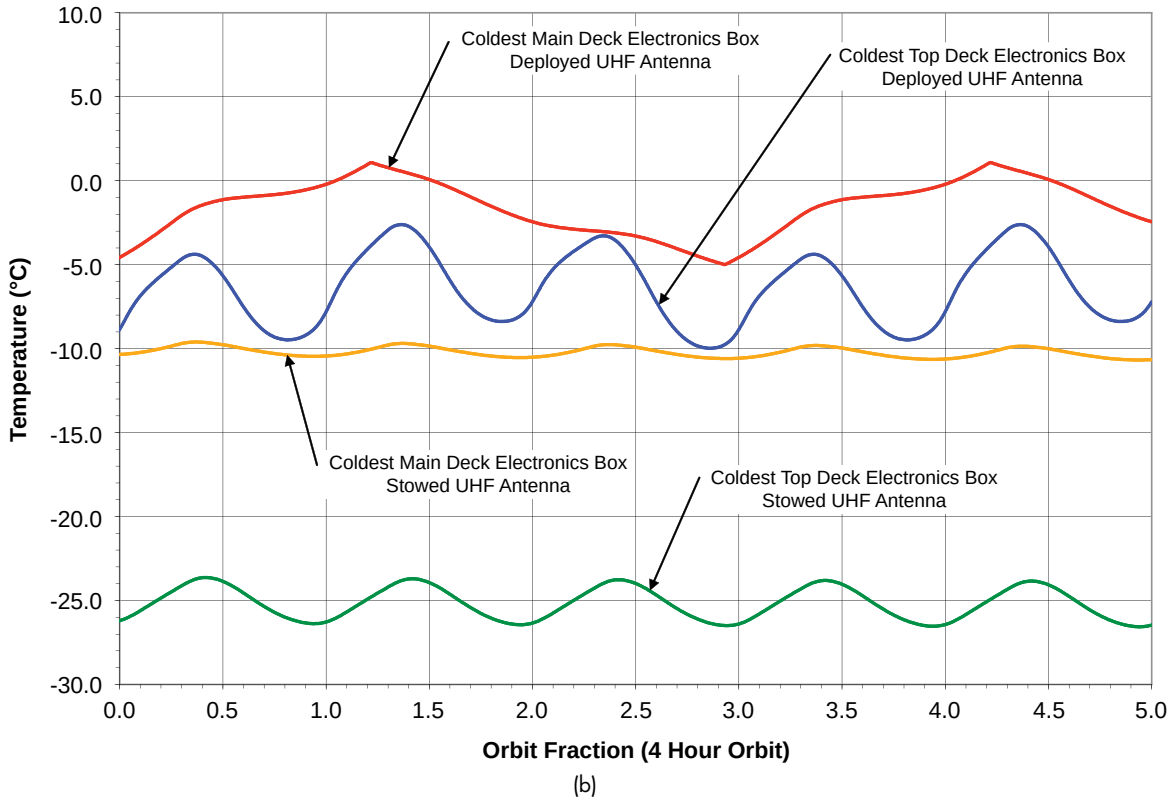

(b)

FIGURE 8
(a) COMMx electronics box worst-case temperature predictions for 2 hours of operation per orbit. (b) COMMx electronics box survival temperature predictions.

References

[1] T. Hoang, M. Brown, R. Baldauff, and S. Cummings, "Development of a Two-Phase Capillary Pumped Heat Transport for Spacecraft Central Thermal Bus," Proceedings of 2002 Space Technology and Applications International Forum (STAIF 2002), Albuquerque, NM, 2002.

[2] L. Ottenstein, "CAPL 3 Flight Experiment Overview," Two-Phase Technology '99 Workshop on Ambient and Cryogenic Thermal Control Devices, Sponsored by NASA/GSFC, ESA/ESTEC and the Aerospace Corporation, May 15–17, 1999.

[3] C. Baker, W. Bienert, and A. Ducao, "Loop Heat Pipe Flight Experiment," SAE Paper No. 981580, 1998.

[4] http://www.marlow.com/

[5] *Loop Heat Pipe User's Handbook*, 2nd Ed., U.S. Naval Research Laboratory, Code 8821, Washington, DC, Sept. 2001.

[6] P.J. Brennan and E.J. Kroliczek, "Heat Pipe Design Handbook," Vol. 1, NASA Contract NAS5-32406, June 1979.

[7] T. Hoang, R. Baldauff, and K. Cheung, "Start-up Behavior of an Ammonia Loop Heat Pipe," AIAA Paper No. 2005-36952, 3rd International Energy Conversion Engineering Conference, August 15–18, 2005, San Francisco, CA.

[8] T. Hoang and J. Ku, "Transient Modeling of Loop Heat Pipes," Paper No. AIAA 2003-6082, 1st International Energy Conversion Engineering Conference, August 17–21, 2003, Portsmouth, VA.

[9] T. Hoang, K. Cheung, and R. Baldauff, "Loop Heat Pipe Testing and Analytical Model Verification at the U.S. Naval Research Laboratory," Paper No. 2004-01-2577, 34th International Conference on Environmental Systems, 2004, Colorado Springs, CO.

[10] T. Hoang, "Mathematical Modeling of Loop Heat Pipes Part II: Secondary Wick Analysis," AIAA Paper No. 2007-4837, 5th International Energy Conversion Engineering Conference, 2007, St. Louis, MO.

acoustics

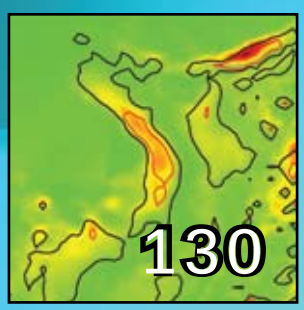

127
Reconstruction of Acoustic Exposure on Orcas in Haro Strait
D.M. Fromm

130
Operational Acoustic Transmission Loss Uncertainty Characterization
R.A. Zingarelli and J.P. Fabre

Reconstruction of Acoustic Exposure on Orcas in Haro Strait

D.M. Fromm
Acoustics Division

Introduction: On 5 May 2003, USS *Shoup* (DDG 86), an *Arleigh Burke*-class Navy Guided Missile Destroyer, transited from the Naval Station Everett via the Strait of Juan de Fuca and the Haro Strait to the Canadian Forces Maritime Experimental Test Range at Nanoose Bay on the eastern side of Vancouver Island, British Columbia. While underway, a sonar training exercise was executed from 10:40 to 14:40 (local time). During the exercise, unusual behavior was observed in one of the resident pods of orcas, raising the question of the sonar's impact on them. Due to two coincidental activities, this question can be addressed in detail.

Coinciding with *Shoup's* transit, a marine mammal class from Friday Harbor Labs led by Dr. David Bain was observing a pod of Southern Resident killer whales (*Orcinus orca*) (J pod).[1] The class shadowed the J pod from their boat, recording its behavior, the GPS location of the boat, and the time of day. Figure 1 shows the tracks of USS *Shoup* and Dr. Bain's boat shadowing the J pod overlaid on the bathymetry.

Additionally, acoustic recordings were made on monitoring hydrophones deployed by Dr. Val Veirs of Colorado College for his Orca Vocalization and Localization (OVAL) project.[2] More than 370 recordings on four hydrophones were made, spanning the time period that *Shoup* was transmitting for its long-range sonar operations.

Modeling Analysis: A detailed reconstruction of the event that related the locations of *Shoup*, the J pod, and the monitoring hydrophones during the time period of *Shoup's* long-range sonar operations was constructed. By combining high-fidelity predictions of the acoustic field with the in situ acoustic recordings, the reconstruction provides a moment-to-moment picture of the events of May 5.

Figure 2 shows an example of the reconstruction at a representative time in *Shoup's* transit. The map plots the positions of *Shoup*, the J pod, and the monitoring hydrophones over the bathymetry contours. (The ellipses are explained later.) The straight red lines indicate the direct path from the acoustic source to the J pod or to the monitoring hydrophones.

Acoustic field predictions were executed along the direct paths using the state-of-the-art, bench-marked, underwater acoustic propagation model RAM, developed at NRL.[3] A high-resolution, 3D description of a complex and highly range-dependent environment was assembled from databases, models, and inputs provided by experts at various Navy laboratories. The two plots of Fig. 3 show transmission loss in dB vs range and depth from *Shoup* to the hydrophones (a) and to the J pod (b).

Due to the complexity and range-dependence of the environment, a small shift in *Shoup's* location causes the details of the acoustic field to change while the mean acoustic field remains fairly stable. Therefore, it was appropriate to use histograms to quantify the received sound pressure levels (SPLs) in the vicinity of the phones and the J pod.

Dr. Val Veirs' acoustic recordings constituted a key part of the analysis for two reasons. First, because the recordings were calibrated, the predicted SPLs from *Shoup* to the monitoring phones could be validated for those times that the recording hydrophones were not overloaded. Second, through a spectral analysis of the recordings, the mode of operation of *Shoup's* sonar, which had not been logged, could be determined. Specifically, it could be proven that the first half of the transmission was directed to the port side of the ship (away from the hydrophones) and the second half of the transmission was directed to the starboard side of the ship (toward the hydrophones).

After receiving the direct path acoustic energy, the hydrophones recorded the reverberation, i.e., sound energy that scattered from interactions with the ocean surface and bottom. The time series showed up to 19 s of reverberation. The received intensity of reverberation from the port-side transmission is comparable to or greater than that in the starboard-side transmission despite the fact that it was directed away from the hydrophones.

Data Interpretation: To understand this, consider the ellipses plotted on the map in Fig. 2. The orange/dark-green ellipses have *Shoup* and the phones as their foci, while the yellow/light-green ellipses have *Shoup* and the J pod as their foci. These are approximate "travel time" ellipses for 1, 3, 5, … 17, 19 s from the smallest to the largest. That is, if the moment in time when the sound arrives along the direct radial path from *Shoup* to the phones (J pod) is time t = 0 s, then reverberation from locations covered by the smallest ellipse arrives 1 s later, and reverberation from the next smallest ellipse arrives 3 s later (from t = 0) and so on.

For the *Shoup*-phone ellipses, the orange/dark-green shows the portions of the travel time ellipse that are not blocked by land and can actually contribute to the reverberation. The yellow/light-green ellipses illustrate the same thing for the J pod. Finally, the green (dark or light) portion of the ellipses corresponds to the reverberation due to the port-side transmission, and the orange/yellow portion of the ellipses corresponds to the reverberation due to the starboard-side transmission. It is evident that a significant amount of acoustic energy from the port-side transmission could

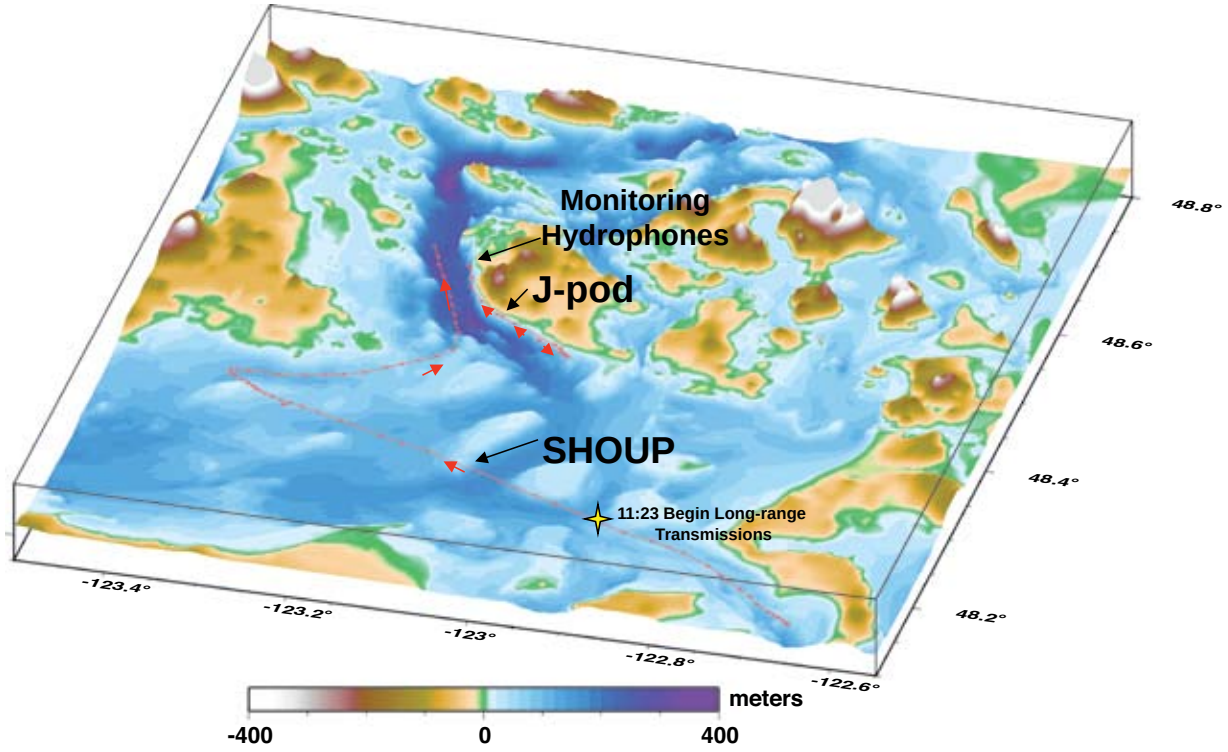

FIGURE 1
Three-dimensional image showing bathymetry and topology of the Haro Strait (deep blue) and surrounding region. The topology above 400 m elevation is in gray. The track of USS *Shoup*, corresponding to times when its sonar was active, proceeds from the lower right-hand corner at time 10:40 and ends at time 14:41 (all times local). The reported track of the boat containing Dr. David Bain and his students, who shadowed the J pod, proceeds from the center of the figure at time 10:47, heading initially southeast, and concludes at time 14:43 heading northwest. The monitoring hydrophones of Dr. Veirs are located shoreward of this last location. *Shoup*'s sonar was initially configured for short-range (less than 2.5 km) operations. From 11:23 until 14:40, it was configured for long-range operations (from 5 to 20 km). The first hydrophone recording available for analysis was from time 11:39.

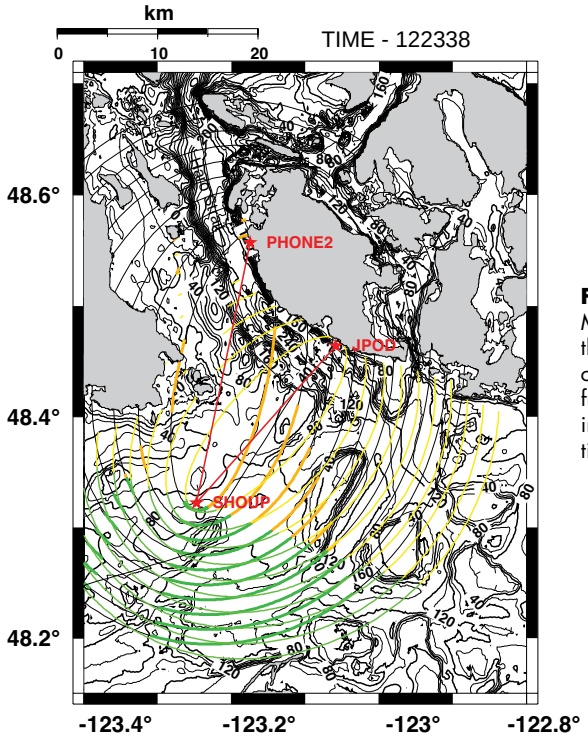

FIGURE 2
Map showing the positions of *Shoup*, the J pod, and the monitoring hydrophones over the bathymetry contours. The straight red lines indicate the direct path from the acoustic source to the J pod or to the monitoring hydrophones. The ellipses indicate location and timing of reverberation (see text).

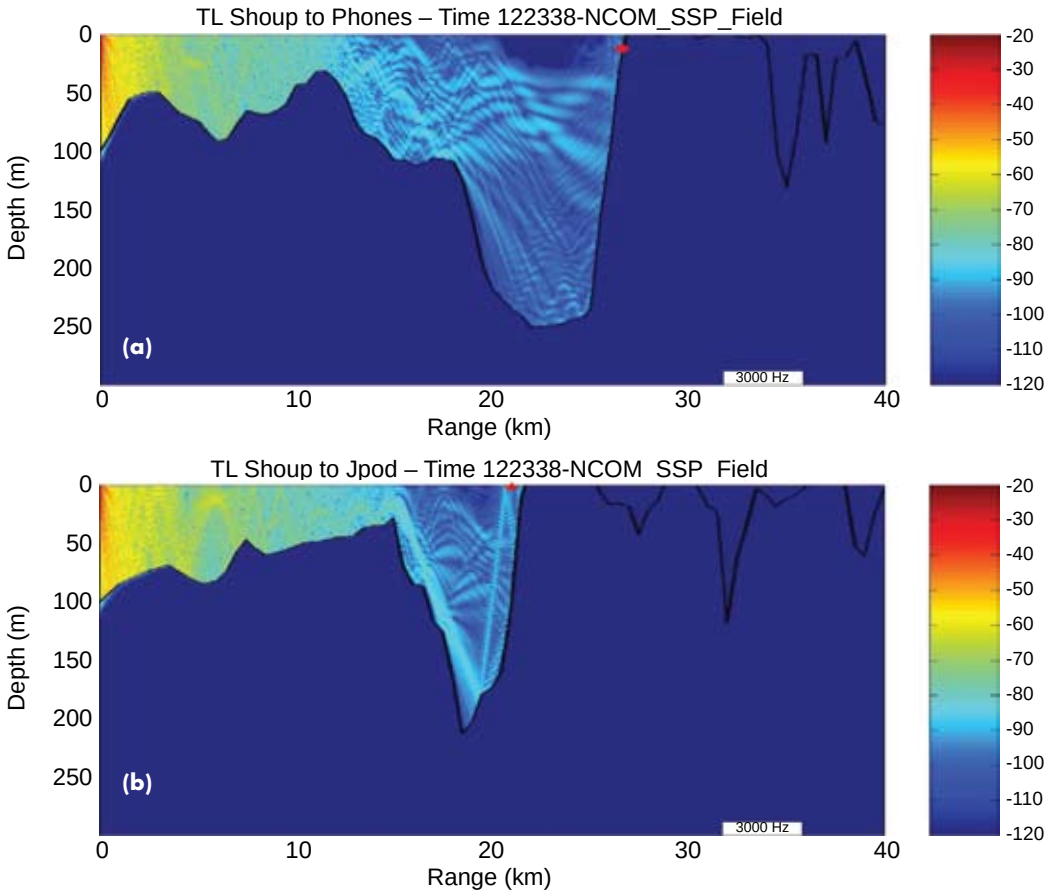

FIGURE 3
Bathymetry and RAM-predicted transmission loss as a function of depth and range for the direct-path radial lines from *Shoup* to the monitoring hydrophones (a) and to the location of the J pod (b).

be scattered from the ocean surface and bottom and received on the hydrophones.

Summary and Conclusions: The comparison of the predicted and measured direct path SPLs on the hydrophones indicated that the model was tending to predict levels ranging from 1 to 10 dB higher than those recorded. Improving the acoustic predictions would require an actual in situ measurement of the sound speed field and a much more detailed description of the bottom properties throughout the region. The predicted SPLs were considered to be an overestimate of the mean SPL received at the monitoring hydrophones and experienced by the J pod.

By combining the model predictions with the acoustic recordings, a time series of the SPL received by the J pod could be created for the entire event that became more accurate as the J pod and *Shoup* both approached the locations of the hydrophones. By integrating this time series a total energy exposure for the J pod could be calculated. From these results, the National Marine Fisheries Service (NMFS) determined that the J pod's exposure levels did not reach the levels for a temporary threshold shift in hearing, let alone a permanent threshold shift. Without the evidence of the directionality of the sonar's mode of operation, the total predicted exposure would have been approximately twice as high and NMFS's conclusion might have been different.

The results of this reconstruction were also used in the development of a risk continuum function to relate acoustic exposure levels to the probability of a behavioral response. This risk continuum function was used in the analysis supporting the recent Environmental Impact Statement for the Hawaii Range Complex.

[Sponsored by COMPACFLT]

References

[1] D. Bain, Field notes provided to the National Marine Fisheries Service NorthWest Region (NMFS NW); subsequently made available to U.S. Navy by NMFS NW for the express purpose of completing this acoustic analysis (2003).

[2] V. Veirs, Acoustic recordings made under the OVAL program and provided to NMFS NW; subsequently made available to U.S. Navy by NMFS NW for the express purpose of completing this acoustic analysis (2003).

[3] M.D. Collins, "A Split-step Pade Solution for Parabolic Equation Method," *J. Acoust. Soc. Am.* **93**, 1736–1742 (1993).

Operational Acoustic Transmission Loss Uncertainty Characterization

R.A. Zingarelli and J.P. Fabre
Acoustics Division

Introduction: Uncertainty is an unavoidable part of any physical measurement or prediction process. Uncertainties in directly measured oceanographic quantities such as bathymetry, water sound speed profiles, acoustic system parameters, and so forth are fairly straightforward to quantify. A method for mapping these values into overall uncertainty in sound transmission loss (TL) levels has been developed at NRL. Here, we briefly review this method and demonstrate its use in a larger framework, incorporating environmental and acoustic prediction models and associated uncertainties to give a unified, operationally useful prediction for confidence intervals on acoustic transmission loss.

Technique: It has long been recognized that range-averaging predicted TL will produce a curve that qualitatively matches the results of a frequency average over some system bandwidth. The physical basis for this was later shown to be an outcome of similar mathematical forms of the two types of averages when the solutions were expressed as sums of modes.[1] This averaging equation is also amenable to calculating bounds on a TL prediction if some method exists of determining the uncertainty in the number of modes. Fortunately, such estimation is straightforward if sound directions are locally approximated as straight lines and the maximum propagation angle is known. The algorithm developed[2] consists of three range averages: one for the TL prediction based on system bandwidth as described in Harrison and Harrison,[1] and one for each of the bounds based on a fractional change in averaging interval corresponding to the fractional change in mode count, which is determined by uncertainties in both environmental parameters and bandwidth. This method provides a significant capability, the estimation of TL uncertainty, at low computational cost, and can be used on any acoustic propagation model, mode-based or otherwise.

Two examples of this method are shown in Fig. 4. The environment depicts an upslope path onto a coastal shelf, and the two frequencies used were chosen to bracket the cutoff frequency for acoustic propagation on the shelf. Typical uncertainties for the environment were used, and the bandwidth of the system was set to one-third octave to simulate common oceanographic survey methodology. At the higher frequency (Fig. 4(a)), the small uncertainties in the deeper water expand greatly as the sound propagates upslope. As the total number of modes decreases, uncertainties in the remaining number of modes become proportionally more important. At the lower frequency (Fig. 4(b)), the cutoff range prediction is evident and the TL uncertainty boundaries effectively become range uncertainty boundaries for the cutoff point.

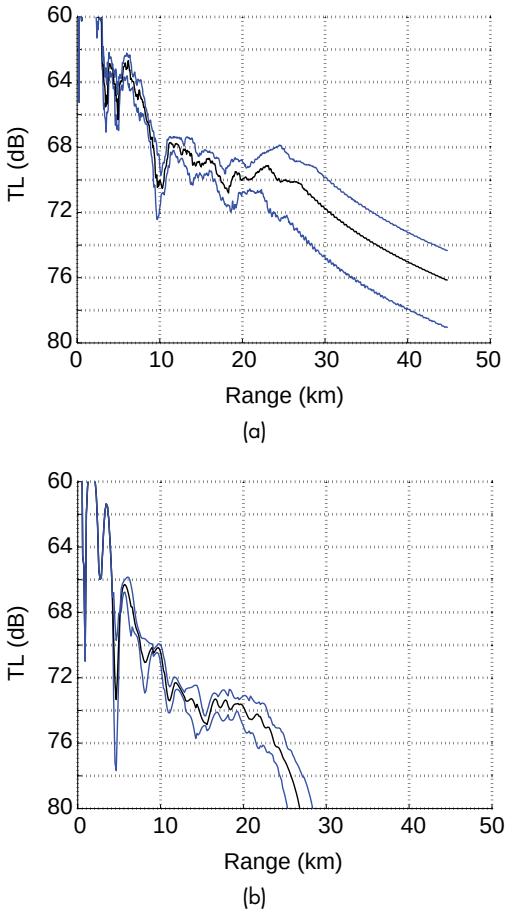

FIGURE 4
Transmission loss calculations for an upslope onto coastal shelf environment at (a) 125 Hz and (b) 12.5 Hz. Mode stripping and, hence, increasing uncertainty with range are shown at the higher frequency, while cutoff depth and the resulting range uncertainty are evident at the lower frequency.

Demonstration: Products such as the Naval Oceanographic Office (NAVO) acoustic performance surface and NRL's Integrated Acoustic Multienvironmental Processing System (IAMPS) currently provide high-fidelity, wide-area estimates of acoustic system performance given the spatially and temporally complex environment. The uncertainty estimation method described above has been incorporated into IAMPS and is providing estimates of acoustic performance with uncertainty for large operational areas and time frames. NRL is transitioning this method to NAVO for use in their acoustic performance surface

and other related applications, and it is becoming part of their emerging acoustic uncertainty capabilities in support of the Fleet. In addition to providing the ability to include non-environmental sources of uncertainty, this transition precludes the need to compute multiple acoustic realizations based on oceanographic (or other) ensembles, thus saving computational time while still including the ensemble variance.

Figure 5 shows an example of predicted area that would be covered by a generic acoustic sensor for a test area in the Pacific Ocean. The uncertainty methodology was applied and overplotted for areas of high (red contours) and medium (black contours) uncertainty. This type of product is very useful to the oceanographic and acoustic analysts and allows them to better understand the quality of their products.

Summary: The ability to quickly and reliably estimate acoustic uncertainty has far-reaching applications. Among these are confidence intervals on acoustic level and detection range predictions, improved capability and verification of ongoing performance surface predictions, better planning of Fleet and survey operations, and further reduction of the overall error in database products from NAVO. This method and its applications have been fully developed and tested at NRL, are transitioning to Naval operational use, and are fast becoming an integral part of the Navy's ability to estimate acoustic uncertainty for better understanding and improved confidence in products supporting many aspects of acoustic tactics and planning.

[Sponsored by NRL]

References

[1] C.H. Harrison and J.A. Harrison, "A Simple Relationship Between Frequency and Range Averages for Broadband Sonar," *J. Acoust. Soc. Am.* **97**, 1314–1317 (1995).

[2] R.A. Zingarelli, "A Mode-based Technique for Estimating Uncertainty in Range-averaged Transmission Loss Results from Underwater Acoustic Calculations," *J. Acoust. Soc. Am.* **124**, EL218–222 (2008).

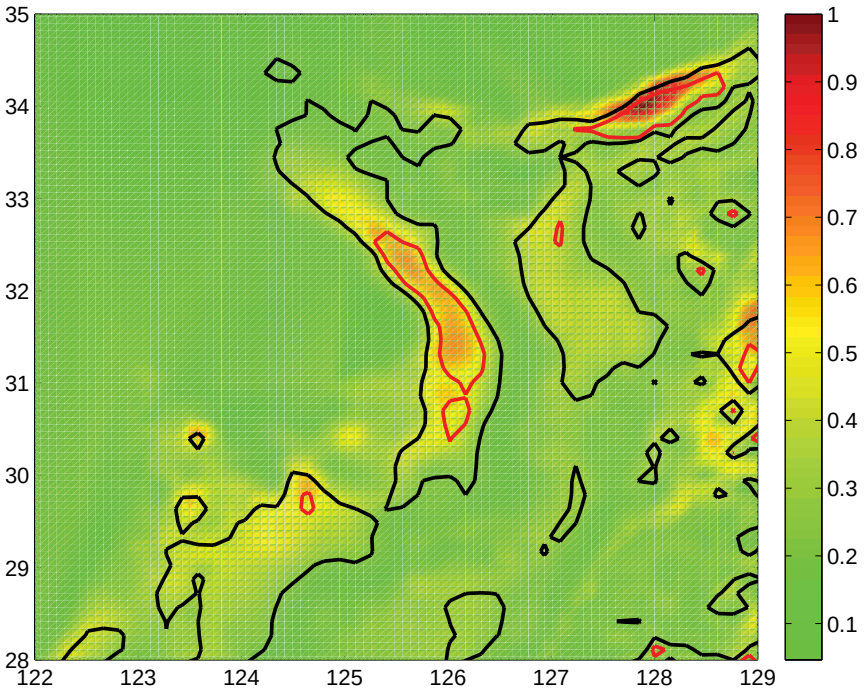

FIGURE 5
Acoustic coverage overplotted with areas of high (red contours) and medium (black contours) uncertainty.

atmospheric science and technology

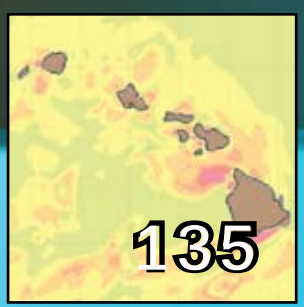

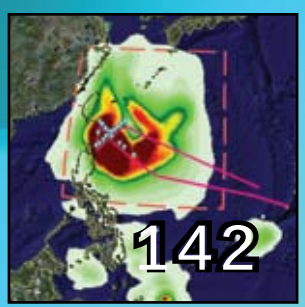

135
Operational Radar Performance Surfaces for RIMPAC 2008
T. Haack and J. Hansen

138
The Atmospheric Neutral Density Experiment (ANDE)
A. Nicholas, T. Finne, I. Galysh, M. Davis, and L. Healy

142
Observing Guidance for Tropical Cyclones
C.A. Reynolds, J.D. Doyle, C. Amerault, and H. Jin

Operational Radar Performance Surfaces for RIMPAC 2008

T. Haack and J. Hansen
Marine Meteorology Division

Introduction: A new system called Atmospheric Radar Performance Surfaces (ATPS) was designed in a joint effort between the Naval Research Laboratory (NRL), the Naval Postgraduate School (NPS), the Space and Naval Warfare (SPAWAR) Systems Center (SSC), and Fleet Numerical Meteorology and Oceanography Center (FNMOC), to provide spatio-temporal guidance about radar propagation conditions during Rim of the Pacific 2008 (RIMPAC08). The ATPS provides expected radar range guidance as a function of location, time, radar, and target type. Supplementary information was provided by ensemble forecasts to estimate the uncertainty associated with environmental ducting parameters impacting electromagnetic (EM) propagation. The ATPS provides range information and the environmental uncertainty enables a "range of ranges" to be communicated. Predicting EM propagation conditions in and around the Fleet during planning/execution of at-sea exercises and operations is of critical military importance. The ATPS enables decision-makers to gain a strategic advantage in placement and positioning of military assets. The inclusion of quantitative uncertainty information provides decision-makers with superior information, allowing for improved risk/opportunity management and more efficient operations.

Military operatives routinely use Numerical Weather Prediction (NWP) forecasts for predicting the spatio-temporal variability in atmospheric conditions that influence all facets of mission planning and execution. In addition to their forecasting capability, these fields are also used to initialize propagation codes to assess EM ducting conditions for various radar and target configurations. However, the current capability is limited by an inability to effectively communicate horizontal variability over a wide region of military activity.

The propagation environment is largely dependent upon vertical variations in water vapor, which often contain sharp discontinuities due to layering of the environment. Surface and boundary layer structure in the atmosphere can produce negative gradients in the modified refractive index (M) for which energy at microwave frequencies are trapped, producing extended detection and communication ranges for sensors operating within the ducting layer. Spatial variability develops due to changes in the sea surface temperature (SST), sea/land breeze and topographic forcing, and evolution of the synoptic and mesoscale conditions that add considerable complexity to the propagation environment. The Navy can exploit this variability for military advantage to ascertain locations within their operating domain for optimal placement of assets.

ATPS Components and Products: Figure 1 shows the components of the new ATPS in which radar and target information come from AREPS (Advanced Refractive Effects Prediction System) databases maintained by SSC, the NRL mesoscale forecast model COAMPS®* provides 3D environmental conditions, the NPS bulk surface model vertically resolves the surface layer providing modified refractivity profiles, and the SSC Advanced Propagation Model (APM) determines the propagation path loss. AREPS further provides probability of detection (POD) threshold values of propagation path loss below which a given target can be detected. The radar's performance is denoted by the maximum detection range and maximum continuous detection range (right and left asterisk, respectively, in Fig. 1(e)) computed for each point in the COAMPS model domain.

An example of a radar performance surface in the Arabian Gulf is shown in Fig. 2, depicting the maximum detection range of a small surface target using a shipboard X-band radar. The spatial complexity and structure originate from variability in the 9-km and 3-km resolution COAMPS fields, with the 3-km grid more faithfully resolving nighttime drainage flows from the steep mountainous coastline to the northeast. While these performance surfaces are for a generic X-band radar, the ATPS system has been made flexible and versatile such that the predicted performance can be obtained for a variety of radars and targets operating at any height within a COAMPS analysis or forecast domain.

RIMPAC08 Operational Demonstration: As a demonstration of the new radar performance surface capability and transition to operations at FNMOC, the complete end-to-end automated ATPS system was seamlessly run in real time twice daily for military exercises in and around the Hawaiian Islands during July 2008 (RIMPAC08). The performance of an X-band airborne radar at three flight levels was selected for evaluation of ATPS and follow-on validation efforts. Due to their differing radar cross sections, ship-sized targets have considerably different detection patterns than smaller surface targets, as shown in Fig. 3. The surfaces display the hallmarks of an island wake in the

*COAMPS® (Coupled Ocean/Atmosphere Mesoscale Prediction System) is a registered trademark of the Naval Research Laboratory.

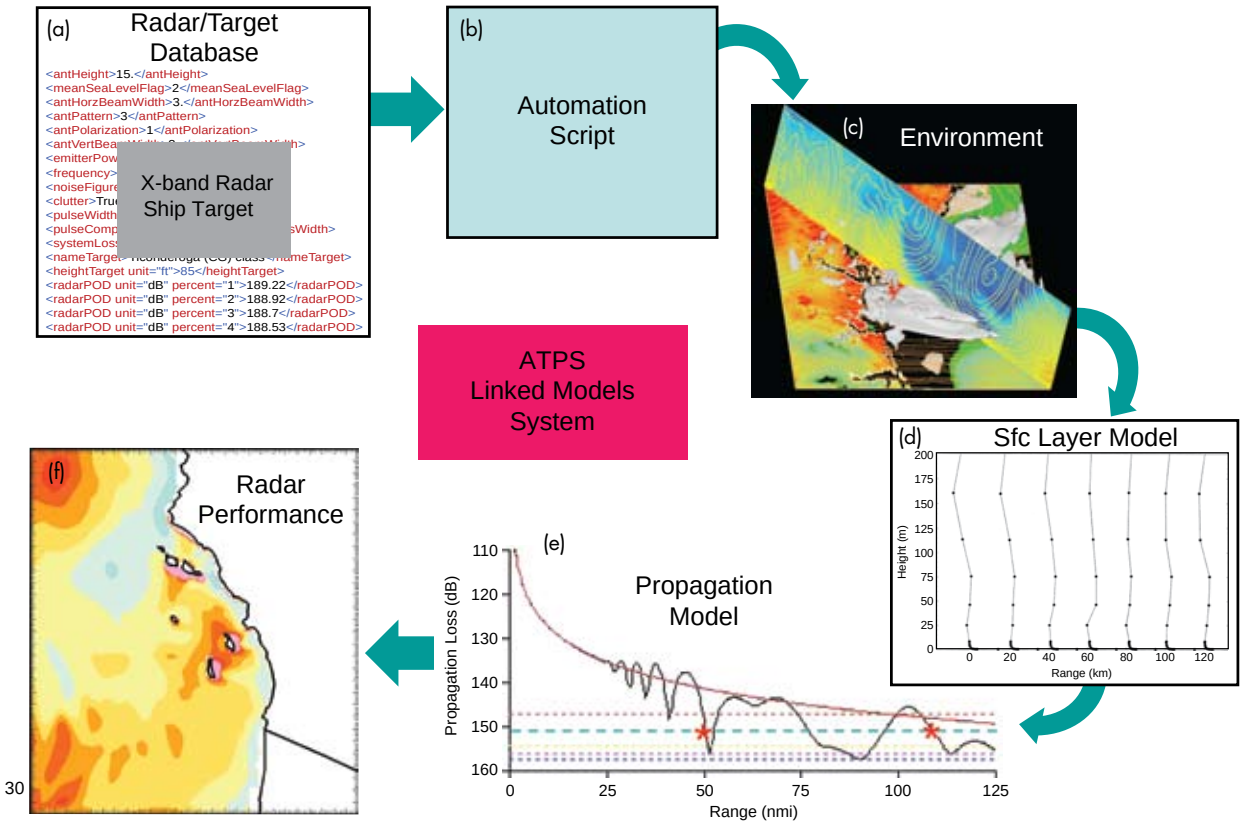

FIGURE 1
ATPS components. Radar/target/threshold input from AREPS database (a), automation script (b), three-dimensional environmental fields from COAMPS (c), high vertical resolution profiles of modified refractivity from the NPS bulk surface layer model (d), propagation path loss determined by APM (e), and the gridded ATPS radar performance output product (f). In Fig. 1(e), the dashed lines denote probability of detection (green line = 90% POD) and the right and left red asterisks are the maximum detection range and maximum continuous detection range, respectively.

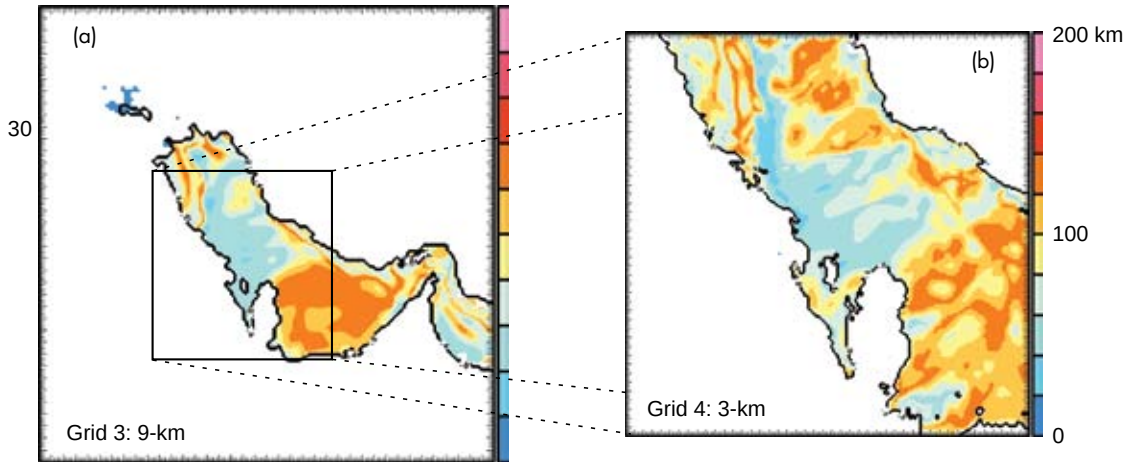

FIGURE 2
Comparison of the radar performance surface for an X-band shipboard radar showing maximum detection range (km) for a 90% POD of a small surface target from COAMPS 9-km resolution fields (a) and 3-km resolution fields (b).

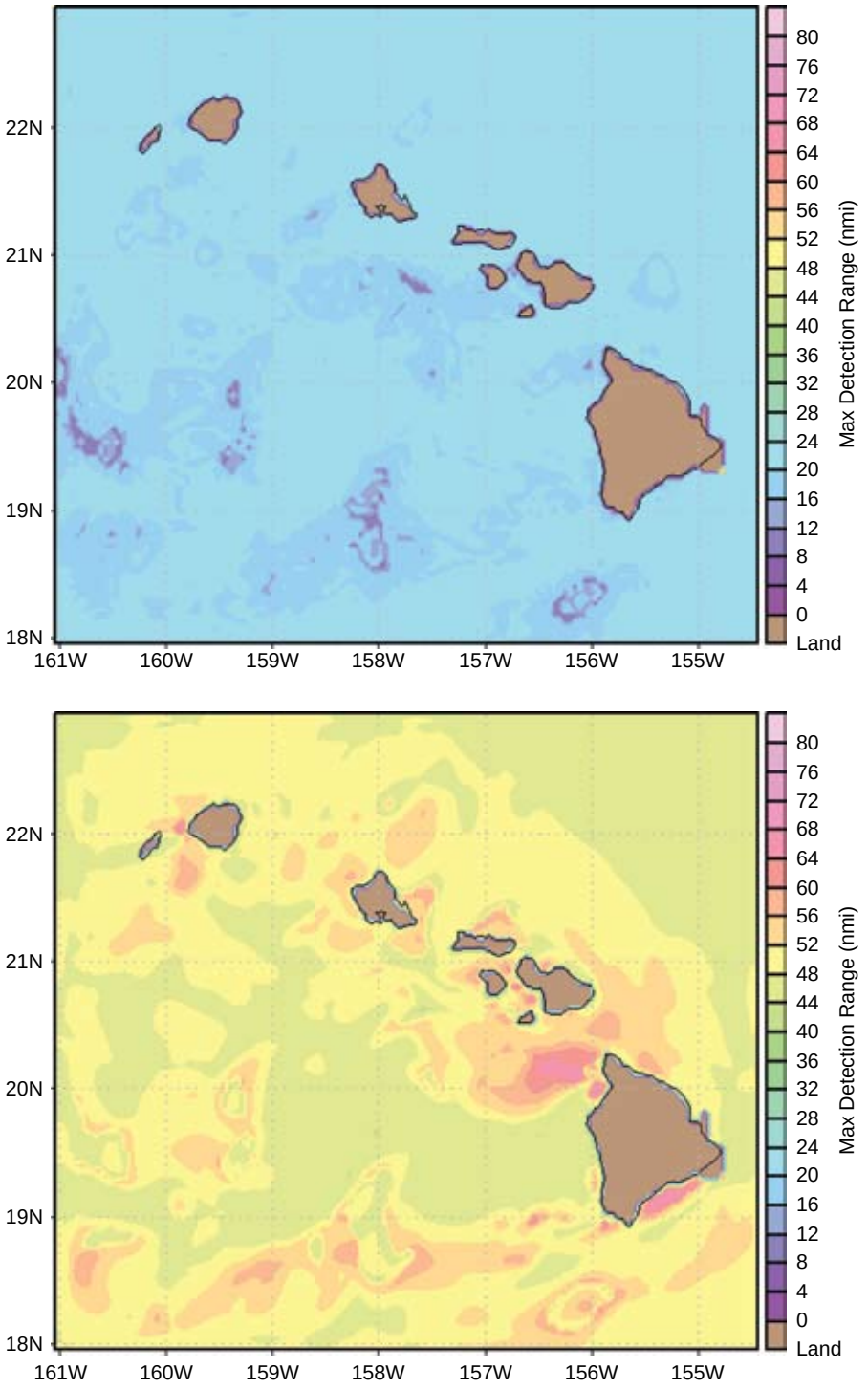

FIGURE 3
Performance surface for an X-band airborne radar at 1000 ft showing maximum detection range (nmi) for 90% POD of a small surface target (top) and a ship-sized target (bottom).

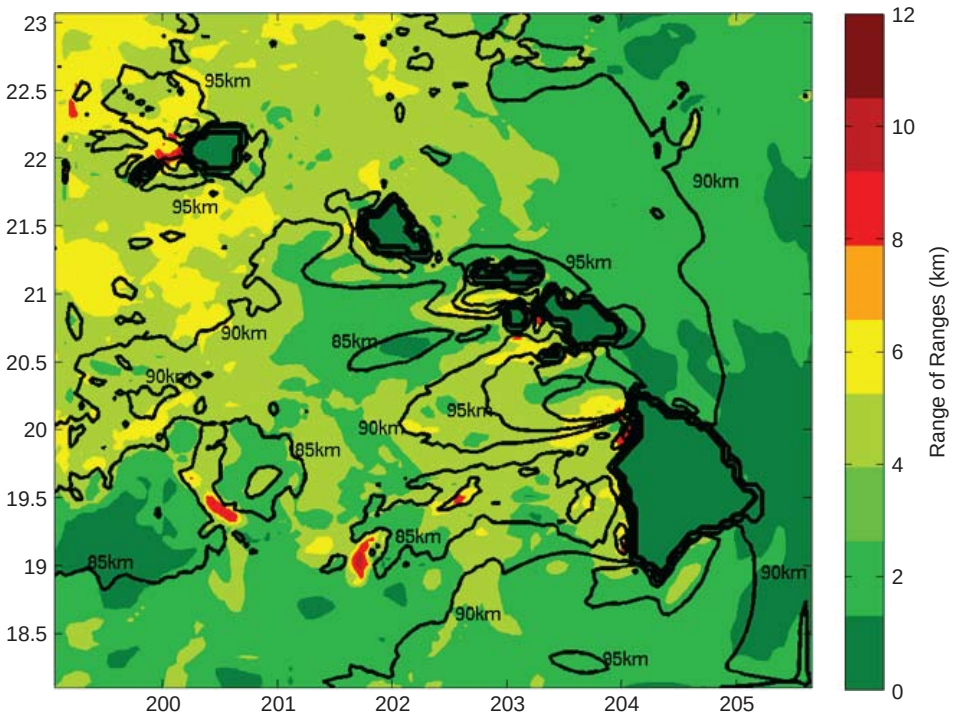

FIGURE 4
The mean detection range (km, solid contours) and 1 standard deviation (km, color fill) of ship-sized target obtained from a 33-member ensemble of COAMPS forecasts communicating environmental uncertainty and the "range of ranges." Green colors denote high confidence in the mean value, and red denotes low confidence.

lee of the islands,[1] for which atmospheric effects can have opposing influence on detection depending upon target size. Note that a ship-sized target has shorter detection ranges in the wake region relative to surrounding locations, whereas a smaller surface target has longer detection ranges.

The deployment of ATPS enables for the first time domain-wide coverage of environmental effects on radar performance and an opportunity to efficiently assess and exploit spatio-temporal variability over broad regions. A complementary RIMPAC08 demonstration project estimated and communicated the uncertainty associated with atmospheric ducting by running a 33-member ensemble of COAMPS integrations for each forecast period. Detection range uncertainty is obtained by computing ATPS fields for each member of the ensemble, yielding the mean maximum detection range and first standard deviation, an example of which is given in Fig. 4. The variability communicates the "range of ranges" that can be used to add confidence to deterministic forecasts or be used to objectively optimize decisions.

Summary: The work presented here represents the combined efforts of several Navy organizations to design, develop, and transition ATPS, which automates the computation of atmospheric radar performance surfaces using COAMPS three-dimensional forecasts as input to describe the environmental effects on EM propagation. This system was successfully deployed as a demonstration product during RIMPAC military exercises in 2008.

[Sponsored by SPAWAR PMW-120]

References

[1] S.D. Burk, T. Haack, L.T. Rogers, and L.J. Wagner, "Island Wake Dynamics and Wake Influence on the Evaporation Duct and Radar Propagation," *J. Appl. Meteoro.* **42**, 349–367 (2003).

The Atmospheric Neutral Density Experiment (ANDE)

A. Nicholas,[1] T. Finne,[1] I. Galysh,[2] M. Davis,[2] and L. Healy[3]
[1]*Space Science Division*
[2]*Space Systems Development Department*
[3]*Spacecraft Engineering Department*

Introduction: The Naval Research Laboratory (NRL) has developed a satellite suite, the Atmospheric Neutral Density Experiment (ANDE),[1] to improve precision orbit determination and prediction by monitoring total atmospheric density between 300 and 400

km. The ANDE Risk Reduction (ANDERR) flight was deployed into orbit by the space shuttle *Discovery* on 21 December 2006 (Fig. 5). The primary ANDERR mission objective, a test of the shuttle deployment mechanism for the follow-on ANDE flight (scheduled for mid-2009), was successful. The primary ANDE mission objectives are to measure the variability of atmospheric density driven by solar and geomagnetic forcings for improved orbit determination and to provide a test object for the U.S. space surveillance network (SSN). A joint effort between NRL's Space Science Division and its Naval Center for Space Technology to routinely process and analyze the ANDE data has led to improved orbit determination and prediction using an atmospheric model correction method. The ANDE data provide a valuable tool for correcting deficiencies in atmospheric models and have led to advancements in miniature sensor technology. These advancements are pivotal for multipoint in situ space weather sensing.

Mission Objectives: The ANDE satellite suite consists of a series of four nearly perfect spherical micro-satellites with instrumentation to perform two interrelated mission objectives. The first objective is to monitor the total neutral density along the orbit for improved orbit determination of resident space objects. The second is to provide a test object for both radar and optical SSN sensors. The DoD Space Test Program will provide launch services for two missions (ANDERR and ANDE), with each mission flying a pair of ANDE spacecraft.

The major source of error in determining the orbit of objects in low Earth orbit (LEO), i.e., altitudes less than 1000 km, is the computation of acceleration due to atmospheric drag. This acceleration is governed by Eq. (1),

$$a_d = -\frac{1}{2} B \rho v^2 , \tag{1}$$

where a_d is the acceleration, ρ is the atmospheric density, and v is the orbital velocity relative to the medium (including cross-track and radial velocities). Equation (2) defines the ballistic coefficient, B, with C_D being the coefficient of drag, A the projected frontal area, and m the mass of the object:

$$B = \frac{C_D A}{m} \tag{2}$$

The constant and well-determined cross section and surface properties of the ANDE spherical spacecraft provide an ideal set of objects for monitoring atmospheric drag and for calibrating SSN assets.

ANDE Data Flow: The 20th Space Control Squadron, USAF, in Dahlgren, Virginia, processes the SSN radar observation data of the ANDERR spacecraft. The product is a set of orbital state vectors and corresponding radar observations, which is provided to NRL up to three times a day. These state vectors are processed at NRL using Special-K orbit determination software to produce a set of ephemerides. These ephemeris files are reformatted into the consolidated predic-

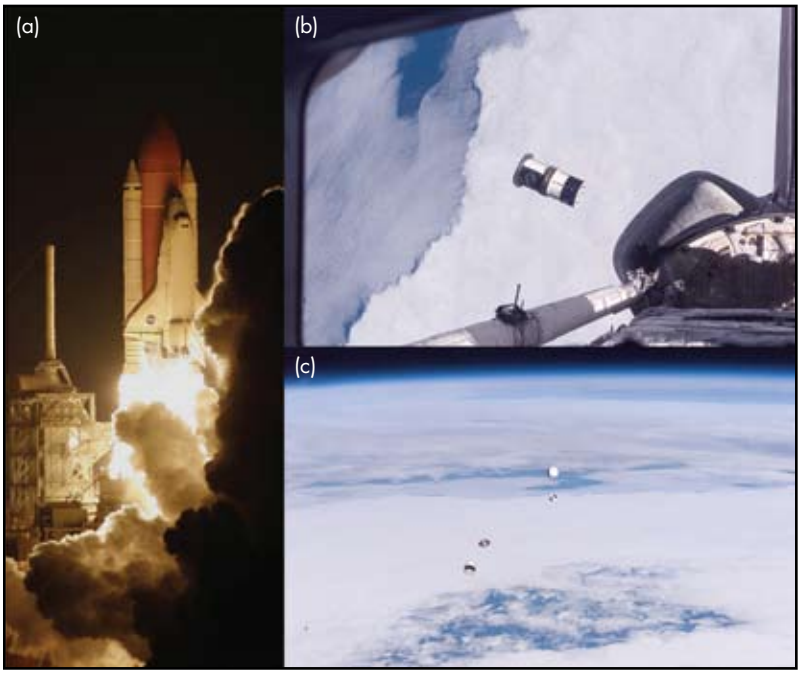

FIGURE 5
The launch (a) and deployment (b,c) of the Atmospheric Neutral Density Experiment Risk Reduction (ANDERR) spacecraft from the space shuttle *Discovery* on 21 December 2006, during the STS-116 mission. (Photos courtesy of NASA)

tion format used by the International Laser Ranging Service (ILRS) tracking stations. A set of predictions is also computed once per day using the NRL Orbit Covariance Estimation and Analysis (OCEAN) orbit determination code. The radar observation data are merged with the satellite laser ranging (SLR) observation data and processed by OCEAN to generate a 2-day augmented set of predictions that includes the atmospheric correction. Figure 6 depicts the two data flow processes.

Data Processing and Analysis: A comparison between the values of C_D for the two spacecraft from the OCEAN run, using an atmospheric model (NRLMSISE-00) and a priori area and mass information, yields excellent agreement between the two objects even as the altitude separation between the two spacecraft increases due to differential drag. The retrieved values of C_D for the two spacecraft are presented as a function of time in Fig. 7(a). These results are non-physical as the value of C_D is well below the theoretical limit of 2; the atmospheric model is overestimating the density, and the OCEAN code is correcting for this by scaling the B term down to fit the observations. The ANDERR data provide a global climate monitoring metric, which showed a consistent overestimation[2] of total density by climatology models by an average of 26.6%.

The primary drivers of the atmosphere are solar radiation heating and geomagnetic heating. The solar driver is input into the atmospheric model in the form of the $F_{10.7}$ cm radio flux, an easy to measure ground-based proxy for the solar ultraviolet flux that heats the atmosphere. The A_p index is a measure of geomagnetic activity at the Earth and is used by atmospheric models to drive the geomagnetic heating in the atmosphere. A wavelet analysis was performed on the C_D density corrections: $F_{10.7}$, A_p, and the solar wind velocity (V_{sw}) time series to further investigate the causes of periodicities observed during 2007. The wavelet power spectra are presented in Fig. 7(b–e) as a function of day of year for 2007. The plots have been formatted to a range of 2 to 20 days with white contours representing the 95% significance level. The short-term oscillations (5, 7, 9 days) were much more prevalent and stronger in both the A_p and V_{sw} data in the first half of 2007 than in the second half of the year. This is also evident in the 9-day period in the C_D atmospheric corrections derived from the ANDERR spacecraft orbits. The strong 18-day periods observed in the $F_{10.7}$ data are also observed in the C_D corrections although there is a significant time lag and atmospheric recovery period associated with this data. The analysis technique applied to the ANDERR data set separates geomagnetic forcing of the atmosphere from solar irradiance forcing of the atmosphere.

Sensor Miniaturization: On the second flight of the ANDE program (scheduled for mid-2009), one spacecraft will carry miniaturized sensors to measure the density and composition of the atmosphere. NRL

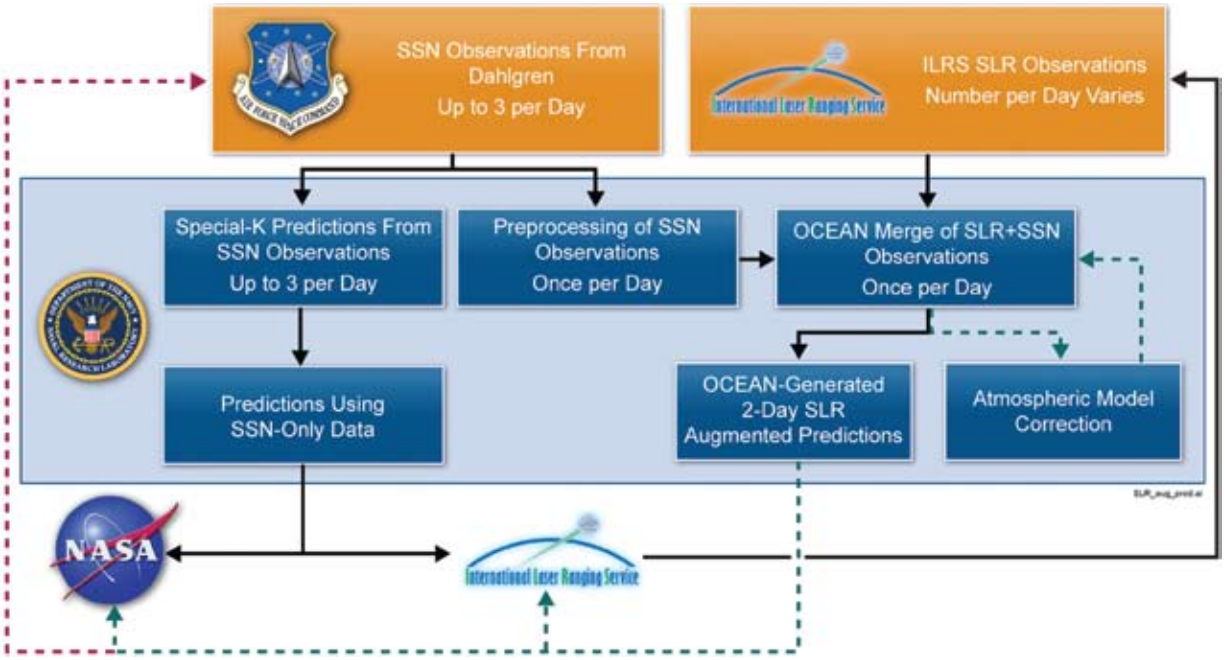

FIGURE 6
The data flow and processing of ANDE observations. The green dashed lines represent functions demonstrated during the ANDERR mission. The red dashed line is expected to be complete after the final ANDE flight.

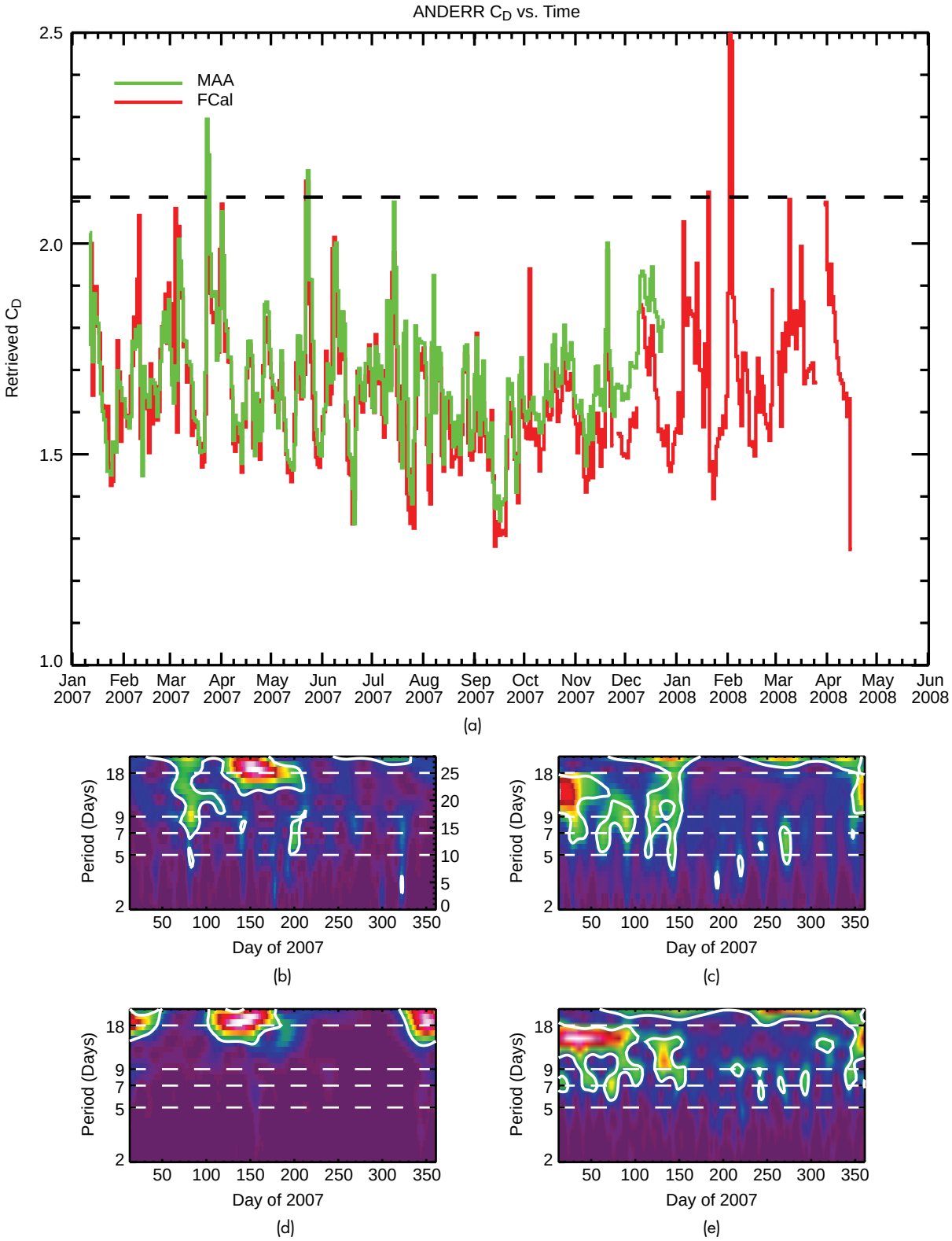

FIGURE 7
(a) OCEAN fitted C_D values, using NRLMSISE-00 for the ANDERR spacecraft. (b, c, d, e) Morlet power spectra for the C_D, A_p, $F_{10.7}$, and V_{sw}, respectively. The white contour is the 95% significance level.

FIGURE 8
The ANDE wind and temperature spectrometer.

has collaborated with NASA Goddard Space Flight Center to develop a small wind and temperature spectrometer (Fig. 8). The technology push to reduce the size, weight, and power of such sensors is pivotal for multipoint in situ space weather sensing.

[Sponsored by NRL and ONR]

References

[1] A.C. Nicholas, S.E. Thonnard, I. Galysh, P. Kalmanson, B. Bruninga, H. Kelly, S. Ritterhouse, J. Englehardt, K. Doherty, J. McGuire, D. Niemi, H. Heidt, M. Hallada, D. Dayton, L. Ulibarri, R. Hill, M. Gaddis, and B. Cockreham, "An Overview of the ANDE Risk Reduction Flight," Proc. of the AMOS Technical Conference, Maui, HI, Sept. 2002.

[2] A.C. Nicholas, J.M. Picone. J. Emmert, J. DeYoung, L. Healy, L. Wasiczko, M. Davis, and C. Cox, "Preliminary Results from the Atmospheric Neutral Density Experiment Risk Reduction Mission," Proc. of the AAS/AIAA Astrodynamics Specialist Conference, paper #AAS 07-265, Mackinac Island, MI, Aug 20–24, 2007.

Observing Guidance for Tropical Cyclones

C.A. Reynolds,[1] J.D. Doyle,[1] C. Amerault,[1] and H. Jin[2]
[1]*Marine Meteorology Division*
[2]*SAIC*

Introduction: Tropical cyclones (TCs), including hurricanes in the Atlantic and typhoons in the Western Pacific, are of great military and civilian interest around the world. In order to improve the prediction of TC intensity, structure, and track, THe Observing-system Research and Predictability EXperiment (THORPEX) Pacific Asian Regional Campaign (T-PARC)/Office of Naval Research (ONR) Tropical Cyclone Structure-08 (TCS-08) field campaign was conducted during August and September 2008. The international campaign, with nine participating nations, aimed to observe TCs and their environment throughout their lifecycle. To accomplish this, four aircraft stationed in Guam, Japan, and Taiwan flew a total of 76 missions (including 21 missions by the NRL P-3), during which 1149 vertical soundings of atmospheric data were taken via instruments dropped from the aircraft. In addition, 223 soundings were taken from instruments dropped from high-altitude balloons drifting westward from their launch site in Hawaii. These atmospheric observations were subsequently ingested into operational weather prediction systems to improve real-time TC forecasts. For the first time ever, the number of these special observations taken in the Western Pacific was similar to the number of special observations taken to improve hurricane forecasts in the Atlantic (Fig. 9).

To support the field campaign, NRL produced real-time products based on global-scale and storm-scale forecast models and their adjoint systems. Adjoints allow for the calculation of the sensitivity of TC forecasts to changes in the initial state in a mathematically rigorous, computationally feasible manner. These products provided information on features and processes that influence the TC track and intensity forecasts, and were instrumental in determining resource allocations and deployments (such as when and where aircraft would take additional observations). NRL uniquely contributed both global and storm-scale products, providing critical information on both large-scale remote influences and the sensitivity of the forecast to fine-scale structures within the storm itself.

Global-scale Products: NRL used the Navy Operational Global Atmospheric Prediction System (NOGAPS) forecast and adjoint models[1] to produce targeted observation guidance twice daily for five fixed regions, plus additional products during high-interest periods, at 150 km resolution. These guidance products provided information on where the 48-h TC forecasts would be most sensitive to errors in the atmospheric analyses, and therefore would be "targets" for additional observations to improve the quality of the analysis in these regions. The target guidance was produced with a 48-h to 60-h "lead time" to allow for flight track planning and deployment. These products were useful both for aircraft deployment purposes and for understanding the physical processes that control tropical cyclone motion. For example, in Fig. 10, the NOGAPS forecast sensitivity (shaded) for TC Jangmi on 00 UTC 28 September 2008, indicates that the 48-h forecast of TC Jangmi (22N, 122E) is sensitive to changes in the peripheral anticyclonic (clockwise) flow to the southeast of the storm center, as well as a weakness in the anticyclonic flow to the north of the storm center (as denoted by the 500-hPa streamlines). The importance of both these features for influencing TC motion has been previously suggested through simple dynamical studies as well as complex numerical integrations.

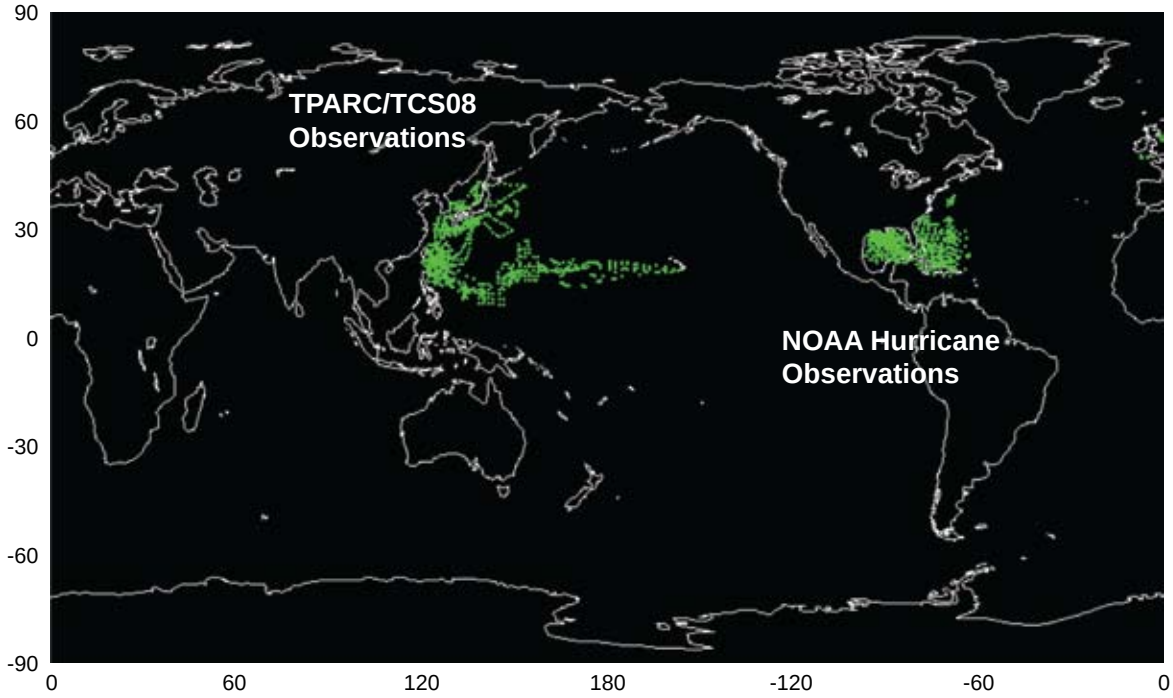

FIGURE 9
Locations (green dots) of the special atmospheric soundings taken from aircraft and high-altitude balloons during September 2008. Figure produced by Fleet Numerical Meteorology and Oceanography Center.

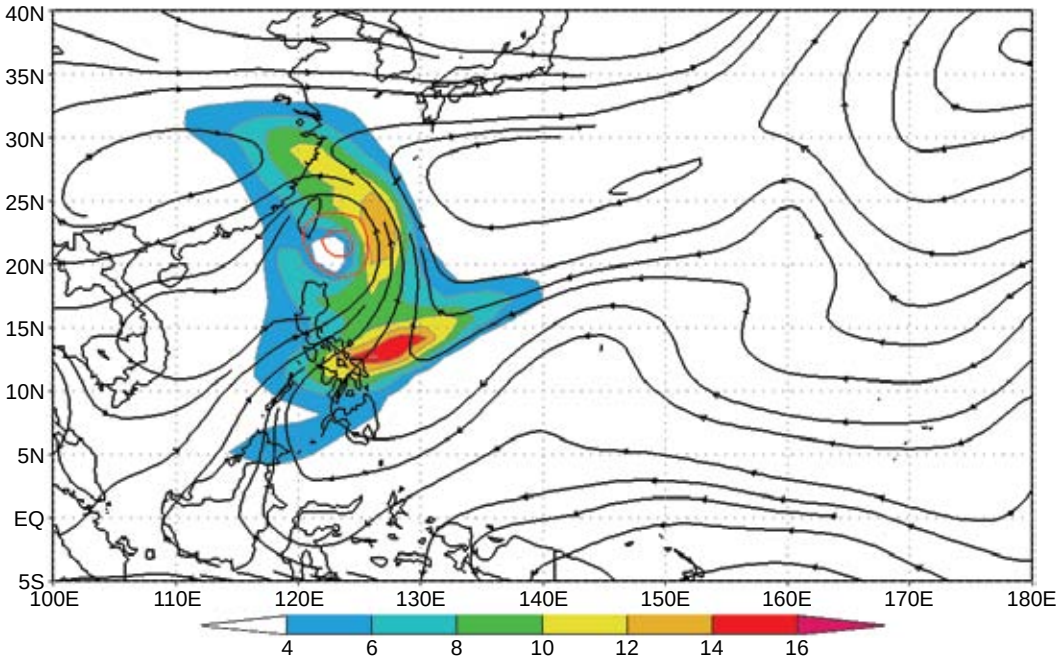

FIGURE 10
Vertically integrated sensitivity of the NOGAPS 48-h forecast of TC Jangmi, valid at 00 UTC 28 September 2008, shaded, J kg^{-1}, along with streamlines for the 500-hPa wind (black), and contours of 850-hPa vorticity at 10 and 20 x 10^{-5} s^{-1} (red). Jangmi is centered at 22N, 122E.

Storm-scale Products: Storm-scale targeted observing products were produced using the Coupled Ocean/Atmosphere Mesoscale Prediction System (COAMPS®) forecast and adjoint system twice daily, centered on storms of interest, at 40-km resolution. These products were produced with 24-, 36-, and 48-h lead times. A unique aspect of this nonhydrostatic adjoint system is that an exact adjoint to the explicit microphysics has been developed[2] and used during T-PARC/TCS-08. An adaptive response function region was used to target favorable areas for TC genesis and development. Results indicate that forecasts of TC formation in the Western Pacific are very sensitive to the initial state. The adjoint-based sensitivity fields indicate structured patterns in the wind, thermal, and microphysical fields that project on to the model-simulated deep convection, which ultimately influences the intensification rate. For example, sensitivity fields for typhoon Sinlaku valid at 1200 UTC 10 September 2008 are shown in Fig. 11. The sensitivity of the final time kinetic energy in the box shown in the figure to the initial vorticity at 2 km indicates a highly structured pattern with anticylonically curved sensitivity maxima (Fig. 11(a)). The region of the perturbation total energy (Fig. 11(b)) maximum is well sampled by the C-130 aircraft soundings deployed during this flight. In general, relatively small adjoint-based basic state perturbations on the order of observational errors (1 m s^{-1}, 1 K) lead to rapid growth rates in the near-surface horizontal velocity of more than 10 m s^{-1} and a 6 hPa deepening rate of the central pressure over 24 h.

Acknowledgments: Support from the sponsor, ONR PE–0601153N, is gratefully acknowledged. The Department of Defense High Performance Computing Challenge project provided real-time computer resources.

[Sponsored by ONR]

References

[1] C.A. Reynolds, M.S. Peng, S.J. Majumdar, S.D. Aberson, C.H. Bishop, and R. Buizza, "Interpretation of Adaptive Observing Guidance for Atlantic Tropical Cyclones," *Mon. Wea. Rev.* **135**, 4006–4029 (2007).

[2] C. Amerault, X. Zou, and J. Doyle, "Tests of an Adjoint Mesoscale Model with Explicit Moist Physics on the Cloud Scale," *Mon. Wea. Rev.* **136**, 2120–2132 (2008).

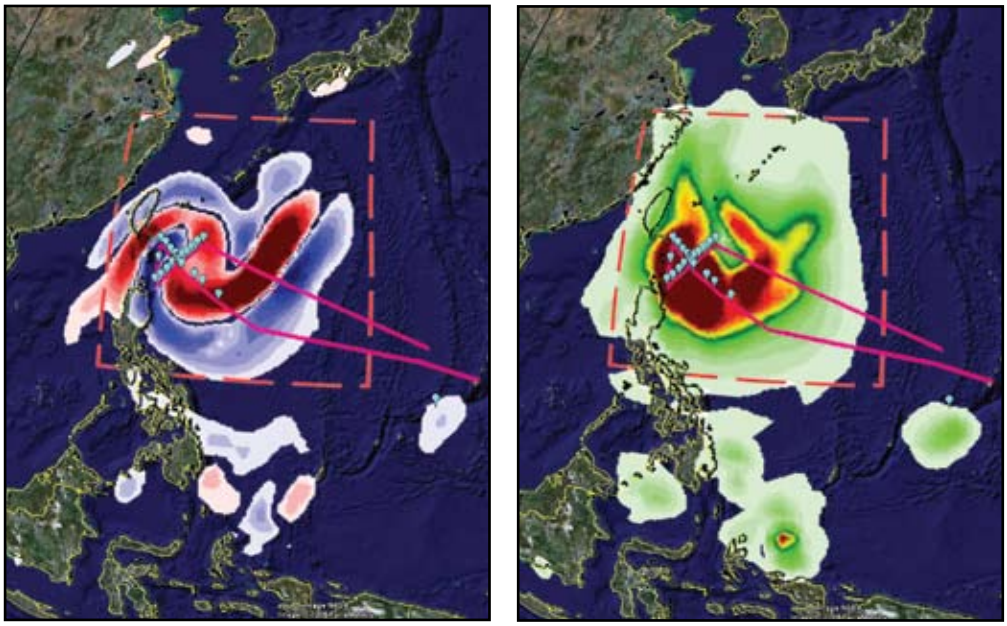

(a) (b)

FIGURE 11

The COAMPS® adjoint sensitivity fields for the (a) vorticity (m^2 s^{-1}) and (b) vertically integrated total energy (J kg^{-1}) valid at 1200 UTC 10 September 2008 for typhoon Sinlaku. The C-130 aircraft flight track is shown by the solid magenta line, and the red dashed box indicates the region over which the response function is applied. The aircraft sounding deployment locations are represented by the turquoise balloon symbols.

chemical/biochemical research

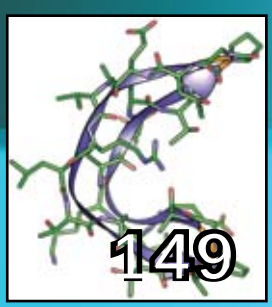

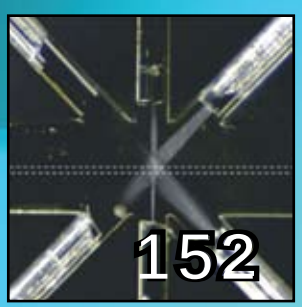

147
Guided Terahertz Waves for Characterizing Explosives
J.S. Melinger and D. Grischkowsky

149
Innovative Foldamers: Engineering Heterochiral Peptides
T.D. Clark and J.L. Kulp III

152
A Multiwavelength Microflow Cytometer
F.S. Ligler, J.S. Erickson, J.P. Golden, J.S. Kim, M. Nasir, P.J. Howell, A.L. Thangawng, L.R. Hilliard, L.C. Shriver-Lake, and G.P. Anderson

Guided Terahertz Waves for Characterizing Explosives

J.S. Melinger[1] and D. Grischkowsky[2]
[1]*Electronics Science and Technology Division*
[2]*Oklahoma State University*

The Problem: One of the most promising and discussed applications of terahertz (THz) spectroscopy is the detection of explosives materials through identification of their vibrational fingerprint spectra. While much progress has been made toward the measurement of THz vibrational fingerprints of explosives,[1] fundamental issues remain to be addressed for THz sensing of explosives to reach its full potential. One issue is that line broadening mechanisms obscure the vibrational spectra of explosives, such that individual vibrational absorption lines merge into broad absorption features. Such line broadening makes identification of explosives more difficult and also impedes a full understanding of the origin of the vibrational fingerprint lines. A detailed scientific understanding of THz vibrational fingerprint spectra is necessary for their rational use in a database of threat materials. A second issue is that THz vibrational transitions tend to be about 100 times weaker relative to mid-infrared vibrational transitions. This emphasizes a need to develop methods to boost the sensitivity of THz measurements for explosives detection.

The Solution: Researchers at NRL and Oklahoma State University (OSU) have collaborated to make innovative use of the metal parallel plate waveguide (PPWG) to measure vibrational fingerprint spectra of explosives solids with unprecedented narrow lineshapes. This approach builds upon previous work by OSU that demonstrated the suitability of the PPWG for performing sensitive THz spectroscopic measurements.[2,3] In a PPWG, THz waves are strongly confined in the narrow gap (20–100 microns) between the plates while propagating over a relatively long path of several centimeters (Fig. 1). We exploit this high sensitivity by depositing a thin film of an explosive (or simulant) on one of the inner metal surfaces. We have used a variety of simple methods to produce thin films of suitable polycrystalline quality, including casting from solution and vacuum sublimation. The measurement method outlined in Fig. 1 is called waveguide terahertz time-domain spectroscopy (THz-TDS),[3,4] and uses well established ultrafast opto-electronic

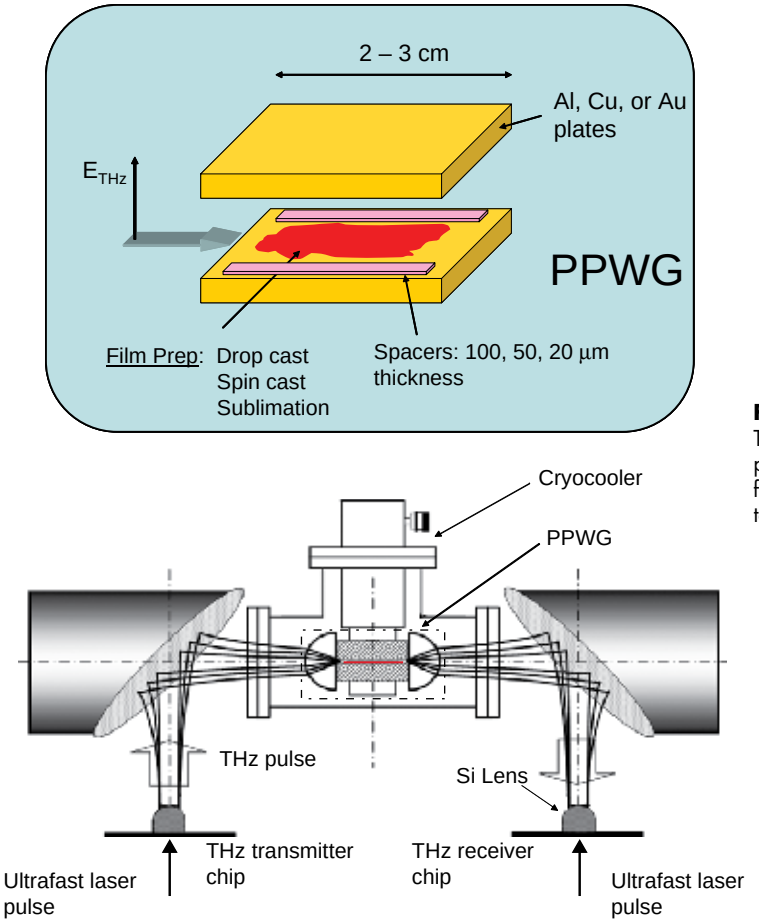

FIGURE 1
Top: Schematic of the metal parallel plate waveguide containing a thin film. Bottom: Schematic of waveguide terahertz time-domain spectroscopy.

techniques to generate and detect sub-picosecond THz pulses.

Vibrational Fingerprints as Narrow as Gas Lines: Virtually all previous THz measurements of explosives solids have suffered from line broadening due to sample disorder. Consequently, the fundamental underlying THz vibrational fingerprint spectrum of explosives and related materials has remained unknown. We have demonstrated the first-ever resolution of these underlying fingerprints using waveguide THz-TDS at cryogenic temperatures.[5,6] In Fig. 2 we compare the THz responses of the explosive simulant 2,4-dinitrotoluene (2,4-DNT) as a film in an aluminum PPWG, and in conventional pellet form, where 2,4-DNT is randomly dispersed in a transparent polyethylene matrix. The persistent ringing patterns of the signal waveforms are the result of THz absorption by vibrational modes. Note that the oscillatory pattern for the pellet sample decays to the noise floor in about 20 picoseconds, whereas the oscillations for the film persist beyond 100 picoseconds. The corresponding vibrational absorption spectra are derived by Fourier transformation of the time-dependent signals (Fig. 2 bottom). The vibrational spectrum of the film shows a dramatic line narrowing effect and resolves several broad absorption features observed in the pellet spectrum. For the film, at least 19 lines are resolved between 0.5 and 2.5 THz, compared to fewer than 10 lines in the pellet sample. Some of the fingerprint lines in the film are as sharp as 7 GHz (0.21 cm^{-1}), which is as narrow as a molecular rotational-vibrational gas line at ambient pressure.

Figure 3 shows that waveguide THz-TDS resolves the previously unseen underlying vibrational fingerprint spectra of the explosives cyclotrimethylene-trinitramine (RDX) and trinitrotoluene (TNT). A highly detailed fingerprint spectrum results for both explosives, showing 18 lines for RDX and 21 lines for TNT. Several of the vibrational lines have linewidths narrower than 10 GHz. A sensitivity enhancement provided by the PPWG is highlighted by the relatively small mass of the explosives films, consisting of approximately 150 micrograms. This represents about 1% of the analyte mass typically needed in THz measurements of standard pellet samples of explosives to achieve similar signal levels.

Structural characterization of the explosives films using optical microscopy and X-ray diffraction indicates a planar ordering of the film on the PPWG surface, where individual micro-crystals form with high crystalline quality (e.g., see Fig. 3). We suggest that the sharp vibrational fingerprint lines observed in our films result from a high degree of crystalline order, which minimizes inhomogeneous line broadening.

Summary and Impact: We have demonstrated a new waveguide-based method for THz characterization

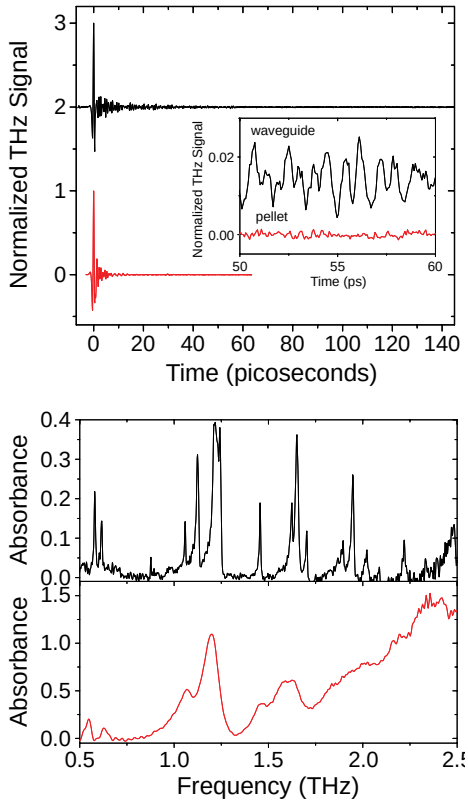

FIGURE 2
Top: Comparison of signal waveforms for pellet (red line) and waveguide THz-TDS (black line) characterizations of 2,4-DNT at 11 K. Bottom: Corresponding absorbance spectra for 2,4-DNT in pellet form (red line) and as a film (black line). An aluminum PPWG is used for waveguide THz-TDS.

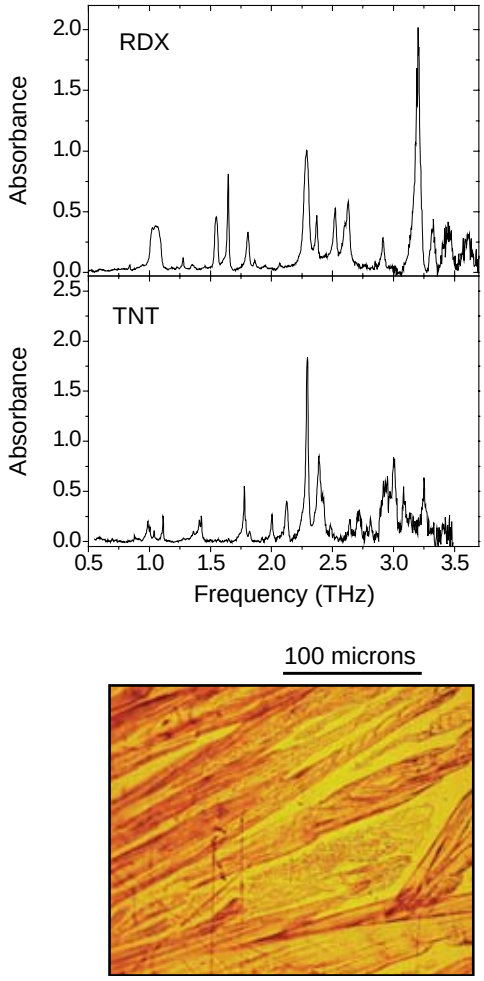

FIGURE 3
Top spectrum: Absorbance spectrum of an RDX thin film in an aluminum PPWG at 13 K. Bottom spectrum: Absorbance spectrum of a TNT thin film in a gold-coated PPWG at 12 K. The optical micrograph shows the TNT film on gold-coated PPWG.

of solids which has resulted in unprecedented narrow-line, high-sensitivity measurements of explosives and related materials. From a fundamental perspective, waveguide THz-TDS provides rigorous input to advance theoretical methods for calculating THz vibrational spectra, which can lead to deeper scientific understandings of the vibrational properties of solid-state materials. More practically, waveguide THz-TDS represents a gateway for the future development of THz-based point detection and forensic analysis of explosives and other threat materials. Further, high-resolution waveguide THz-TDS spectra can augment THz fingerprint databases used for remote sensing applications.

[Sponsored by NRL and ONR]

References

[1] J. Chen, Y. Chen, H. Zhao, G. Bastiaans, and X.-C. Zhang, "Absorption Coefficients of Selected Explosives and Related Compounds in the Range of 0.1-2.8 THz," *Optics Express* **15**, 12060–12067 (2007).
[2] G. Gallot, S.P. Jamison, R.W. McGowan, and D. Grischkowsky, "Terahertz Waveguides," *J. Opt. Soc. Am.* **17**, 851–863 (2000).
[3] J. Zhang and D. Grischkowsky, "Waveguide Terahertz Time-domain Spectroscopy of Nanometer Water Layers," *Optics Letters* **29**, 1617–1619 (2004).
[4] J. S. Melinger, N. Laman, S. Sree Harsha, and D. Grischkowsky, "Line Narrowing of Terahertz Vibrational Modes for Organic Thin Polycrystalline Films Within a Parallel Plate Waveguide," *Appl. Phys. Lett.* **89**, 251110 (2006).
[5] N. Laman, S. Sree Harsha, D. Grischkowsky, and J.S. Melinger, "7 GHz Resolution Waveguide THz Spectroscopy of Explosives Related Solids Showing New Features," *Optics Express* **16**, 4094–4105 (2008).
[6] J.S. Melinger, N. Laman, and D. Grischkowsky, "The Underlying Terahertz Vibrational Spectrum of Explosives Solids," *Appl. Phys. Lett.* **93**, 011102 (2008).

Innovative Foldamers: Engineering Heterochiral Peptides

T.D. Clark and J.L. Kulp III
Chemistry Division

Innovative Foldamers: The field of foldamer design promises new routes to important compounds for use in sensors, smart materials, and catalysts. The term "foldamer" refers to a molecule that folds into a structurally stable state in solution.[1] Proteins and peptides are an important class of natural foldamers that carry out a host of essential functions in biology, including molecular recognition, information storage, catalysis, and controlled crystallization of inorganic materials. The desire to mimic such functions with synthetic molecules inspires the field of foldamer design.

Of the foldamers under development, β helices — peptide helices containing amino acids with alternating chirality — represent an intriguing and relatively unexplored subclass of peptide-based foldamers. Very few β-helical peptides exist in nature, and all of these compounds adopt their active β-helical structures in hydrophobic membrane environments. However, for many potential biomimetic or bioinspired applications, water or other polar solvents will likely be the medium of choice. In our research, therefore, we pose the question: Can engineered β helices discretely fold in polar media such as methanol, and ultimately water?

Peptide Engineering: In designing β helices, we must overcome several challenges, including the tendency of β helices to adopt multiple structures in solution (structural polymorphism), and the tendency of water to disrupt the hydrogen bonds that stabilize folded peptide structures. Structural polymorphism and aggregation are undesirable for functional foldam-

ers as these physical phenomena effectively decrease the concentration of the desired structure, leading to lower activity. To limit structural polymorphism, we developed a method to trap a singular β-helical structure by linking the two strands and forming a cyclic peptide (Fig. 4).[2] The cyclic construction also helps to stabilize the folded structure against the disrupting effect of water. To further stabilize the peptide in polar media, we designed hydrophilic sites and two stabilizing electrostatic interactions into the structure (peptide 1, Fig. 5(a)). After synthesis and purification, we found that the resulting peptide folded stably in the highly polar solvent methanol — an unprecedented achievement in the field of β-helical peptide foldamers.[3]

Structural Characterization: Circular dichroism (CD) uses differential adsorption of polarized light to reveal general structural characteristics in biological molecules. Our initial studies began in methanol, an alcohol solvent often employed as a surrogate for water. In methanol, the CD spectrum is characteristic of a β-helical structure. As we added increasing amounts of water, the peptide partially unfolded into a bracelet-like structure.

We further probed the peptide's aggregation state and thermal stability by CD. The CD spectra of peptide 1 in methanol and water are independent of concentration, suggesting the peptide is monomeric under the conditions studied. The CD signals in methanol and water do not change appreciably from 5 to 65 °C, indicating both structures are surprisingly thermostable; for comparison, most proteins unfold at 45 °C.

Another technique that allows several different means for establishing molecular structure is nuclear magnetic resonance (NMR). NMR perturbs and monitors the nuclear spins of atoms, which are sensitive to local chemical environments, thus making NMR a powerful technique for investigating the three-dimensional structure of molecules. Computer modeling using NMR data with simulated annealing molecular dynamics (SAMD) generates structures consistent with the experimental measurements — effectively allowing us to determine the coordinates of the atoms in the molecule. Using NMR and SAMD, we were able to generate images of the molecular structures of peptide 1 in methanol (Fig. 5(b)) and water (Fig. 5(c)). In water, the molecule consists of three subgroups all having topography with antiparallel strands and two turn regions; in methanol, the peptide forms the intended structure — a well-defined β helix (Fig. 5(b)).

Second-Generation Peptide: Having achieved a β-helical structure in methanol, we next sought to design a new peptide that would adopt a similar structure in water. For this second-generation peptide, we increased the length of the peptide, which we expected would increase the number of helical hydrogen bonds, thus increasing the overall stability of the helical fold. Furthermore, we designed peptide 2 (Fig. 6) to be stabilized by six electrostatic interactions in the expected helical structure. The CD spectrum of peptide 2 in buffered water confirmed the formation of a β helix and validated our approach to the problem. This demonstration of a β helix in water furthers our goal of developing β helices as a versatile class of foldamers.

Conclusions and Outlook: We have presented the design and biophysical characterization of the first β-helical peptide foldamers that adopt stable structures in polar solvents. By joining the strands with turns, we trapped the peptides into a discrete structural state — a prerequisite for a fully functional foldamer. Our studies prove the β helices can fold stably in polar solvents; the fundamental principles established in this work will enable the future design of predictable β-helical structures. These innovative heterochiral peptides promise numerous potential applications as sensors, smart materials, and catalysts, thus enhancing NRL's multidisciplinary technology platform.

[Sponsored by ONR and AFOSR]

References

[1] S. Hecht and I. Huc, eds., *Foldamers: Structure, Properties, and Applications* (Wiley-VCH, 2007).

[2] M. Sastry, C. Brown, G. Wagner, and T.D. Clark, "Cyclic Peptide Helices: A Hybrid β-Hairpin, β-Helical Supersecondary Structure," *J. Am. Chem. Soc.* **128**, 10650–10651 (2006).

[3] J.L. Kulp III and T.D. Clark, "Engineering a β-helical D,L Peptide for Folding in Polar Media," *Chem. Eur. J.*, **2009**, 15(44), 11867-11877.

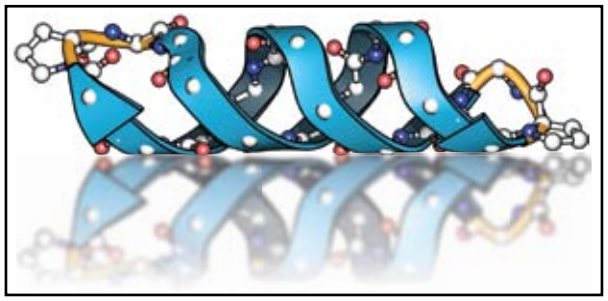

FIGURE 4
Peptide backbone structure of a β-helical supersecondary structure developed, synthesized, and characterized at NRL.

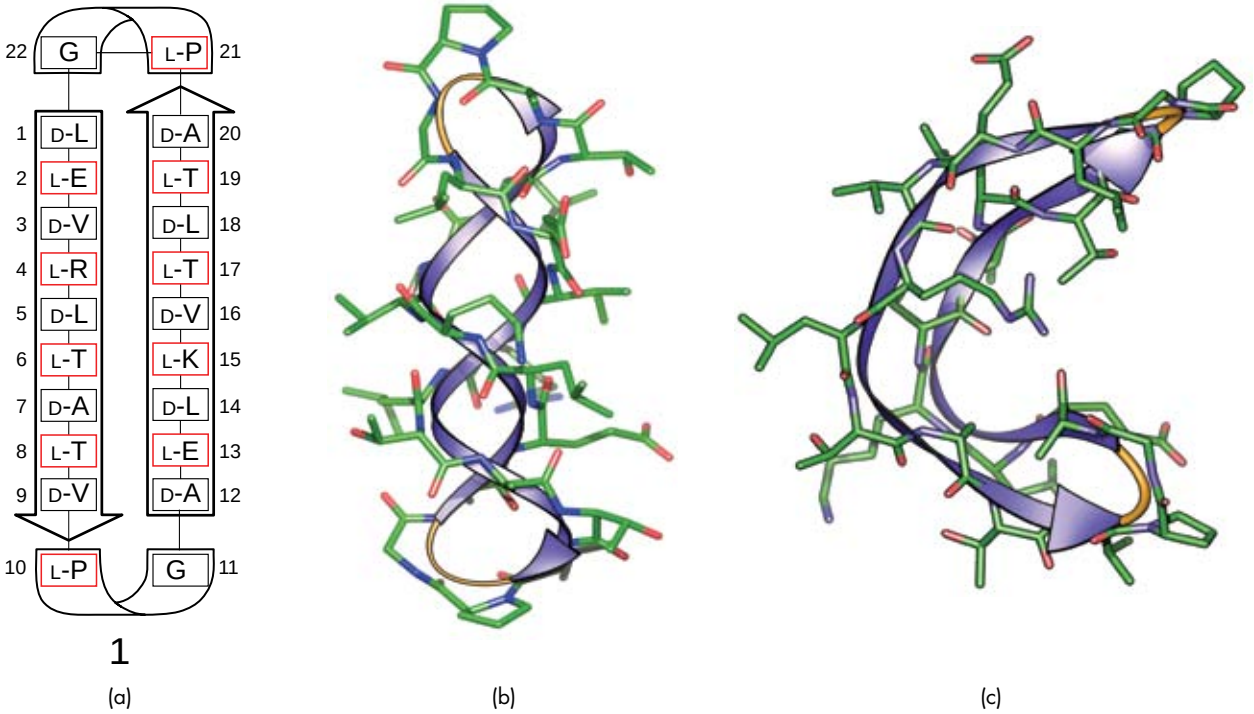

FIGURE 5
(a) Sequence and numbering scheme for peptide 1 using one-letter codes for amino acid residues; D,L-convention for denoting chirality describes amino acids that are non-superimposable on its mirror image — human hands being the most common example of chirality; D-amino acids and glycine are boxed in black, L-amino acids are boxed in red. (b) and (c) Nuclear magnetic resonance derived structures, computed by simulated annealing molecular dynamics, of peptide 1 in methanol (b) and buffered water (c).

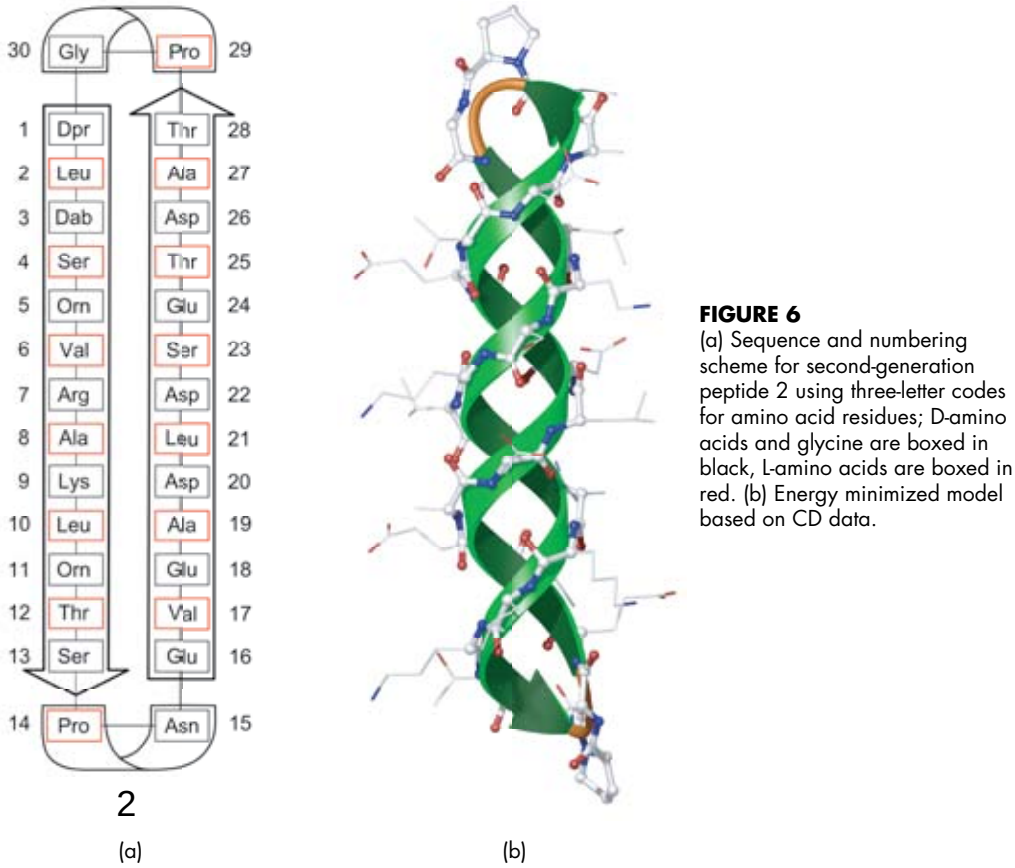

FIGURE 6
(a) Sequence and numbering scheme for second-generation peptide 2 using three-letter codes for amino acid residues; D-amino acids and glycine are boxed in black, L-amino acids are boxed in red. (b) Energy minimized model based on CD data.

A Multiwavelength Microflow Cytometer

F.S. Ligler, J.S. Erickson, J.P. Golden, J.S. Kim, M. Nasir, P.J. Howell, A.L. Thangawng, L.R. Hilliard, L.C. Shriver-Lake, and G.P. Anderson
Center for Bio/Molecular Science and Engineering

Introduction: Fluorescence-based flow cytometry dates back to the 1960s. Essentially, cells or particles are aligned in a flow stream and optically interrogated. Size, density, and fluorescence at multiple wavelengths can be quantified. In many cases, tags, such as fluorescently labeled antibodies, are mixed with the samples prior to analysis so that specific targets or cell functions can be identified. Currently, large, complex, laboratory-based flow cytometers are required to perform medical diagnostics, such as white blood cell counts and immunoassays to detect infection, or for environmental monitoring applications, such as classification of marine algae.

In the traditional design, the sample containing the particles or cells is pumped out of a small tube into a much larger, concentric pipe that is carrying filtered water. This hydrodynamic focusing puts all the particles into the center of the wider "sheath" stream, which then is tapered to a smaller diameter. The particles are thus "focused" and pass single-file through the laser beams for analysis. Over the last decade, flow cytometers have become smaller in size and less expensive, but this sheath flow design is not amenable to miniaturization to the point that the systems are portable. NRL's Center for Bio/Molecular Science and Engineering has developed a microfluidic sheath flow system that is robust, simple to fabricate, and very compact. This sheath flow device forms the basis of a microflow cytometer that has demonstrated the capability for 4-color analysis that is competitive with the larger, commercial systems.

The NRL Microflow Cytometer: Figure 7(a) shows a diagram of the microflow cytometer. The sample stream is shown in red. A picture of an actual chip in action can be seen in Fig. 7(d). The sample stream enters from a small middle channel and is flanked on either side by two sheath streams. These sheath streams are usually just water or a clean buffer solution. Because the flow rates of the sheath streams are much faster than the sample stream, the sample stream is compressed between them. Figure 7(b) shows a computer model of the cross section immediately after the streams are brought together. The sample stream is separated from the walls, but it still touches the ceiling and floor of the channel. This problem is eliminated as the liquid flows through the part of the channel with the chevron-shaped grooves in the ceiling and floor of the channel. As the fluid flows through the grooved region, the chevron grooves move fluid from the sides to the top and bottom of the channel, squeezing the sample stream vertically. The result is that the sheath stream completely wraps around the sample stream, yielding the cross-section shown in Fig. 7(c).

Once the sample is flowing in a narrow, confined stream surrounded by sheath fluid, it can be evaluated using the optical fibers shown in Fig. 7(e). The light from two lasers is launched into the channel using optical fibers. Two fibers, directly opposite the two excitation fibers, are used to carry the excess light away so that it will not interfere with the measurement. Two more fibers are used to collect the light that has interacted with cells or particles as they pass through the interrogation region. Some of the collected light is simply laser light that has bounced off the particles; this light scatter signal is proportional to particle size and density. Laser light which is absorbed by fluorophores either attached to or in the cells or particles is emitted at longer wavelengths. Filters at the other end of the fibers discriminate the colors prior to quantitation of the fluorescence using photomultiplier tubes.

Multiplexed Detection Assays: The microflow cytometer detects and distinguishes particles coded with two fluorescent dyes. These coded particles are coated with antibodies that bind specific targets such as bacteria or toxins. After exposure to the sample to be tested, tracer antibodies carrying a dye that fluoresces at a third wavelength bind to any target captured on the coded particles. The microflow cytometer measures the levels of the third fluorescent dye to detect and quantify the amount of the target present in the sample (Fig. 8).

With the ability to distinguish the multiple coded particles and detect the target analyte on each particle, the microflow cytometer is capable of detecting multiple targets simultaneously. Our initial 6-plex assay demonstrated limits of detection highly comparable to those obtained using a commercial laboratory system with the same (killed) targets, antibodies and coded particles. We obtained the following detection limits: 103 cells/ml for *E. coli*, 104 cells/ml for *Listeria*, 105 cells/ml for *Salmonella*, 1.6 ng/ml for choleratoxin, 0.3 ng/ml for Staphylococcal enterotoxin B, and 8 ng/ml for ricin.

Conclusion: This microflow cytometer system has demonstrated the analytical capability for applications in miniaturized, automated, point-of-care instrumentation for hospitals and portable field-deployable sensor systems for medical diagnostics, environmental monitoring, and biodefense.

[Sponsored by NRL]

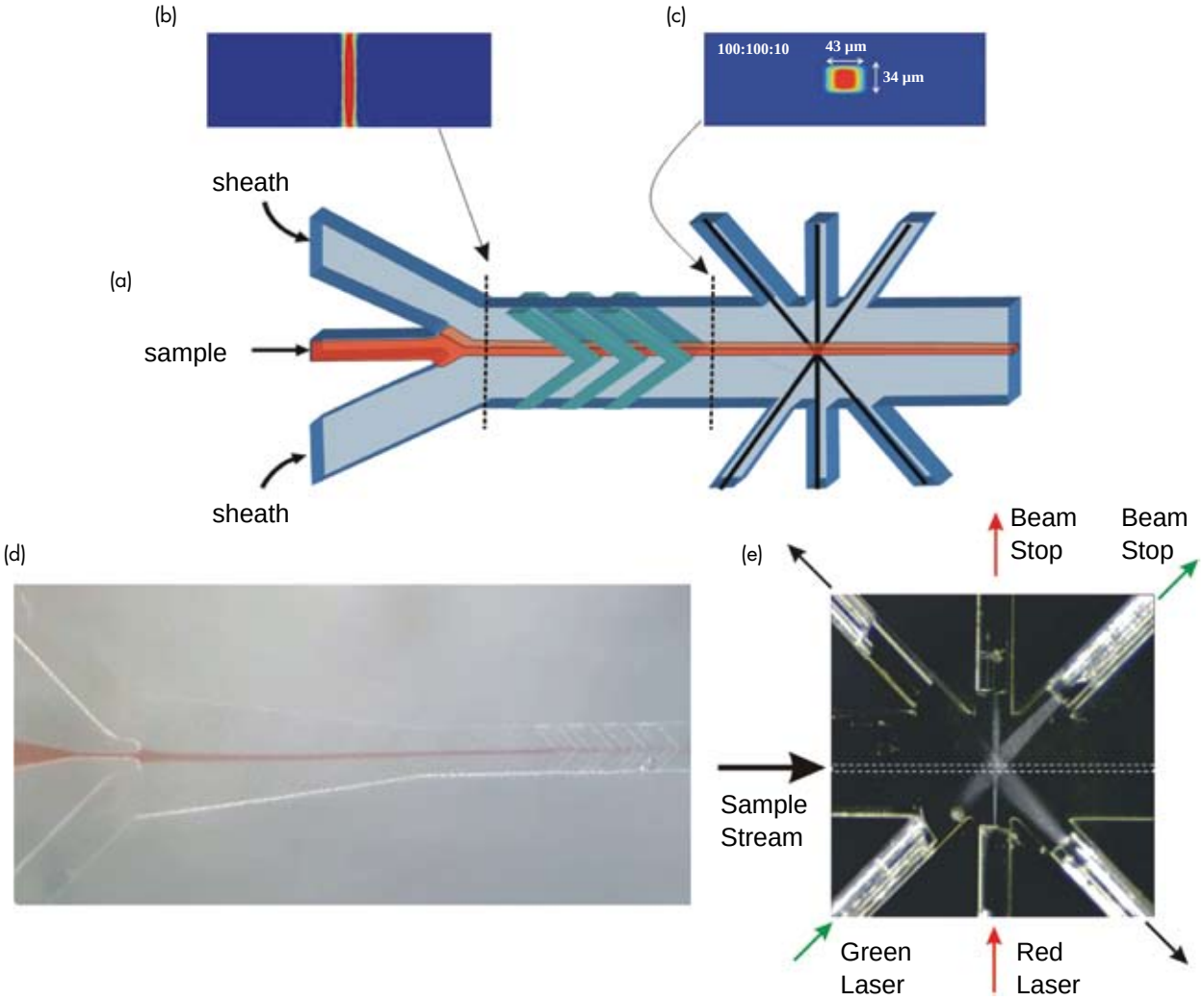

FIGURE 7
(a) diagram of microflow cytometer channel showing sheath and sample inlets and interrogation region, (b) cross-section of flow channel before chevrons, (c) cross-section of flow channel after chevrons showing sheath flow, (d) photograph of core stream with dye, (e) photograph of optical fibers illustrating the focusing of the numerical apertures of a single-mode excitation fiber and two multi-mode collection fibers on the interrogation region.

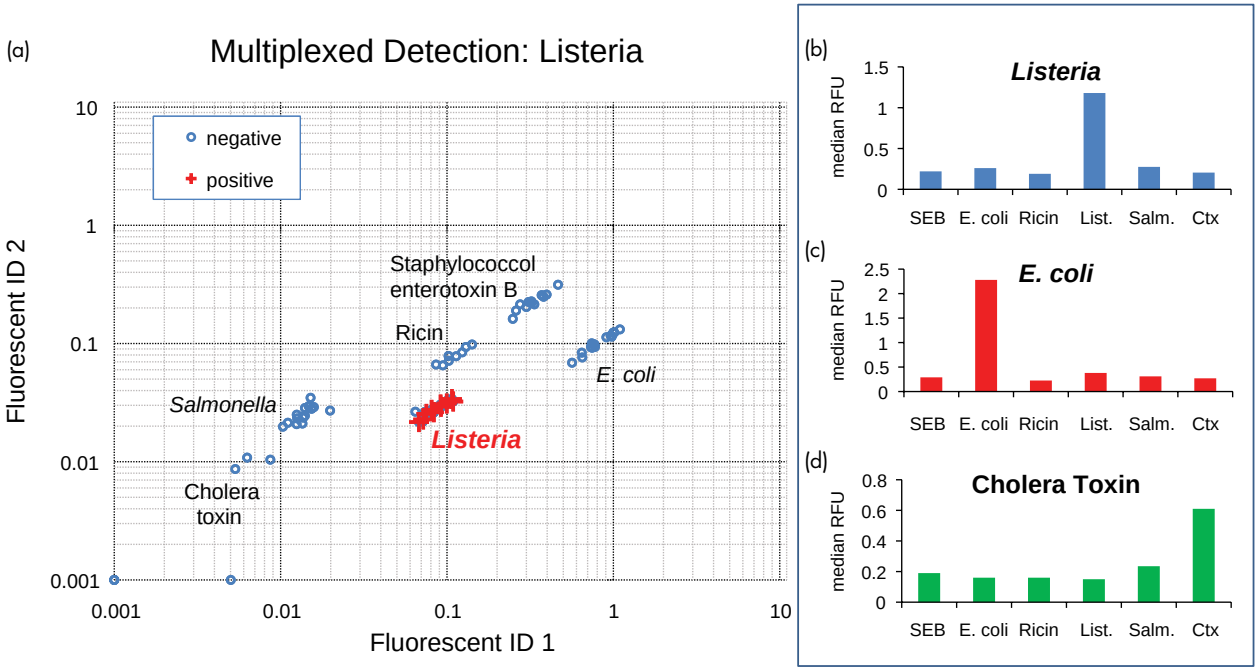

FIGURE 8
The microflow cytometer is capable of detecting multiple biothreat targets using its ability to distinguish fluorescently coded particles, each of which can be specific for a different target. By measuring the amount of fluorescent light, measured in relative fluorescence units (RFU) at two different wavelengths, the particles are identified, while fluorescence at a third wavelength is used to determine the presence or absence of each target. (a) shows the plot of the different particle sets identified based on the amount of two different fluorophores embedded in each particle. The presence of *Listeria* in this assay is indicated by the red marks on each particle that exhibited fluorescence at a third wavelength. The bar graphs on the right quantify the fluorescence at the third wavelength in particle sets to which different targets were added: (b) *Listeria* (10^7 cfu/ml), (c) *E. coli* (10^7 cfu/ml), and (d) cholera toxin (1000 ng/ml).

electronics and electromagnetics

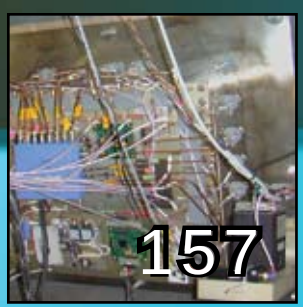
157

160

162

157
The Multifunction Electronic Warfare (MFEW) Advanced Development Model
G.C. Tavik and N.M. Thomas III

160
Transportable Electronic Warfare Module (TEWM)
D.E. Tremper, R.S. Cortesi, J. Heyer, J.Geib, and D. Bay

162
Laser Decoy System for Small Ground Platforms
R. Evans and S. Moroz

The Multifunction Electronic Warfare (MFEW) Advanced Development Model

G.C. Tavik[1] and N.M. Thomas III[2]
[1]*Radar Division*
[2]*INNOLOG*

Introduction: In the almost 30 years since the development of the AN/SLQ-32 Surface Ship Electronic Warfare (EW) system, the number and sophistication of radar emitters and antiship missiles have increased dramatically. The resulting need for improved situational awareness, combat system coordination, threat detection and identification, and support for future improvements in electronic countermeasures against new and emerging threats led the Office of Naval Research (ONR) to establish a Technology Transition Agreement (TTA) in 2004 with the Chief of Naval Operations (CNO), the program managers for the new construction DDG 1000, and the Surface EW Improvement Program (SEWIP). This TTA established an ONR program under the Fleet Force Protection (FFP) Future Naval Capability (FNC) to develop and demonstrate a Multifunction Electronic Warfare (MFEW) Advanced Development Model (ADM), and mature and transition critical EW system technology to full-scale engineering development.

Based on the TTA and the secret DDG 1000 EW component specifications, ONR and NRL established the following key performance factors (KPFs) to focus the MFEW development: (1) frequency and spatial coverage, (2) sensitivity for signal detection, (3) system response time from signal detection to emitter reporting, (4) electromagnetic environment requirements (for both on- and off-board emitters), (5) signal angle-of-arrival (AOA) measurement accuracy, (6) antenna radar cross section (RCS), (7) emitter classification requirements, including false emitter reporting rate, and (8) performance requirements against specified emerging threats.

ONR and NRL initiated the MFEW ADM program in FY05 by selecting and tasking seven contractors to study, develop, and propose system architectures for an MFEW ADM. In addition to the KPF objectives, ONR required that the design be modular and open; capable of being scaled to the size and operational requirements of multiple platforms; capable of future growth to perform additional EW functions; and capable of incorporation into an integrated sensor/communications system-of-systems under the real-time control of a Resource Allocation Manager (RAM). Based on these architecture design efforts, the Northrop Grumman Corporation (NGC) was selected in September 2005 to develop the MFEW ADM.

MFEW ADM Design and Fabrication: The MFEW design is based on a multi-element interferometer antenna (Fig. 1) combined with a frequency scanning architecture that uses a set of 16 to 24 wideband (400 MHz) tuners and digital receivers, each followed by a bank of digital narrowband (~32 MHz) filters and a corresponding set of detectors. The frequency scanning process is weighted by a priori estimates of signal concentration and known emitter parameters to optimize system response time while searching all frequency bands. The narrow bandwidth of the individual detec-

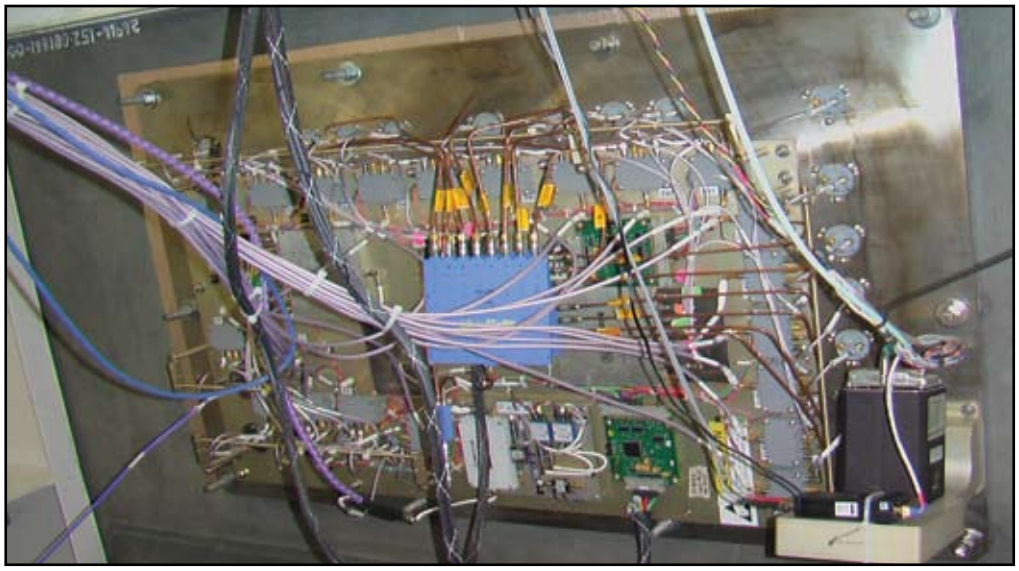

FIGURE 1
MFEW ADM antenna assembly as viewed from inside the above-deck shelter. The antenna elements are located around the perimeter of the electronics mounting plate, embedded in the deckhouse composite structure.

tion channels maximizes sensitivity while minimizing the effects of electromagnetic interference (EMI). Precision direction finding (PDF) is accomplished with an array of two orthogonal interferometers made from 14 of the 20 low-RCS dual sinuous receive elements that form the antenna. Degradation of AOA accuracy due to multipath signal reception is mitigated by a modified version of the multiple signal classification (MUSIC) algorithm.[1] The individual digital tuners and receivers are dynamically allocated between High Probability of Intercept (HPOI) detection and PDF functions as required. The quantity of receivers in a system, which impacts system response time, may be scaled based on cost/performance factors as required for any particular ship class or mission.

The MFEW ADM incorporates a data processor and associated output interfaces based on the Electronic Surveillance Enhancement (ESE) subsystem, which was previously developed by NGC for SEWIP Block 1. The new processor software is designed to operate with the NRL-developed Advanced Multi-Function RF Concept (AMRFC) Resource Allocation Manager,[2] and the NGC-developed human machine interface (HMI).

Test and Demonstration: The MFEW ADM was fabricated and delivered to the NRL in October 2007 (Fig. 2). NRL installed the system in two CONEX (Container Express) boxes; one containing the above-deck assembly, including the interferometer array embedded in a section of the new DDG 1000 destroyer composite deckhouse material, and the other containing the below-deck assembly, including the HMI operator controls and displays. These in turn were mounted on a ship motion simulator at the NRL Chesapeake Bay Detachment (CBD) for testing (Fig. 3). Demonstrations included the detection and tracking of relevant land-based, shipboard, and airborne emitters within this maritime environment.

After a final demonstration to the TTA sponsors in May 2008, the system was shipped to San Diego and installed on the USS *Comstock* (LSD 45) (Fig. 4) in preparation for the RIMPAC 2008 multinational fleet exercises off the coast of Hawaii. *Comstock* and MFEW actively participated in the TAPA II (Technical Cooperation Program Anti-ship Missile Project Arrangement) technology segment of the exercise jointly with Canada and Australia.

Summary: The MFEW ADM program designed, built, tested, and demonstrated a critical new EW capability on a very aggressive schedule. It performs remarkably well against nearly all of the KPFs, and the MFEW technology is now being transitioned to the SEWIP Block 2 acquisition program. The resulting upgrade will be installed in various configurations throughout the Fleet starting in 2013. Detailed analysis of the MFEW test data continues in preparation for a final NRL report in 2009.

[Sponsored by ONR]

References

[1] R. Schmidt and R. Franks, "Multiple Emitter Location and Signal Parameter Estimation," *IEEE Trans. Antennas Propag.* **34**(3), 276–280 (1986).

[2] G.C. Tavik, C.L. Hilterbrick, J.B. Evins, J.J. Alter, J.G. Crnkovich, J.W. deGraaf, W. Habicht II, G.P. Hrin, S.A. Lessin, D.C. Wu, and S.M. Hagewood, "The Advanced Multifunction RF Concept," *IEEE Trans. Microw. Theory Tech.* **53**(3), 1009–1020 (2005).

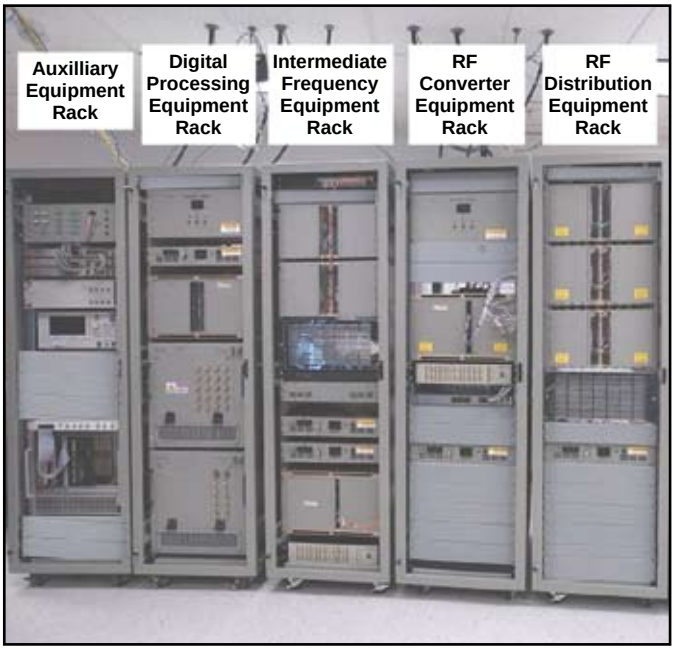

FIGURE 2
MFEW ADM equipment racks.

FIGURE 3
MFEW ADM above-deck shelter (on top of the Ship Motion Simulator) and below-deck shelter (on top of Building 12) at NRL-CBD. Inset shows the above-deck shelter in motion during testing with airborne emitters mounted on an NRL Learjet.

FIGURE 4
MFEW ADM shelters mounted aboard the USS *Comstock* (LSD 45) during installation in San Diego.

Transportable Electronic Warfare Module (TEWM)

D.E. Tremper, R.S. Cortesi, J. Heyer, J. Geib, and D. Bay
Tactical Electronic Warfare Division

Introduction: Traditionally, the incorporation of advanced electronic warfare (EW) capabilities, either as existing payload upgrades or as new system installations, has required extensive timelines and platform-specific integration planning. Research efforts have often targeted specific EW applications and operational environments to facilitate the transition of the technology, rather than develop cross-domain functionality. Often these separate EW systems address the same threats or frequency bands but are each platform-centric.

Under an Office of Naval Research (ONR) funded Future Naval Capability (FNC) program, research was performed by the Tactical Electronic Warfare Division (TEWD) at NRL to develop an advanced EW capability for use on unmanned platforms. The primary thrusts were in the areas of antiship missile defense (ASMD) and countersurveillance. The ASMD and countersurveillance missions are not platform-specific, nor are they limited to unmanned vehicles. Scientists at NRL continued to evolve the initial unmanned vehicle EW concept[1] into a platform-independent payload applicable to both manned and unmanned assets. This evolution resulted in the Transportable EW Module (TEWM), a platform-agnostic EW payload, shown in Fig. 5, which is capable of being rapidly transferred from vessel to vessel, aircraft, vehicle, or fixed site, or vice versa.

Development of a common EW core for application across a variety of military operations not only avoids the platform-centric payload approach, it also allows for distributed EW payloads that can easily be networked. The TEWM system was designed from the start to support TEWM-to-TEWM communication and data sharing. Future network interfaces will allow TEWM to connect to available communication links in order to either passively or actively tie into available situational awareness data streams, as well as coordinate distributed EW operations.

TEWM System Overview: Like its unmanned vehicle predecessor, the TEWM design incorporated an electronic support (ES) receiver integrated with a wideband digital radio frequency memory (DRFM) based electronic attack (EA) capability. DRFM-based payloads have the capability to apply standard noise jamming techniques, as well as generate high-resolution false targets with realistic amplitude and Doppler modulation, engage multiple threats simultaneously, and generate multicomponent wave forms that combine false targets with obscuration jamming. DRFM flexibility allowed TEWM to be designed from the start as an EW hardware core that supports a variety of potential operations. High-power transmission is achieved through high-gain antennas and high-power modules developed for tactical aircraft and equally applicable to surface use. Electronic components are air-cooled, unlike the original unmanned vehicle payload, which relied on forced convection cooling.

FIGURE 5
TEWM being operated by NRL scientists.

Although not demonstrated during at-sea prototype testing, TEWM and networks of TEWM systems are designed to be controlled by as few as one Jammer Control Station (JCS). JCS is a graphical user interface developed using the NRL SIMDIS visualization tool, which provides users with a real-time 3D situational awareness picture, including platform positions and motions, and payloads' status and activities, as well as RF detections and bearings with threat, neutral, and friendly assignment. As shown in Fig. 6, JCS operators can specify search and threat parameters, operate payloads manually, and point and click RF beams for interrogation or to activate jamming across any networked and available TEWM. Single or multipayload networked control and coordination can be managed by a single JCS operator.

RIMPAC 2008 Experimentation: During FY08, the TEWM system was demonstrated as part of a large-scale EW experiment during the international Rim of the Pacific (RIMPAC) 2008 exercises in July. RIMPAC is a biannual, international maritime exercise that takes place in the Pacific Ocean near Honolulu, Hawaii, under the direction of the United States Pacific Command (PACOM). NRL scientists installed the TEWM hardware onboard the DDG 93 *Chung Hoon*, as

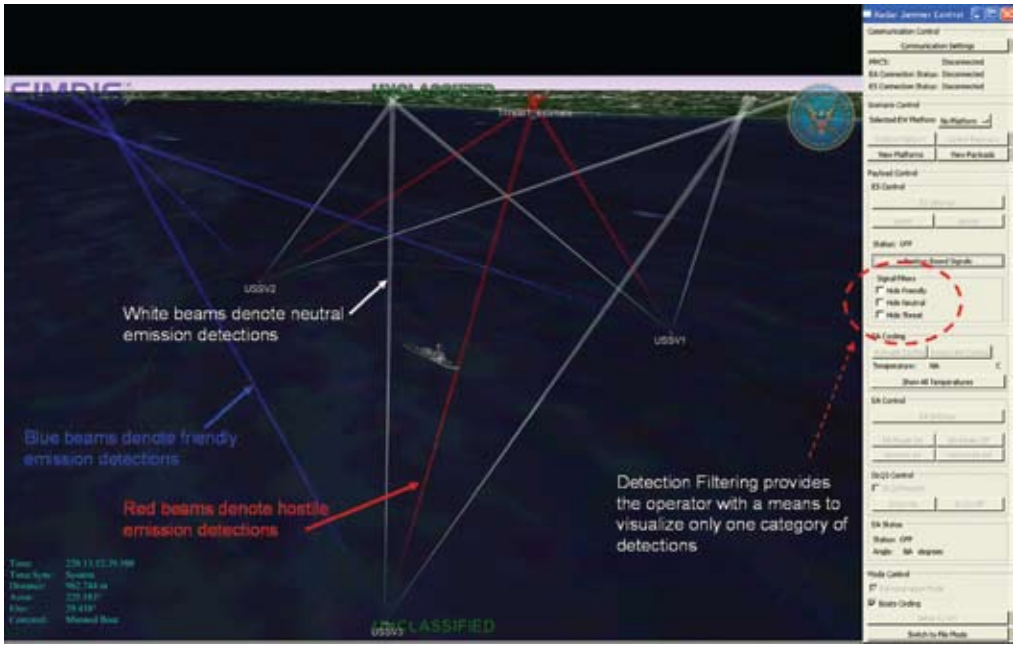

FIGURE 6
Distributed EW control demonstrated by JCS.

shown in Fig. 7, for RIMPAC 2008 in order to demonstrate the system's capabilities in ASMD and counter-surveillance applications. Hardware was installed on the deck of the *Chung Hoon* in 30 minutes. Bringing TEWM up to full operation took less than 2 hours. Directional transmit and receive antennas limited the interference between TEWM and onboard emitters.

The RIMPAC at-sea experiment demonstrated TEWM's capability to generate advanced EA waveform concepts for area defense and self-protection against maritime patrol aircraft, multirole fighters, and captive-carry ASM simulators. Additional experiments are planned for 2009 aimed at controlling TEWM across an existing military network, as well as coordinating the operation of two networked TEWM systems.

Summary: Traditional EW development has followed a platform-centric approach leading to costly and lengthy planning and integration. The TEWD at NRL is actively pursuing a compact, low-cost, capability-centric EW payload in order to support the rapid transfer of sophisticated capabilities between platforms and domains. This platform-agnostic approach will facilitate the integration of distributed and coordinated EW concepts into military operations currently not found in the Fleet.

[Sponsored by ONR]

Reference

[1] D. Tremper and J. Heyer, "Unmanned Sea Surface Vehicle Electronic Warfare," *2007 NRL Review*, p. 159–161.

FIGURE 7
TEWM installed on the DDG 93 *Chung Hoon*.

Laser Decoy System for Small Ground Platforms

R. Evans and S. Moroz
Tactical Electronic Warfare Division

Introduction: Increasingly, U.S. Navy ships are operating in the littorals, where they may be exposed to a variety of threat weapons including laser-directed threats. These laser-guided threats are also of very high concern to the Marines as they operate lightly armored vehicles in hostile areas. A laser decoy concept was developed demonstrating a capability to counter these types of threats. With relatively small-sized vehicles, the laser decoy needs to be compact and affordable. Short threat alert times dictate a very rapid response from the laser decoy. These constraints were met in the laser decoy that was developed and demonstrated as part of the EWISSP (Electronic Warfare Integrated System for Small Platforms) project.

One of the Office of Naval Research (ONR) Future Naval Capability (FNC) programs, EWISSP was developed as a low-cost integrated system to improve the survivability of small surface platforms against precision guided threats. The EWISSP design included sensors to detect the threat, processing to classify the threat type, and countermeasure responses to negate the effectiveness of the threat. The small platforms with small crew size can be protected with the automated operation of EWISSP. Although the Marines' Expeditionary Fighting Vehicle (EFV) was the initial transition target for the EWISSP technology, the system was designed to work with the full array of small surface platforms including the Light Armored Vehicle (LAV), the Landing Craft Air Cushion (LCAC), and the Landing Craft Utility (LCU) ships. EWISSP was jointly developed by a team including ONR, NRL, and Northrop Grumman. The NRL focus was in the development and demonstration of the Laser Countermeasure (LaCM) to detect, identify, and counter laser-guided threats to the small surface platforms.

LaCM Description: Laser-guided weapons are precisely directed by an operator who illuminates the intended impact point with a laser beam. Guidance logic in the weapon detects this pointing laser reflection from the intended target and corrects the weapon's trajectory to impact the illumination point. A first step to countering these threats is to detect that the pointing laser designator energy is illuminating the defended platform. For this demonstration, the Goodrich Company's laser detection sensor was combined with signal processing logic to alert the EWISSP system to an attack.

Major LaCM components included a countermeasure laser to confuse the threat weapon, an optic combination to direct the LaCM laser energy toward the threat, and an erectable 2-meter mast to provide an improved defensive geometry. On alert of an attack, the LaCM mast is deployed from a stowed position that maintains the platform's relatively low profile. Next, the LaCM beam is configured by optics at the top of the mast to direct the countermeasure energy. This is followed by transmission of the energy from the LaCM laser to jam the threat sensor, preventing the threat weapon from hitting the targeted platform. Figure 8 illustrates the LaCM countermeasure concept that presents both omnidirectional and spot ground jamming beams that can counter the full range of laser-guided threats.

LaCM Testing: As part of the testing, the LaCM defended platform was attacked by threat seekers carried on a helicopter. The helicopter flew a full range of trajectories representative of those typically followed by threats. Figure 9 shows the LaCM hardware with the mast erected on a surrogate HMMWV (High Mobility Multipurpose Wheeled Vehicle) test platform

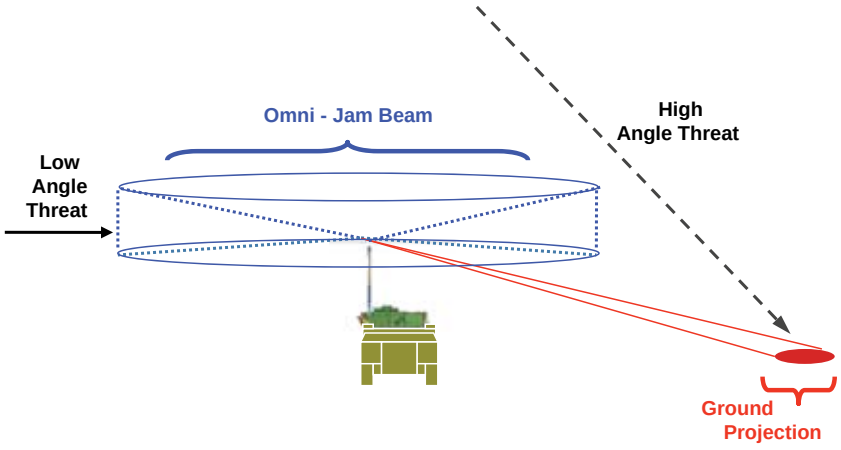

FIGURE 8
Laser Countermeasure (LaCM) concept.

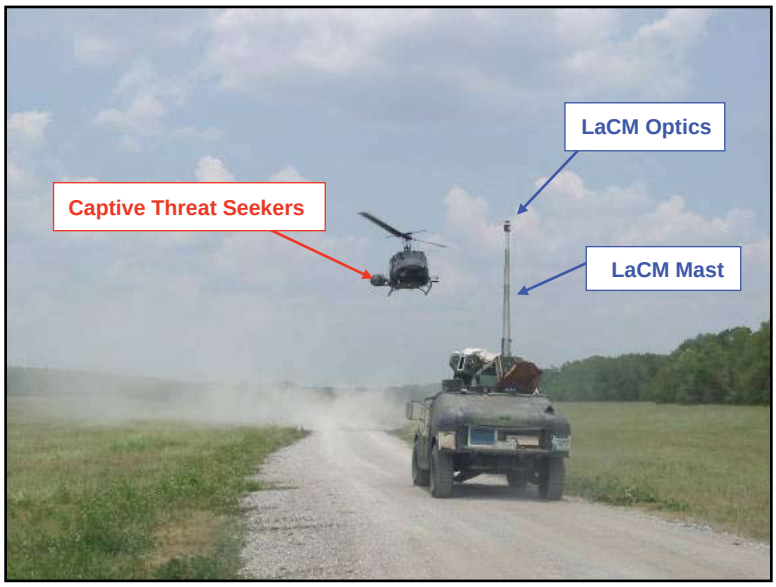

FIGURE 9
LaCM testing with captive seekers on helicopter.

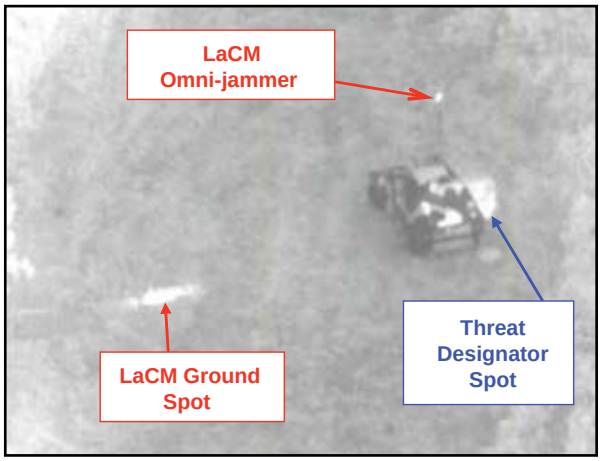

FIGURE 10
Reference infrared image of LaCM testing.

along with instrumented threat seekers installed on a test helicopter. This testing covered a wide range of backgrounds and attack geometries. A representative scene presented to the threat seekers is presented in the infrared image of Fig. 10. The center of the LaCM omni-jammer is seen as the small dot. The ground spot from the laser decoy lures the threat away from the HMMWV that is being illuminated by the threat's laser designator. During the testing, the LaCM was highly effective in countering the threat seekers over a full set of engagement geometries.

Summary: The helicopter testing followed an extensive test series that was conducted at multiple test sites with many climatic and background conditions. In all of the tests, the concept was demonstrated to effectively counter the precision laser-guided threats.

[Sponsored by ONR]

information technology and communications

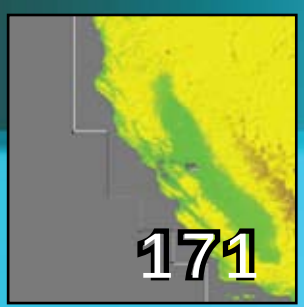

167
Free-Space Optical Link to an Explosive Ordnance Disposal (EOD) Robot
W.S. Rabinovich, J.L. Murphy, M. Suite, M.F. Ferraro, R. Mahon, and P.G. Goetz

169
A Maritime Information Exchange Model (MIEM) for Sharing Actionable Intelligence
C. Dwyer, R. Hayes-Roth, D. Reading, and G. Small

171
Tiled Image Archival and Distribution for Seafloor and Terrestrial Imagery
E. Ioup, J. Sample, and F. McCreedy

172
Cross-Domain Payload Migration
C.M. Huffine

Free-Space Optical Link to an Explosive Ordnance Disposal (EOD) Robot

W.S. Rabinovich, J.L. Murphy, M. Suite, M.F. Ferraro, R. Mahon, and P.G. Goetz
Optical Sciences Division

Introduction: The Optical Sciences Division, in collaboration with scientists from the Remote Sensing Division and the Naval Center for Space Technology, field-tested a free-space optical (FSO) link for a counter-IED (improvised explosive device) robot. Traditional radio frequency (RF) link command and control of these robots is not possible in the presence of IED RF jammer systems. To solve this problem, a free-space optical link using quantum well based modulating retroreflectors was prototyped and installed on one version of a robot. Two field tests were run. During the first test at the Naval Explosive Ordnance Disposal Technology (NAVEODTECH) Division, Indian Head, the link operated in the presence of RF jammers and showed continued command and control on the robot without interference. The system was demonstrated to several military personnel including the Program Executive Officer (PEO) for Littoral and Mine Warfare. During the second test, at Naval Surface Warfare Center Dahlgren, the link was tested for range. A maximum range of 1 km, limited by line of sight, was demonstrated. This matches the maximum range for the RF link.

Free-space optical communication has emerged in recent years as an attractive alternative to conventional RF techniques due to its very large bandwidth, low probability of intercept, and immunity from interference or jamming. These features are inherent in the short wavelength of optics, but to be exploited, require high quality telescopes and extremely accurate pointing and tracking. As a result, optical communication systems can have a large system impact in terms of weight, power, and platform stability, which may be unacceptable for small platforms. Small, remotely controlled robots fall into this category of platforms. They often require high bandwidth links to return video and other data, but they may also work in environments in which a large amount of RF interference may be present, limiting their communication range. However, a conventional optical communication system may not be appropriate for them. Even for modest ranges on the order of 1 km and data rates on the order of 1.5 Mbps, a conventional FSO system will require pointing accuracy on the order of a degree for the transmitter and receiver. This implies that a gimbaled optical system with an automated acquisition and pointing system is needed on the robot.

In this effort, as an alternative to a conventional FSO system, we investigated the use of a retroreflecting optical system. It is possible to establish a two-way optical link using a single conventional laser transmitter. This transmitter is located on a large platform (or at a ground station) that has sufficient power, payload capacity, and platform stability to operate it. It can communicate data to a second, small platform conventionally by modulating its laser with the desired signal. If the laser is strong enough, the small platform can receive the data using a detector with a wide field of view, obviating the need for a large pointed receive telescope. However, such a system does not allow the small platform to transmit data back to the large platform. To do this, we used a modulating retroreflector (MRR).

An optical retroreflector is a passive optical component, such as a corner cube prism, that reflects light incident upon it exactly back along its path of incidence. Retroreflectors typically have a large field of view (about 30 degrees full angle for glass retroreflectors) and very high efficiency. Retroreflectors are often used in road signs to increase their readability at night.

Retroreflectors can also act as optical communication systems. By mounting an electro-optic shutter in front of the corner cube, the retroreflected beam can be modulated with the data signal. In operation, the large platform illuminates the small platform with a continuous-wave (unmodulated) laser beam. This beam strikes the modulating retroreflector and is passively reflected back to the large platform. The shutter is then turned on and off with an electrical signal that carries the small platform's data. This impresses the data stream upon the retroreflected beam, which then carries it back to the large platform. Figure 1 shows a schematic of a modulating retroreflector. For the past ten years, NRL

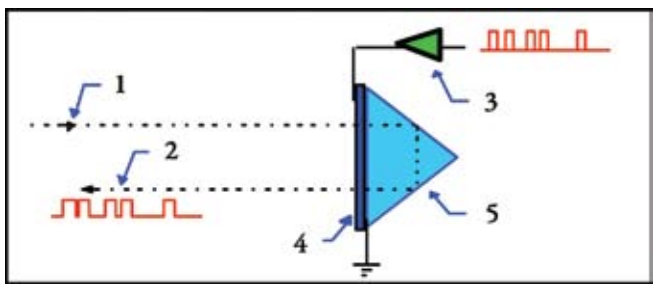

FIGURE 1
A modulating retroreflector diagram: (1) interrogation beam; (2) reflected modulated beam; (3) driver from the information source; (4) transmissive multiple quantum well modulator; and (5) solid retroreflector.

has developed MRR systems using large area semiconductor multiple quantum well modulators.[1,2] These sophisticated solid state devices can operate at the Mbps data rates needed for transmitting video imagery.

Modulating Retroreflector Terminal for the Packbot: In the summer of 2008, NRL, working in collaboration with the NAVEODTECH Division, conducted a rapid prototyping experiment to test the feasibility of using MRR links for explosive ordnance disposal (EOD) robots, specifically the Packbot. The Packbot currently uses a 1.5 Mbps 802.11 RF link between its control station and the robot to return video from the Packbot's cameras and to send commands to the Packbot.

We created an MRR terminal with six MRR/photoreceiver elements, giving an angular coverage of 180° in azimuth and 30° in elevation. Full 360° coverage can be accomplished with more MRRs. All the modulators were driven with the same signal, for a total power draw of about 1.2 W. The MRR terminal created for the Packbot had a diameter of about six inches and is shown in Fig. 2. An Ethernet modem that was developed to drive MRRs interfaced the Packbot's data link to the MRR array.

An MRR free-space optical link is inherently asymmetric. It can use a small unpointed terminal on one end, but it requires an actively pointed laser interrogator on the other. We chose to use a laser interrogator developed for NRL under the ONR Dual Mode Optical Interrogator (DMOI) program. This terminal is shown in Fig. 2.

Optical Link Tests: Our initial link tests were conducted at the NAVEODTECH facility in Indian Head, MD. The Packbot was first set up in a field, and the optical link was established starting at ranges of about 30 m. The Packbot was then driven over the field out to ranges of about 250 m, limited by line-of-sight distances. Video return over the optical link was smooth over the whole range, as was control of driving. The robot could be turned ±90° without moving out of the field of view of the MRR terminal. At full range, the actuator arms were controlled over the optical link by both NRL operators and EOD personnel. Operation was essentially identical to operation over the Packbot RF link. Figure 3 is a photograph of the Packbot while being controlled by the optical link, along with the control console. At a later point in the day, a separate demonstration that used a small RF jammer was conducted. The jammer was turned on and the Packbot was driven, under its RF link, as close as we could get to the jammer. At a range of about 20 m from the jammer, the RF link failed. We then switched to the optical link and drove the Packbot up to the jammer and around it.

The primary tests of the Packbot-MRR optical link were conducted at Naval Surface Warfare Center Dahlgren, down Shock Tube road. This road provided a 1 km line of sight. We were able to control the robot over the full length of the road, even at distances at which the primary RF link could not work.

These tests demonstrated that an optical link could act as a drop-in replacement for an RF robot data link. The bandwidth allowed full video to be returned from the robot, which is needed for driver feedback. Future work will examine even more compact systems and approaches to non-line-of-sight links.

Acknowledgments: We acknowledge the support of Dr. Kurt Hacker of NAVEODTECH in both funding this effort and helping with robot integration and testing. We also acknowledge the support of the Office of Naval Research for modulating retroreflector technology and the DMOI terminal, and the Rapid Reaction Technology Office for the development of

(a)

(b)

FIGURE 2
(a) The EOD Packbot robot carrying the modulating retroreflector array and (b) the Novasol Dual Mode Optical Interrogator (DMOI) used in the experiment.

(a) (b)

FIGURE 3
Packbot, with MRR terminal mounted aft, being controlled by the optical link (a) and a view of the control console (b) while conducting tests at NAVEODTECH at Indian Head, MD.

the modulating retroreflectors and photoreceivers used in this project. We also acknowledge Wade Freeman, Steve Frawley, and Mike Colbert of SmartLogic, Inc. for modem development, and Eric Saint-George, Stan Uecke, and John Sender of Novasol for the DMOI optical interrogator.

[Sponsored by NSWC]

References

[1] G.C. Gilbreath, W.S. Rabinovich, R. Mahon, M.R. Corson, M. Ferraro, D.S. Katzer, K. Ikossi-Anastasiou, T. Meehan, and J.F. Kline, "Large Aperture Quantum Well Shutters for Fast Retroreflected Optical Data Links in Free Space," in *Laser Radar Technology and Applications IV,* held in Orlando, FL, and Munich, Germany, June 16, 1999, ed. G.W. Kamerman and C. Werner, *Proc. SPIE* **3707**, 666–672 (1999).

[2] W.S. Rabinovich, R. Mahon, H.R. Burris, G.C. Gilbreath, P.G. Goetz, C.I. Moore, M.F. Stell, M.J. Vilcheck, J.L. Witkowsky, L. Swingen, M.R. Suite, E. Oh, and J. Koplow, "Free-space Optical Communications Link at 1550 nm Using Multiple-quantum-well Modulating Retro-reflectors in a Marine Environment," *Opt. Eng.* **44**(5), 056001 (2005).

A Maritime Information Exchange Model (MIEM) for Sharing Actionable Intelligence

C. Dwyer,[1] R. Hayes-Roth,[2] D. Reading,[3] and G. Small[4]
[1]*Space Systems Development Department*
[2]*Naval Postgraduate School*
[3]*Western Information Technology Services Corp.*
[4]*Harris Corp.*

Introduction — A Mandate to Share: The 9/11 Commission Report and related Presidential directives have highlighted the need to share information between different government agencies, military services, and international allies. With sponsorship from the Navy and the Office of the Secretary of Defense (OSD), NRL provided the technical leadership for the Comprehensive Maritime Awareness (CMA) Joint Capabilities Technology Demonstration (JCTD) aimed specifically at developing and demonstrating effective means for sharing maritime intelligence to improve interdiction of suspicious or threatening vessels, cargo, and people. To accomplish sharing in an effective manner, we need to enable humans and computers to understand situation intelligence so that they can respond quickly to significant events. As the number of sensors and internetworked systems increase, the data volumes continue to soar, so people will need to rely on the machines to assess and filter more and more of the data. Human attention will need to focus on key events and making important judgments.

The Department of Defense (DoD) plans to improve information sharing by making information assets *understandable* and *accessible*. We term information understandable when it consists of familiar types and values. We consider it accessible when computerized services can obtain it for us. Thus, one goal of the CMA JCTD was to make actionable intelligence about maritime situations understandable and accessible in that way. The key to achieving that goal was to create a set of types and values that could be used to describe beliefs about maritime entities, relations, and events, as well as the evidence for those beliefs. The Maritime Information Exchange Model (MIEM) addresses that need by prescribing how to express such beliefs and evidence.

Conceptual Models of Situations and XML Schemas: The MIEM comprises a *conceptual model* for the entities and relationships needed to describe dynamically evolving maritime situations, consisting of beliefs and evidence. As situations evolve, these beliefs change, and the MIEM provides a way to characterize and capture those changes. Beyond being just a con-

ceptual model, the MIEM consists of actual information encoding models expressed as Extensible Markup Language (XML) schemas. These XML schemas provide a grammar for writing syntactically correct XML-tagged documents that express specific maritime situations. These schemas consist of specified terms for key entities such as vessels, cargo, and people, attributes of these entities, and permissible types of values that can be associated with these attributes. In addition, the MIEM schemas provide types and values for various types of metadata that can qualify or embellish the situation data themselves. These metadata can characterize how strongly something is believed, the evidence for or against that belief, time qualifiers for when the belief is valid, sources of evidence, and restrictions on access, for example.

The MIEM schemas are intended for use by service-oriented architecture (SOA) systems or other schema-aware software applications. The MIEM describes how information should be expressed when it is transferred between two independent systems, namely as XML-tagged text. Each independent system, which can be a source or a consumer of maritime intelligence, may use its own database techniques for maintaining its view of situation data. The MIEM provides a target for producers or consumers, who can translate into and out of the MIEM as appropriate. In the future, systems could choose to use the MIEM as a schema for document or database storage directly, because XML-based storage products are becoming increasingly common. However, that practice goes beyond the immediate purpose and significance of the MIEM.

Levels of Actionable Intelligence: In assessing how intelligence becomes actionable, we identify nine increasing levels of value that information sharing systems need to address. These nine levels are listed and briefly illustrated in Table 1. Where most DoD systems operate at levels 1, 2, or 3, the MIEM can support information sharing at all nine levels, including the exchange of multiyear case files tracking vessels or persons of interest.

The principal features of MIEM comprise ways to describe key domain entities, key secondary concepts, and extensive and universally applicable metadata. MIEM consists of modular XML schemas that can be restricted or extended wherever required to meet the needs of a specific application. The key domain entities include conveyance and vessel, person, crew and passenger, cargo and facilities, and measurements such as time, position, length, and weight. The key secondary concepts address lifecycle issues including states, transitions, voyages and epochs, events, anomalies, and threats. The extensive metadata provide ways to describe source, confidence, alternatives, pedigree, and caveats, as well as ways to distinguish past, present, and predicted future states.

Summary — Sharing Maritime Intelligence: The MIEM provides the foundation for a collabora-

TABLE 1 — Levels of Valued Added Information Supported by the MIEM

Level	Type	Example	Value Added
9 (**highest**)	Case files for key entities	Histories, highlights, comprehensive details	Enables in-depth predictive analysis
8	Threats and anomalies	Dangerous undeclared cargo	Increased preemptive threat reduction
7	"Of interest" conditions and watch lists	Suspicious cargo on board	Increased analytical efficiency
6	History, behavior, and future projections	Voyages and predicted courses	Enables basic predictive analysis
5	Multiple alternatives and analysis	Ambiguity, uncertainty	Direct evidence of certainty
4	Degree of belief and pedigree	Evidence, quality	Direct information about quality
3	Fused data and inferred beliefs	Position, crew	Synergistic improvement in situational awareness
2	Caveats and simple metadata	Sensor type, classification	Indirect quality assessment
1 (**lowest**)	Sensor system reports	Automatic Information System (AIS)	Reduced development costs for customers

tive approach to sharing and continually improving intelligence. To further the objectives of cross-agency sharing, the Navy has established a partnership with the Department of Homeland Security Enterprise Data Management Office (DHS EDMO) and the program management office for the National Information Exchange Model (NIEM PMO). Under this agreement, the MIEM will become the authoritative information sharing model for maritime data throughout the entire Federal Government.

[Sponsored by Deputy Under Secretary of Defense for Advanced Systems and Concepts]

Tiled Image Archival and Distribution for Seafloor and Terrestrial Imagery

E. Ioup, J. Sample, and F. McCreedy
Marine Geosciences Division

Introduction: The Navy and other Department of Defense activities collect and archive large amounts of imagery of the Earth's seafloor and terrestrial surfaces for distribution to users in the tactical, intelligence, or scientific communities. This imagery is high resolution and collections can be quite large; the compressed 1 meter per pixel imagery of the U.S. is approximately 3 terabytes. Storing the high-resolution imagery as flat files on a hard drive or in a database is problematic because the system must perform time-consuming loading, decoding, and post-processing of large numbers of images for every request by a user. The tile archival and distribution system developed by the Naval Research Laboratory's Mapping, Charting, and Geodesy Branch of its Marine Geosciences Division solves these problems and provides a sophisticated and comprehensive method of imagery management.

Tile Organization and Creation: The tile archival and distribution system works by preprocessing imagery once before it is used. Our system stores all imagery as fixed size image tiles at a number of predefined map scales. The lowest map scale partitions the world into two tiles: a tile matrix of one row and two columns. All consecutive scales have double the number of rows and columns as the previous scale. Figure 4 shows the Western Hemisphere divided by several scales of tiles. This system allows for arbitrarily high map scale, although it is rarely necessary to have more than 20 scales. An image tile may be any size but we chose to use 512 × 512 images. A 512 × 512 image tile provides a compromise between limiting image size and limiting the number of images required to fill a user's map.

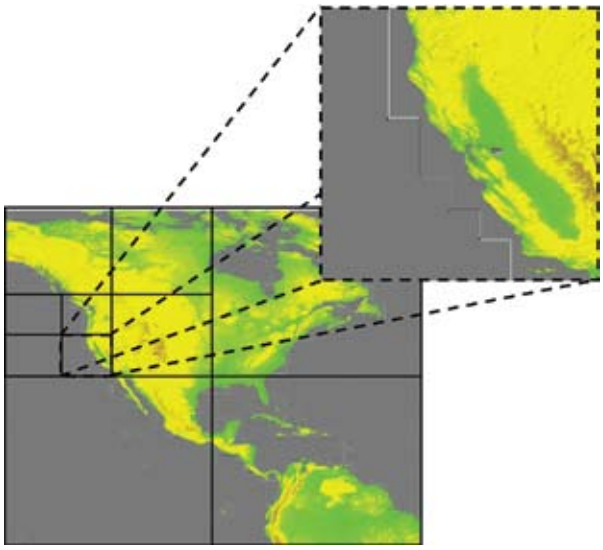

FIGURE 4
An example world image broken into successively higher resolution tiles. Higher resolution tiles cover the same geographic area, but contain more highly detailed imagery.

The process of tile creation involves a few basic steps. First, the image is decoded from its original image file format and, if necessary, reprojected into a geodetic projection. Our reprojection algorithm performs a pixel-by-pixel reprojection to ensure that tiles align on the edges, but improves performance by creating a matrix of conversions and linearly interpolating between values. (This algorithm is the subject of an NRL patent application filed in 2007.[1]) Next, the image is resized to the closest native tile scale and pasted into the appropriate tiles. When all original images have been processed, the highest scale is used to create the lower scales. Each tile in the lower scale can be created by resizing and combining tiles in the higher scale. Data updates are performed by using new data to create tiles to replace old tiles and recreating the lower scales in areas that changed.

Tile Image Distribution: The tile archival and distribution system is especially well suited to online distribution of imagery. We have created a tile server to provide direct access to tiled imagery over the Internet. Each image tile is accessible from the tile server via a unique URL containing the scale, row, and column of the tile. This URL allows both Web browser clients and standalone clients to access tiles quickly and easily. These clients will retrieve tiles from the tile server and manage the map view themselves. Clients determine which tiles are necessary for a particular geographic area desired by the user. These clients will only usually display the map scales natively supported by the tile server, thus no costly image processing must be per-

formed on either the server or client. Google Earth and other tile-based clients are compatible with this methodology.

Our tile server also supports the Web Map Service (WMS), a standard and popular method of distributing imagery over the Internet. WMS allows users to request imagery of any size over any geographic area. To fulfill a WMS request, the tile server mosaics the tiles of the closest map scale to the request and rescales the result to match the desired image size. This method is superior to using the original imagery, which requires loading each high-resolution image file, constituting possibly terabytes of imagery for large areas, in order to fulfill a request.

Mobile and disconnected systems have limited resources available for imagery storage and processing, both of which are taxed if required to handle high-resolution imagery. Deploying tiled data provides a number of advantages. We can deploy tiles covering limited areas and at lower resolution than the original imagery in order to save storage space. Our mobile applications require little processing power because no image processing is necessary to directly use tiles.

Conclusion: The NRL-developed tile archival and distribution system has provided significant advancements in how imagery of the Earth's surface and seafloor is currently used by a number of Department of Defense agencies, including the National Geospatial-Intelligence Agency, the Marine Corps System Command, Naval Explosive Ordnance Disposal, and NRL's Naval Center for Space Technology.

[Sponsored by NRL]

Reference

[1] E.Z. Ioup, H.C. Mesick, and J.T. Sample, "Method for Efficiently Transforming a Raster Image from One Map Projection to Another Map Projection," U.S. Patent Appl. 11/673,363, Feb. 2007.

Cross-Domain Payload Migration

C.M. Huffine
Space Systems Development Department

Cross-Domain Payload Migration: Space payload development typically occurs over relatively long timelines, given the risks, costs, and other factors. This fact motivates developers to investigate other payloads and platforms, in aviation and terrestrial systems, for example, as a means of gaining experience with state-of-the-art technology and exercising the methods and processes used in engineering high-reliability space systems. Increasingly, systems developed for aviation and terrestrial platforms serve as risk-reducing prototypes for eventual space missions. Remote operation of payloads deployed in unmanned aviation platforms and unattended ground systems provides a realistic operating environment for simulating control of a space payload.

The tradespace of hardware and software required to successfully support many Navy, Marine Corps, and DoD missions exhibits commonality that could be used across multiple payload and platform domains. Comparison of characteristics and requirements between payload domains shows many solutions to be more alike than different. The Naval Research Laboratory has demonstrated on several payload developments the feasibility of designing advanced, state-of-the-art systems for use across multiple domains and the reduced development costs which result, especially for shared software systems.

Moving Beyond Single-Purpose Payloads: In examining the organizations, companies, laboratories, and other facilities often supporting DoD development activities, it is common to note a stovepiped mentality. The space development organizations tend to be separated from the aviation and ground solutions people. These structures often mirror that of the sponsoring organization, resulting from security classification, from separation of funding sources, and other factors. For a more than a decade, DoD has specifically focused on breaking down stovepipes so that within organizations there is more visibility across the portfolio of projects and development efforts. Current economic realities and the need to share information help bring down stovepiping.

The Naval Research Laboratory provides a unique environment to support those efforts with a broad multidisciplinary approach across our divisions. Since many of our sponsoring organizations are also in a position to see across the multiplatform solution space, they are able to recommend development projects and solutions that can end up being more efficient. Encouraging NRL scientists and engineers and our DoD sponsors to think ahead during the specification and design phase about applying their work across multiple domains is advantageous. In the Space Systems Development Department, it has been a philosophy to "solve the problem once" to the largest extent possible. We continue to strive to meet that ideal.

Case Study — Copperfield-2: The Copperfield-2 (CuF2) payload system for use in ground, aviation, and space platforms serves to demonstrate a core R&D product NRL has successfully demonstrated across multiple platforms. The CuF2 system was developed as an experimental platform for a flexible, reconfigurable payload. When the first concepts were put together, the design focused on a single type of aviation

platform. However, as the architecture evolved, the engineers made design decisions and trades that supported "future proofing" the system and provided for expanded utility. With the broader capability designed into the hardware and software, CuF2 became a core product and acted as a springboard to a number of other unforeseen projects, each program adding further capability valuable to follow-on work. This produced a library of hardware and software applications, and a menu from which modular systems could be constructed. The history of the development shows the migration across platform domains.

Not all of the platforms and domains listed in Table 2 came to fruition in an actual demonstration, but in no case did a limitation of the payload design prevent further application. While CuF2 started life with a specific radio requirement in mind, its success has been defined by its capability to adapt to new signals that were of no interest when the payload was first designed.

Furthering Cross-Platform Applicability: As development continues with the next generation of payloads under the Software Reconfigurable Payload (SRP) portfolio of products, providing built-in flexibility becomes a design rule. The "best practices" used in the design, implementation, and construction of space payloads, with their higher complexity and expense, are also in line with the best practices one uses in the development and design of aviation payloads, and really help to increase the reliability of any system. Engineering trades must be undertaken to optimize capability versus cost, however: it is often difficult to articulate in a requirements document "latent capability."

The biggest challenge one finds in developing cross-domain solutions is selecting high-performance components for terrestrial and aviation applications that will also operate successfully in the higher radiation levels encountered in the space environment. Thermal, vibration and shock, and vacuum effects can all be readily accommodated through careful management of the environmental control systems. Indeed, shock and vibration are often a more challenging problem in aviation and terrestrial systems — rocket rides are short in duration, and extremes of temperature are very unusual events. Sitting on the tarmac in the desert for 8 hours of sunlight often presents a more challenging thermal design problem than the one encountered in the design of space payloads. Figure 5 shows the variety of payload operating domains and corresponding packaging techniques.

Different types of electronic components used in payloads respond differently to radiation environments depending on their underlying technology. RF components are inherently more tolerant due to the semiconductor processes used to construct them. High-speed processors and field-programmable gate arrays (FPGAs) tend to be "softer" and can be affected by total-dose radiation, producing a slow degradation of performance, or by highly energetic bursts of radiation, causing "single-event upsets" that change memory states. Permanent failure may even result when a highly charged particle hits a particularly susceptible semiconductor device, causing "single-event burnout." In the realm of digital processing, radiation tolerant parts are available — but parts today tend to be at least a decade behind parts that are commercially available for use in terrestrial and aviation applications. NRL experience has shown that a compromise design with radiation-hardened circuitry, but much of the same software components, provides for the best portability for cross-domain applications. On-orbit experience has also shown that within the tradespace of cost, complexity, and reliability, selected commercial non-radiation-hardened components can be successfully flown and provide useful mission life. Sponsors must, however, understand the cost-benefit trade and the risks involved.

TABLE 2 — Payload Migration History

Platform	Domain	Year
Predator class UAS	Aviation	2001
Firescout class UAS	Aviation	2003
TacSat-1	Spacecraft	2004
Tier-II UAS	Aviation	2005-6
TIE/TacSat-2	Spacecraft	2006
Subsurface	Subsurface	2006-7
GlobalHawk	Aviation	2008
MSS	Terrestrial	2008
TacSat-1A	Spacecraft	2008/9

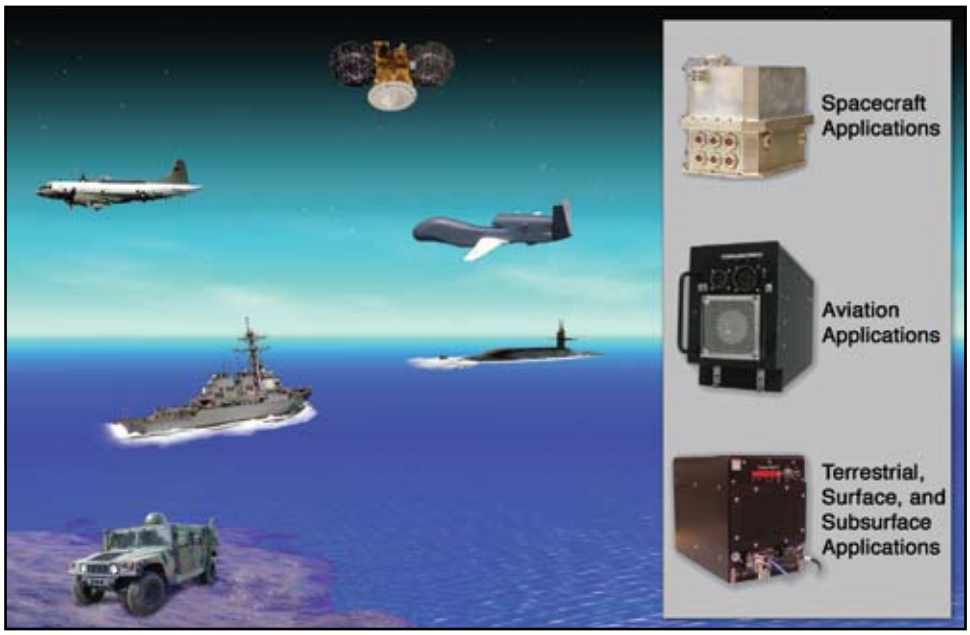

FIGURE 5
Various form factors and hardware examples for those domains.

Conclusions: Payload design engineers have within their toolbox the ability to create systems that are relevant beyond a single operational domain. Keeping the most challenging attributes of each domain in mind during the design process, intelligent engineering trades can be made that maximize capability. NRL experience in providing terrestrial, aviation, and space platforms validates the flexibility, extensibility, and cost and schedule savings that may be realized. The goal of "solving the problem once" is obtainable, and in the longer term provides more capability to more payload systems with reduced overall cost.

[Sponsored by ONR]

materials science and technology

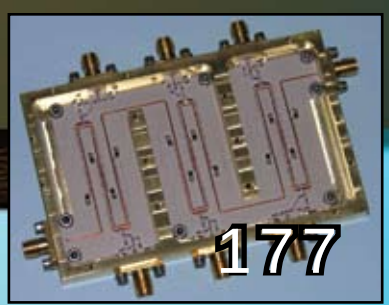
177

180

182

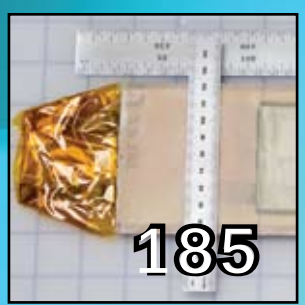
185

177
Tunable Filter and Multiplexer for Improved Transmitter Electromagnetic Compatibility
D.R. Jachowski, C. Rauscher, S.W. Kirchoefer, W. Kruppa, A.C. Guyette, and J.M. Pond

180
Risk Mitigation for High Temperature Superconducting Generators
R.L. Holtz

182
CT-Analyst Integration in Chemical/Biological/Radiological (CBR) Analysis Applications
A. Moses

185
Multifunctional Structure-Battery Composites for Marine Applications
J.P. Thomas, M.A. Qidwai, W.R. Pogue III, and A. Rohatgi

Tunable Filter and Multiplexer for Improved Transmitter Electromagnetic Compatibility

D.R. Jachowski, C. Rauscher, S.W. Kirchoefer,
W. Kruppa, A.C. Guyette, and J.M. Pond
Electronics Science and Technology Division

Introduction: The challenge of using high-power transmitters, or "jammers," is complicated by the desire for these transmitters to be compatible with friendly-force systems that operate in the same region of the electromagnetic spectrum. Electromagnetic compatibility is particularly difficult to achieve when practical constraints, such as size, weight, and power, dictate that these transmitters operate efficiently — a mode of operation in which their amplifiers are more prone to generate spurious signals that interfere with friendly-force systems.

To address the issue of electromagnetic compatibility in transmitters, MITRE Corporation is developing an extensible transmitter architecture that will broadcast less friendly-force interference. MITRE enlisted NRL to develop filters able to suppress interference transmission without compromising the transmitter's task. Within a four-month time frame, NRL's Microwave Technology Branch developed a novel high-power contiguous-channel frequency multiplexer for suppression of amplifier second harmonics and a novel microsecond-tunable notch filter for excision of selectable narrow frequency bands from an amplifier's input. Figure 1 illustrates the integral role of these filters in the transmitter's output module.

Ridge-Waveguide Multiplexer: The multiplexer selectively combines the outputs of two sub-octave-frequency-banded power amplifiers, preserving signal power while suppressing harmonic and other out-of-band interference. Composed of two ten-resonator channel filters and a manifold, it was designed using commercial general-purpose electromagnetic-analysis and circuit-simulation software.[1] As shown in Fig. 2(a), each channel filter employs T-profile ridge waveguide, known for its compact size, low passband insertion loss, and wide stopbands. Dielectric fill of the gap between the ridges and opposing waveguide wall lowers the waveguide cutoff frequency and reduces filter size. Notched ridge-waveguide sections create evanescent-mode coupling between adjacent ridge-waveguide resonators for further size reduction.[1] Notch depths are varied to adjust couplings, while widths are kept equal to facilitate manufacturing. As shown by the partially disassembled multiplexer in Fig. 2(b), a coaxial manifold connects channel filters to a common antenna port, inhibiting modes that would degrade stopband performance. N-type connectors are used for convenience, and integrated coaxial-to-ridge-waveguide transitions and port matching networks help to reduce the overall size.

The transmission and reflection characteristics of the 375 mm × 108 mm × 57 mm unplated aluminum multiplexer, with no post-assembly tuning, are plotted in Fig. 2(c). The 531–977 MHz and 1030–1636 MHz channels have less than 0.5 dB insertion loss, and their respective second harmonics are attenuated by more than 60 dB. Compared with conventional approaches, this new multiplexer technology enables substantial savings in size while retaining excellent electrical performance, power handling, and manufacturability. The approach to design and realization appears accurate enough that post-assembly tuning will not be needed, further reducing cost and improving reliability.

Tunable Microstrip Notch Filter: The tunable notch filter selectively removes jamming energy in a

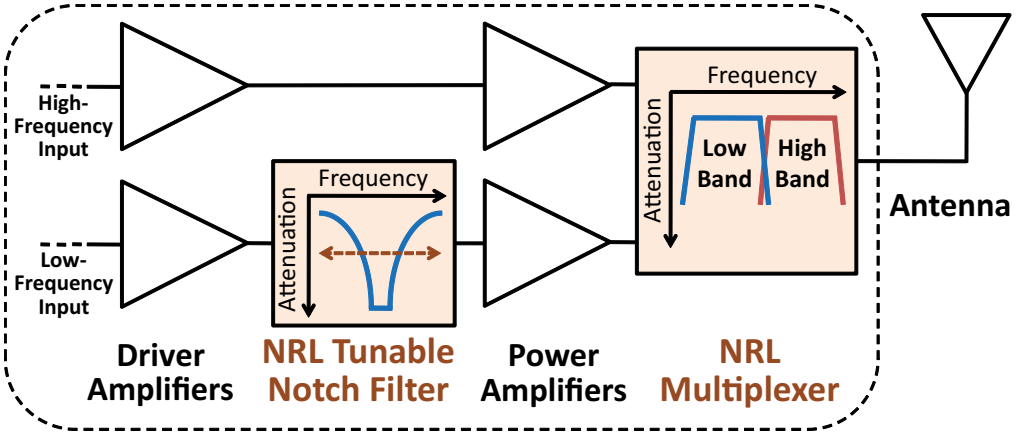

FIGURE 1
Simplified functional block diagram of MITRE's experimental transmitter output module, including NRL's two-channel multiplexer and tunable notch filter.

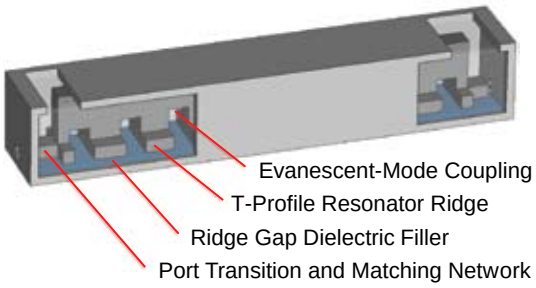

(a)

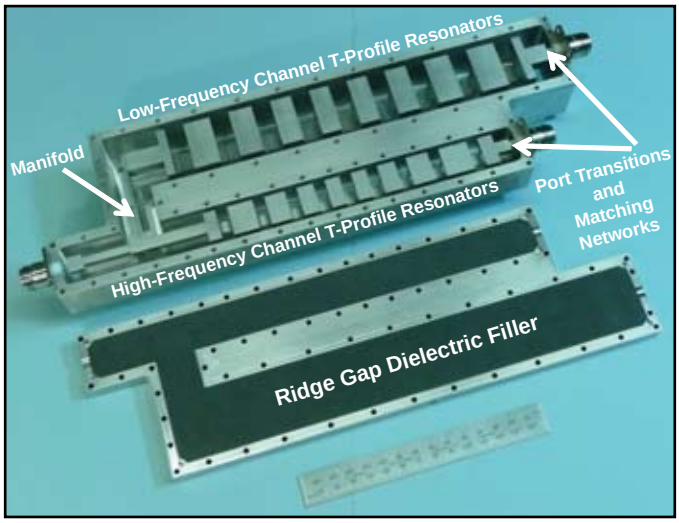

(b)

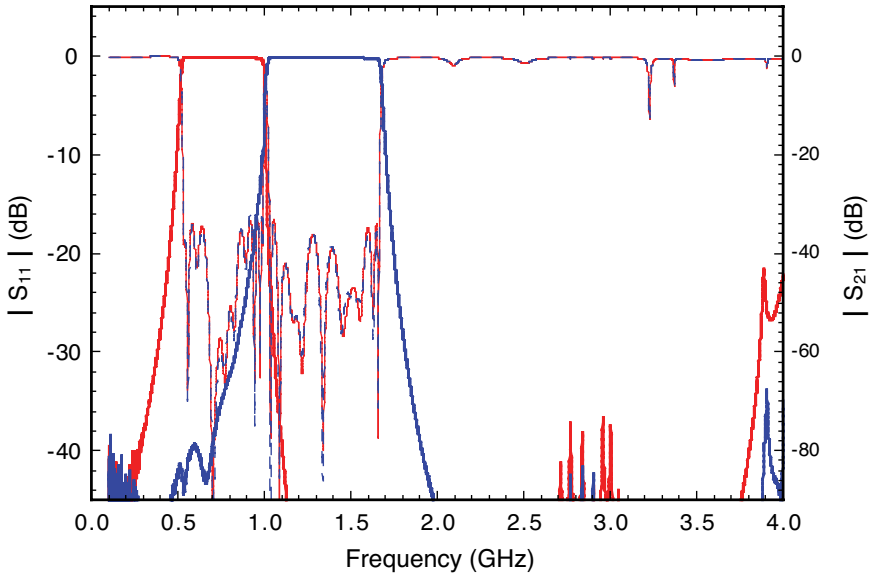

(c)

FIGURE 2
(a) A partial cutaway rendering of a single ridge-waveguide channel filter, together with (b) a photo of the 531–1636 MHz, partially disassembled, two-channel ridge-waveguide frequency multiplexer and (c) a plot of the multiplexer's measured transmission and reflection characteristics.

selectable frequency band before it can be amplified and broadcast, enabling equipment interoperability through a new level of control over transmitted spectral content. MITRE's requirement for sub-microsecond tunability of a narrow 60 dB stopband over nearly an octave frequency range cannot be met with conventional reflective notch filters, in which resonator resistance limits stopband attenuation and selectivity, especially with the added resistance of semiconductor frequency-tuning elements. However, the requirement can be met with absorptive notch filter technology[2,3] recently developed at NRL, in which resonator and associated tuning element resistance limits minimum 3-dB bandwidth rather than stopband attenuation. Within the stopband, signal power not reflected is dissipated in the resistance of resonators and their tuning elements, enabling theoretically infinite attenuation. And while changes in operating frequency correspond with commensurate changes in couplings and tuning-element resistance that degrade the performance of conventional notch filters, absorptive notch filters can correct for these commensurate changes with a simple offset between the tuned frequencies of coupled pairs of resonators, enabling stopband attenuation and bandwidth to be preserved across a broad range of operating frequencies.

The 102 mm × 64 mm × 9 mm microstrip absorptive notch filter, comprised of a cascade of three two-resonator absorptive notch sub-circuits, is shown in Fig. 3 with its measured performance. Using com-

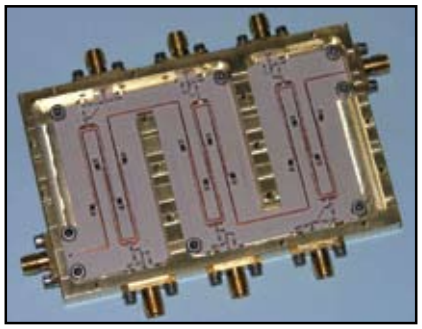

(a)

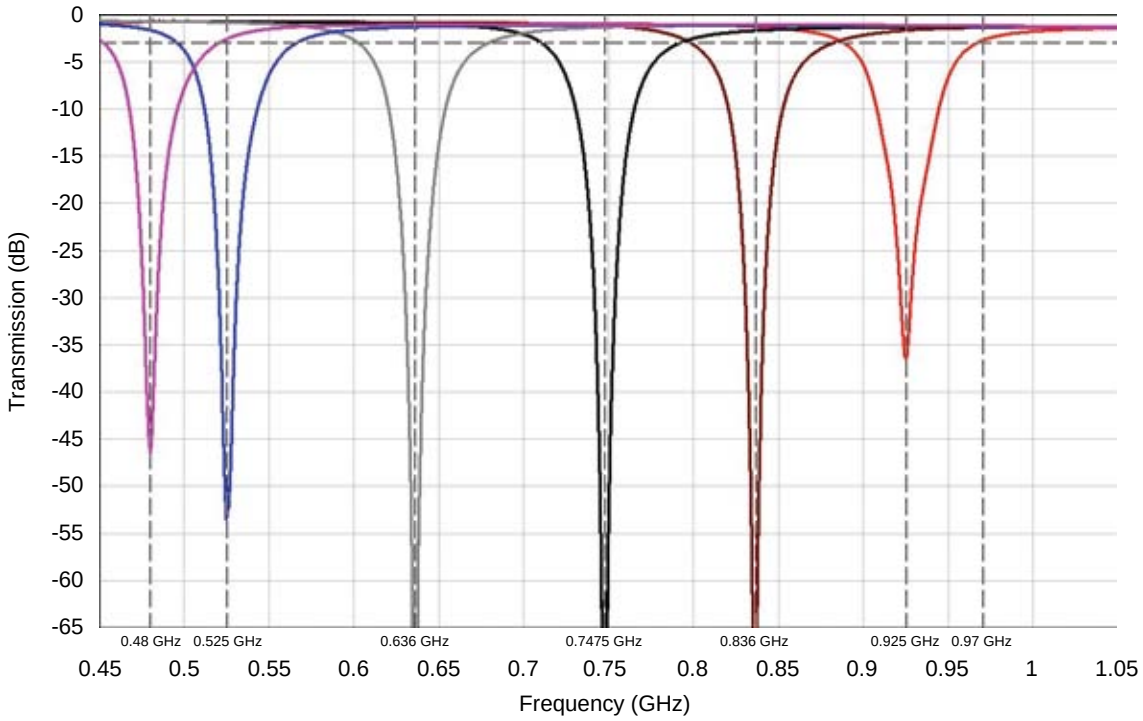

(b)

FIGURE 3
(a) Photograph and (b) measured transmission characteristic of the sub-microsecond-tunable microstrip absorptive notch filter with a 480–925 MHz (or more than 92%) tuning range, tuned to six different operating frequencies: 480, 525, 636, 747.5, 836, and 925 MHz.

mercial hyperabrupt varactor diodes as tuning elements, the filter maintains a 3-MHz-wide stopband attenuation of more than 60 dB across a majority of its 480–925 MHz tuning range. Passband insertion loss ranges from 0.7 dB to 1.2 dB, 3-dB bandwidth remains less than 84 MHz while varying less than 24% over the tuning range, and, thanks to 100-MHz-bandwidth lowpass bias networks, transition time from one 60-dB-attenuation operating frequency to another is 720 ns. The filter achieves an unprecedented combination of frequency tuning range and speed, electrical performance, and size using only inexpensive, commercially available materials and components.

Summary: NRL developed two critical, novel components for insertion into a new MITRE transmitter architecture: a multiplexer and a tunable notch filter, both having small size, low cost, and good performance. The success of MITRE's subsequent transmitter demonstration suggests a practical near-term path to improved equipment compatibility and interoperability, and supports the Navy's near-term equipment acquisition plans by showing the feasibility of demanding Navy requirements and by serving as a design reference for industry.

Acknowledgments: This work was sponsored by Naval Sea Systems Command (NAVSEA). Marc St. John of MITRE initiated the effort and Gary Shuler of NAVSEA supported it.

[Sponsored by NAVSEA]

References

[1] C. Rauscher, S.W. Kirchoefer, J.M. Pond, A.C. Guyette, and D.R. Jachowski, "A Compact Ridge-Waveguide Contiguous-Channel Frequency Multiplexer," *IEEE Trans. Microw. Theory Tech.* **57**(3), 647–656 (2009).

[2] D.R. Jachowski, "Compact, Frequency-agile, Absorptive Bandstop Filters," *2005 IEEE MTT-S Int. Microwave Symp. Dig.*, 513–516 (2005).

[3] D.R. Jachowski, "Narrow-band Absorptive Bandstop Filter with Multiple Signal Paths," U.S. Patent No. 7,323,955, January 29, 2008.

Risk Mitigation for High Temperature Superconducting Generators

R.L. Holtz
Materials Science and Technology Division

Background: High temperature superconducting (HTS) motors and generators will enable high-efficiency, high power density naval propulsion, and compact electrical generators for weapons and ship systems. The second-generation high temperature superconductors (2G-HTS) based on yttrium-barium-copper-oxide (YBCO) coated conductor architectures have undergone a processing technology breakthrough that has led to manufacturability of long lengths of these materials, sufficient for demonstrations of large motors and generators. Ensuring superior fatigue properties of the HTS materials compatible with the life-cycle of naval machinery is a key issue. NRL has been working closely with superconductor manufacturer Superpower, Inc., electric motor manufacturer Baldor Reliance, General Dynamics Electric Boat Division, and Naval Surface Warfare Center Carderock Division (Philiadelphia) on risk mitigation demonstrations for a 10 MW HTS generator design. NRL's responsibility in this collaboration is assessment of the reliability of HTS coil design, particularly with respect to thermomechanical fatigue associated with cooling/warming between room temperature and the cryogenic temperatures at which the machines operate.

Coil Architecture for HTS Machinery: Figure 4 depicts a rotor coil architecture for an HTS motor or generator. The windings of HTS tapes are placed into a steel or other metallic rotor structure, and secured by epoxy impregnation. The epoxy provides both mechanical support against the high stresses experienced by the coil, and electrical insulation. The principal risk factor for the reliability of such coils is thermomechanical stress as the coil is cooled to cryogenic temperatures. If a coil is subsequently warmed and cooled multiple times, such as for major maintenance, overhaul, or repair of the machine, there is a potential for low cycle fatigue damage. In the life of a ship generator, such thermal cycles would occur perhaps up to 20 to 30 times.

The large thermomechanical stresses develop because between room temperature and 77 K, the thermal contractions of epoxies with suitable strength and electrical properties are typically around 1%, while the thermal contractions of the HTS tapes and of the steel are much lower, around 0.25%. Thus, large tensile stress develops in the epoxy, which potentially could rupture the HTS tapes, damage electrical connections, or crack the interface between the epoxy and the HTS or the interface between the epoxy and the steel rotor body.

Coil Electrical Characteristics: The main measurements we perform on HTS coils are the voltage versus current curves, and the time dependence of voltage for fixed currents. Typical behaviors at 77 K are shown in Fig. 5. The voltage-current curves are characterized by a voltage that grows exponentially as current increases above a "critical current." In an ideal HTS tape, the DC resistance is zero for currents below the critical current. In a real coil, there are splices of HTS tapes, as well as joints of HTS tapes with copper conductors. These

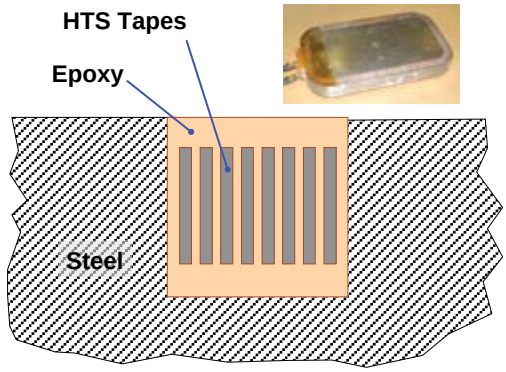

FIGURE 4
Schematic of the cross-sectional coil architecture. HTS windings are placed into steel body and epoxy-impregnated. The inset shows an example of a prototype coil.

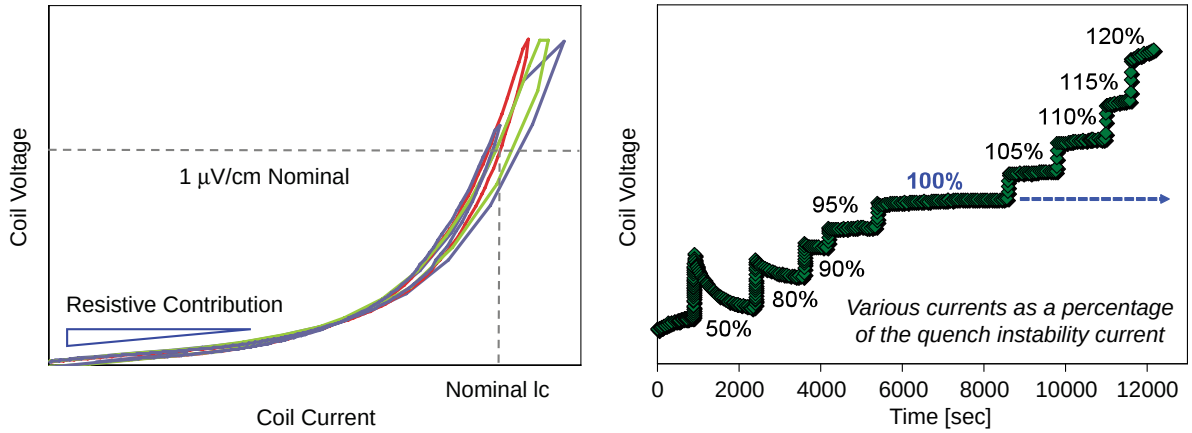

FIGURE 5
(a) Typical voltage-current curves for an HTS coil. This plot shows the curves following several different thermal cycles. The nomimal criticial current, Ic, is defined as the current at which the voltage is 1 microvolt per centimeter. The linear behavior at low currents is due to a resistive (non-superconducting) contribution. (b) Typical voltage-time curves for the same HTS coil. For each value of current, the voltage is monitored for some period of time to determine if it is stable. The highest current at which the voltage exhibits long term stability is designated the quench instability current.

have a small DC resistance, which manifests as a linear behavior at low currents in the voltage-current curves, indicated in Fig. 5(a). For thermomechanical fatigue reliability evaluation, any increases in the resistance following thermal cycling would indicate damaged electrical connections or splices.

When the current exceeds the critical current anywhere in the coil, heat is produced, which raises the temperature, which reduces the critical current even further, leading to a thermal runaway process known as "quench." This manifests as a voltage that increases with time at constant current, as seen for the higher currents in Fig. 5(b). An important figure of merit therefore is the maximum current that can be used in the coil without causing thermal runaway. We term this the "quench instability current." For thermomechanical fatigue reliability assessment, we measure this quench instability current as a function of thermal cycles. Changes in this property would indicate either damage to the HTS tapes, or cracks separating the epoxy from the HTS or the steel body, which degrade the thermal conductivity.

Results: Figure 6 shows results from NRL's recent evaluation of a prototype HTS generator coil. No systematic changes of the resistive component, Fig. 6(a), or quench current, Fig. 6(b), are seen for up to 20 thermal cycles between room temperature and cryogenic temperatures.

Significance: Prior work at NRL on the electromechanical properties of HTS tapes established limits on the stresses and strains that could be tolerated.[1] By incorporating earlier NRL results into the design of coils, risk of degradation due to thermal cycling is mitigated. Actual measurements on prototype coils under the current NRL program confirm the fatigue integrity of coil designs, and demonstrate that HTS technology is reliable for large, fatigue-critical, shipboard machinery applications.

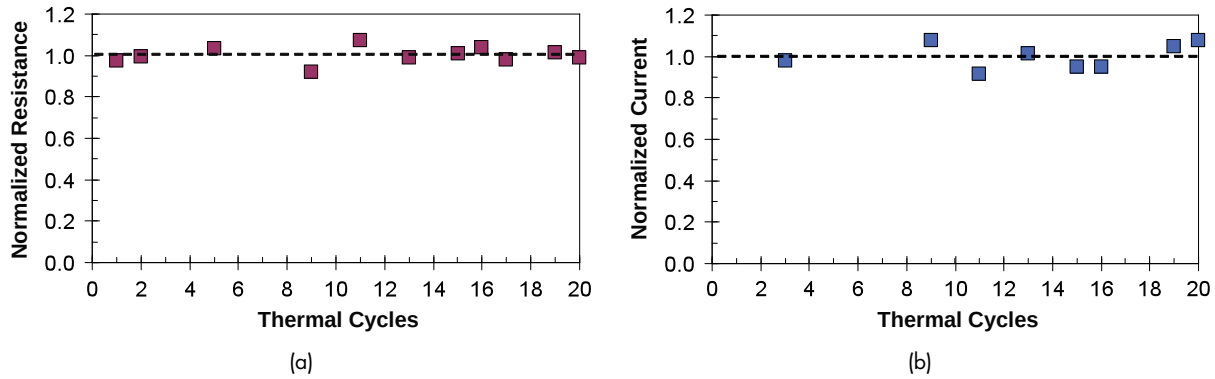

FIGURE 6
Experimental results on an HTS coil showing the thermal cycling stability of the (a) resistive contribution to the voltage-current characteristics, and (b) the quench instability current. Results are normalized to the average values in both plots.

Acknowledgments: HTS coils were provided by Superpower, Inc., Schenectady, NY.

[Sponsored by ONR and NRL]

Reference

[1] R.L. Holtz, R.J. Soulen, M. Osofsky, J.H. Claassen, G. Spanos, D.U. Gubser, R. Goswami, and M. Patten, "High Temperature Superconductors for Naval Power Applications," *2006 NRL Review*, pp. 149–151.

CT-Analyst Integration in Chemical/Biological/Radiological (CBR) Analysis Applications

A. Moses
Laboratory for Computational Physics and Fluid Dynamics

Introduction: Modern information systems used in the fight to prevent or respond to chemical, biological, and radiological (CBR) attacks are greatly improved by incorporating complex plume modeling as a resource in their applications. This is one of the principal reasons that NRL's CT-Analyst (Contaminant Transport Analyst) has become such a valuable software tool in the field of CBR analysis. CT-Analyst accurately models the transport and dispersion of contaminants for instantaneous situation assessment. By taking advantage of compressed data structures pre-computed in a high performance computing (HPC) environment, it runs in real time, without having to re-compute each time a change is made to a given scenario. CT-Analyst is also designed for smaller scales than other similar tools — specifically cities, downtowns, and other complex urban environments. The computing speed and the focus on areas where attacks are likely to occur distinguish CT-Analyst as one of the top tools for use by first responders, crisis management teams, simulation designers, and others interested in fast and reliable plume predictions. CT-Analyst is also versatile in its connectivity with other applications; its application programming interface opens it to developers in a range of applications, and allows it to interface with many widely available public tools. Thus, CT-Analyst's integration with applications in the CBR arena makes it a powerful asset to the military, homeland security, local authorities, and software developers.

Geographical Information Systems: CT-Analyst's core functionality is to produce time-dependent plumes over a geographic area, and while the tool itself contains its own user-friendly graphical user interface (GUI), other products can also be used to display this kind of information. Some of the latest tools used to map, visualize, and process local and global geography are Geographical Information Systems (GIS), which range from publicly available programs, such as Google Earth, to more industry-specific tools. The advantage of a program such as Google Earth in particular is that it is well known by household users and by corporate and government institutions alike. The wide familiarity of this program makes it ideal for exporting CT-Analyst data and making it readily understood and usable by anyone. Google Earth's KML file format can show all the display states CT-Analyst offers, including plumes, total footprint, backtrack, consequence, and others (Fig. 7).

Simulations: CT-Analyst has been integrated alongside a number of simulation tools as well, with its plume predictions replacing the often simplified oval or standard Gaussian puff models that are part of many of these systems. One Semi-Automated Forces (OneSAF) is a military simulation used for demonstrating complex entity interaction, taking into account environmental factors and unit behaviors. OneSAF's existing model of representing plumes was replaced by CT-Analyst's, correctly modeling smoke and other

FIGURE 7
CT-Analyst plumes displayed in Google Earth, showing the same colors and density information as in the CT-Analyst program.

airborne hazards so that line of sight and contamination could be computed, ultimately affecting the behaviors of units and the outcome of a given scenario. This greatly benefited the accuracy and effectiveness of the OneSAF model and emphasized the value of CT-Analyst capabilities.

CT-Analyst is also being incorporated into another simulation tool, Virtual Battlefield 2 (VBS2), a product of Bohemian Interactive. VBS2 is a gaming product that allows players to train in a variety of scenarios, including terrorist attacks, urban combat, or other types of missions. Like OneSAF, VBS2 natively features a very basic plume model, one that essentially operates on only a visual level, and involves no knowledge of terrain, buildings, or any other part of the geometry (Fig. 8). In this ongoing integration project, the objective is to have an interface between the VBS2 game engine and CT-Analyst, so that plumes are produced in CT-Analyst based on in-game events and then sent back into the game for display and for effects on the players.

Preparedness Tools: First responders and emergency planners have a variety of CBR analysis tools at their disposal. One of them, Chemical Biological Response Aide (CoBRA), features a highly detailed database of known contaminants and an incident reporting system that allows responders and officials at varying levels to both input and receive information from all the other users of the software. CT-Analyst was incorporated into CoBRA (Fig. 9) with several capability goals: 1) to have the CT-Analyst GUI embedded inside of CoBRA so that actual or practice events could be input, 2) to have such events saved out and inserted into the incident reporting system, 3) to allow other users to recall these reports and display the exact scenario within their own copy of the GUI, and 4) to locate important federal buildings in a scenario and determine if they are in the affected areas. All of these goals were satisfied in the integration project, with CT-Analyst able to quickly and easily distribute scenarios involving contaminant releases, and detect and report affected buildings.

Summary: CT-Analyst's core ability to produce time-dependent plumes in complex urban environments is useful in a variety of applications in the CBR field. Among the common GIS systems, simulation tools, and emergency preparedness applications in use today, CT-Analyst has found a role in each. CT-Analyst is enhancing products that people are already using, and is certain to be important in other products undergoing development or yet in the planning stages.

[Sponsored by NRL]

FIGURE 8
Plumes as they appear in VBS2; work is ongoing to replace this format with time-dependent plumes from CT-Analyst.

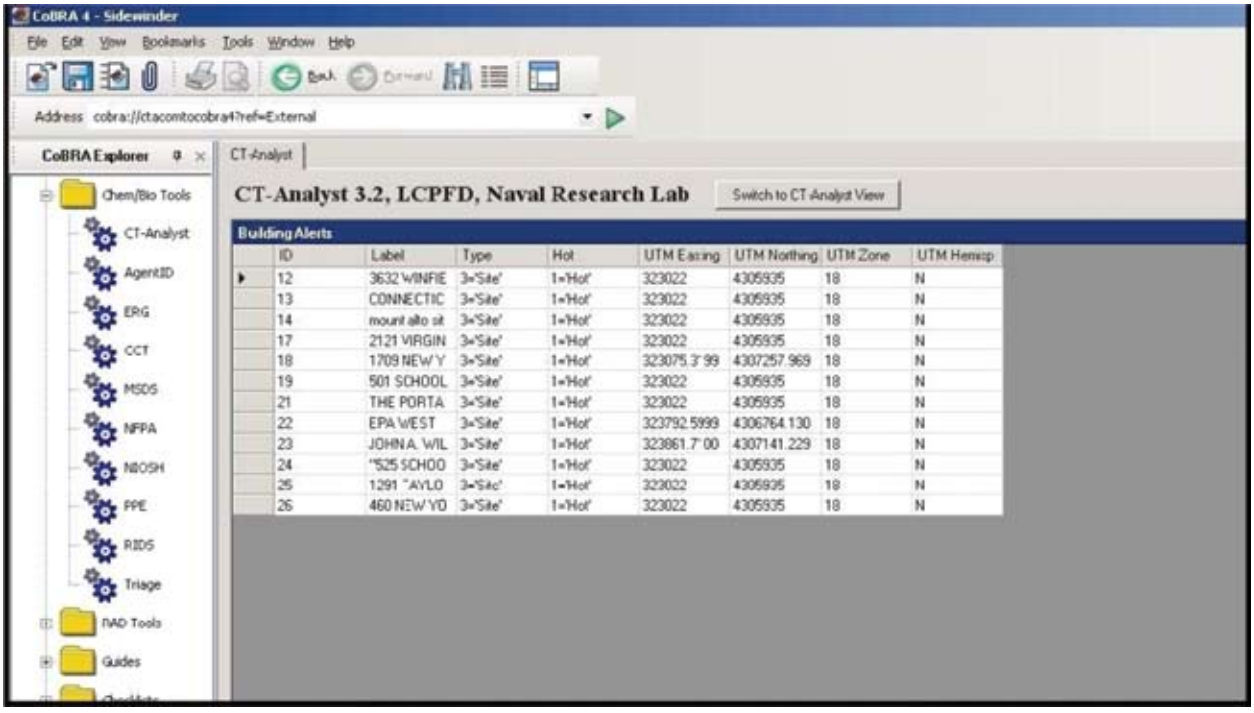

FIGURE 9
CT-Analyst incident reporting information embedded in CoBRA.

Multifunctional Structure-Battery Composites for Marine Applications

J.P. Thomas,[1] M.A. Qidwai,[2] W.R. Pogue III,[1] and A. Rohatgi[2]
[1]*Materials Science and Technology Division*
[2]*Science Applications International Corporation*

Introduction: There is current interest in increasing the time-on-station endurance of unmanned underwater vehicles (UUVs) through the use of hybrid power systems consisting of fuel cells for cruise-mode and batteries for the sprint-mode portions of a mission. Today, most electric-powered UUVs use large batteries that are contained within the hull. In moving to hybrid power systems, significant hull space can be freed up for additional fuel-oxidizer or payload by relocating the battery cells into the UUV skin and other structural components.

In previous works, we have examined the use of multifunctional structure-power materials/components for increasing the available energy and/or decreasing weight in small-scale unmanned systems.[1] The present work focuses on the integration of high-energy lithium-ion (polymer) battery cells into fiber-reinforced polymer composite materials for application to larger-scale marine systems. The operational environment (i.e., seawater at depth) and large-scale structural and energy storage capacity requirements have posed new challenges in the multifunctional design process. Galvanic corrosion and buoyancy are of fundamental concern, as are battery safety, charge/discharge control, and power bussing.

Laminates and Sandwiches: Traditional (unifunctional) marine composites are either fiber-reinforced polymer laminates or fiber-reinforced polymer facesheets/foam core sandwich designs for enhanced bending performance and buoyancy. Both of these fundamental design configurations are addressed in this work. Laminates are used as skin, casing, and bulkheads, whereas sandwich composites are used in structural frame components and skins. The reinforcements are unidirectional carbon- and glass-fibers or woven cloth. The glass layers are used primarily on the exterior surfaces to provide electrical/galvanic isolation of the carbon layers. Core materials are closed-cell or syntactic foams depending upon the targeted depth rating.

Composite Testing: Three types of structure-battery (SB) composites have been designed, fabricated, and tested to demonstrate potential for underwater marine applications.[2] The first is an SB laminate with the cells "framed" within foam channels and then bonded between flat and conformal laminate layers. The second is an SB sandwich panel with cells embedded in a foam core. The third is a modular (easily removable) SB stiffener with cells framed in a foam channel bonded between laminate layers (Fig. 10).

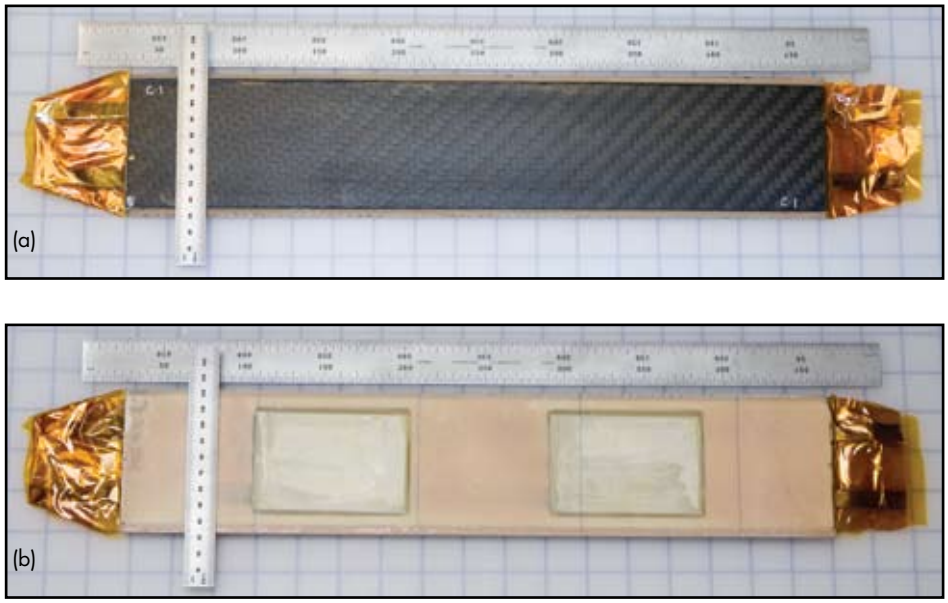

FIGURE 10
Modular structure-battery stiffener showing top (a) and bottom (b) views and the two embedded lithium cells. This SB stiffener can be (reversibly) attached to a structure to provide a significant increase in flexural stiffness and strength with energy storage capacity.

Unifunctional equivalents have also been fabricated for comparing mechanical performance. Performance objectives for the new SB composites include: 1) volumetric energy density of 50 Wh/L or greater; and similar or better: 2) structural properties, 3) buoyancy levels, and 4) dimensions relative to the unifunctional counterparts.

High-performance carbon- and glass-epoxy materials (prepregs and wet layup) from SP Gurit (Marine Composites Division) were used in the fabrication of all specimens.[2] The prepregs use the SE84LV epoxy resin (80 °C cure), and the wet layups use the Ampreg 22 resin (50 °C cure). The S-1800 SAN closed-cell foam was used for framing the battery cells and as a buoyant core material for the sandwich composites. Kokam USA rechargeable lithium ion cells (type SLPB 356495; 3.7 mm × 64 mm × 95 mm) were used and are nominally rated at 3.8 V and 2100 mAh capacity.

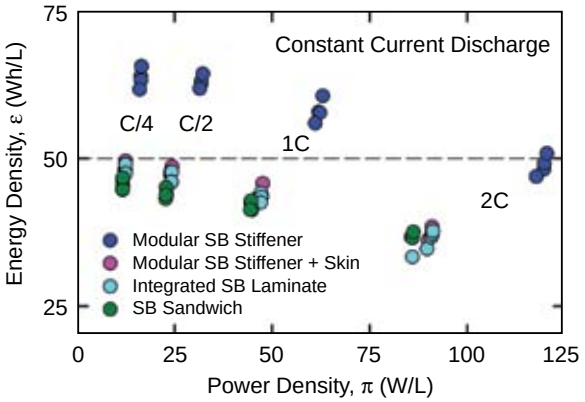

FIGURE 11
Ragone performance of the SB composites at four discharge rates. The fabricated specimens were slightly thicker than planned, which accounts for the slight underperformance (<50 Wh/L) of the integrated and sandwich SB composites.

Results: Flexure testing to characterize mechanical bending stiffness, and Ragone testing, which measures energy storage capacity as a function of power discharge rate, were conducted to characterize the structural and electrical performance.[3] Flexure testing demonstrated that the apparent bending stiffness of the multifunctional SB composites was equal to or better than that of the unifunctional counterparts. Volume normalized Ragone data (Fig. 11) show that the modular SB stiffener (without and with attached skin laminate) possesses the maximum energy density, followed by the SB sandwich and the SB laminate.

The results demonstrate the feasibility of integrating lithium-ion cells into structural composites to provide energy storage capability (50 Wh/L in this case) without degrading structural performance and buoyancy. Work is ongoing to characterize the flexural strength and the Ragone behavior under hydrostatic pressure. Critical issues for future investigation include 1) developing a fabrication process for co-curing of the composite materials with the battery cells without degradation of energy storage capacity, and 2) improving the electrical safety and power connections through integrated battery management circuitry and multifunctional use of the carbon-epoxy layers for power bussing.

[Sponsored by ONR and NRL]

References

[1] J.P. Thomas, M.A. Qidwai, J.N. Baucom, and W.R. Pogue, "Multifunctional Structure-Power for Electric Unmanned Systems," Paper NBR–1, NATO AVT-141 Specialists' Meeting on Multifunctional Structures / Integration of Sensors and Antennas, Vilnius, Lithuania, October 2–5, 2006.

[2] W.R. Pogue, M.A. Qidwai, J.P. Thomas, and A. Rohatgi, "Structure-Battery Composites for Marine Applications – Part I: Multifunctional Design and Fabrication," Paper 050, 2008 SAMPE Fall Technical Conference, Memphis, Tenn., Sept. 8–11, 2008.

[3] A. Rohatgi, J.P. Thomas, M.A. Qidwai, and W.R. Pogue, "Structure-Battery Composites for Marine Applications – Part II: Multifunctional Performance Characterization," Paper 068, 2008 SAMPE Fall Technical Conference, Memphis, Tenn., Sept. 8–11, 2008.

nanoscience technology

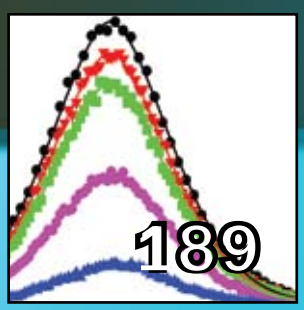

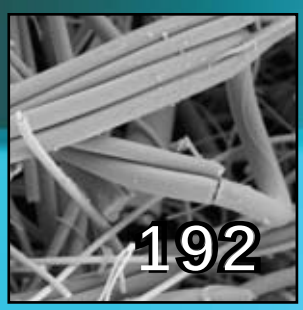

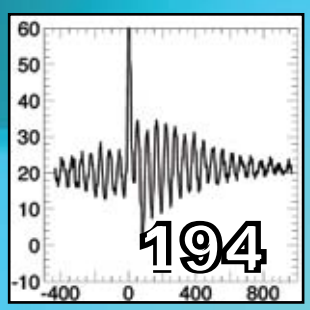

189
Charge Transfer Between Quantum Dots and Peptide-Coupled Redox Complexes
I.L. Medintz, T. Pons, S.A. Trammell, and H. Mattoussi

192
Making the Most of a Scarce Metal
C.N. Chervin, A.M. Lubers, J.W. Long, and D.R. Rolison

194
Optical Pulse Control of Electron and Nuclear Spins in Quantum Dots
S. Carter, S. Economou, A. Shabaev, T. Kennedy, A. Bracker, and T. Reinecke

Charge Transfer Between Quantum Dots and Peptide-Coupled Redox Complexes

I.L. Medintz,[1] T. Pons,[2] S.A. Trammell,[1] and H. Mattoussi[2]
[1]*Center for Bio/Molecular Science and Engineering*
[2]*Optical Sciences Division*

Introduction: Nanotechnology has great potential for creating a new generation of multifunctional hybrid bio-inorganic assemblies that are capable of enhancing Navy capabilities and DoD battle systems in general. The unique properties of luminescent quantum dots (QDs) have made them an integral building block in this burgeoning field.[1] In addition to their well known size-dependent emission spectra, QDs are extremely sensitive to the presence of additional charges either on their surfaces or in the surrounding environment, which can alter both their photoluminescence (PL) and absorption properties.[2] Since the advent of successful techniques to interface QDs with biological molecules, there has been a strong desire to understand the interactions of QDs with redox-active complexes to create new sensors capable of monitoring specific biological and abiotic processes.[2] However, as there is only a minimal understanding of these systems, rational design of QD-redox assemblies with control over both architecture and redox levels is needed to provide insight into the underlying mechanisms. Here we label peptides with a variety of metal complexes expressing different oxidation potentials and ratiometrically self-assemble them on the QD surfaces. This unique configuration allows us to gain insights into the underlying quenching processes involved and exploit them for biosensing.

Quantum Dot Conjugate Architecture: We have previously shown that polyhistidine-terminated peptides can rapidly self-assemble onto QDs with high affinity and control over conjugate valence (i.e., number of peptides per QD).[2,3] In this study, we exploit this self-assembly process and use CdSe-ZnS QDs capped with either negatively charged dihydrolipoic acid (DHLA) or neutral poly(ethylene glycol)-terminated DHLA ligands (DHLA-PEG).[3] Peptides expressing terminal hexahistidine (His_6) tags and unique cysteine or aminolated residues at the opposite end were labeled with reactive metal complexes including a ruthenium chelate (Ru), a bis-bipyridine ruthenium chelate (ruthenium-bpy), and a ferrocene metal complex. These were ratiometrically self-assembled to the QDs for subsequent spectroscopic analysis; see Fig. 1.

Cyclic Voltammograms and Energy Levels: We first determined the redox levels of the QDs and metal complexes used. Figure 2(a) shows the cyclic voltammograms collected from layers of unconjugated QDs and the metal complex–labeled peptides immobilized on indium tin oxide (ITO) electrodes. The ruthenium and ferrocene peptide complexes show reversible forward (oxidation) and reverse (reduction) scans while the ruthenium-bpy appears to be predominantly oxidized. In comparison, the QDs exhibit a single irreversible broad peak centered between 0.2 and 0.24 V regardless of surface ligand present, which is attributed

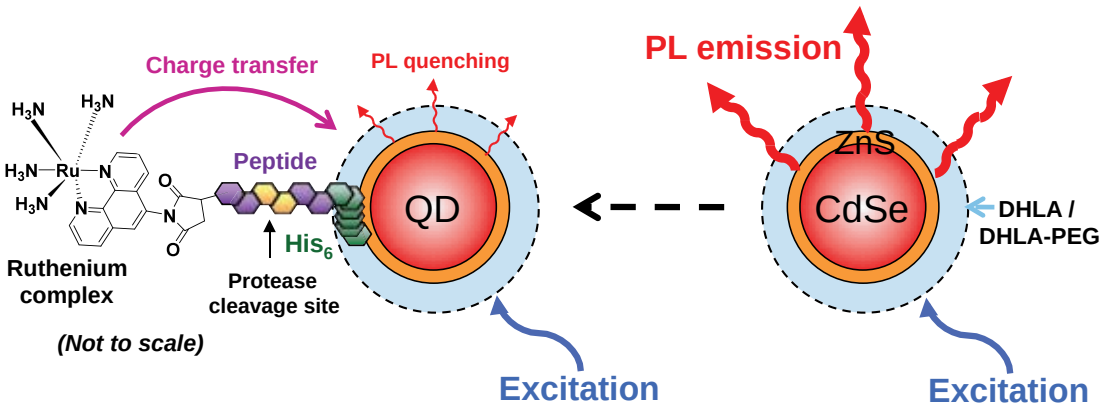

FIGURE 1
Schematic of the charge-transfer-induced quenching of QD PL. Hexahistidine (His_6)-appended peptides are labeled with redox-active metal complexes and self-assembled on CdSe-ZnS QDs capped with either DHLA or DHLA-PEG ligands. The structure of the ruthenium complex is shown. As a result of proximity and redox interactions, charge transfer to the QD results in a quenching of its PL, with a magnitude that depends directly on the number of peptides assembled per QD. Using an amino acid sequence in the peptide that is recognized by a protease allows the assembly of a specific protease sensor. By exploiting the changes in PL quenching following enzyme digestion we are able to realize quantitative monitoring of the enzymatic proteolysis involved.

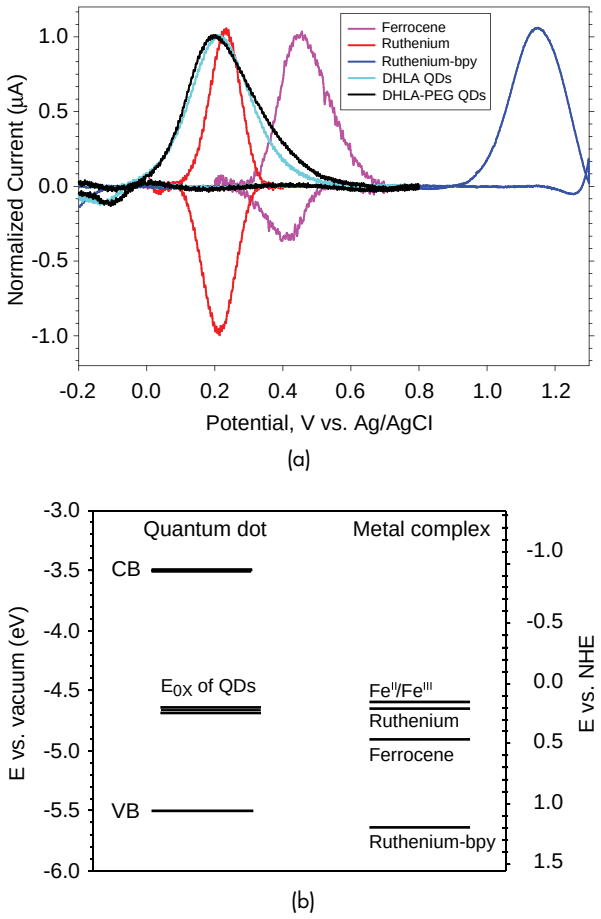

FIGURE 2
(a) Superimposed and background-corrected cyclic voltammograms collected from 590-nm emitting QDs capped with DHLA or DHLA-PEG and peptides labeled with a ruthenium chelate, a bis-bipyridine ruthenium chelate (ruthenium-bpy), and a ferrocene metal complex. (b) Positions of the energy levels corresponding to the QD oxidation peak (E_{ox}), and the oxidation potentials of the metal complexes and the control Fe^{II}/Fe^{III} compound.

to their oxidation. Figure 2(b) shows the extrapolated positions of the QD conduction bands (CB) and valence bands (VB), along with the corresponding QD oxidation peak (E_{ox}) and the oxidation potentials of the metal complex–peptides and of an atomic iron control (Fe^{II}/Fe^{III}). These observations indicate that both the ruthenium complex and atomic iron with their lower oxidation potentials should promote charge transfer from the metal center to the QD when self-assembled into hybrid conjugates. In contrast, ferrocene and ruthenium-bpy with their higher oxidation potentials present less favorable configurations for charge transfer to the QDs.[2]

Spectroscopic Analysis: We next examined the effects that assembling the metal complexes had on the QD photoemission. Figure 3(a) shows representative PL spectra collected from solutions of conjugates having an increasing average number of Ru-peptides per DHLA-functionalized QD. Data clearly show that the proximity of Ru-labeled peptides to the nanocrystals produces a significant and progressive loss of PL; this loss also directly tracks the Ru-peptide valence in the conjugate. Further insight was provided by examining the effects that self-assembling Ru-peptides had on QD absorption properties. The differential absorption plots shown in Fig. 3(b) show that there is bleaching of the QD absorption along with a long red tail contribution in the presence of Ru-peptide, the magnitude of which increases progressively with QD-conjugate valence. This broad red tail change in absorption which accompanies the observed quenching is attributed to electrons populating the QD surface states. Interestingly, QDs functionalized with neutral DHLA-PEG ligands displayed similar quenching from Ru-peptides while the changes in absorption suggested charge-transfer to both the QD surface and core-states. These results were confirmed by using atomic iron as a control, as its low oxidation potential suggested it should also promote charge transfer–based QD quenching.[2] In comparison, the other metal complexes exhibiting higher oxidation potentials did not elicit any significant changes to the QD absorption or PL properties. We also found that the magnitude of Ru-peptide quenching was dependent upon QD size, with larger, red-emitting QDs less quenched on average than smaller, blue-green QDs.[2]

Proteolytic Assays: We exploited this charge transfer process to demonstrate the use of Ru-peptide-based quenching as a signal-transduction modality for monitoring enzymatic proteolysis. Peptides incorporating sequences recognized by the protease chymotrypsin were self-assembled to QDs and exposed to increasing amounts of this enzyme in the absence and presence of a specific inhibitor. Concentration-dependent protease cleavage of the Ru-peptides resulted in concomitant QD PL increases which were converted into enzymatic velocity by correlating quenching efficiencies into the number of intact Ru-peptides per QD-conjugate following enzymatic digestion. This also allowed the derivation of standard Michaelis-Menten kinetic values which describe the enzymatic processes; see Fig. 4. The activity of several other proteases was also monitored with this sensing configuration and in each case the kinetic data agreed reasonably with the expected values.[2]

Conclusions: We combined the electrochemical properties of redox-active metal complexes, peptide-driven self-assembly, and the surface-sensitive quantum dot photoluminescence to elucidate and understand a few aspects of charge transfer between metal complexes and luminescent CdSe-ZnS QDs.

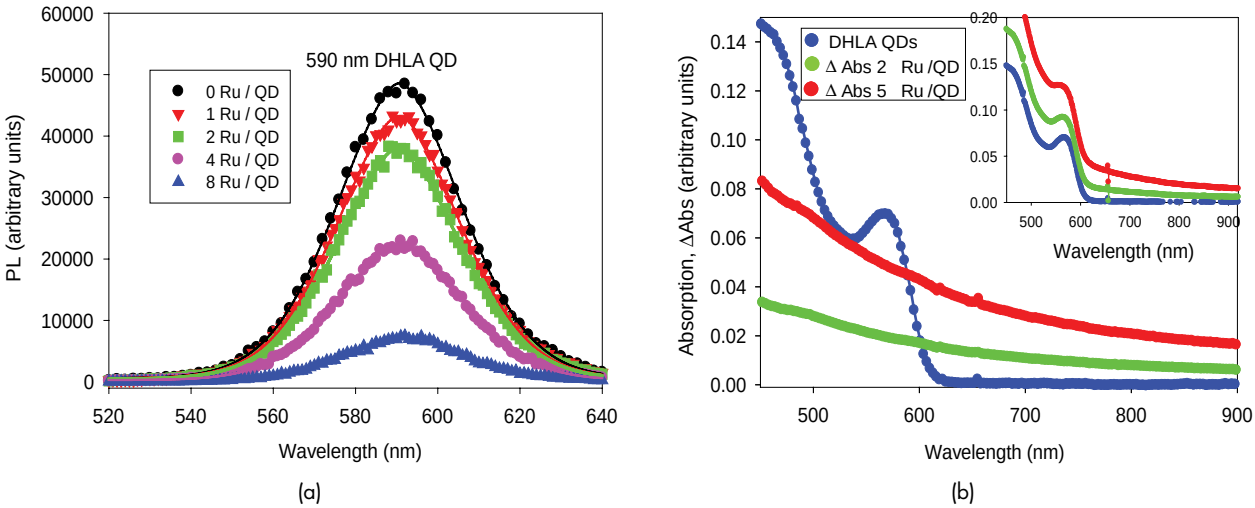

FIGURE 3
(a) Photoluminescence spectra collected from solutions of DHLA-capped QDs at increasing Ru complex-to-QD ratio. (b) Effects of redox coupling on the QD absorption profile. Plots of QD absorption together with differential absorption (ΔAbs) spectra for DHLA QDs self-assembled with increasing number of Ru-peptides. Inset shows the raw absorption data.

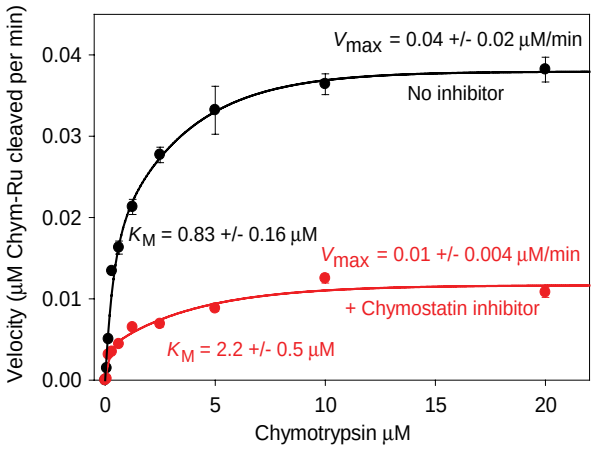

FIGURE 4
Enzymatic assay of chymotrypsin activity utilizing QD–Ru peptide conjugates, showing enzymatic velocity versus increasing chymotrypsin concentration in the presence and absence of a specific chymostatin inhibitor. The changes in kinetic parameters (higher Michaelis constant K_M and lower maximal velocity V_{max}) are characteristic of a mixed inhibition process.

We find that charge transfer and quenching are highly dependent on the relative position of the oxidation levels of QDs and metal complex used; they are also directly responsive to the controlled number of metal complexes brought in close proximity to the nanocrystal surface. The ability to control the number of metal complexes is not something easily achievable with other experimental approaches such as spin-coating or layer-by-layer assembly. Exploiting the underlying PL quenching processes allowed us to demonstrate specific enzymatic sensors. This approach highlights NRL's unique capability to combine an understanding of nanoscale materials and biological functionalities to create new hybrid bio-inorganic sensors. These results strongly suggest that other QD charge transfer configurations may be viable and will allow similar architectures to be designed for a variety of nanoscale roles of direct relevance to the Navy, including sensing, catalysis, and energy harvesting.

Acknowledgments: The authors thank Phil Dawson and Juan B. Blanco-Canosa of the Scripps Research Institute for assistance with peptides. The authors acknowledge the Defense Threat Reduction Agency (DTRA) and the NRL Institute for Nanoscience for financial support.

[Sponsored by NRL and DTRA-ARO]

References

[1] I.L. Medintz, H.T. Uyeda, E.R. Goldman, and H. Mattoussi, "Quantum Dot Bioconjugates for Imaging, Labeling and Sensing," *Nature Materials* **4**, 435–446 (2005).

[2] I.L. Medintz, T. Pons, S. Trammell, A. Grimes, D. English, J. Blanco-Canosa, P. Dawson, and H. Mattoussi, "Interactions Between Redox Complexes and Semiconductor Quantum Dots Coupled via a Peptide Bridge," *J. Am. Chem. Soc.* **130**, 16745–16756 (2008).

[3] K. Susumu, H.T. Uyeda, I.L. Medintz, T. Pons, J.B. Delehanty, and H. Mattoussi, "Enhancing the Stability and Biological Functionalities of Quantum Dots via Compact Multifunctional Ligands, *J. Am. Chem. Soc.* **129**, 13987–13996 (2007).

Making the Most of a Scarce Metal

C.N. Chervin, A.M. Lubers, J.W. Long, and D.R. Rolison
Chemistry Division

Introduction: Precious indeed are the platinum-group metals (PGMs): ruthenium, Ru; rhodium, Rh; palladium, Pd; osmium, Os; iridium, Ir; and platinum, Pt. The earthly scarcity and concomitant cost of PGMs have always tempered their adoption in the vast array of strategic and commercial technologies in which their inclusion would yield improved performance. We can now attain the impressive electronic and electrochemical properties of ruthenium oxide — high electronic conductivity, high capacitive charge storage for pulse power, and fast electron transfer for catalysis, analysis, or sensing — by distributing modest amounts of the material onto dirt-cheap, insulating substrates, namely paper made of silica fibers.

In the pursuit of a robust, flexible, and inexpensive electronic and catalytic substrate, we adapted our prior protocol for depositing 4-nanometer-high webs of ruthenium dioxide (RuO_2) throughout the interior of silica (SiO_2) nanoarchitectures.[1] Now, in place of specialty porous silica, commercially available silica filter paper is soaked in chilled solutions of RuO_4 in petroleum ether; the RuO_4 decomposes to RuO_2 as the solution warms to room temperature. The initially white silica membrane turns black as nanoscale RuO_2 nucleates on the fibers (Fig. 5(a)). The macroporous voids between the fibers (hundreds of nanometers to several micrometers between the submicron- to micron-diameter silica fibers, Fig. 5(b)) offer ample headspace for deposition of nanoscopic RuO_2 while retaining facile perfusion of fluids through the membrane. The time for equilibration and RuO_2 deposition is less than one day and is carried out in ambient atmosphere without specialized reactors.

Improved Properties on the Nanoscale: The resistance of the as-prepared $RuO_2||SiO_2$ composite decreases by four orders of magnitude upon heating in flowing oxygen to 200 °C. The marked increase in conductivity arises because the disordered, as-deposited oxide nanoparticles convert into a nanoscopic skin (Fig. 5(c)) of the more conductive, crystalline rutile form. The four-point probe-derived conductivity of the calcined $RuO_2||SiO_2$ nanocomposite is 0.5 S cm^{-1} at room temperature in air with only ~300 μg cm^{-2} of RuO_2 per geometric area of silica paper.[2]

The $RuO_2||SiO_2$ fiber membranes express an electrochemical surface area of ~90 m^2 g^{-1} (RuO_2), exhibit a thermopower consistent with metallic RuO_2, and support fast electron-transfer reactions in aqueous and nonaqueous electrolytes. The $RuO_2||SiO_2$ composite retains the mechanical attributes of the SiO_2 membrane, which is flexible, has a degree of compressibility (softness), and can be easily molded through pressure to form quality interfacial contact with uneven surfaces. All of these are important attributes in fabricat-

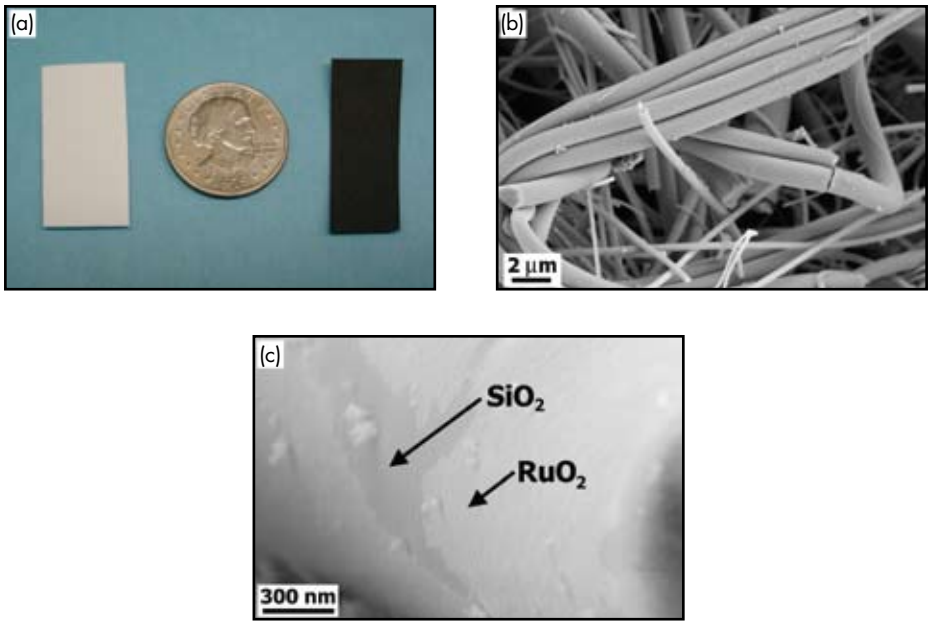

FIGURE 5
The morphology of RuO_2 nanoskins on SiO_2 fiber paper. (a) SiO_2 paper before (white) and after sub-ambient temperature deposition of RuO_2 (black). (b-c) Scanning electron micrographs of a 200 °C-calcined $RuO_2||SiO_2$ composite: the morphology of the paper is unaltered by RuO_2 deposition, which forms a through-connected nanoscale shell on the membrane fibers leaving only small islands of uncoated SiO_2.

ing practical devices that incorporate these conductive papers.

This inexpensive, practical manifestation on the macroscale of a metallic-like conductor on the nanoscale is accomplished at low ruthenia mass loadings (~5 weight %) and volume fraction (<0.1 volume %), thereby maximizing the utilization of this expensive platinum-group metal; the 2009 cost of materials runs less than $0.20 USD per square centimeter of conductive composite. The conductivity we report is normalized using the geometric dimensions of the insulating silica paper, and so does not completely express the remarkable behavior of the conductive nanoskin. Contrast the density-normalized conductivity of RuO_2 in three forms:

Form of RuO_2	Density-normalized electronic conductivity S cm^2 mg^{-1}
RuO_2||SiO_2 paper, calcined at 200 °C	50
Pressed pellet of RuO_2 powder harvested from the subambient synthesis, calcined at 200 °C	14
Polycrystalline RuO_2	12

Expressing the same oxide as a nanoskin wrapped contiguously around a curved dielectric imparts a fourfold enhancement in the electron conductivity.

The 2- to 3-nanometer-thick coatings of RuO_2 that cover the convex walls of the silica fibers also exhibit atypically high specific capacitance for electron–proton charge storage — five times that — at crystalline RuO_2. In acidic electrolyte, 90% of the total electron–proton charge is stored at the outer surface of the ruthenia phase in the RuO_2||SiO_2 fiber membranes.[2] In a 2-nanometer spherical particle of rutile RuO_2, more than 90% of the crystalline subunits are expressed at the surface of the particle. The electrochemical capacitive response we obtain indicates that the nanocrystalline RuO_2 shell can be considered to be equivalent to a single oxide layer stabilized by the supporting silica fiber. In analogy with graphene,[3] the ruthenia nanoskin on the silica fiber paper acts as an exfoliated layer of the conductor.

Future Applications: The ever-increasing energy and power demands of Navy and Marine Corps missions will require advancements in such portable power technologies as fuel cells. All of the features discussed above, including the ease and low expense of the synthesis, make this new electrode structure a prime candidate as an electron–proton conductive, gas-diffusion electrode in which neither carbon nor ionomer will be required to form a fuel-cell electrode. We have preliminary evidence that Pt nanoparticles are readily electrolessly deposited only at the ruthenia nanoshell of the RuO_2||SiO_2 membrane, as seen in Fig. 6. This advanced electrode structure wires protons and electrons along the electrically conductive nanoshell of RuO_2 and thereby removes two limiting components in fuel-cell electrodes: (i) carbon to support the metal electrocatalytic nanoparticles and provide an electron path through the electrode structure; and (ii) ionomer to transport protons to the proton-conducting solid membrane (e.g., Nafion™) that physically separates the anode from the cathode. The weight loadings of Pt should easily reach ≤100 μg cm^{-2} for such paper-based electrode architectures, which would meet future Department of Energy targets for hydrogen-fed fuel cells.

[Sponsored by ONR]

References

[1] J.V. Ryan, A.D. Berry, M.L. Anderson, J.W. Long, R.M. Stroud, V.M. Cepak, V.M. Browning, C.I. Merzbacher, and D.R. Rolison, "Electronic Connection to the Interior of a Mesoporous Insulator with Nanowires of Crystalline RuO_2," *Nature* **406**, 169–172 (2000).

[2] C.N. Chervin, A.M. Lubers, K.A. Pettigrew, J.W. Long, M.A. Westgate, J.J. Fontanella, and D.R. Rolison, "Making the Most of a Scarce Platinum-group Metal: Conductive Ruthenia Nanoskins on Insulating Silica Filter Paper," *Nano Lett.* **9**(6), 2316–2321 (2009).

[3] Q.-H. Yang, W. Lu, Y.-G. Yang, and M.-Z. Wang, "Free Two-dimensional Carbon Crystal—Single-layer Graphene," *New Carbon Mater.* **23**, 97–103 (2008).

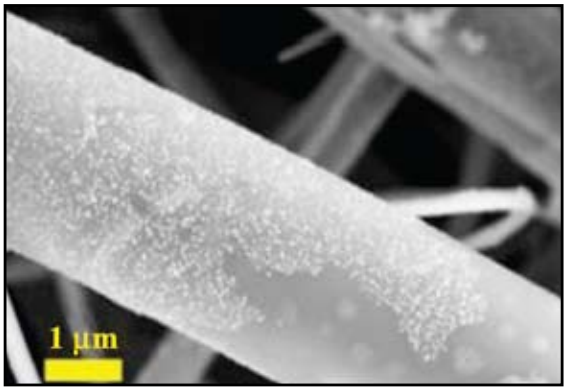

FIGURE 6
Scanning electron micrograph of a 200 °C-calcined RuO_2||SiO_2 fiber membrane after electroless deposition of Pt from a 2 mM H_2PtCl_6 solution in 0.5 M H_2SO_4. The Pt ions reduce at the electrified RuO_2 coating, forming nanoparticles associated with the through-networked nanoskin without forming electrically unaddressable Pt on bare SiO_2.

Optical Pulse Control of Electron and Nuclear Spins in Quantum Dots

S. Carter,[1] S. Economou,[1] A. Shabaev,[2] T. Kennedy,[1] A. Bracker,[1] and T. Reinecke[1]
[1]*Electronics Science and Technology Division*
[2]*George Mason University*

Introduction: Quantum information has the potential to revolutionize secure communications and computation, both important to the Department of Defense. The unique properties of quantum bits (qubits, units of quantum information) and the phenomenon of entanglement (non-local, non-classical correlation) prevent eavesdropping over quantum communication channels and enable the solving of problems that grow exponentially difficult with classical computation, including decryption of codes with long encryption keys.

Electron spins in quantum dots (QDs) are being widely investigated as qubits for storage and processing of quantum information, with the two different directions of the spin, up or down, forming the two states of the qubit. NRL is a leader in developing semiconductor QDs for quantum information, both in materials development and in probing the quantum nature of these nanometer-scale structures. Controlling the spin in these QDs, including increasing the spin coherence time, is a key area of NRL research. The electron spin coherence time in a QD, or lifetime of the qubit, can be at least microseconds, but the coherence is easily masked by the many (10^4 – 10^5) randomly oriented nuclear spins that also exist in the QD (see Fig. 7(a)). The net nuclear spin acts as a temporally fluctuating magnetic field that randomizes the phase of the electron spin qubit. We use a train of picosecond laser pulses at wavelengths near an electronic QD transition to manipulate the electron spin polarization and thereby control the nuclear spin polarization. This technique can be used to extend the electron spin coherence time in QDs, making this system more attractive for quantum information applications.

Optical Spin Control: The primary effect of the laser pulses is to partially orient electron spins along the optical axis (z-direction in Fig. 7(a)). The spins then precess about a field composed of a perpendicular applied magnetic field of 3 T and the net nuclear spin field. This precession is observed for an ensemble of QDs at ~4 K (Fig. 7(b)) using time-resolved Faraday ellipticity (TRFE), which measures the electron spin projection along the optical axis as a function of time. The oscillations decay within a few hundred picoseconds due to inhomogeneity in the spin precession frequencies. The signal at negative delays is due to spins that precess with a frequency synchronized to a multiple of the laser pulse repetition rate (~81 MHz). Synchronized spins are efficiently polarized due to constructive interference over many pulses, while non-synchronized spins are not efficiently polarized. This phenomenon is known as spin mode-locking, and the associated nuclear dynamics have been previ-

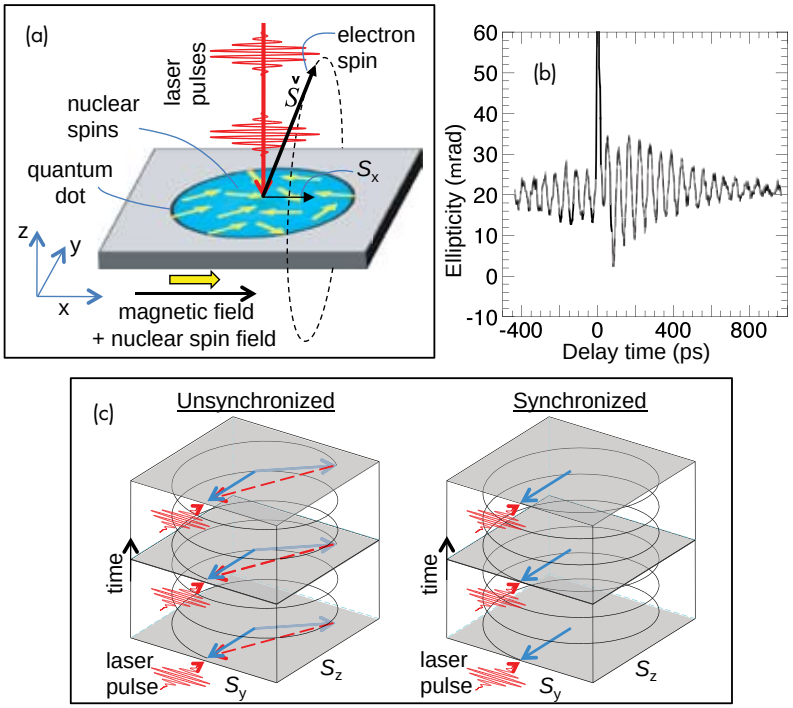

FIGURE 7
(a) Illustration of a quantum dot illuminated by a pulse train, showing nuclear spins (yellow) and the precessing electron spin. (b) Time-resolved Faraday ellipticity signal for an ensemble of QDs. (c) Illustration of electron spin precession for synchronized and unsynchronized spins. The unsynchronized spin polarization is ~2.5 times smaller than shown here. Red dashed arrows indicate the jump in the unsynchronized spin polarization from before a laser pulse (faint blue arrows) to after a laser pulse (blue arrows).

ously explored for laser wavelengths resonant with the QD transition.[1,2] With the laser detuned from the QD transition, we find that a significant non-precessing spin component S_x is generated along the magnetic field axis, with the direction determined by the sign of detuning.

The nuclear spin dynamics depend on electron spin synchronization to the pulse train and the value of S_x. For an unsynchronized electron spin, the spin vector will suddenly jump each time a pulse hits (see Fig. 7(c)). These sudden jumps are likely to induce nuclear spin flips due to the hyperfine interaction. The direction of the nuclear spin flips is random for $S_x = 0$, but is directional for nonzero S_x. The nuclear spin flips change the electron spin precession frequency and can either push electron spins toward synchronization or away from it. The amplitude of the TRFE is a measure of how well the nuclear spins synchronize electron spins to the pulse train. Figure 8(a) displays the TRFE amplitude vs. QD detuning from the laser (δ_{QD}) for a series of pump intensities. At low intensities, for which the nuclear effects should be small, the amplitude is nearly symmetric about zero detuning, and it decays with detuning due to decreased coupling to the laser. At higher intensities there is a shift toward negative detunings due to increased spin synchronization for negatively detuned QDs. Theoretical calculations confirm this behavior (Fig. 8(b)), indicating that electron spins are pushed toward synchronization for negatively detuned QDs and away from synchronization for positively detuned QDs. The difference is due to the changing sign of S_x. This result is further illustrated in Fig. 8(c), which displays the calculated probability distribution of the nuclear polarization for positive, negative, and zero detuning.

Conclusions: We have demonstrated that the direction of nuclear spin flips can be controlled with the detuning of an optical pulse train. This allows us to control the nuclear polarization and fix it at a precise value determined by the repetition rate of the laser. A fixed nuclear polarization will increase the coherence time of electron spin qubits and allow better control of the spin precession frequency. Precise nuclear control also suggests using nuclear spins, which have very long spin coherence times, to store quantum information.

[Sponsored by ONR]

References

[1] A. Greilich, D.R. Yakovlev, A. Shabaev, A.L. Efros, I.A. Yugova, R. Oulton, V. Stavarache, D. Reuter, A. Wieck, and M. Bayer, "Mode Locking of Electron Spin Coherences in Singly Charged Quantum Dots," *Science* **313**, 341–345 (2006).

[2] A. Greilich, A. Shabaev, D.R. Yakovlev, A.L. Efros, I.A. Yugova, D. Reuter, A.D. Wieck, and M. Bayer, "Nuclei-Induced Frequency Focusing of Electron Spin Coherence," *Science* **317**, 1896–1899 (2007).

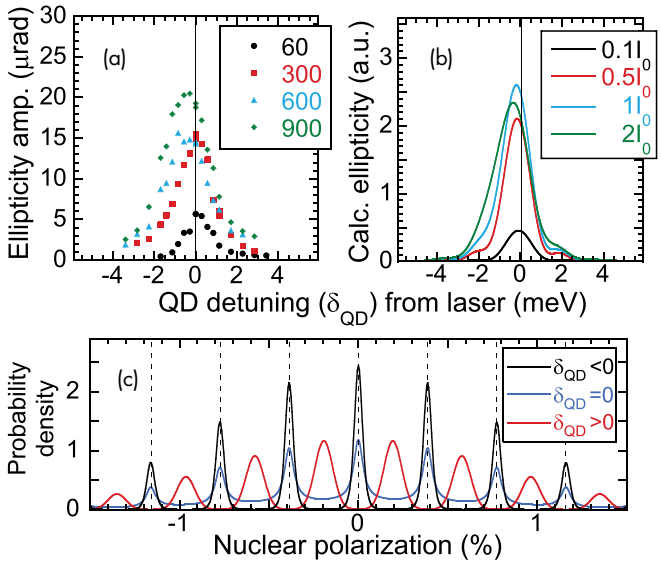

FIGURE 8
(a) Oscillation amplitude of TRFE vs QD detuning for a series of pulse intensities (in W/cm^2). (b) Calculated ellipticity vs QD detuning for a series of pulse intensities. (c) Calculated probability distribution of the nuclear polarization for three QD detunings: –0.8, 0, and +0.8 meV. Vertical dashed lines mark the nuclear polarizations that synchronize spin precession.

ocean science and technology

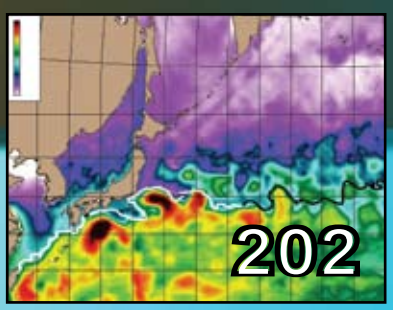

199
A Thinning Arctic Ice Cap as Simulated by the Polar Ice Prediction System (PIPS): 2000–2008
P.G. Posey, R.H. Preller, L.F. Smedstad, and C.N. Barron

202
Predicting “Ocean Weather” Using the HYbrid Coordinate Ocean Model (HYCOM)
E.J. Metzger, H.E. Hurlburt, A.J. Wallcraft, O.M. Smedstad, J.A. Cummings, and E.P. Chassignet

206
Littoral Battlespace Characterization Using Small Unmanned Aerial Systems
K.T. Holland, D. Lalejini, and K. Plavnick

208
The Environmental Post-Mission Analysis System: Through-The-Sensor to the Warfighter
B.Y. Lin, S.A. Myrick, W.E. Avera, and M.M. Harris

A Thinning Arctic Ice Cap as Simulated by the Polar Ice Prediction System (PIPS): 2000–2008

P.G. Posey, R.H. Preller, L.F. Smedstad, and C.N. Barron
Oceanography Division

Introduction: Even though the Arctic is one of the most hostile operational environments in the world, numerous vessels transit the Arctic regularly in summer when coastal melting opens the shortest connection between much of the North Atlantic and North Pacific. Free drifting icebergs, 24-hour seasonal darkness, sub-zero temperatures, and a lack of dependable logistical support can make Arctic operations extremely challenging for ships, aircraft, and submarines. Accurate forecasts of changing ice conditions can be applied to anticipate changing conditions and mitigate operational challenges. Applications of the second- and third-generation Polar Ice Prediction System (PIPS) are used to model and diagnose continuing thinning of Arctic ice and larger summertime ice-free areas. A significant decrease in overall ice cover has been observed in relation to the anticipated median ice extent. In 2007, the summer minimum sea ice extent in the Arctic was 40% below the minimum sea ice extents of the 1980s and more than 20% below the previous record minimum of 2005. Forecasts from the second-generation ice prediction system, PIPS 2.0, agree well with documented observations concerning the current diminishing ice cap (Fig. 1).

Current Forecasting Capabilities: The Naval Research Laboratory (NRL) is continuing to develop increasingly capable ice forecast systems tailored to fit the needs of their Navy customers. PIPS 2.0 has been producing operational Arctic forecasts for the Navy since 1996. PIPS 2.0 couples the Hibler dynamic/thermodynamic ice model[1] to the Bryan and Cox ocean model[2] to cover all sea ice areas in the northern hemisphere. The model uses a rotated 0.28° spherical coordinate system to avoid the problem of a numerical singularity at the pole, such that grid spacing varies from 17 to 33 km over the domain. PIPS 2.0 provides operational 72-hour forecasts of ice drift, ice thickness, and ice concentration to the National Ice Center (NIC).

PIPS Results 2000 to 2008: Evaluation of PIPS 2.0 forecasts from 2000 to 2008 reveal a slow overall decrease in Arctic ice with a minimum during the summers of 2007 and 2008. This decrease is occurring both in area of ice coverage and total ice volume. For example, in the central Arctic, ice exhibits a seasonal cycle with minimum volume in September. PIPS 2.0 indicates that this annual minimum in ice volume has undergone a 35% loss from 0.59×10^9 m^3 in 2000 to a low of 0.38×10^9 m^3 in 2008 (Table 1). A similar decreasing pattern also occurs in both the western and eastern Arctic regions during the same time period. PIPS 2.0 monthly ice thickness fields from September (Fig. 2) show how "ice free" the coastal regions have become each summer during the past few years (2007–2008) and how the overall pattern of ice thickness varies. Since open ocean areas absorb more solar heating than ice covered areas, the reduction of ice extent in the summer creates an overall warmer ocean that slows winter regrowth of the ice cover. This leads to thinner wintertime ice and decreases in overall ice volume during the yearly cycle as periods of cooling are not able to restore ice thickness to previously observed levels. Even though extremely low temperatures in the northern hemisphere during the winter of 2007 helped to increase the ice area visible from satellite data to a more "normal" level, especially along the northern Greenland coast, the overall Arctic ice volume was lower in 2008 due to thinner ice than in past years.

Future Capabilities in Ice Forecasting: Sufficient measurements of sea ice conditions, effective assimilation of these observations, and thorough evaluation of forecast skill and error trends are critical to improving the quality of operational models and forecasts. In continuing efforts to provide state-of-the-art capabilities for ice forecasts, NRL has developed the next-generation operational ice forecast system, PIPS 3.0. This new capability couples the Los Alamos Sea Ice Model (CICE)[3] to the global Navy Coastal Ocean Model (NCOM),[4] taking advantage of developments in modeling and assimilation over the last ten years to predict ice conditions, ice currents, temperature, and salinity at a higher resolution (5–9 km in the Arctic) and with greater accuracy. PIPS 3.0 is now producing daily 48-hour forecasts at the Naval Oceanographic Office (NAVOCEANO) and will have competed its validation tests by mid-2009.

Conclusions: The Arctic has been and will continue to be a region of strategic and operational interest. The dramatic changes seen during the last decade impact the traversal of the region by introducing changing conditions expected to increase shipping activity and thereby increase overall operational risks. A history of nowcasts and forecasts from the operational ice prediction systems developed by NRL can be used to construct a baseline of ice conditions, cycles, and trends to enable more robust assessment of the extent and environmental impacts of Arctic ice changes. As higher-resolution forecast systems are developed, more accurate and detailed forecasts will

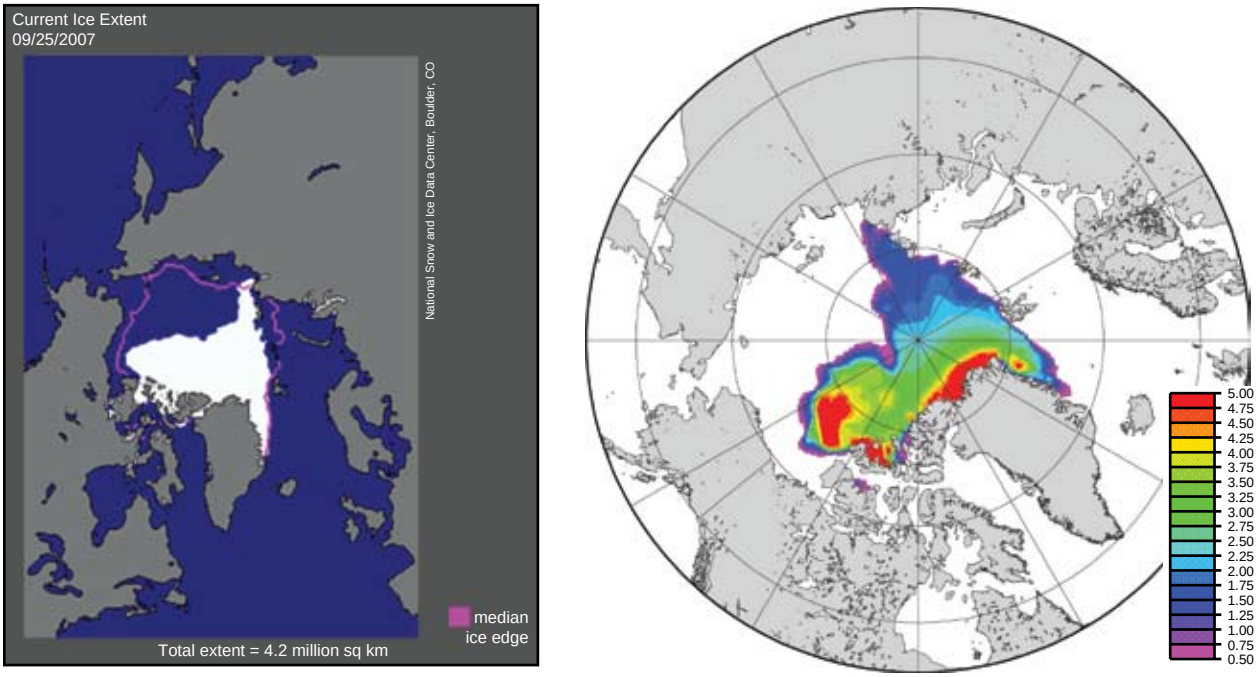

(a) (b)

FIGURE 1
(a) September 2007 Arctic sea ice extent (white), compared to the September median ice extent (pink line) calculated from 1979 to 2000 (Source: National Snow and Ice Data Center) compared to (b) the PIPS 2.0 monthly mean September ice thickness (m) for 2007.

TABLE 1 — PIPS 2.0 Yearly Maximum and Minimum Values of Total Ice Volume for the Central Arctic

Total Central Arctic Ice Volume $\times 10^9$ m^3				
	Maximum		Minimum	
Year	Month	Value	Month	Value
2000	May	0.90	Sep	0.59
2001	May	0.93	Sep	0.69
2002	May	0.99	Sep	0.75
2003	Apr	0.95	Sep	0.58
2004	May	0.91	Sep	0.58
2005	Apr	0.93	Sep	0.62
2006	May	0.85	Sep	0.52
2007	May	0.86	Sep	0.49
2008	Mar	0.67	Sep	0.38

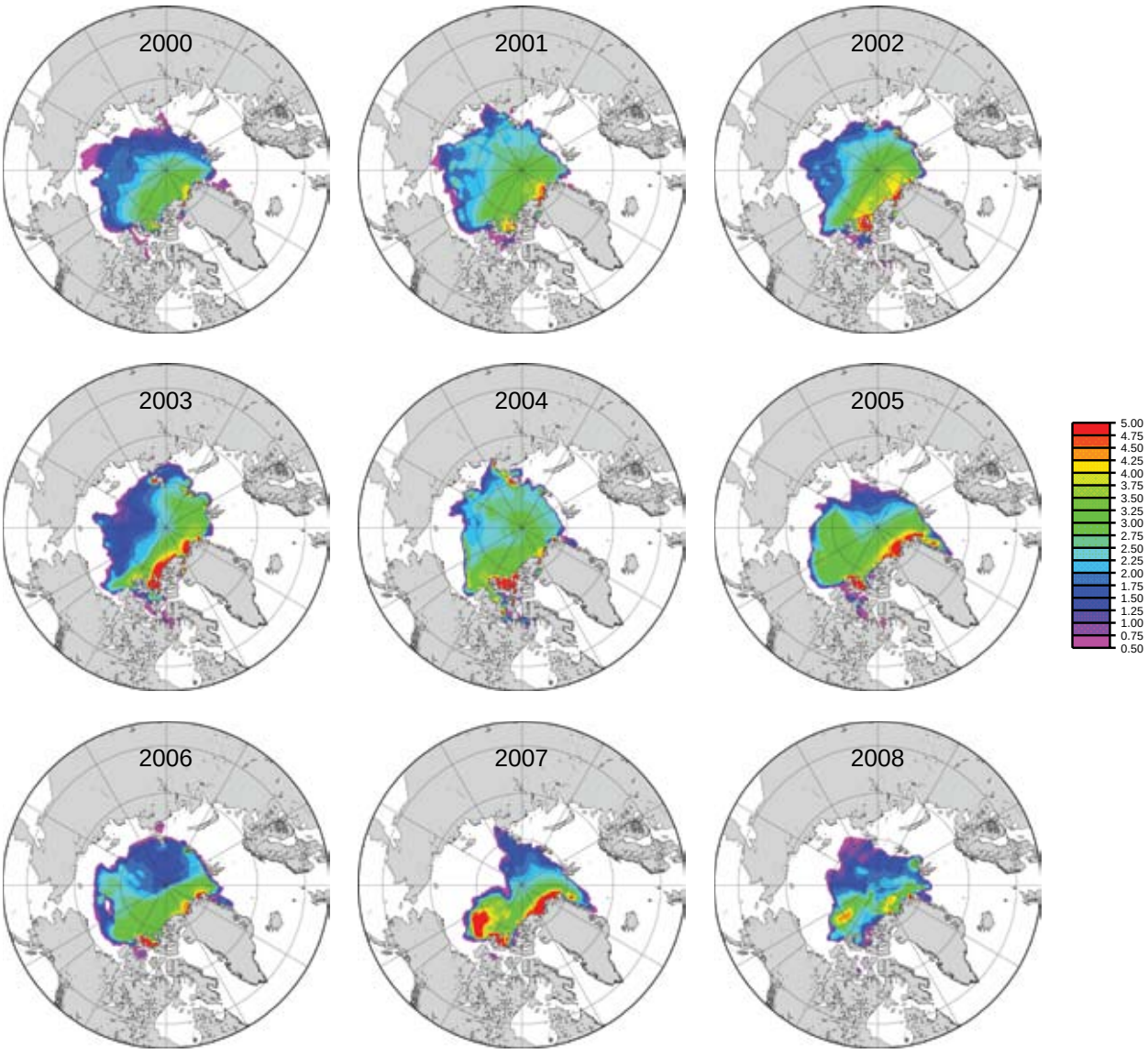

FIGURE 2
PIPS 2.0 September monthly mean ice thickness (m) from 2000 to 2008.

become available for use in predicting, understanding, and adapting to changing Arctic ice conditions.

Acknowledgments: The authors would like to thank Mr. Michael Phelps of Jacobs Engineering for archiving and plotting the ice forecast products. For historical PIPS 2.0 model forecasts see http://www730/pips2. This work is made possible through the support of the Office of Naval Research.

[Sponsored by ONR]

References

[1] W.D. Hibler, "A Dynamic Thermodynamic Sea Ice Model," *J. Phys. Oceanogr.* **9**, 815–864 (1979).

[2] M.D. Cox, "A Primitive Equation, 3-Dimensional Model of the Ocean," Geophysical Fluid Dynamics Laboratory Ocean Group Technical Report No. 1 (Princeton, NJ, 1984).

[3] E.C. Hunke and J.K. Dukowicz, "An Elastic-Viscous-Plastic Model for Sea Ice Dynamics," *J. Phys. Oceanogr.* **27**, 1849–1867 (1997).

[4] C.N. Barron, A.B. Kara, P.J. Martin, R.C. Rhodes, and L.F. Smedstad, "Formulation, Implementation and Examination of Vertical Coordinate Choices in the Global Navy Coastal Ocean Model (NCOM)," *Ocean Modelling* **11**(3-4), 347–375 (2006), doi:10.1016/j.ocenmod.2005.01.004.

Predicting "Ocean Weather" Using the HYbrid Coordinate Ocean Model (HYCOM)

E.J. Metzger,[1] H.E. Hurlburt,[1] A.J. Wallcraft,[1] O.M. Smedstad,[2] J.A. Cummings,[1] and E.P. Chassignet[3]
[1]*Oceanography Division*
[2]*QinetIQ North America/Planning Systems, Inc.*
[3]*Florida State University*

Introduction: Development of an advanced global ocean prediction system has been a long-term Navy interest. Such a system must provide the capability to depict (nowcast) and predict (forecast) the oceanic "weather," some components of which include the 3D temperature, salinity, and current structure, the surface mixed layer, and the location of mesoscale features such as eddies, meandering currents, and fronts. The space scale of these eddies and meandering currents are typically ~100 km and current speeds can easily exceed 1 ms^{-1} in the Gulf Stream (Atlantic) and Kuroshio (Pacific). Numerical ocean models with sufficiently high horizontal and vertical resolution are needed to depict the 3D structure with accuracy superior to climatology and/or persistence (i.e., a forecast of no change). The existing two-model operational system, run daily at the Naval Oceanographic Office (NAVOCEANO), is based on the 1/32° Navy Layered Ocean Model (NLOM) and the 1/8° Navy Coastal Ocean Model (NCOM). Unlike NLOM, NCOM has high vertical resolution, but it has medium range horizontal resolution (15 km at mid-latitudes near 40°N) that is eddy-permitting. The next-generation system is based on a single model, the HYbrid Coordinate Ocean Model (HYCOM), that was developed as part of a multi-institutional consortium between academia, government, and private industry. At 2.2 times the horizontal resolution of NCOM, the HYCOM system is eddy-resolving, a distinction associated with important dynamical implications for both ocean model dynamical interpolation skill in the assimilation of ocean data and for ocean model forecast skill.[1] It represents the world's first eddy-resolving global ocean prediction system with both high horizontal and high vertical resolution and has been running daily in the operational queues at NAVOCEANO since 22 December 2006. The HYCOM system has been validated against observational data[2] and is scheduled for operational testing in 2009.

Prediction System Description: The ocean component of the nowcast/forecast system is 1/12° global HYCOM (mid-latitude resolution of ~7 km) with 32 hybrid vertical coordinate surfaces. The truly generalized vertical coordinate can be isopycnal (density tracking — often best in the deep stratified ocean), levels of equal pressure (nearly fixed depths — best used in the mixed layer and unstratified ocean), or sigma-levels (terrain-following — often the best choice in shallow water). HYCOM combines all three approaches by choosing the optimal distribution at every grid point and time step. The hybrid coordinate extends the geographic range of applicability of traditional isopycnic coordinate models toward shallow coastal seas and unstratified parts of the world ocean. It maintains the significant advantages of an isopycnal model in stratified regions while allowing more vertical resolution near the surface and in shallow coastal areas, hence providing a better representation of the upper ocean physics.

HYCOM employs the Navy Coupled Ocean Data Assimilation (NCODA), which is a fully 3D multivariate optimum interpolation scheme, to assimilate observational data. The data include surface observations from satellites, such as altimeter sea surface height (SSH) anomalies, sea surface temperature (SST), and sea ice concentration, plus in situ SST observations from ships and buoys and temperature and salinity profile data from XBTs, CTDs, and Argo floats. The 3D ocean environment can be more accurately nowcast and forecast by combining these diverse observational data types via data assimilation and using the dynamical interpolation skill of the model.

Real-time Results: Where possible, the real-time system is evaluated using independent observations; some examples follow. Figure 3 shows simulated SSH

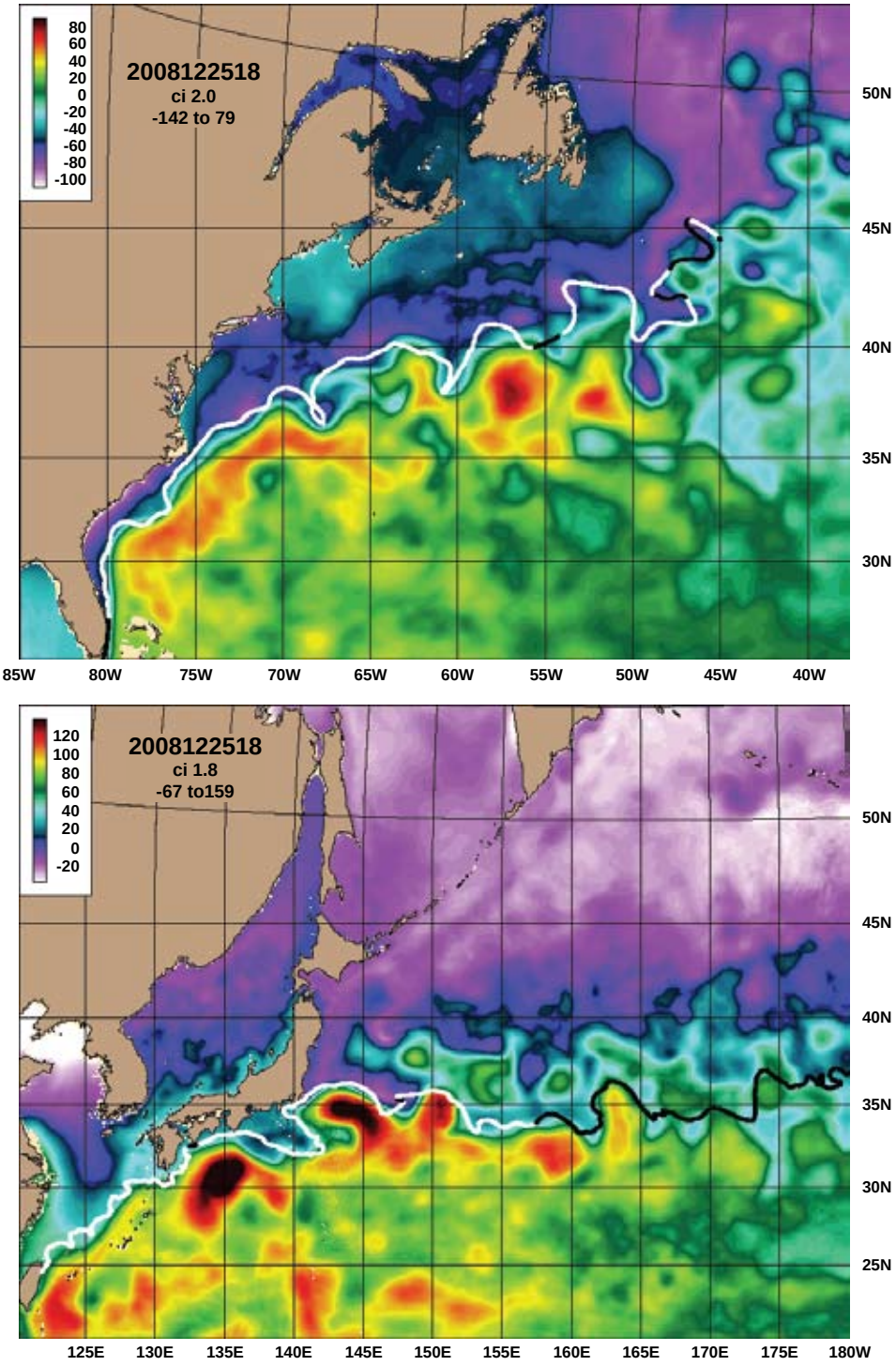

FIGURE 3
Sea surface height (cm) from the 1/12° global HYCOM/NCODA forecast system for the Gulf Stream in the Atlantic Ocean (top) and the Kuroshio in the Pacific Ocean (bottom) on 22 December 2008. The ribbon of high gradient color shows the location of these western boundary currents; embedded within the meandering flow are warm and cold core eddies. The currents generally flow parallel to the isolines of height and are strongest where the gradients are the tightest. An independent infrared (IR) analysis of the north edge of both current systems performed by the Naval Oceanographic Office is overlain on each image. A white (black) line means the IR analysis is based on data less (more) than four days old.

for the Gulf Stream and the Kuroshio current systems. The assimilation of satellite altimeter SSH anomalies is essential to accurately map the circulation in these highly chaotic regions dominated by flow instabilities. Infrared-based frontal analyses showing the northernmost edge of the currents are overlain on the images. They provide an independent analysis of the current positions and clearly indicate the ocean nowcast/forecast system is accurately mapping these western boundary currents.

Figure 4 shows an example that uses drifting buoy trajectories to validate the flow field in the Kuroshio. Drifting buoy temperature (but not velocity) is assimilated into the system, allowing the trajectory to be an independent validation source. The white box focuses on a warm core eddy about to detach from the Kuroshio, and a pair of drifting buoys is noted on the western and eastern sides. These two drifters pass within a half degree of each other while traveling in opposite directions. Close examination indicates the two buoys are on opposite sides of a saddle point that still connects the main current with the detaching eddy. Thus, the system is able to accurately assimilate the altimeter data and act as a dynamical interpolator.

SST forecast skill of the system is examined in Table 2. Shown are the mean error (bias), root-mean-square-error (RMSE), skill score (a non-dimensional quantity with perfect skill having a value of 1), and correlation as a function of forecast length. The bias and RMSE gradually grow with forecast length. The spatial distribution of the mean error is shown in Fig. 5 for the analysis time and for a 3-day forecast. The

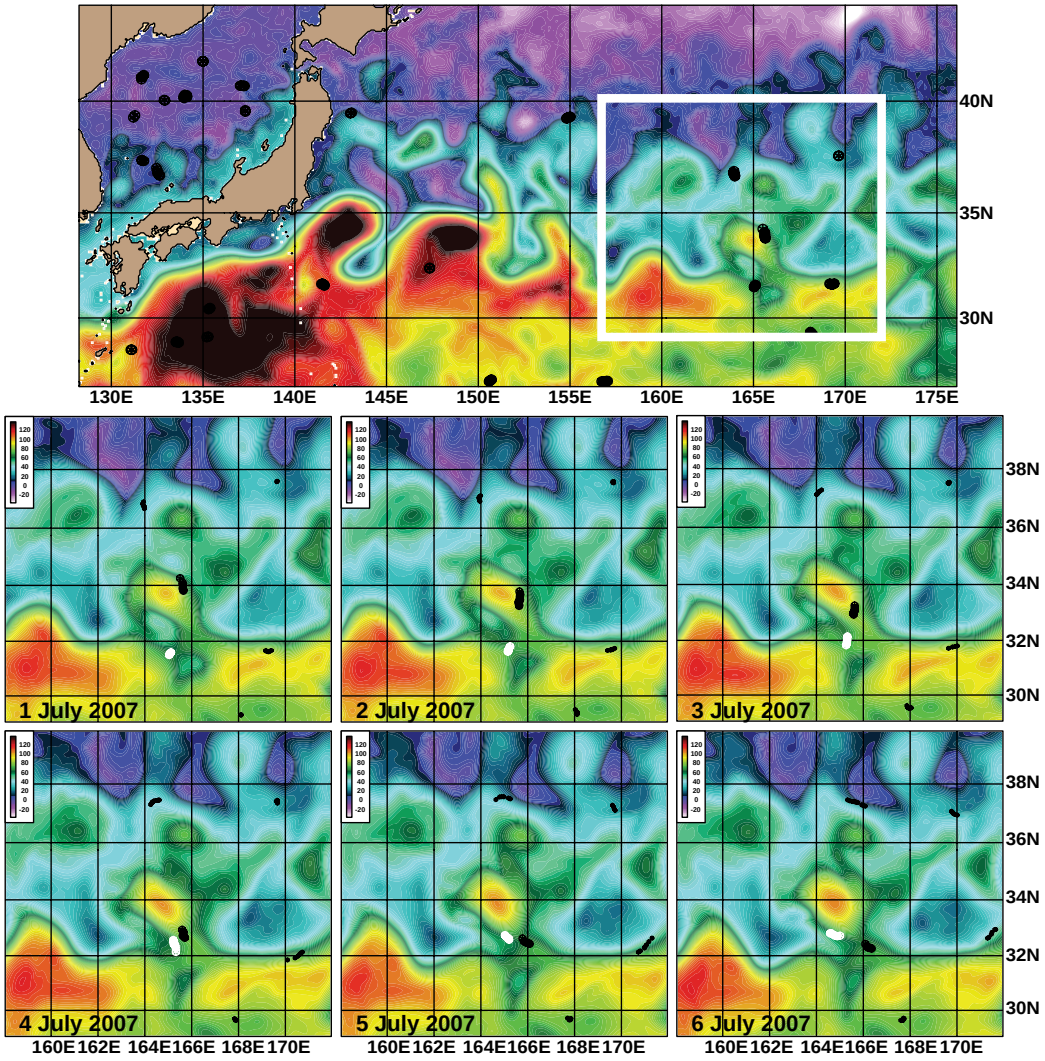

FIGURE 4
Sea surface height (cm) from the 1/12° global HYCOM/NCODA forecast system for the Kuroshio on 1 July 2007 (top). Drifting buoy tracks over a 1-day time period are overlain on each panel. The white box defines the focused area of the bottom six panels that span the time frame 1–6 July 2007. A warm core eddy is about to detach from the Kuroshio, and two drifting buoys (highlighted in white and black) are traversing its western and eastern sides.

TABLE 2 — SST Error Statistics vs ~33,000,000 MCSST Observations; Analysis Between 45°S and 45°N

	Mean Error	RMSE	Skill Score	Correlation
Analysis	-.02	.36	.99	1.0
1-day forecast	-.09	.44	.99	1.0
2-day forecast	-.14	.52	.99	.99
3-day forecast	-.18	.60	.98	.99
4-day forecast	-.22	.67	.98	.99
5-day forecast	-.26	.72	.98	.99

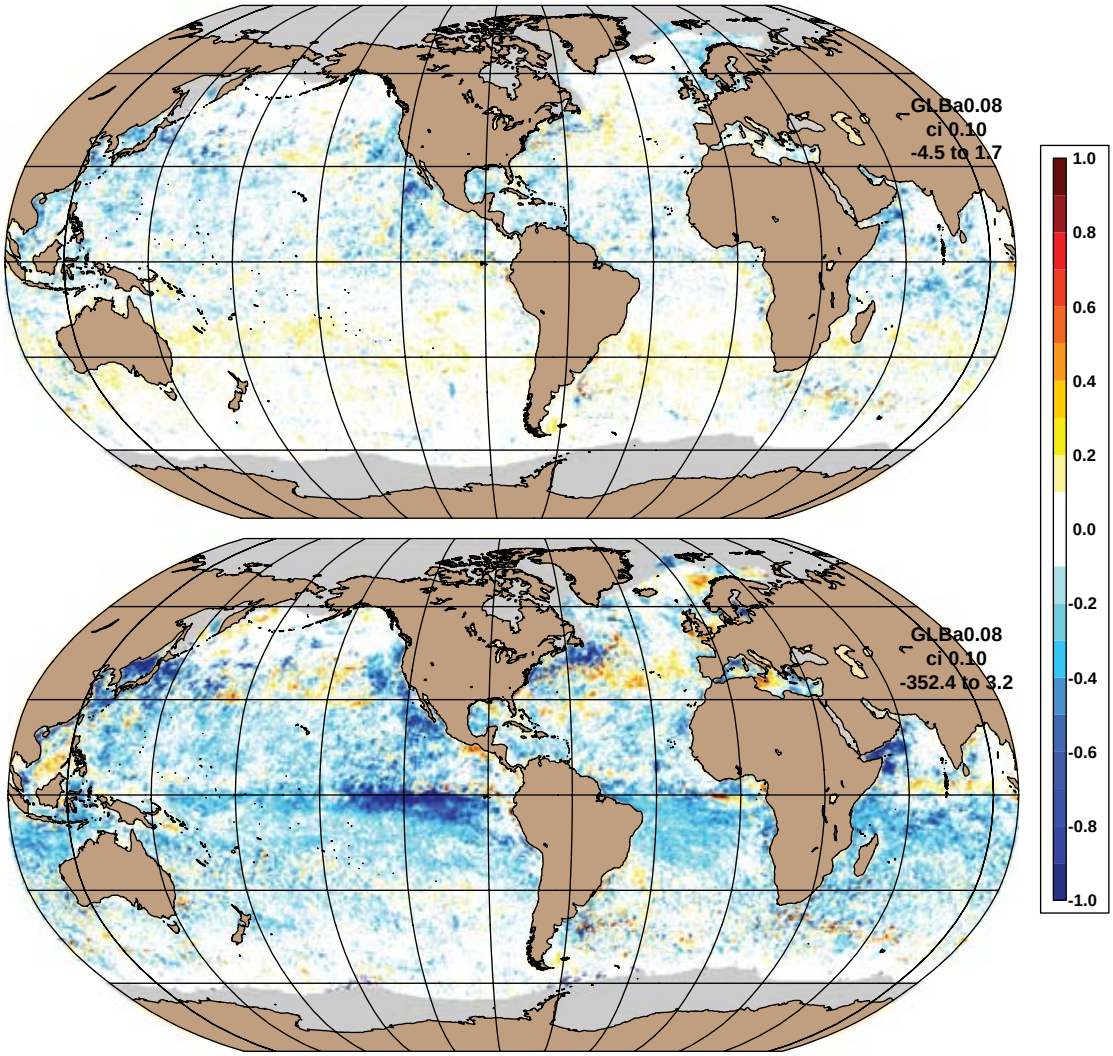

FIGURE 5
Sea surface temperature (SST) mean error (bias) relative to ~33,000,000 multi-channel SST (MCSST) observations at the analysis time (top) and for a 3-day forecast (bottom). Red (blue) colors indicate simulated SST is warmer (cooler) than observed. Values between ±0.1 °C are white. The gray area near the poles is an annual average ice coverage mask.

system has demonstrated forecast skill lasting up to about a month for the meandering currents and eddies in some regions.

Impact: A next-generation 1/12° global ocean nowcast/forecast system is running in real time at NAVOCEANO. It is designed to replace an existing nowcast/forecast system and have more than twice as fine grid resolution. It can more accurately depict such features as western boundary currents and sharp ocean fronts, thus providing improved environmental awareness to the Fleet.

[Sponsored by ONR, NOPP, and HPCMO]

References

[1] H.E. Hurlburt, E.P. Chassignet, J.A. Cummings, A.B. Kara, E.J. Metzger, J.F. Shriver, O.M. Smedstad, A.J. Wallcraft, and C.N. Barron, "Eddy-resolving Global Ocean Prediction," in M. Hecht and H. Hasumi, eds., *Ocean Modeling in an Eddying Regime*, Geophysical Monograph 177 (American Geophysical Union, Washington, DC, 2008).

[2] E.J. Metzger, O.M. Smedstad, P. Thoppil, H.E. Hurlburt, A.J. Wallcraft, D.S. Franklin, J.F. Shriver, and L.F. Smedstad, "Validation Test Report for Global Ocean Prediction System V3.0 – 1/12° HYCOM/NCODA: Phase I," NRL Memorandum Report NRL/MR/7320--08-9148 (Washington, DC, 2008).

Littoral Battlespace Characterization Using Small Unmanned Aerial Systems

K.T. Holland,[1] D. Lalejini,[1] and K. Plavnick[2]
[1]*Marine Geosciences Division*
[2]*Naval Oceanography Special Warfare Command*

Motivation: Few environmental regions are as dynamic as the littoral, where dramatic changes in winds, waves, and bathymetry can occur over time scales as short as a few hours. A long-term goal for the Littoral Dynamics Team within the Naval Research Laboratory (NRL) is to extract littoral meteorological and oceanographic (METOC) conditions from intelligence, surveillance, and reconnaissance (ISR) imagery collected by either space or airborne platforms in near real time. Our most recent efforts have focused on developing capability to provide actionable battlespace awareness for amphibious operations through the analysis of motion imagery from Small Unmanned Aerial Systems (SUAS). These systems are relatively inexpensive and are widely used within the Department of Defense.

Technical Approach: Although we have investigated a number of suitable platforms, our military customers commonly use the Raven B SUAS manufactured by Aerovironment, Inc. This platform, with a wingspan of 1.4 m and a weight of 1.9 kg, is ideally suited for low-altitude ISR. The system can carry either dual color video cameras with digital pan/tilt/zoom or a single infrared (IR) camera, downlinked live to a ground control station (GCS). Within the GCS, the video is timestamped and aligned with position and attitude metadata. Although direct orthorectification of imagery frames is possible using an external laptop computer, time latencies and sensor misalignments can result in geo-referenced mosaics with substantial errors. Instead, NRL has developed an image matching approach based on scale-invariant tie-points to automatically create mosaics suitable for littoral characterization that can be geo-registered using optimized metadata with only limited manual intervention.

Exercise Demonstration: This approach was demonstrated during 21–28 July 2008 in support of Exercise Trident Warrior 2008 and Exercise Rim of the Pacific (RIMPAC) 2008 while working from Bellows Beach, Hawaii. Our joint civilian and military team managed and flew the Raven B for purposes of collecting surf zone imagery in support of U.S. Navy and Marine Corps amphibious operations (Fig. 6). Military support, including transmission of our products to the fleet, was coordinated through the Naval Oceanographic Operations Command, ISR Oceanography Directorate. This was the first time Raven B had been used for this purpose during a major exercise.

Five flights (averaging 55 minutes duration) over 4 days resulted in nearly 600 images and video clips. These clips were analyzed immediately after collection to create a number of timely environmental products (Figs. 7 and 8). These products were used by METOC personnel aboard the USS *Bonhomme Richard* (LHD 6) who indicated that these products were useful in planning RIMPAC landings at Bellows Beach.

A related part of the demonstration purpose was to develop, refine, and assess the concepts of operations (CONOPs) and tactics, techniques, and procedures (TTPs) associated with collecting Raven B overhead imagery for littoral characterization, planning, and tactical decision-making. By flying at various altitudes and flight paths (dwells, orbits, and strip maps), we were able to develop an optimal collection strategy and demonstrate that this system could provide quality, timely, and actionable intelligence that impacted operations through improved battlespace METOC characterization. For example, cloudy weather conditions on some mornings would have precluded the use of higher altitude surveillance platforms. The overall demonstration proved that effective METOC characterization of the littoral battlespace was possible by exploiting tactical, non-traditional METOC sensors, specifically imagery from a locally controlled SUAS.

FIGURE 6
UAS operator preparing to launch Raven B on Bellows Beach, HI. USS *Bonhomme Richard* (LHD 6) is visible near the horizon.

FIGURE 7
Image mosaic created while on-scene showing Bellows Beach landing area.

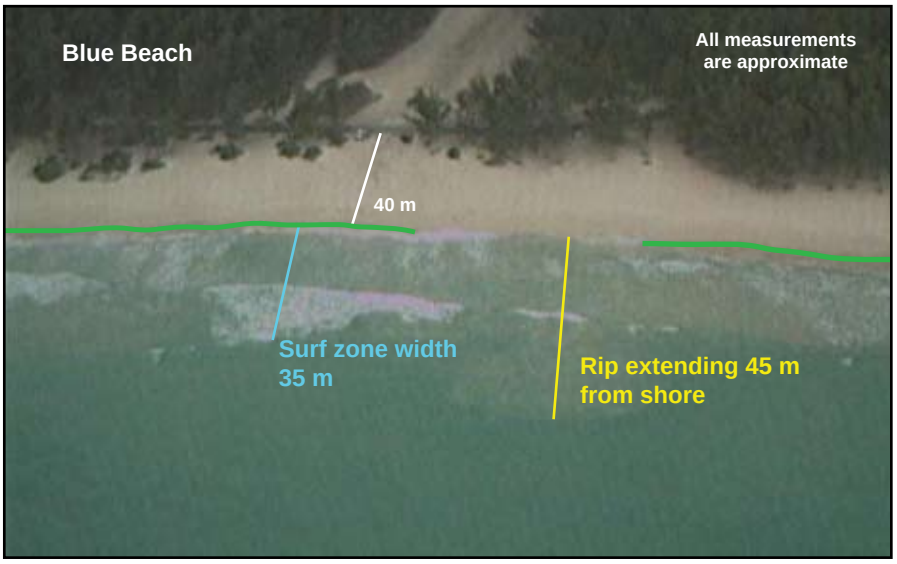

FIGURE 8
Example of an analyzed image product created from mapped Raven B video frame. Shoreline location and measured widths of littoral features are indicated.

Future Plans: Present METOC products that can be derived from these systems include geo-rectified mosaics showing surf zone characteristics, shorelines, hazards to navigation, and preferred vessel pathways. Some of our techniques for standardizing product types and formats require further development. In addition, numerical analysis of these videos has been shown useful for estimating wave direction and period, and will be used to derive bathymetry in the near future. We anticipate working with further amphibious demonstrations similar to Trident Warrior during 2009.

[Sponsored by ONR]

The Environmental Post-Mission Analysis System: Through-The-Sensor to the Warfighter

B.Y. Lin, S.A. Myrick, W.E. Avera, and M.M. Harris
Marine Geosciences Division

Managing a Sea of Environmental Data: The highly skilled, but leaner crews of today's Navy are tasked with compiling ever-increasing amounts of environmental knowledge. The mine hunter's arsenal bristles with data-gathering equipment: side-scan sonar, unmanned underwater vehicles, and meteorological sensors. Compounded with the work required to deploy, retrieve, and maintain this equipment, downloaded data from these platforms can easily overwhelm operators, and post-mission analysis may fall behind. Navy scientists at NRL develop data processing tools and algorithms to enable the warfighter to do more work in fewer steps, but there is a need for seamless data processing integration "to ensure data are visible, available, and usable, when needed and where needed, to accelerate decision-making."[1] NRL's Environmental Post-Mission Analysis (EPMA) system addresses this need with a powerful, cross-platform data analysis system that manages the compilation and integration of environmental data. EPMA is being developed for the mine warfare community, but will also have broader data analysis applicability. The system ingests and processes field data and formats it into products that can be used in analysis tools and prediction models to allow informed and timely decision-making.

Marshalling Through-the-Sensor Output: In the course of processing environmental data, one encounters no end of data format varieties. For example, an operator may download raw side-scan sonar imagery in proprietary format, convert it to a common processing format, and then export it as a geo-rectified TIFF image. Each of these manifestations of the data has a specific purpose. In the EPMA system, this smallest operable collection of data is called an EPMA data set, and it is tagged with an EPMA data type. To manage and integrate disparate data outputs, EPMA defines a unified, extensible data type system to help discriminate into what processes a data set can be fed. In the most basic sense, an EPMA data type is a triplet of attributes: logical parameter, conceptual representation, and physical storage format. A collection of *bathymetry* may be arranged in a *grid* of points, stored in a *CHRTR* formatted file (Fig. 9). Along with extra metadata externalized by the data type, this aggregation, or attribution, gives EPMA more actionable information about the data set than what can be inferred from the file name or file extension alone.

Process Automation: NRL is a leading developer of tools and algorithms for advanced image processing, environmental modeling and prediction, and visualization of the battlespace, among other capabilities. In the EPMA system, a processing module encapsulates each of these capabilities, and presents an input and output interface using the EPMA data type system. These processing modules can be chained together based on type compatibility in a semi-automated workflow. Moreover, EPMA can manage the mundane details of file management and processing job control, freeing the operator to focus on higher levels of information interpretation and tactical decision-making.[2]

Developing a Sustainable Open Framework: Systematic and effective software reuse is left out of the design and implementation of many software systems. Software reuse can reduce development cycles and costs, decrease maintenance effort and expense, lengthen software life-spans, and speed technology transition times. EPMA's system architecture has been designed to take full advantage of software reuse. EPMA defines interfaces and a plug-in framework that allows new modules to be added in with a plug-and-play capability (Fig. 10). A module might be a basic, input-output processing block, an extension of the user interface or visualization technique, or might also combine other modules in a new workflow. The new plug-ins can be added at runtime, giving the user new operational capabilities. From the viewpoint of the module developer, EPMA is a robust application programmer's interface (API) that offers high-level data management, process control, and a set of reusable user interface widgets, such as map views.

Post-Mission Analysis for the Future: All aspects of the EPMA system are engineered to address the data-driven needs of the future net-centric warfare. Good software design combined with the cutting-edge capabilities developed by NRL make EPMA not only

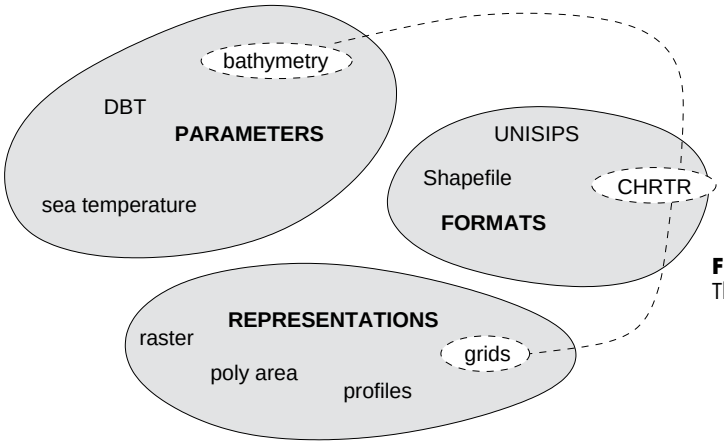

FIGURE 9
The EPMA data type system.

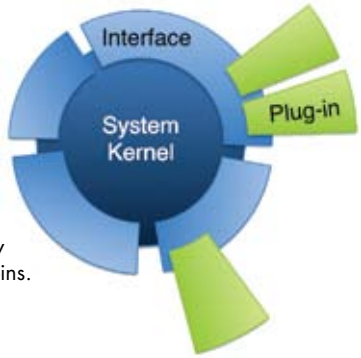

FIGURE 10
Extending capability through EPMA plug-ins.

an immediately useful application for the mine warfare community, but also a solid framework for general-purpose data analysis operations. Its utility has been shown with the first major release of EPMA Build 1.0. EPMA Build 2.0, slated for a 2009 release, boasts a matured implementation of the system.

Acknowledgments: This work was sponsored under Program Element 0603704N by the Oceanographer of the Navy with program management provided by SPAWAR PMW 180, Captain Wang, and Program Manager Dr. Ed Mozley; and NAVOCEANO under OPNAV N852 Mine Warfare Branch funds. We also acknowledge the dedicated engineers and scientists at the Naval Oceanographic Office who are jointly developing the EPMA with NRL.

[Sponsored by NAVOCEANO]

References

[1] J.P. Stenbit, "Department of Defense Net-Centric Data Strategy," Department of Defense memorandum, May 9, 2003, http://www.defenselink.mil/cio-nii/policy/datastrategy.shtml.

[2] M. Harris et al., "Environmental Data Collection, Sensor to Decision Aid," Sixth International Symposium on Technology and the Mine Problem, May 9–13, 2004, Monterey, CA, http://handle.dtic.mil/100.2/ADA426504.

optical sciences

213
Project CHLOE: High Altitude Defense Against Anti-Aircraft Missiles
R.M. Mabe, K.A. Sarkady, and B.A. Nichols

215
Transparent Spinel Ceramic
J.S. Sanghera, G. Villalobos, W. Kim, S. Bayya, and I.D. Aggarwal

217
Lightning Strike Sensing System for the Space Shuttle Launch Pad
A. Davis, J. McVicker, P. Karatsinides, A. Dandridge, and C. Kirkendall

Project CHLOE: High Altitude Defense Against Anti-Aircraft Missiles

R.M. Mabe,[1] K.A. Sarkady,[1] and B.A. Nichols[2]
[1]*Optical Sciences Division*
[2]*Alaire Inc.*

Introduction: NRL is conducting research to mitigate the threat posed by Man-Portable Air Defense Systems (MANPADS) to civilian aviation. Since the 1970s, the International Civil Aviation Organization has documented at least 42 civilian aircraft attacked with these systems. Twenty-nine of these attacks have resulted in loss of the aircraft and life. Attempts as recent as the Mombasa attack of an Israeli airliner in 2002, the attack of a DHL cargo plane in Iraq in 2003, and the arrest of an arms dealer attempting to smuggle MANPADS into the United States in 2003 are evidence of the continued threat posed to civilian aviation by these weapons.

Project CHLOE: Project CHLOE is a Department of Homeland Security (DHS) Homeland Innovative Prototypical Solutions (HIPS) project intended to demonstrate game-changing leaps in payload technologies at the prototype level that can enable the defeat of MANPADS from a persistent, high-altitude orbit. Project CHLOE is determining the system-level operational effectiveness, maturity of components, subsystems, software, system approach, and suitability for employing Counter-MANPADS (C-MANPADS) technologies from High Altitude Endurance Unmanned Aerial Systems (HAE UAS). The intent of CHLOE is to provide persistent, broad-area protection of commercial aviation from altitudes above the National Airspace System (NAS), that is, above 18 km mean sea level (MSL). The first stage of CHLOE was to determine the viability of MANPAD launch detection with existing technologies. To that end, NRL was tasked to conduct a rapid modification and prototyping of existing Tactical Aircraft Directed Infra-Red Countermeasure (TADIRCM) two-color infrared (IR) missile warning system (MWS) components to support a high-altitude flight demonstration and evaluation.

Technical Challenges: DHS desired the CHLOE flight demonstration be conducted from altitudes above the NAS and selected the National Aeronautics and Space Administration's (NASA) ER-2 as the test platform. The ER-2 is capable of achieving altitudes in excess of 21 km MSL. Standoff detection from these altitudes required an order of magnitude improvement in sensitivity over the current TADIRCM sensor design. The TADIRCM two-color missile warning sensors were designed to counter MANPADS at tactical ranges less than 10 km. NRL and DRS Technologies redesigned the missile warning sensor optics and electronics, achieving the required performance for the flight demonstration.

Additionally, most of the other components were only certified to maximum altitudes of 30,000 ft. This precluded a direct mounting of the TADIRCM Early Operational Assessment (EOA) pod on the ER-2. With the assistance of NRL's Spacecraft Engineering Department, the MWS was redesigned to fit in the ER-2's experimental Q-bay. Since this was a test of the missile warning function only, the laser-based directed infrared countermeasure was not installed. The repackaged MWS was integrated into NASA's Dryden Flight Research Center and flight tests were conducted there. Figure 1 shows the MWS installed in the upper portion of the ER-2 Q-bay, and Fig. 2 shows the MWS sensor installation in the lower Q-bay hatch. The design provided for a system field of regard of 360° in azimuth from an elevation of 40° to 90° below the horizon.

Demonstration Results: Initial flight operations were conducted in the areas surrounding Edwards AFB, California, to check MWS operability and measure urban clutter levels at various altitudes. The flights confirmed operation throughout the ER-2 operational envelope. During these flights, MWS operability was validated at various altitudes using a missile simulator. The simulator comprised a set of propane burners designed to generate infrared signatures with spectral characteristics similar to those of a threat missile at broad aspect. The MWS was able to detect and declare as a threat the simulator at slant ranges up to 30 km. The system was also able to geo-locate the simulator position with an average error of 50 m. The flights also measured urban clutter at various altitudes up to the maximum altitude of the ER-2. The data collected provide valuable insight into the effect of background clutter on MANPAD detection from high altitude.

Following the local flight operations, the ER-2 and support crew were moved to Kirtland AFB in Albuquerque, New Mexico, to support flight operations over the White Sands Missile Range during DHS C-MANPADS live fire tests. Five MANPAD launches were observed from altitudes in excess of 21 km MSL. The MWS detected, tracked, and declared all five of the launches. Figure 3 is a single sensor frame showing the declaration of two launch events. The red boxes declare as threats the near-simultaneous launch of two MANPADs toward targets near the end of the valley at the upper left. The data were obtained from 20 km MSL. The results were similar for the other observed events.

The MWS demonstration portion of Project CHLOE was successful in demonstrating the efficacy of MANPAD detection from altitudes above the NAS. During the demonstration, all observed MANPAD

FIGURE 1
CHLOE processing equipment mounted in upper ER-2 Q-bay.

FIGURE 2
CHLOE sensors mounted in lower ER-2 Q-bay hatch.

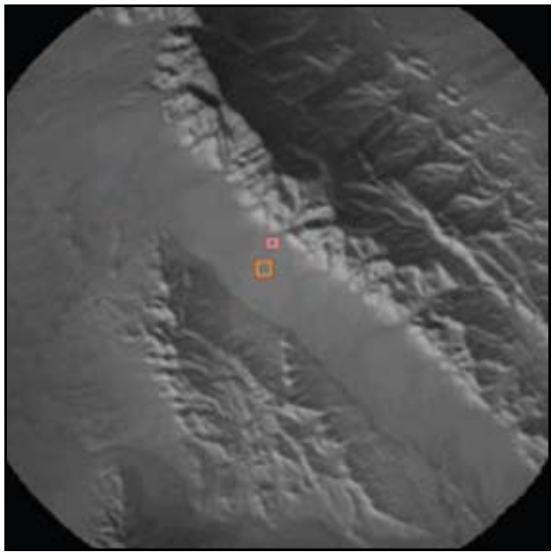

FIGURE 3
Detection and declaration of near-simultaneous MANPAD launches, from 65,000 feet.

launches were detected and declared as threats. The demonstration also provided valuable insight into the background clutter levels to be expected at these altitudes. Based on post-demonstration analysis, the higher clutter levels observed over urban areas will require a sensor with a higher resolution than the redesigned MWS sensor to provide adequate threat declaration probability with a reasonable false cue rate. This higher resolution sensor will provide additional benefits in a greatly reduced pointing error for handoff to a MANPAD countermeasure. Additionally, higher resolution will result in reduced geo-location errors and provide more accurate launch position reports to the nation's law enforcement agencies.

[Sponsored by the Department of Homeland Security]

Transparent Spinel Ceramic

J.S. Sanghera, G. Villalobos, W. Kim, S. Bayya, and I.D. Aggarwal
Optical Sciences Division

Spinel Ceramic: Spinel ($MgAl_2O_4$) is a cubic crystalline material with a unique combination of ruggedness and excellent transmission from the ultraviolet (0.2 μm) to the mid-infrared (5 μm) region. This positions spinel as the de facto material of choice for numerous Department of Defense and commercial infrared window applications. However, single crystal spinel is difficult to make in dimensions greater than a few millimeters using traditional high temperature (>2000 °C) melt growth techniques. On the other hand, attempts to make polycrystalline spinel by traditional hot pressing of powder has led to inhomogeneous material, typified by opaque nontransmitting regions, thereby making it unsuitable for practical applications. However, NRL has solved this problem.

NRL's Technology: We have identified that the poor quality of commercial spinel ceramic is attributed to the inhomogeneous mixing of the sintering aid (LiF) with the spinel powder. This leads to porosity and trapped sintering aid. Therefore, we have developed a novel and patented process to uniformly coat the sintering aid onto every spinel powder particle and enable its removal during the hot-pressing process at around 1600 °C.[1] This enables full densification and fabrication of uniformly transparent high-optical-quality spinel ceramic. The process is scalable to make large windows, but also by designing suitable hot-press molds, it is possible to make thick windows and conformal optics including lenses and dome shapes (Figs. 4 and 5).

Applications: The availability of high-optical-quality spinel ceramic in different shapes and sizes makes it an excellent window material for many applications. Some of the applications being pursued for spinel are described in the following paragraphs.

DDG 1000. The DDG 1000 destroyer (Fig. 6) requires high-strength, large-sized windows for the bridge that exhibit both visible and infrared transmission to 5 μm and must withstand up to 8 psi waveslap. Since NRL's hot-press process is scalable to large sizes, the bridge window could be made from one large piece of spinel, or alternatively it could be made by edge diffusion bonding of two or more smaller windows together. The feasibility of both of these approaches has been demonstrated (Fig. 4).

Photonic Mast for Virginia Class Submarines. Existing windows on the mast use silica glass and crystalline germanium for transmission of visible and mid-infrared light, respectively (Fig. 6). Unfortunately, both materials are weak and prone to damage, despite the

FIGURE 4
A 12-in. x 16-in. x 0.5-in. single pane of spinel ceramic and a 6-in. x 3-in. x 0.5-in. part made by edge diffusion bonding two smaller pieces.

FIGURE 5
Examples of a thick (1.5-in.) spinel window and a dome.

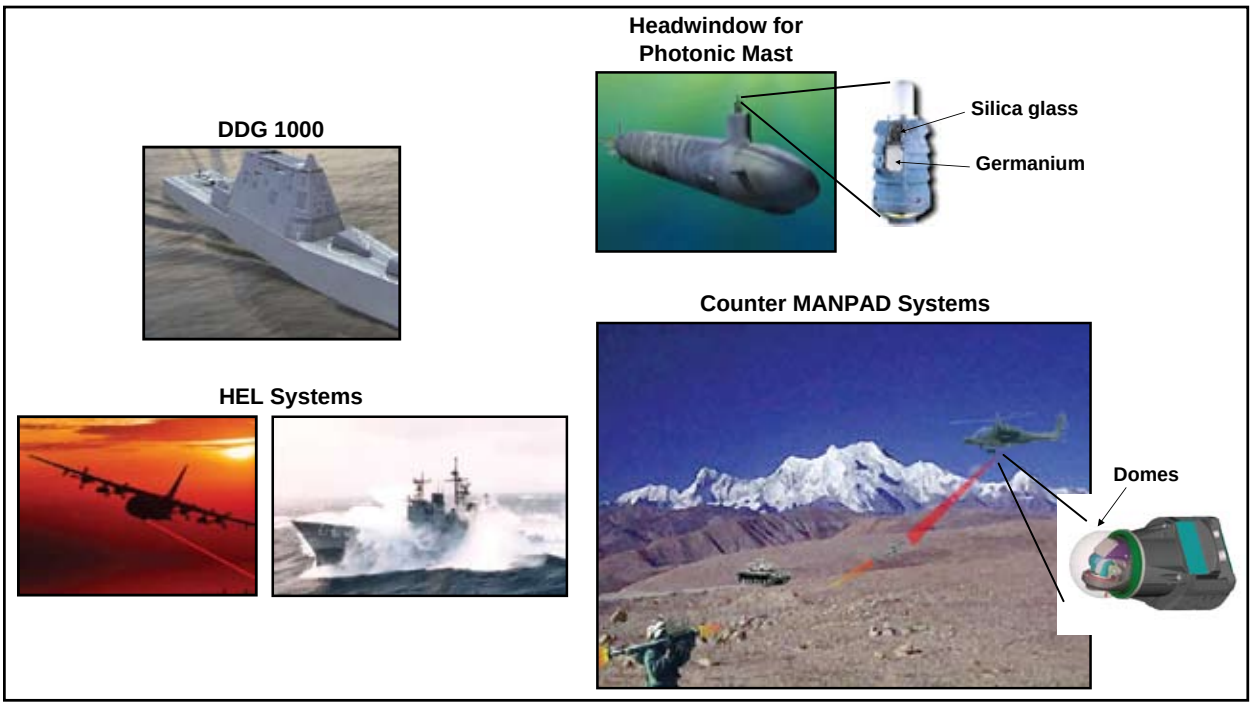

FIGURE 6
Several applications that will benefit from development of transparent spinel ceramic.

fact that they are 1.5 in. thick. The replacement of both windows with a single window of spinel will enhance survivability and significantly reduce maintenance and life cycle costs. The challenge is how to make thick spinel windows. By refining the hot-press process, we have successfully demonstrated preparation of 1.5-in. thick spinel ceramic with very good optical quality (Fig. 5).

High Energy Lasers. High energy lasers (HEL) are being developed for directed energy weapons systems, but the exit aperture (i.e., window) has been identified as the single point of failure due to a combination of poor thermal, optical, and mechanical properties (Fig. 6). This is especially true for glass windows since they possess very low thermal conductivity, which leads to thermal shock. Their low strength also makes them unsuitable for applications in hostile environments. On the other hand, spinel's excellent ruggedness enables its use in hostile environments and its higher strength enables the use of thinner windows, thereby reducing weight. NRL has developed technology to make ultra-high-purity spinel powder, which has been used to make spinel ceramic with a record low absorption loss of 6 ppm/cm at 1.06 μm. A combination of low absorption loss and high strength lead to very low optical path distortion of the laser beam.

Domes for Missile Protection Systems. Rugged infrared transmitting domes are needed in systems to counter Man-Portable Air Defense Systems (MANPADS) and provide platform and personnel protection against infrared seeking missiles (Fig. 6). Existing materials, such as crystalline silicon, are weak and

also do not provide visible transmission, while sapphire provides limited transmission at a wavelength of 5 μm. However, spinel provides both visible transmission and better transmission than sapphire at 5 μm, and without compromising the mechanical performance. Consequently, we have modified the hot-press die design and process and successfully demonstrated fabrication of spinel domes (Fig. 5).

In addition to the applications described above, the availability of high-optical-quality spinel ceramic with high strength will also enable fabrication of lightweight blast shields, face shields, and goggles for personnel protection from improvised explosive devices (IEDs) as well as conformal windows for reconnaissance. NRL's spinel technology has been licensed to industry and the "Transparent Spinel Ceramic" technology was selected as the winner of the 2008 National Award for Excellence in Technology Transfer by the Federal Laboratories Consortium.

Acknowledgments: We acknowledge the help of Bryan Sadowski and Fritz Miklos of SF Associates and thank NRL 6.2, NAVSEA, and Joint Technology Office for High Energy Lasers (JTO-HEL) for funding this effort.

[Sponsored by NRL and ONR]

Reference

[1] G. Villalobos, J.S. Sanghera, S.B. Bayya, and I.D. Aggarwal, "Fluoride Salt Coated Magnesium Aluminate," U.S. Patent 7,211,325, May 1, 2007.

Lightning Strike Sensing System for the Space Shuttle Launch Pad

A. Davis,[1] J. McVicker,[2] P. Karatsinides,[2]
A. Dandridge,[1] and C. Kirkendall[1]
[1]*Optical Sciences Division*
[2]*Global Strategies Group, Mission Systems*

Introduction: NRL Optical Sciences Division scientists designed and fabricated a fiber-optic magnetic field gradient sensing system for use by NASA on the space shuttle launch pad at Kennedy Space Center (KSC), Florida. The system is being used to monitor the occurrence and intensity of lightning strikes on and in the vicinity of the launch pad and space shuttle during prelaunch operations. The NRL system is integrated with the NASA Ground Lightning Monitoring System (GLMS), which records the intensity of the dynamic magnetic fields that result from lightning and triggers a warning if nearby lightning is strong enough to cause damage to the electronic systems employed on either the shuttle or the launch pad. Current lightning strike monitoring capabilities at the pad are not robust enough to screen lightning events, thus resulting in extensive, time-consuming inspections to verify the integrity of the electronic systems whenever any electrical storm activity occurs nearby. The NRL magnetic field gradient sensing system provides improved sensing bandwidth, resolution, and accuracy, and when incorporated into the GLMS, it alerts NASA as to when inspection of the electrical systems is required. Additionally, it indicates when inspection is not required, thus avoiding unnecessary expenditures of time and money.

System Description: The system has electronically passive, remote-sensing heads that are deployed both on the launch pad and aboard the space shuttle (Fig. 7). The use of passive sensors on the space shuttle launch pad is an important safety feature due to the presence of hydrogen and oxygen used to fuel the shuttle. Three search coils (X, Y, and Z axes) are used to generate dynamic voltages proportional to the time derivative of the local magnetic field as induced by lightning activity. This voltage is passed to an optical head that contains three fiber-optic interferometers (one for each vector axis of the magnetic field) where it is converted to optical phase. Three-by-three (inputs by outputs) optical couplers are used to form the interferometers; the voltage from the search coil is converted to optical phase by a crystal phase modulator in the sensing leg of the interferometer while the reference leg is left unperturbed. Demodulation of interferometers of this design does not require that an active carrier be imposed on the interferometer's output, thus maintaining the passive nature of the sensing system. The optical heads containing the interferometers are connected by fiber-optic cables to an NRL avionics system in the instrumentation room located underground below the launch pad. These fiber-optic cables again maintain the electronically passive nature of the sensing system and are not susceptible to electromagnetic interference (EMI). The cables deployed on the launch pad are between 1 and 2 km in length; however, the system is capable of employing cables up to tens of kilometers long. Each NRL avionics box is configured to support up to four three-axis sensing heads. The system undergoes a 1-min autocalibration routine on power up and runs a continuous calibration update in the background during operation. Digital demodulation algorithms, with 5 MHz of processing bandwidth, are used to recover the dynamic magnetic waveforms from the optical carriers. These waveforms are passed to the NASA GLMS system.

Four NRL three-axis search coil sensors and the associated optical heads and avionics systems, all designed and fabricated by scientists and engineers in the Optical Sciences Division, were installed and tested

FIGURE 7
GLMS placement on the space shuttle *Discovery* launch pad.

by NRL and NASA personnel on Pad A at KSC in April 2008. The system has since undergone vigorous performance and acceptance testing. NRL and NASA engineers are collaborating to make system operational refinements that will optimize the system's lightning strike detection capabilities. On 31 May 2008, the system was used to monitor the intensity of lightning strikes that occurred near *Discovery* for the STS-124 mission. In December 2008, the NASA Engineering Readiness Review board approved the GLMS system, which employs the NRL Field Gradient Sensing system, for use on the space shuttle launch pad.

[Sponsored by NASA, Kennedy Space Center]

remote sensing

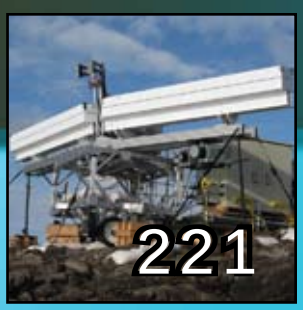

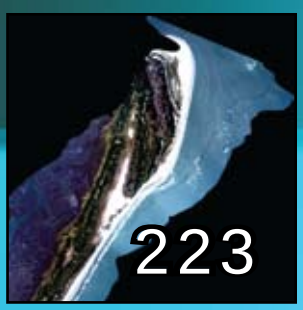

221
Polarimetric Radar Imaging of the Ocean Surface
M.A. Sletten and K. Scheff

223
Airborne Remote Sensing of Trafficability in the Coastal Zone
C.M. Bachmann, C.R. Nichols, M.J. Montes, R.-R. Li, P. Woodward, R.A. Fusina, W. Chen, V. Mishra, W. Kim, J. Monty, K. McIlhany, K. Kessler, D. Korwan, D. Miller, E. Bennert, G. Smith, D. Gillis, J. Sellars, C. Parrish, A. Weidemann, W. Goode, A. Schwarzchild, and B. Truitt

228
Impulsive Noise Suppression via Adaptive Filtering
G.S. San Antonio

Polarimetric Radar Imaging of the Ocean Surface

M.A. Sletten[1] and K. Scheff[2]
[1]*Remote Sensing Division*
[2]*Radar Division*

Introduction: Understanding the relationship between ocean surface waves and the radar backscatter they generate is key to the development of new radar-based techniques to measure ocean parameters, such as wave height and current speed and direction, of importance to both the Navy and the civilian sector. This knowledge is also needed to improve the Navy's ability to distinguish between signals generated by important, man-made targets and the competing radar backscatter produced by the ocean surface itself. The NRL Remote Sensing Division and Radar Division have collaboratively developed a unique radar, the NRL Focused Phased Array Imaging Radar (NRL FOPAIR), to investigate this relationship. The ability of this system to rapidly image the surface and determine the backscattered signal's sensitivity to polarization provides a powerful means to explore this important area of research.

System Description: The NRL FOPAIR is an updated version of a system first conceived and built by the University of Massachusetts–Amherst in the mid-1990s.[1] While typical land-based radars provide an "image" by mechanically scanning a narrow beam across the scene of interest, the FOPAIR accomplishes this by coherently combining data collected by many receive antennas arranged in a linear, side-by-side manner, an arrangement known as a phased array. A separate transmit antenna is used to illuminate the scene. Using this approach, the data required to build the entire image can be collected in less than a millisecond, as opposed to several seconds in the case of mechanical scanning. The NRL FOPAIR also employs both dual transmit antennas and dual receive arrays to allow collection of data spanning all possible combinations of transmit and receive polarizations. The relationship between the polarization state of the transmitted and received signals is intimately tied to the shape of the surface waves, and thus this "polarimetric" capability is an extremely valuable research tool. In addition, the NRL FOPAIR's data acquisition system (DAS) can support a sustained data rate in excess of 400 MB/s, providing the means to generate these polarimetric images at a high frame rate, i.e., to generate polarimetric "movies" that allow the relationship between the highly dynamic surface waves and the backscatter they produce to be studied in unprecedented detail.

Figure 1 is a block diagram of the NRL FOPAIR system. The basic transmit waveform (a linear, frequency-modulated chirp) is generated by a field programmable gate array (FPGA), converted to an analog signal by a Maxim digital-to-analog converter (DAC), and then multiplied up in frequency to 9.875 GHz before final amplification and routing through transmit switches and the horizontally (H) and vertically (V) polarized antennas. In the receive section of the system, three tiers of switches are used to individually select each of the 64 elements of the receive array and route its signal into the receiver. The entire bank of 64 receive elements is addressed sequentially in less than 1 millisecond. The analog receive signal is digitized and then stored by the DAS, which consists of analog-to-digital converters and a disk array for storage. In order to increase the angular coverage of the system, the radar is actually split into two identical halves, one looking 9° left, the other 9° right.

Figure 2 shows examples of the imagery produced by the system. These data were collected during system development when the radar was deployed on a bluff overlooking the Chesapeake Bay. Images for which both the transmit and receive signals are vertically polarized (VV) are shown in Fig. 2(a), while Fig. 2(b) shows the corresponding image when both are horizontally polarized (HH). The "spiky" character of the ocean wave backscatter in the latter is apparent and is generally attributable to breaking or near-breaking waves.[2] Characteristics like these can be fully exploited once a complete understanding of the radar ocean scattering mechanisms is developed.

Recent Hawaii Deployment: In August 2008, the FOPAIR system was deployed overlooking the Pacific Ocean at Makapuu Point State Wayside Park on the island of Oahu, where high quality data was collected over a wide range of wind and wave conditions. Figure 3 is a photograph of the system taken during this deployment. Significant effort was devoted to planning the installation of the radar, electrical power, and two personnel trailers near the edge of the 500-foot cliff at this remote site. Major effort was also required to address Hawaii State Park permitting requirements. Makapuu Point was chosen, despite its logistical and bureaucratic hurdles, due to its truly unique combination of deep water, extremely long fetch (that is, the distance over which the wind blows unimpeded by land), and strong, steady winds. These site characteristics in conjunction with the NRL FOPAIR's unique capabilities will make data analysis much more fruitful and tractable than for previous sea scatter experiments, which used less capable radars in more environmentally complicated locations.

[Sponsored by NRL/ONR]

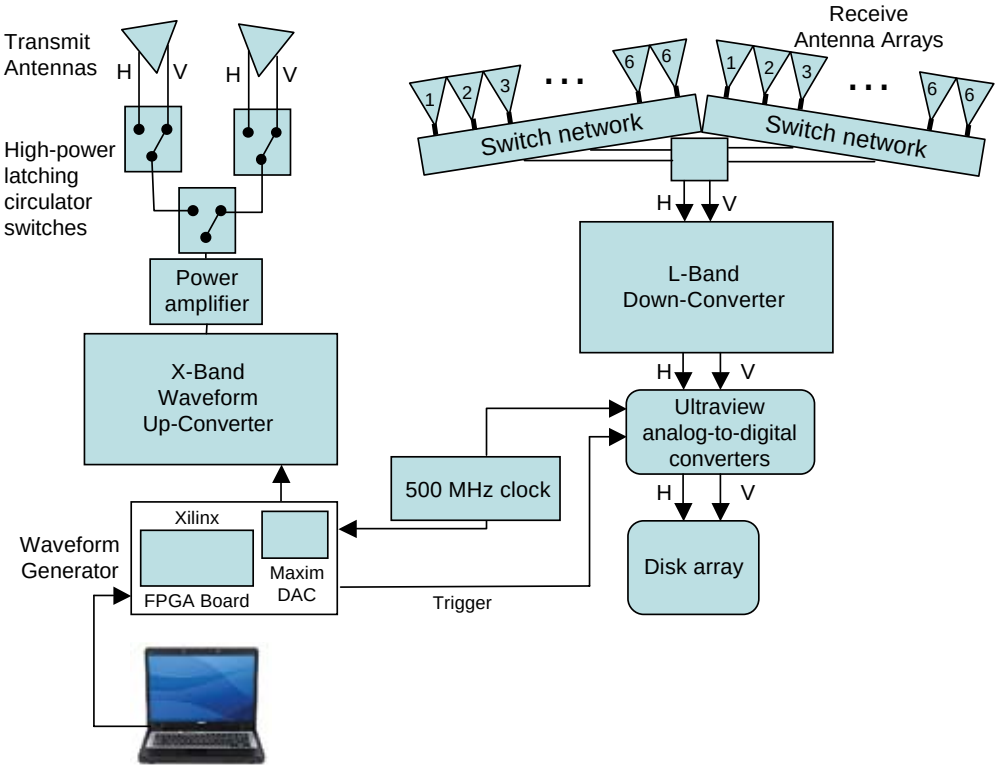

FIGURE 1
Block diagram of the NRL FOPAIR system.

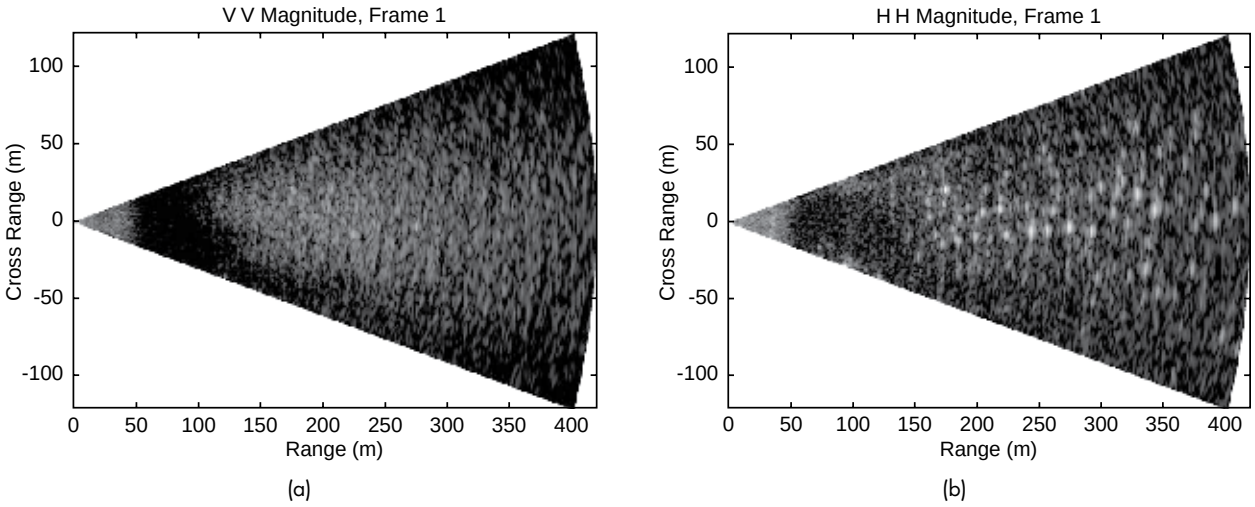

FIGURE 2
(a) Vertical-transmit vertical-receive image of the surface of the Chesapeake Bay. (b) Same as (a), but polarization is horizontal-transmit horizontal-receive.

FIGURE 3
Photograph of the NRL FOPAIR deployed at Makapuu Point on Oahu, Hawaii.

References
[1] R.E. McIntosh, S.J. Frasier, and J.B. Mead, "FOPAIR: A Focused Array Imaging Radar for Ocean Remote Sensing," *IEEE Transactions on Geoscience and Remote Sensing* **33**(1), 115–124 (1995).
[2] P.A. Hwang, M.A. Sletten, and J.V. Toporkov, "Analysis of Radar Sea Return for Breaking Wave Investigation," *Journal of Geophysical Research* **113**, C02003 (2008), doi:10.1029/2007JC004319.

Airborne Remote Sensing of Trafficability in the Coastal Zone

C.M. Bachmann,[1] C.R. Nichols,[2] M.J. Montes,[1] R.-R. Li,[1] P. Woodward,[2] R.A. Fusina,[1] W. Chen,[1] V. Mishra,[3] W. Kim,[3] J. Monty,[3] K. McIlhany,[4] K. Kessler,[5] D. Korwan,[1] D. Miller,[1] E. Bennert,[1] G. Smith,[1] D. Gillis,[1] J. Sellars,[6] C. Parrish,[6] A. Weidemann,[7] W. Goode,[7] A. Schwarzschild,[8] and B. Truitt[9]

[1]*Remote Sensing Division*
[2]*Marine Information Resources Corporation*
[3]*Purdue University, Laboratory for Applications of Remote Sensing*
[4]*U.S. Naval Academy*
[5]*Kessler Soils Engineering*
[6]*NOAA National Ocean Service*
[7]*Oceanography Division*
[8]*University of Virginia*
[9]*The Nature Conservancy*

Introduction: In September 2007, NRL, in partnership with multiple institutions, undertook a combined airborne multi-sensor remote sensing campaign and in situ validation effort. The experiment, VCR'07, took place at the Virginia Coast Reserve (VCR), a National Science Foundation–funded Long Term Ecological Research (LTER) Site on the Eastern Shore of Virginia. The study area comprised an 1880 km^2 region of barrier islands, shallow water lagoons, and mainland marsh systems (Fig. 4). This article describes the results of a subset of experiments conducted during the campaign demonstrating the retrieval of soil bearing strength directly from hyperspectral remote sensing on the VCR barrier islands. Bearing strength, or "trafficability," is a key parameter needed by military planners to identify littoral penetration points. The study also developed and tested new methods for retrieval of shallow water bathymetry, another important parameter needed by amphibious craft during landing.

Background: Hyperspectral imaging (HSI) sensors record the reflected solar radiation from land and water and have been used to retrieve important information in a variety of applications including precision land-cover mapping; in-water retrievals such as bathymetry, bottom type, and suspended constituents; retrieval of biophysical and geophysical parameters on land; and detection and determination of man-made structures and objects. HSI sensors are unique in having a large number of narrow, contiguous spectral channels. They have sufficient spectral resolution to identify different surface characteristics based solely on spectral signatures, and allow mapping of retrieved quantities with a high degree of precision.

Airborne Data Acquisition: For VCR'07, NRL mounted three remote sensing instruments in a de Havilland Twin Otter aircraft (Fig. 4): a CASI-1500 visible near-infrared (VNIR) hyperspectral camera operating in the 0.38–1.04 micron spectral range, a Surface Optics hyperspectral short-wave infrared (SWIR) camera operating in the 0.9–1.7 micron range, and a single-channel mid-wave infrared (MWIR) camera operating in the 3–5 micron range. This article focuses on the results obtained using the CASI-1500.

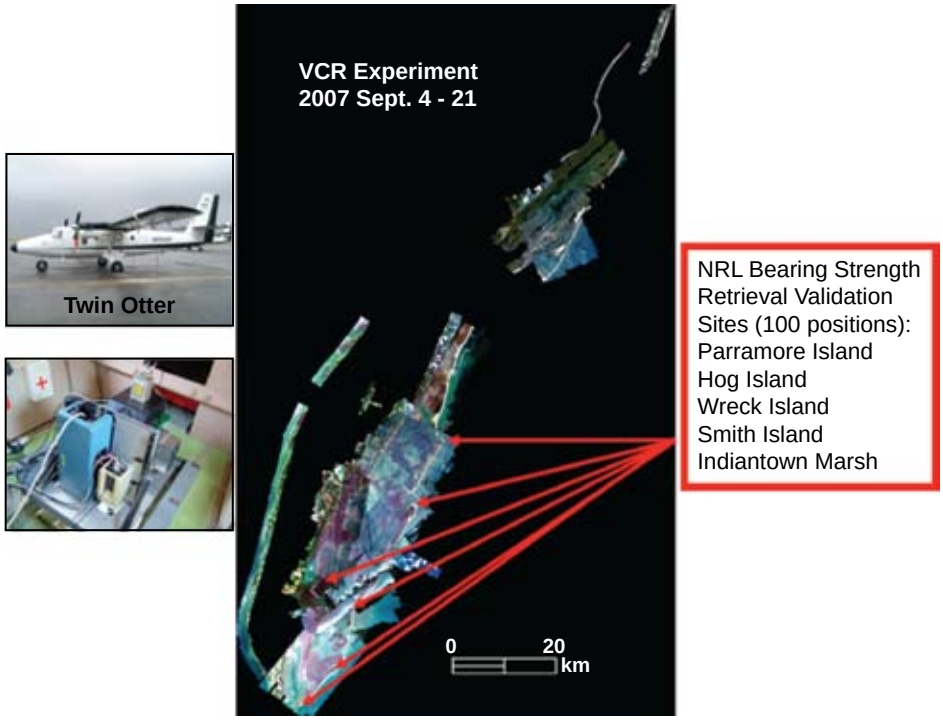

FIGURE 4
Left: Twin Otter aircraft and the three NRL sensors (CASI-1500, Surface Optics SWIR, and mid-wave IR) during VCR'07. Right: Composite of VCR'07 CASI-1500 quicklook images, with arrows indicating locations of primary bearing strength retrieval validation sites.

Bearing Strength from Hyperspectral Imagery: Soil bearing strength depends on a number of key factors including soil composition, grain size, and water content. HSI sensors can discern these properties for the surface layer of a substrate: HSI soil composition mapping has been well documented in the literature;[1] some studies have demonstrated the ability to model grain size from HSI;[2] and liquid water absorption features visible at several parts of the reflectance spectrum allow quantitative estimates of moisture content.

To determine the relationship between HSI surface data and the potential bearing strength of the substrate overall, the VCR'07 team undertook in situ spectral and geotechnical measurements to characterize bearing strength, moisture content, grain size profile, and corresponding spectral reflectance of different typical substrates (Fig. 5). These measurements were used to develop a spectral look-up table for bearing strength, which was then used to produce maps of substrate bearing strength directly from the CASI hyperspectral imagery. Figures 6 and 7 show examples of in situ data retrieval. Figure 8 shows the CASI retrieval product. The validation efforts showed that although HSI sees only the surface reflectance, this layer provides diagnostic information to indicate an estimated bearing strength of the substrate.

Shallow Water Bathymetry: At visible and near-infrared wavelengths, reflectance from the water column is determined by a variety of factors including water depth, bottom type, and the presence of suspended constituents such as color-dissolved organic matter (CDOM), suspended sediments, chlorophyll, and phytoplankton.[3] Thus the general problem of retrieving depth as well as other water properties has been approached using spectral look-up tables[4] in which a forward radiative transfer model such as Hydrolight[5] is executed repeatedly with varying water column properties, depth, and bottom types. To be comprehensive, these look-up tables must be large and may need to be tuned to specific coastal types because bottom types and water properties may vary significantly with coastal type.

In very shallow water (< 2 m depth), there is a range of wavelengths in the near-infrared for which the dominant factors determining reflectance are bottom type and depth, with water column constituents playing a secondary role. During VCR'07, we measured reflectance as a function of depth for various typical bottom types, and determined the optimal wavelengths for which a simpler model involving a library of regressions for each bottom type could optimally be applied in the very shallow limit. One of the optimal wavelengths for this occurs near 810 nm, a local minimum

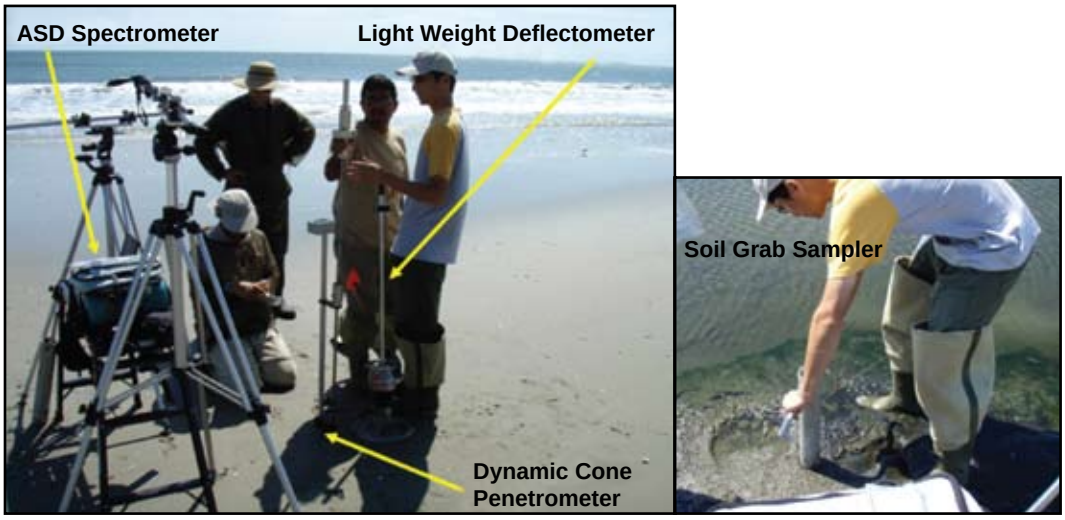

FIGURE 5
In situ calibration/validation instruments: Analytical Spectral Devices (ASD) full-range spectrometer; light weight deflectometer (LWD), which measures dynamic deflection modulus (bearing strength); dynamic cone penetrometer (shear strength); and soil grab sampler (for laboratory grain size profile and moisture analyses).

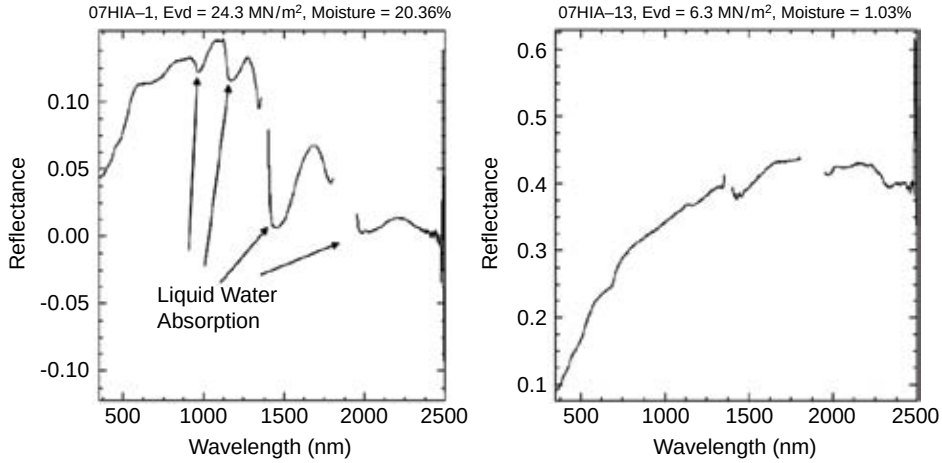

FIGURE 6
In situ water content /spectral measurements. ASD reflectance spectra for (left) sand near the shoreline and (right) sand near the arid backdune. The shoreline site with a moderate measured moisture level shows liquid water absorption features in the spectrum; the backdune site with a low measured moisture level has a spectrum absent of these liquid water absorption features. The corresponding bearing strength measured by the LWD was high at the shoreline site and low at the backdune site.

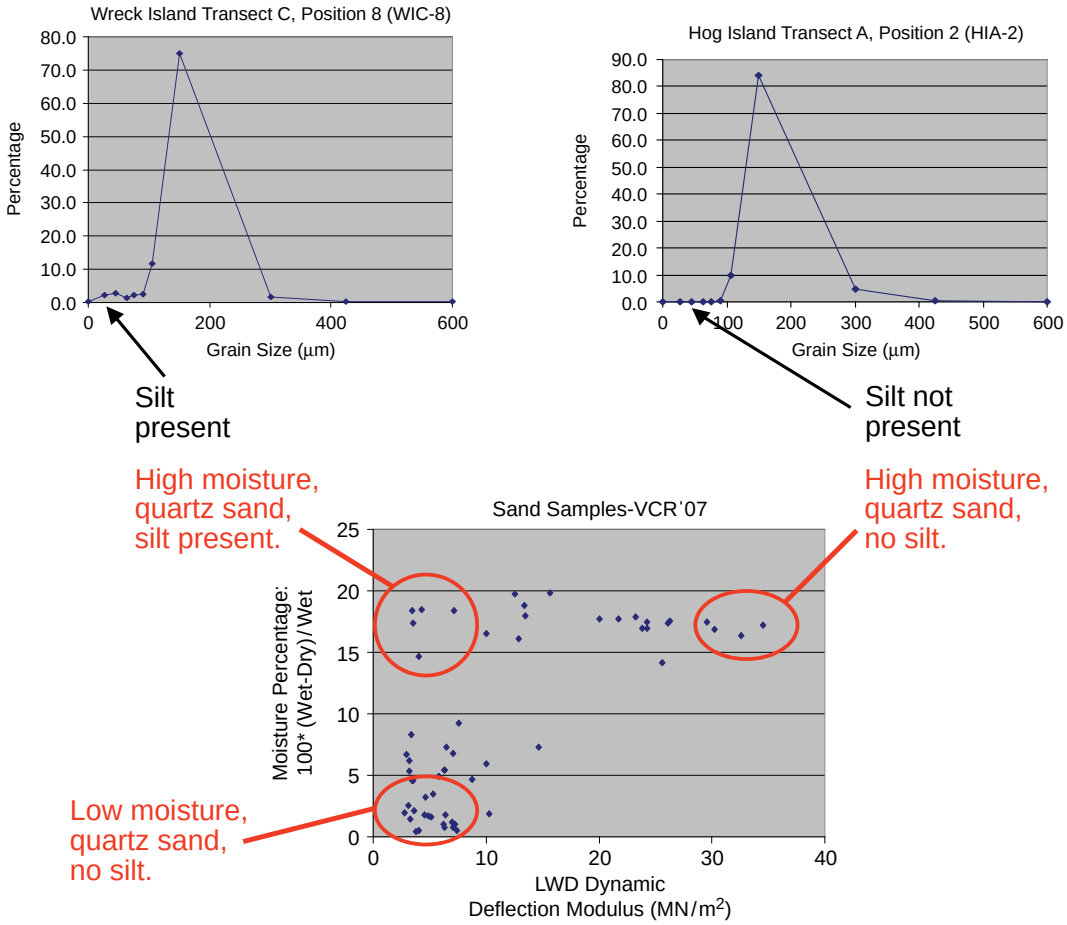

FIGURE 7
Correlation of in situ grain size, moisture, and bearing strength measurements. Scatterplot of percent moisture vs LWD-measured dynamic deflection modulus (bearing strength) for beach shoreline and backdune samples. Presence or absence of silt leads to dramatically different bearing strength when moderate moisture is present. Since silt is a significant contributing factor to bearing strength, we looked for diagnostic features that might indicate the presence or absence of silt quantitatively. Correlation of grain size and ASD spectral data (not shown) provided evidence for the presence of diagnostic VNIR spectral features for grain size.

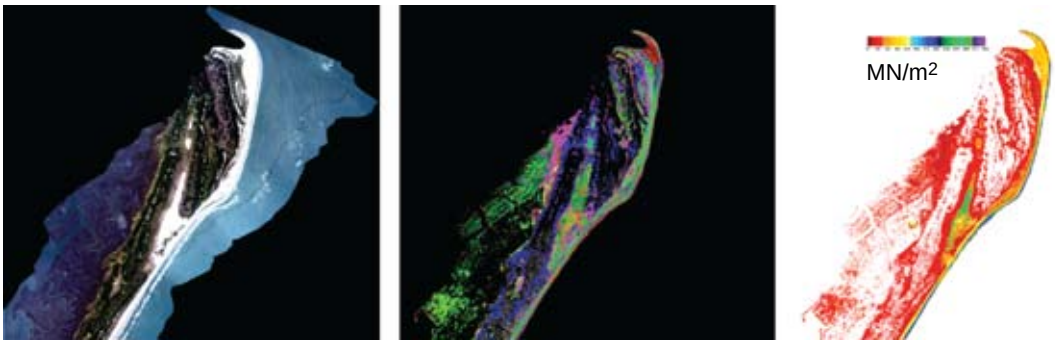

FIGURE 8
Demonstration of a bearing strength retrieval product. Left to right: CASI-1500 HSI scene, Hog Island, VA; closest matching spectrum in the spectral-geotechnical look-up table (LUT); and resulting retrieved bearing strength estimate in MN/m^2.

in liquid water absorption[6] and thus a local maximum in reflectance (Fig. 9). The results shown in Fig. 10 demonstrate the retrieval of very shallow depth in the vicinity of one of the VCR barrier islands using this approach. Kinematic GPS data taken in the intertidal zone were used to demonstrate the high accuracy of the retrieved very shallow bathymetry product.

Conclusions: VCR'07 successfully demonstrated new retrievals from hyperspectral imagery. These included a novel bearing strength map suitable for trafficability analysis in a barrier island coast type. A simplified approach to retrieving bathymetry from HSI in the very shallow limit was also validated. Operational lidar systems such as Scanning Hydrographic Operational Airborne Lidar Survey (SHOALS) do not produce reliable depth retrievals in very shallow waters. In joint HSI/lidar platforms such as the Compact Hydrographic Airborne Rapid Total Survey (CHARTS), the new approach, therefore, could fill a gap in bathymetric retrieval.

[Sponsored by ONR and the National Geospatial-Intelligence Agency]

References

[1] J.E. Baum, S. Orloff, S.M. Hsu, and H.-h. Burke, "Separability of VNIR/SWIR Reflectance Signatures of Prepared Soil Samples: Airborne Hyperspectral vs. Field Measurements," in *Imaging Spectrometry IX*, eds. S.S. Shen and P.E. Lewis, *Proc. SPIE* **5159**, 198–209 (2003).

[2] H.A. Ghrefat, P.C. Goodell, B.E. Hubbard, R.P. Langford, and R.E. Aldouri, "Modeling Grain Size Variations of Aeolian Gypsum Deposits at White Sands, New Mexico, Using AVIRIS Imagery," *Geomorphology* **88**(1–2), 57–68 (2007).

[3] C.D. Mobley, *Light and Water: Radiative Transfer in Natural Waters* (Academic Press, 1994).

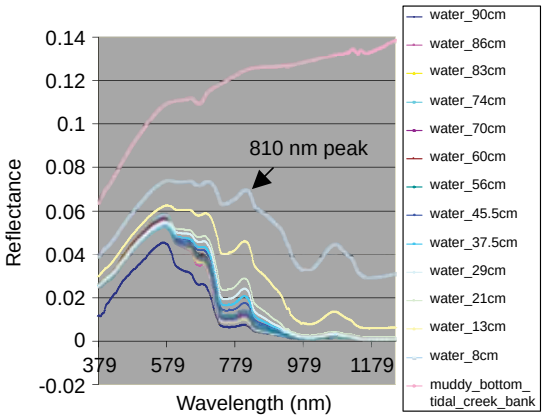

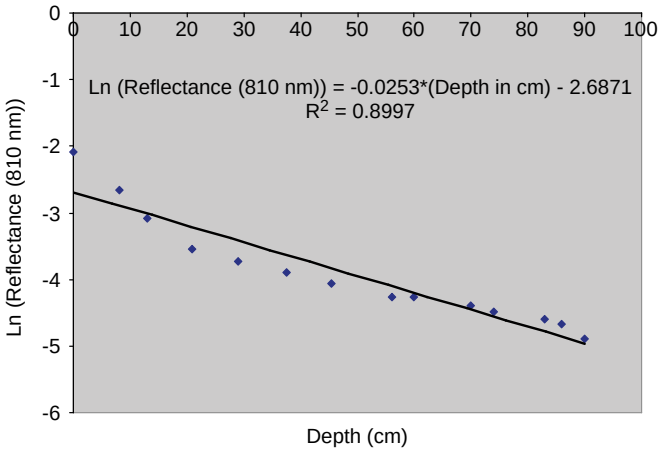

FIGURE 9

Top: In situ spectrometry site on salt marsh tidal creek bank with muddy bottom, at high and low tide, Parramore Island, VA. Bottom left: In situ spectral reflectance vs depth profiles. Bottom right: Regression at the 810 nm feature.

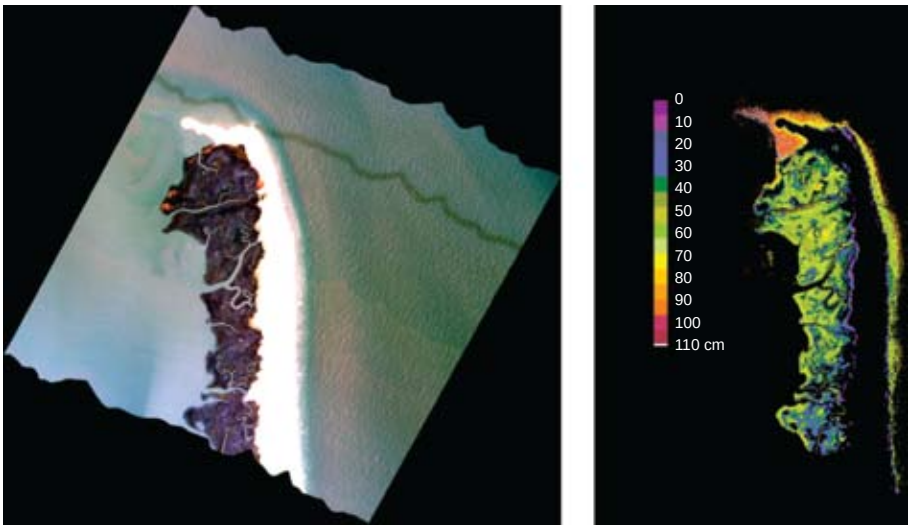

FIGURE 10
Shallow water bathymetry product. Left: NRL CASI-1500 image of Wreck Island, VA. Right: Retrieved depth using the 810 nm regressions for each bottom type determined in preprocessing from the spectral libraries; depth is quantized in the color scale, but actual retrieval is continuous.

[4] C.D. Mobley, W.P. Bissett, J.H. Bowles, C.O. Davis, T.V. Downes, A. Gleason, D.D.R. Kohler, R.A. Leathers, E.M. Lochard, M.J. Montes, R.P. Reid, and L.K. Sundman, "Interpretation of Hyperspectral Remote-sensing Imagery via Spectrum Matching and Look-up Tables," *Applied Optics* **44**(17), 3576–3592 (2005).
[5] C.D. Mobley and L.K. Sundman, Hydrolight 4.1 Technical Documentation, Sequoia Scientific, Inc., Seattle (2000).
[6] J.A. Curcio and C.C. Petty, "The Near Infrared Absorption Spectrum of Liquid Water," *J. Optical Soc. Amer.* **41**(5), 302–304 (1951).

Impulsive Noise Suppression via Adaptive Filtering

G.S. San Antonio
Radar Division

Introduction: Wide area surveillance is a common task for many of the nation's defense agencies. Coverage needs to be persistent 24 hours a day and through varying interference environments. High Frequency Over-the-Horizon Radar (HF-OTHR) is capable of providing wide area coverage that is on the order of hundreds of thousands of square kilometers. The challenges of using OTHR are manifold. Operating in an often crowded and noisy frequency spectrum (3–30 MHz) coupled with the complex and ever-changing state of the ionosphere presents difficulties higher-frequency radars do not face. In this article we describe a technique for suppressing impulsive noise-like disturbances that often corrupt OTHR data. This new technique is enabled by recent advances in high-speed computing that allow near-real-time implementation of sophisticated adaptive signal processing algorithms.

Background: OTHR is a surveillance radar technology that both the U.S. Navy and U.S. Air Force have used over the past forty years because of its wide area coverage capability and low operating cost.[1] Researchers at the Naval Research Laboratory (NRL) developed one of the first OTHR systems in 1961 called MADRE. Currently NRL is helping to develop advanced OTHR systems while also serving as technical advisors to the Navy's AN/TPS-71 Relocatable OTHR (ROTHR) program which consists of three radar sites providing surveillance coverage of the Caribbean Sea, Central America, and South America. Figure 11 shows a ROTHR receive antenna array and Figure 12 shows the approximate coverage area of the three radars.

OTHR operates by either refracting signals off layers of the ionosphere (skywave) or propagating a

FIGURE 11
AN/TPS–71 ROTHR receive array.

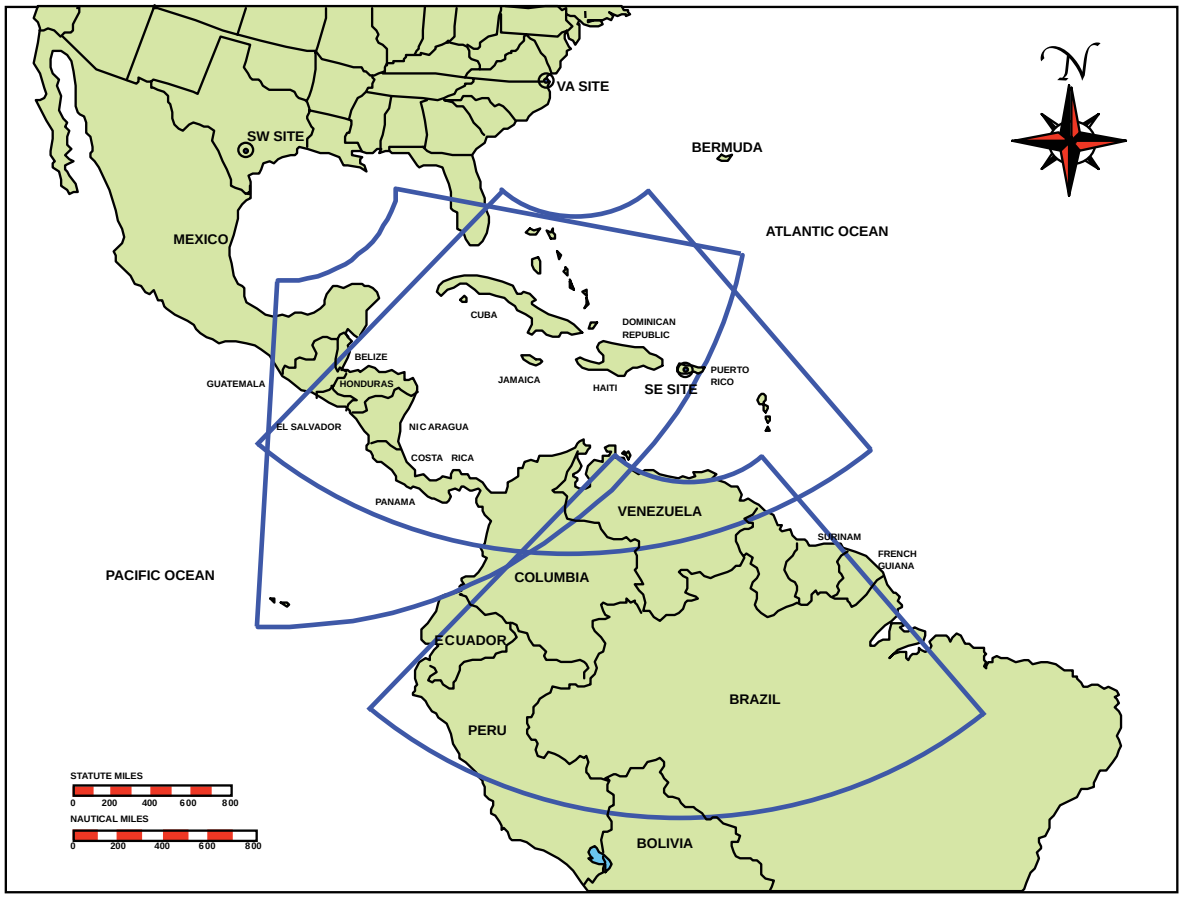

FIGURE 12
Conceptual illustration of OTHR operational environment.

surface wave over the conductive ocean that follows the curvature of the Earth. Among the many sources of performance limitation, impulsive noise is a major contributor. Impulsive noise differs from normal noise sources like thermal noise and cosmic background noise in that it is highly transient with very large amplitude peaks. Traditional Gaussian statistical assumptions fail to properly model this type of noise, and therefore normal target detection algorithms may perform poorly, often with very high false-alarm rates. Recognizing that current data models were inadequate, a signal-plus-noise model was developed that can be used to accurately estimate when data has been corrupted by impulsive noise and subsequently filter the data so as to remove the impulsive noise.

Noise Modeling: Atmospheric noise, power lines, and sporadic local interferers such as engine noise are all types of noise sources that are not well modeled by Gaussian probability distributions. Noise generated by these sources is inherently transient in nature (e.g., a single car driving near the array, a single arc from a power line transformer, or a lighting strike from a distant thunder storm). To this end, a probability distribution describing such random processes should possess "heavy tails" to accurately express the probability of an extreme valued random event. The drawback of modeling using heavy tailed distributions is that detector design can quickly become intractable due to complex expressions for probability density functions (PDFs). An alternative to using heavy tailed distributions is to allow a degree of non-stationarity. Simply put, non-stationarity means that the moments or statistics of a random process change (usually with time or space if we are considering a space-time random process).

In the extreme, non-stationarity could be taken to mean that the random process has different statistics everywhere. It is exactly this interpretation that allows us to hypothesize a space-time point process model for the noise field present in OTHR data. The full data model is composed of three independent parts: backscattered energy from targets, background/thermal Gaussian noise, and other noise that appears like impulsive events. The OTHR data is modeled as the combination of two space-time point processes: the first models targets and ground clutter (point-like in range-Doppler domain) and the second models

impulsive noise (point-like in inverse range-Doppler domain, that is, the fast time–slow time domain before range-Doppler processing). Given this hypothesized data model, modern statistical estimation methods can be used to adaptively filter the impulsive noise.

Adaptive Noise Filtering: Adaptive signal processing describes a method of processing data in such a way that important information is inferred from data in a real-time manner and is allowed to influence the way in which data is processed. More reliable and robust performance is achieved at the expense of slightly diminished peak performance. The adaptive impulsive noise filtering algorithm that has been developed works by first estimating the statistics of target and noise random processes jointly, and then constructing a filtering matrix to recover an estimate of the received data with the impulsive noise removed.

The estimation step requires finding the joint maximum likelihood target range-Doppler power spectrum and noise time-pulse power spectrum estimates. Maximum likelihood (ML) estimation problems are known to be difficult and often analytically intractable. Only recently with the advent of highly parallelized computer architectures have such problems been solvable in near real time. Our solution to the ML estimation problem makes use of a well know statistical algorithm called the expectation maximization (EM) algorithm. Using this iterative algorithm, an ML estimate may be found. Construction of an appropriate filtering matrix is based on finding the minimum mean squared error (MMSE) estimate of the impulsive noise free data. Figure 13 shows the results of applying this algorithm to a set of simulated OTHR data.

An alternative to the model-based maximum-likelihood approach we have described is to systematically identify data samples corrupted by impulsive noise and remove these samples from the data. Simulations and analysis of real OTHR data revealed that the ML approach performed better than several methods previously developed for HF-OTHR data based on extraction and replacement.[2] Additionally, these extraction and replacement techniques are highly dependent on the severity of the impulsive noise corruption and the

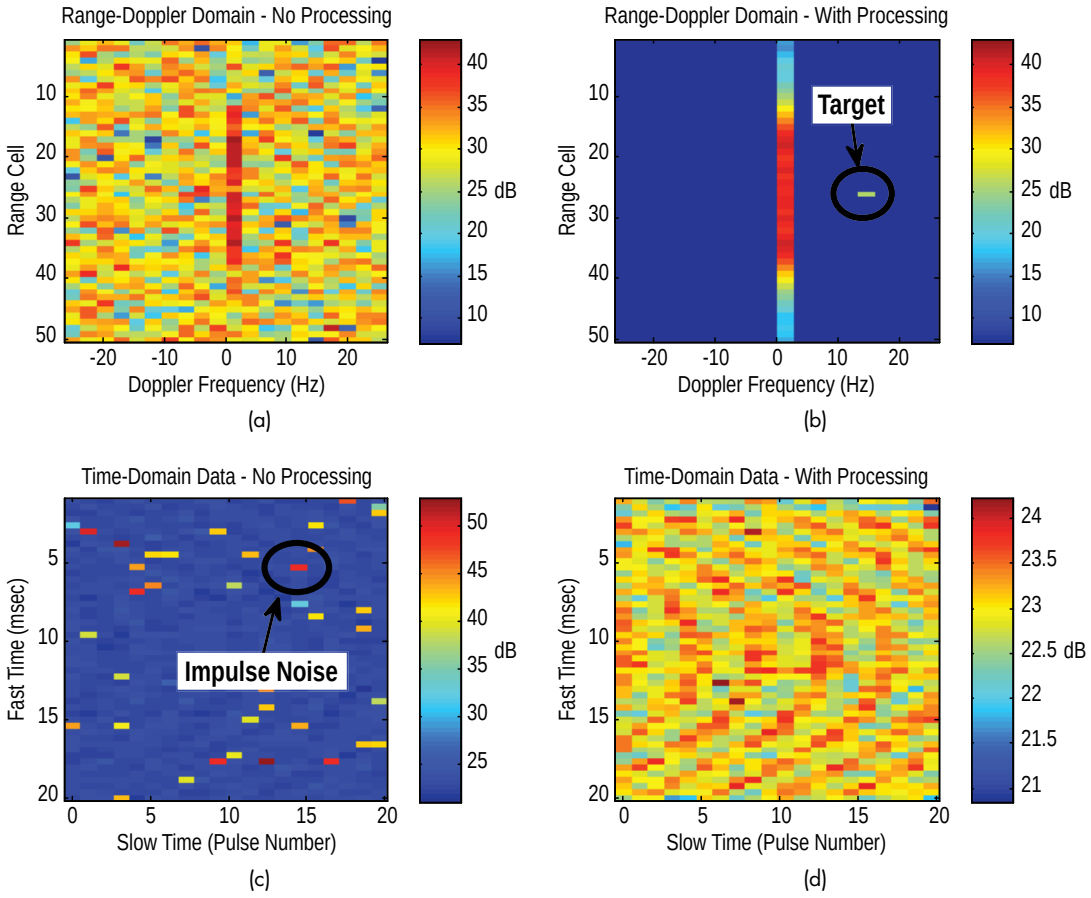

FIGURE 13
Example of adaptive noise suppression technique operating on simulated data. (a) Range-Doppler image with no noise suppression processing; (b) time-domain representation of data, with impulsive noise present; (c) Range-Doppler image after impulsive noise suppression, target can be detected; (d) time-domain data after impulsive noise has been filtered.

method used to replace the extracted samples (usually linear prediction).

Conclusion: Non-cooperative interference will always be a problem for surveillance sensor systems. It is possible, however, to minimize its impact on system performance given the correct signal processing. In this article a new technique for solving the impulsive noise suppression problem was presented. In the future, researchers at NRL will continue to push the limits of OTHR technology by developing new and innovative signal processing solutions.

Acknowledgment: This work was supported by the Missile Defense Agency.

[Sponsored by AFRL/Air Fund]

References

[1] J.F. Thomason, "Development of Over-the-Horizon Radar in the United States," in *Proceedings of the International Radar Conference, Adelaide, Aust., Sept. 3–5 2003*, pp. 599–601.

[2] J.R. Barnum and E.E. Simpson, "OTH Radar Sensitivity Improvement by Temporal Excision of Impulsive Noise," Rome Laboratory, Griffiss Air Force Base, NY, Technical Report RLTR 94-169, Sept. 1994, contract F30602-93-C-0112.

simulation, computing, and modeling

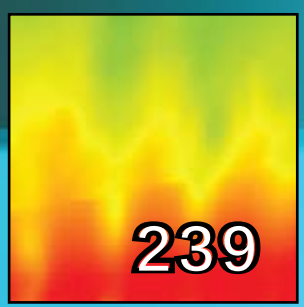

235
The DIME/PMESII Model Suite Requirements Project
R. Hillson

239
Simulation of Supersonic Military Aircraft Jet Noise
K. Kailasanath, J. Liu, and R. Ramamurti

241
Numerical Modeling of Plasmas Using the TurboWAVE Framework
D.F. Gordon, P. Sprangle, A.C. Ting, R. Fernsler, M. Lampe, S. Slinker, and B. Hafizi

The DIME/PMESII Model Suite Requirements Project

R. Hillson
Information Technology Division

Introduction: By necessity and doctrine, the projection of "soft power" is becoming increasingly important to the U.S. Department of Defense. The elements of soft power are often abstracted as *Diplomatic, Information, Military,* and *Economic* (DIME) actions and their *Political, Military, Economic, Social, Information,* and *Infrastructure* (PMESII) effects. DIME/PMESII spans the range of operations other than combat, including humanitarian aid, disaster relief, and non-combatant evacuation operations (Fig. 1(a)).[1] DIME/PMESII operations are complex, with unpredictable effects and interactions. Under sponsorship of the Office of the Secretary of Defense, the Naval Research Laboratory (NRL) Adversarial Modeling and Exploitation Office (Code 5508) has completed an initial effort to document the requirements for an integrated suite of models to forecast the effects of DIME actions on the PMESII variables.[2,3] Also considered are the effects of DIME actions on the *Funding*, *Recruitment*, *Information*, and *Support* (FRIS) systems of non-state actors.[4] This proposed model suite would assist stakeholders in selecting appropriate mixtures of strategies for DIME/PMESII missions, and in planning for the acquisitions required to support such missions. We have also attempted to identify gaps and deficiencies within the domain of available models and their implementations, to provide direction for future research.

DIME/PMESII Requirements: Two types of model requirements were identified: 1) descriptive requirements (DRs) and 2) architectural or framework requirements.[2] The former define the kinds of DIME actions and PMESII effects that the models and simulations should represent. The latter define the requirements for a software framework and its possible architectural realizations, and are not discussed further here. The DRs specify "what" is to be done rather than "how" to do it, and do not suggest any specific algorithms or models.

Descriptive Requirements: The DRs attempt to articulate the ingredients necessary to represent DIME/PMESII features and processes. The requirements are indexed by category — DIME *actions* and PMESII/FRIS *effects* — and take into account *actor*, *context*, and *entity/organization* (Figs. 1(b,c)). The DRs were derived using a technical approach that combines a military scenario-based activities analysis and a definitional-based noun taxonomy development (Fig. 2(a)). Each DR has a title, a descriptive phrase referred to as a *task statement* (Fig. 2(b)), and a list of task-specific *nouns* and *actions*. Two examples follow:

Descriptive Requirement A-D-9 (Action-Diplomatic-9):
Title: Refugee Assistance
Task Statement: The model suite will reflect actions associated with refugee assistance, and the effect those actions have on diplomatic efforts with the multinational community as measured across the PMESII elements.
Nouns: refugee, encampment, security, repatriation, sanitary facilities, food distribution,…
Actions: provide, secure, repair, construct,…
Action Links: Logistics, Refugee Info, Refugee Repatriation,…

Descriptive Requirement I-IS-1 (Impact-Infrastructure-1):
Title: Restoration of Essential Public Services
Task Statement: The model suite will reflect military actions to restore/provide public service utilities to the host nation population, and the effect those military actions have as measured across the PMESII elements.
Nouns: utilities, public services, capacity,…
Actions: restore, provide,…
Action Links: Consequence Management, Humanitarian Assistance, Non-combatant Evacuation Operation, Foreign Internal Defense,…

Measures of Merit: Representative *Measures of Merit* (MoMs) are defined for the descriptive requirements (Fig. 3(a)). Among these, *Measures of Action* (MoAs) and *Measures of Performance* (MoPs) describe the characteristics and target behavior of mission systems with respect to pre-defined criteria. *Measures of Effectiveness* (MoEs), in contrast, are mission-specific, and measure how effectively the mission is being executed. If a humanitarian aid task is to restore public facilities, an MoP might measure how many gallons per day of potable water is being produced relative to a facility's known production capability, while an MoE might measure whether sufficient potable water for physiological and medical purposes is being successfully purified and distributed to specific populations at specific locations.

Applying the Descriptive Requirements: The DR set is representative, open, and extensible. It provides a starting point for assessing the capabilities of existing models, and for identifying research areas that may require the development of new models. Assume that a suite of models has been built and/or acquired that partially spans the DR set. A stakeholder would first select a set of DRs that span the domain of the projected DIME/PMESII mission, and would then select and run a subset of models that best address the descriptive requirements selected. Figure 3(b) illustrates the complete modeling process.

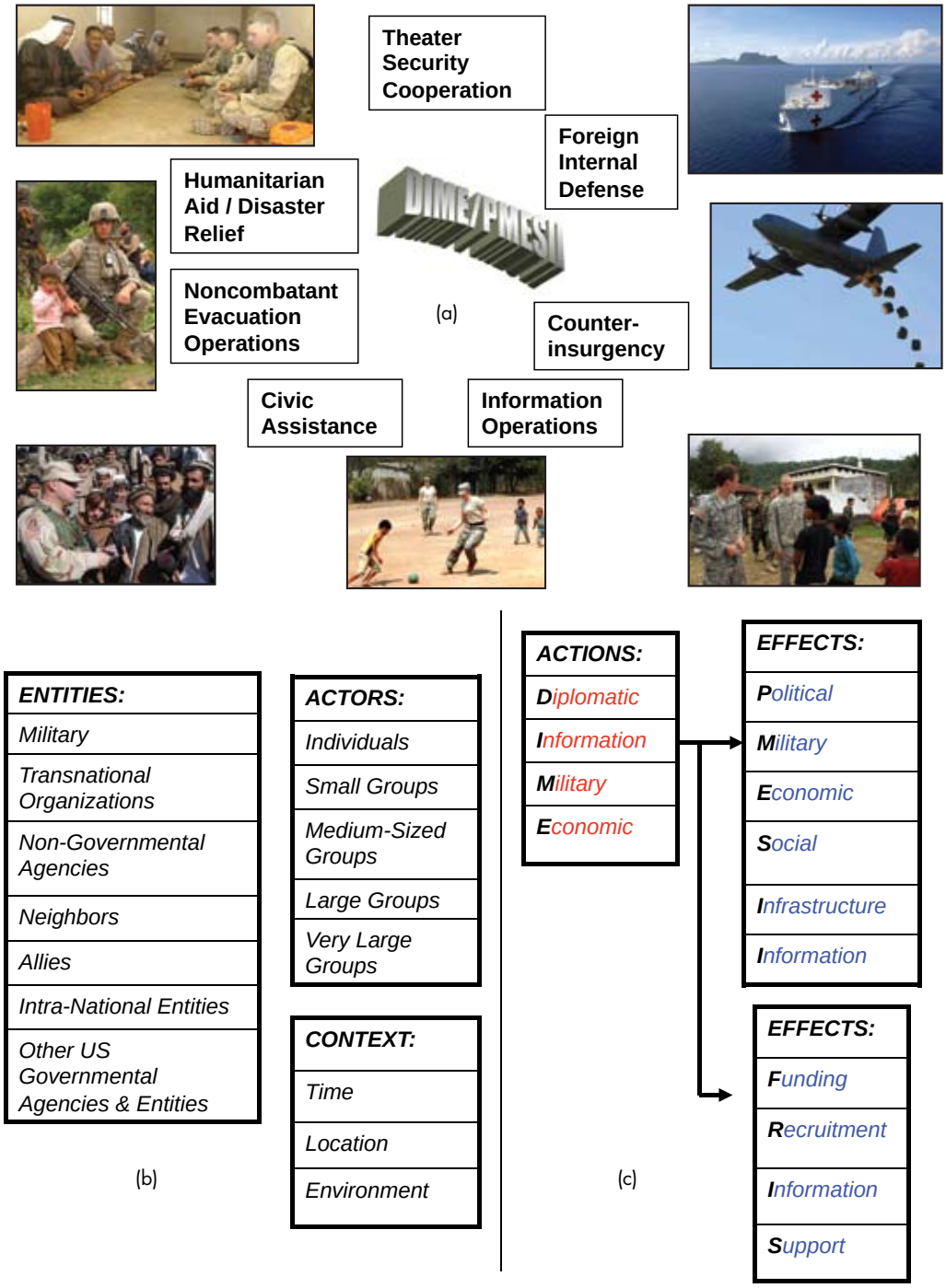

FIGURE 1
(a) DIME actions and PMESII effects span the entire range of military operations other than combat. (b) DIME/PMESII may involve both military and non-military entities and actors. (c) In the descriptive requirements developed for a proposed DIME/PMESII modeling and simulation suite, the PMESII effects have been augmented by the FRIS effects.

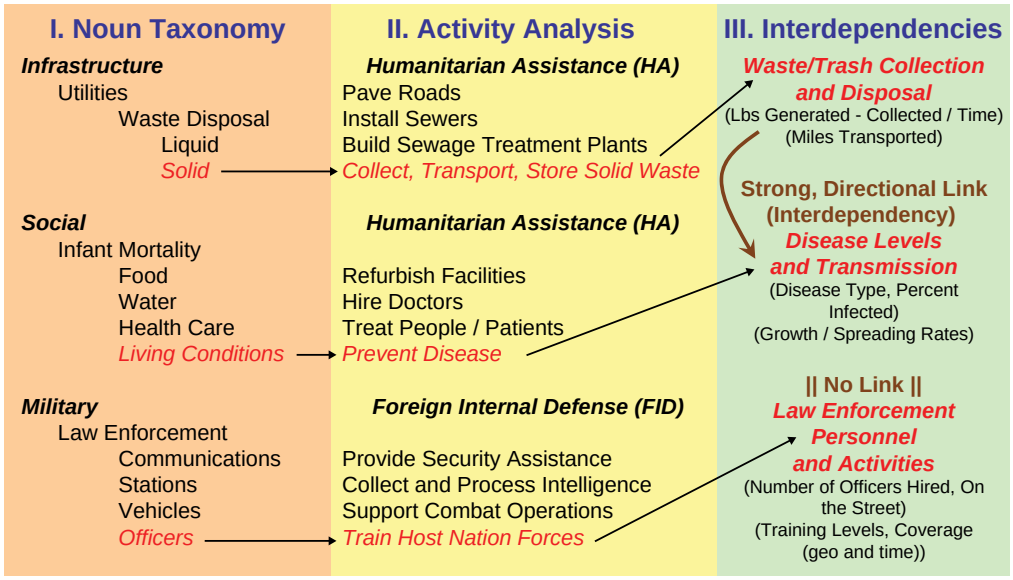

(a)

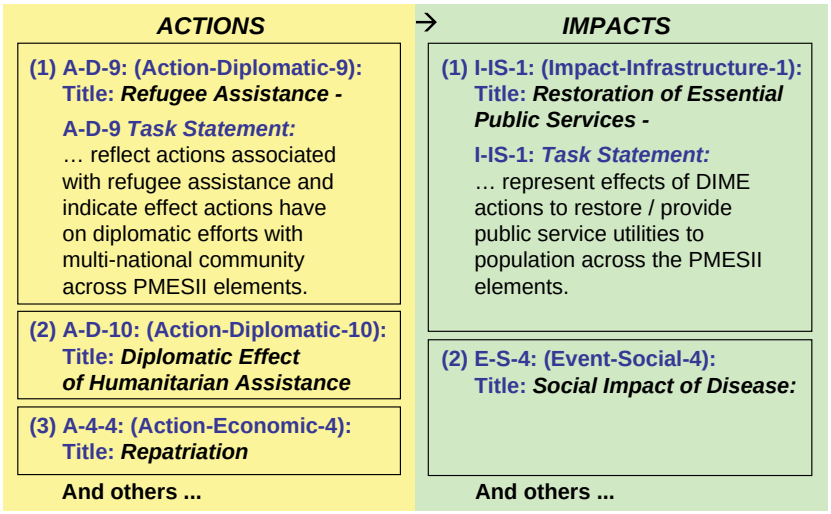

(b)

FIGURE 2
(a) Nouns, activities, and interdependencies related to the descriptive requirement I-IS-1 (Impact-Infrastructure-1, *Restoration of Essential Public Services*) for two concurrent DIME/PMESII missions, Humanitarian Aid (HA) and Foreign Internal Defense (FID). Each DR lists *Nouns* and *Actions* relevant to the requirement. *Interdependencies* may exist between different types of actions. *Restoration of Essential Public Services* will affect the *Infrastructure*, *Social* structure, and the host nation *Military*. There is a clear interdependency between the adequacy of waste disposal and the level of disease, but neither type of activity is linked to law enforcement. (b) To model a humanitarian aid (HA) mission, simulations must be developed and run that satisfy diverse descriptive requirements, many of which are interconnected. In this example, three representative descriptive requirements for modeling HA actions are mapped onto two representative requirements for modeling the HA impacts.

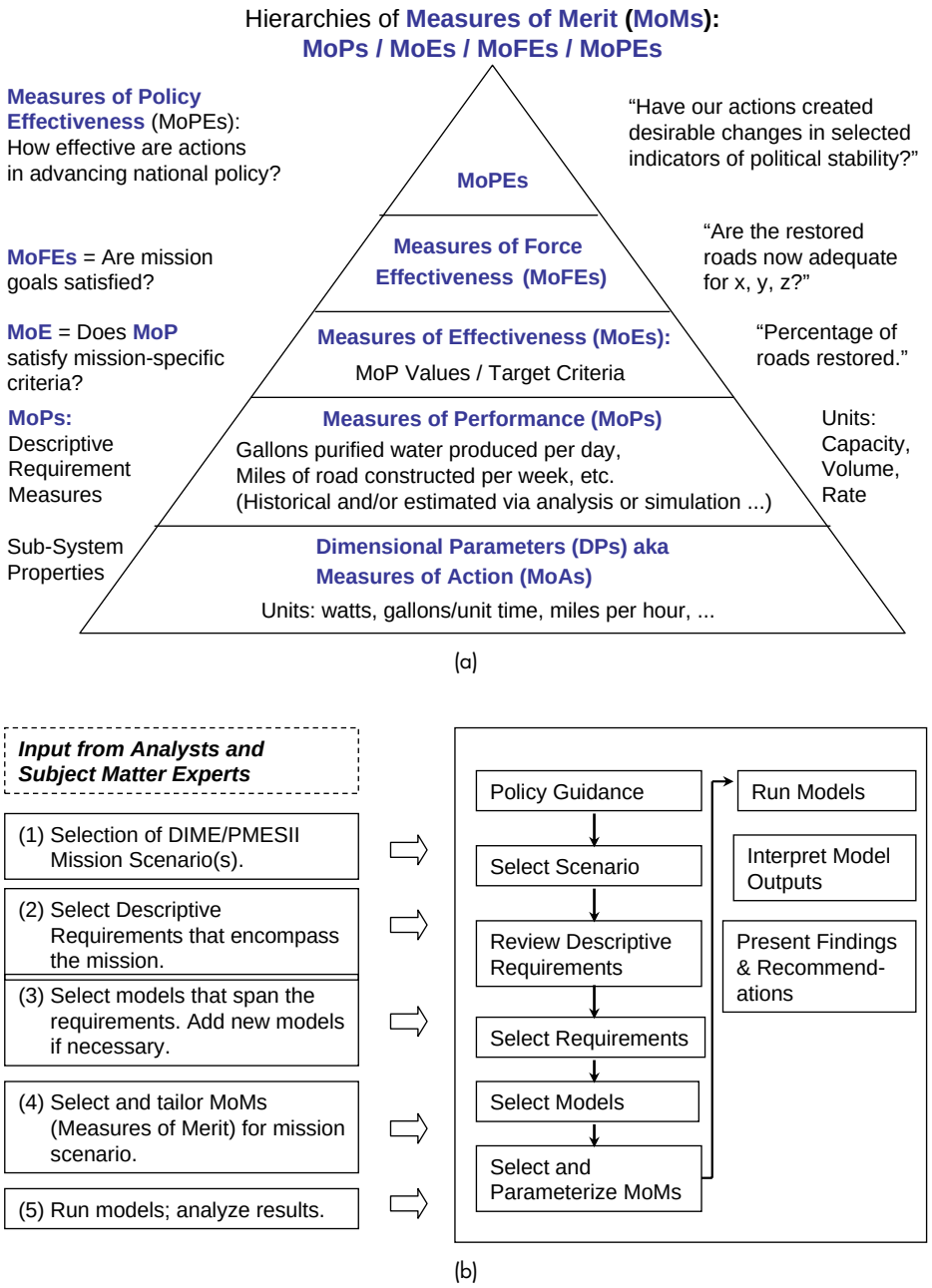

FIGURE 3
(a) The DIME/PMESII descriptive requirements include representative Measures of Merit. Measures of Action (MoAs) and Measures of Performance (MoPs) can be completely defined a priori, but Measures of Effectiveness (MoEs) are mission-specific, and cannot be completely defined in advance of the mission specification. (b) The DIME/PMESII-FRIS modeling process.

Gaps and Deficiencies: Hundreds of DIME/PMESII models exist. In this study, we were able to contrast and compare the properties of a small subset of existing models against the descriptive requirements and the framework requirements.[2] We provisionally identified certain gaps and deficiencies in the current model domain, although we did not attempt to rank these. Notable gaps include the following:

Lack of model integration scheme. Integration of several models is required to richly represent the complexity and interdependencies of the DIME/PMESII problem space. Each model may have its own formats for internal data representation, but the models must be capable of exchanging diverse data types transparently, while interpreting the data accurately within each model. To facilitate this, flexible middleware capable of bridging together any arbitrary collection of models is required.

Absence of models that cover the full range of military activities (Fig. 1(a)). The military operations that are typically modeled represent the realm of conflict. Modeling of other specific operations such as the effectiveness of the training of host nation security forces by U.S. military personnel, or the effects of U.S. operations to provide for infrastructure security are currently not modeled.

Lack of "return on investment" (ROI) assessment. Current DIME/PMESII models provide sophisticated projections of "possible futures." What is lacking is a model, or methods, that will permit us to confidently relate these possible futures to quantitative predicted changes in indicators that are historically correlated with desirable outcomes — for example, increases in the legitimacy and effectiveness of a host nation's government performance.[5] This capability would permit us to compare the relative cost effectiveness of different proposed combinations of DIME actions, while allowing for constraints imposed by budget, schedule, and mission. In summary, a complete ROI approach would let us design experiments to (1) systematically alter different combinations of model input parameters and (2) observe the correlations, both positive and negative, in the contingent forecasts (possible futures) in the solution space.

Summary: The U.S. military is playing an increasing role as a co-provider of humanitarian aid and civic services, as well as being tasked with additional non-combat roles in support of national policy. NRL has written top-level requirements for the development of an integrated suite of DIME/PMSEII models to assist in planning these kinds of missions. This work has resulted in descriptive requirements, framework requirements, a comparison of a small set of existing model capabilities with respect to the descriptive requirements and framework requirements, proposed measures of effectiveness, sample scenario analysis, and gaps and deficiencies analysis. NRL's efforts provide a roadmap for evaluating current and future developments in this area.

Acknowledgments: Many individuals have contributed to this effort. Particular thanks is due to Myriam Abramson, David Armoza, and Ruth Willis (NRL); Doug Clark and Ted Woodcock (Gard Associates), Ivar Oswalt and Robert Tyler (Visitech), Steve Kasputis (Reallaer); and Jerry Smith, William Young, Trena Lilly, and Virginia Robbin Beall (OPNAV N81).

[Sponsored by OPNAV N81]

References

[1] DoD Directive Number 3000.05, "Military Support for Stability, Security, Transition, and Reconstruction (STTR) Operations," 28 November 2005; Number 3000.07, "Irregular Warfare (IW)," 1 December 2008; Number 2205.2, "Humanitarian and Civic Assistance (HCA) Activities," 2 December 2008.

[2] "DIME/PMESII Requirements Project," Final Report, submitted by the Naval Research Laboratory to OPNAV N81, December 2008.

[3] NSAD-R-08-016, "Naval Research Laboratory (NRL) Diplomatic, Information, Military, Economic (DIME) Political, Military, Economic, Social, Information, Infrastructure (PMESII) Modeling Requirements Workshop, held 5 December 2007 - Final Report," prepared by National Security Analysis Department, Johns Hopkins University Applied Physics Laboratory. For Official Use Only (FOUO).

[4] Kris A. Arnold, *PMESII and the Non-State Actor: Questioning the Relevance*, School of Advanced Military Studies, Ft. Leavenworth, Kan., 25 May 2006.

[5] U.S. Agency for International Development (USAID), "Measuring Fragility: Indicators and Methods for Rating State Performance," prepared for USAID by ARD, Inc., June 2005.

Simulation of Supersonic Military Aircraft Jet Noise

K. Kailasanath, J. Liu, and R. Ramamurti
Laboratory for Computational Physics and Fluid Dynamics

Background: There is a growing need to reduce significantly the noise generated by high-performance, supersonic military aircraft. The noise generated during takeoff and landing on aircraft carriers has direct impact on shipboard health and safety issues. Also, noise complaints are increasing as communities move closer to military bases or when there are changes due to base closures and realignment. There is a significant amount of literature dealing with noise reduction in civilian, subsonic aircraft; some of the techniques found effective for those aircraft might be applicable for supersonic military jets. A distinct difference between civilian aircraft engines and advanced military

aircraft engines is that military engines tend to have low bypass ratios and high velocities. During certain flight conditions — such as during takeoff or landing — the exhaust from these engines tends to be non-ideally (under/over) expanded. Non-ideally expanded exhaust flows contain shock cells in the jet exhaust, causing high-amplitude screech tones and broadband shock-associated noise, components that increase the overall noise level. Therefore, our current research is focused on understanding these non-ideally expanded exhaust flow conditions and characterizing the noise sources, so that noise reduction techniques may be successfully pursued.

Approach: A monotonically integrated large-eddy simulation (MILES)[1] approach has been developed at NRL to simulate computationally the flow dynamics and near-field acoustics of supersonic jet exhaust flows. A finite-element flow solver[2] using unstructured grids allows us to model the jet exhaust nozzle geometry accurately, and the MILES approach directly computes the large-scale turbulent flow structures. No explicit subgrid scale model is used and the modeling of the subgrid scales is implicitly provided by the embedded flux limiter in this approach.

Numerical simulations can play a significant role in the test and evaluation of various noise reduction concepts, but for the results of the simulations to be credible, they need to be compared to and evaluated against relevant experimental data. The experimental conditions should include geometries and flow conditions that are representative of realistic engine configurations and operating conditions. The simulations in this study were compared to experimental data obtained at the University of Cincinnati (UC).[3]

The jet exhaust nozzle geometries used in this research are representative of realistic engine nozzles in use on military aircraft and were designed by GE Aircraft Engines. These nozzles do not have smoothly varying contours. Instead, they are convergent-divergent nozzles: they typically have a conical converging section, a sharp throat, and a conical diverging section, a design which allows the area ratio (ratio of the area at the throat to the area at the exit of the nozzle) to be changed in flight to adapt to local conditions and thrust requirements.

Numerical Simulations of the Flow Field and Noise: Monotonically integrated large-eddy simulations of imperfectly expanded jet flows from a convergent-divergent nozzle with a design Mach number of 1.5 were carried out. Total pressure ratios ranging from over-expanded to under-expanded jet conditions were investigated. A typical computed flow field from the nozzle exhaust is shown in Fig. 4. The quantity depicted in the figure is the non-dimensional density (non-dimensionalized using the background ambient density). Key features of the flow field are also identified. Results showed that spacing of the shock cells and the length of the potential core (an indicator of jet mixing) increased as the total pressure ratio increased, and these results were in good agreement with experimental data from UC. The good agreement suggests that the computations are resolving the details observed in the laboratory experiments.

In principle, no shocks or other pressure waves are expected at the design condition. Unexpectedly, weak shock cells were observed at the design condition. Experiments confirmed this observation. Results from the simulations have identified the cause of these waves to be the sharp contraction at the nozzle throat. Hence, these studies suggest that the flow fields from realistic military engine nozzles are not likely to be shock-free under any operating condition.

Comparison of the Noise Spectra: Near-field sound pressure level (SPL) spectra at various locations in the exhaust flow were calculated and compared with the experimental measurements at UC. A screech tone was observed in both experiments and simulations, and both the intensity and frequency were in good agreement between the numerical predictions and the

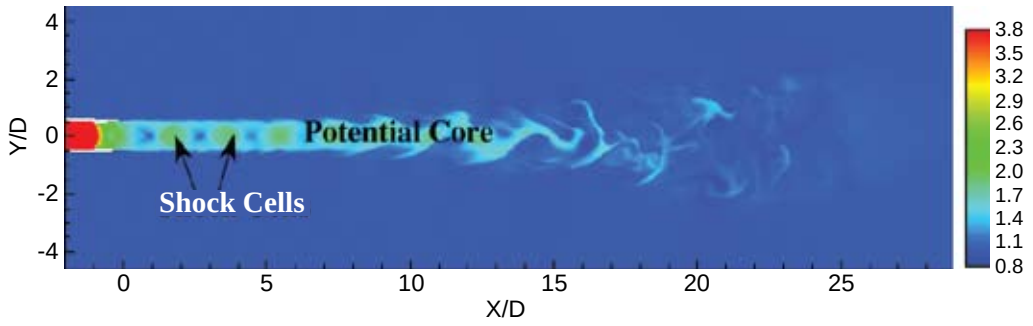

FIGURE 4
Normalized density distribution showing the key features of the computed flow field from the exhaust nozzle of a supersonic jet.

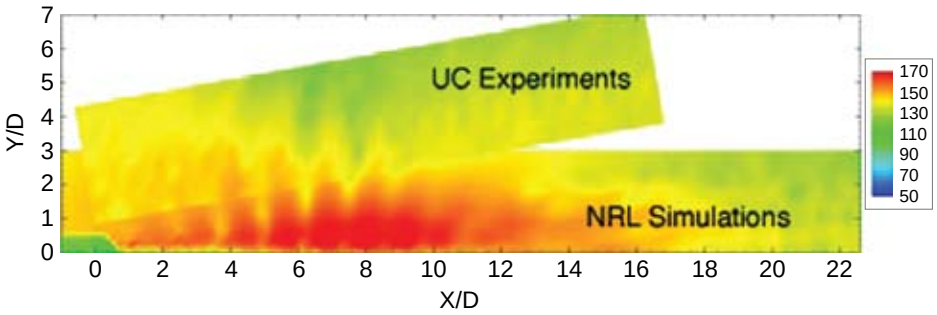

FIGURE 5
Sound pressure levels from the exhaust nozzle of a supersonic jet: comparison of simulations and experimental data. The axial (X/D) and radial (Y/D) distances are non-dimensionalized by the jet diameter (D) at the nozzle exit.

experimental measurements (see Fig. 5). The good agreement highlights the complementary nature of the two approaches. Since it is difficult to measure sound pressure level inside the jet experimentally without modifying the jet, measured data from inside the jet is not available. In the simulation, the fine grid (used for resolving the details of the flow) is restricted to a region close to the nozzle exit due to the limitations of current computer resources (it would be prohibitively expensive to grid the entire flow flow field using the fine grid). Therefore, the direct overlap between the computed region and the region where detailed measurements were taken is small. However, the transition between the results from the simulations and those from the measurements is almost flawless (as seen in Fig. 5) and shows that the two approaches together can produce a more complete picture of the noise field than can be obtained by either approach alone. Further analysis of the results has provided new insight into the sources of jet noise and has been reported elsewhere.[3]

Concluding Remarks: Our simulations were able to accurately describe the flow field and noise from supersonic military aircraft jets. The excellent agreement shown between the results of our simulations and the measurements made at the University of Cincinnati indicates that such experiments and simulations can play complementary roles in the investigation of noise generation from supersonic jet flows. This was the first step in a multi-year effort. After this successful initial step to validate the computational methodology and characterize the noise sources, work on specific noise reduction techniques has begun.

Acknowledgments: This research was sponsored by the Strategic Environmental Research and Development Program (SERDP) and the NRL 6.1 Computational Physics Task Area. The authors are grateful to Prof. Ephraim Gutmark from the University of Cincinnati for sharing the experimental data and general insights into nozzle flow and acoustics. We also thank Prof. Rainald Lohner from the George Mason University for help with the FEFLO computer code.

[Sponsored by SERDP and NRL]

References

[1] F.F. Grinstein and C. Fureby, "On Monotonically Integrated Large Eddy Simulation of Turbulent Flows Based on FCT Algorithms," Ch. 3 in *Flux-Corrected Transport: Principles, Algorithms, and Applications*, eds. D. Kuzmin, R. Löhner, and S. Turek (Springer, 2005), pp. 79–104.

[2] R. Lohner, "FEM-FCT: Combining Unstructured Grids with High Resolution," *Communications in Applied Numerical Methods* 4, 717–729 (1988).

[3] J. Liu, K. Kailasanath, D. Munday, and E. Gutmark, "Investigation of Near-Field Acoustic Properties of Imperfectly Expanded Jet Flows Using LES," AIAA Paper 2009-0015, presented at the 47th AIAA Aerospace Sciences Meeting, Orlando, Florida, Jan. 5–8, 2009.

Numerical Modeling of Plasmas Using the TurboWAVE Framework

D.F. Gordon,[1] P. Sprangle,[1] A.C. Ting,[1] R. Fernsler,[1] M. Lampe,[1] S. Slinker,[1] and B. Hafizi[2]
[1]*Plasma Physics Division*
[2]*Icarus Research, Inc.*

Introduction: The turboWAVE framework is a set of software modules used for simulating a wide range of phenomena involving plasmas. Plasma physics arises in several research areas of interest to the Navy, including ultra-intense laser propagation in air, guided electrical discharges, and advanced accelerators. The approach used to model a plasma can differ greatly from one problem to the next because of the variety of scales, geometries, and physical processes that are important in each case. For example, particle models are useful for accelerators, while fluid models are useful for discharges. In virtually all cases, the need for high performance computing eventually arises. The turboWAVE framework is designed to simulate a variety of

physical systems using the massively parallel architectures that are likely to be available in the near term, including those currently provided by the Department of Defense High Performance Computing and Modernization Program (DoD-HPCMP).

Framework Description: One of the key elements of the turboWAVE framework is the facility for parallel processing. This facility is built on a set of C++ classes which support domain decomposition with respect to fields and particles. The framework also provides classes that are useful for extracting information from large datasets, and writing out diagnostic files in a parallel environment. The framework provides a variety of numerical algorithms, such as electromagnetic field solvers, rapid elliptical solvers, fluid advection routines, particle pushers, and others. These are all designed to work in any number of dimensions, and in some cases are able to function in multiple coordinate systems.

Advanced Accelerators: The turboWAVE modules that implement the particle-in-cell (PIC) technique are designed to model advanced accelerator concepts such as the Laser Wakefield Accelerator (LWFA). The LWFA uses an ultra-intense laser pulse to drive a plasma wave, which can be used to accelerate electrons. Due to the extreme electric fields produced in the plasma wave (GV/cm), the length of the accelerator can be orders of magnitude shorter than a conventional accelerator of the same energy scale. TurboWAVE models such accelerators using a fully electromagnetic field solver coupled to a fully relativistic particle pusher. It includes an optional optimization called the ponderomotive guiding center algorithm,[1] which averages over optical periods. Figure 6 shows data from a turboWAVE simulation in which a 2-TW, 50-fs laser pulse is focused into a plasma with an electron density of about 10^{18} cm^{-3}. The data is a volumetric rendering of the scalar potential associated with the relativistic plasma wave driven by the laser radiation. Structures of this type, which are in motion at nearly the speed of light, can trap and accelerate electrons from either the background plasma or an external source. The accelerated spectra observed in turboWAVE have been shown to agree with those observed in experiments at NRL.[2,3]

Laser Guided Discharges: The turboWAVE modules that solve the hydrodynamic equations for a multi-species plasma are collectively called SPARC (Streamer Propagation and ARCing). These modules are designed primarily for modeling laser guided discharges and laser heated air plasmas. A laser guided discharge uses the plasma filament formed in ambient air by a femtosecond laser pulse as a conducting path which guides an electrical discharge in a chosen direction. Simulating this phenomenon involves electrostatics, air chemistry, and hydrodynamics. The space and time scales involved span orders of magnitude, so specialized algorithms, such as an adaptive grid, are needed to make the simulations practical. A SPARC simulation of streamer propagation is shown in Fig. 7. A streamer consists of an elongated body of plasma immersed in an electric field. The field at the tip of the streamer is larger than the ambient field due to field enhancement. This enhanced field causes avalanche ionization which further elongates the streamer. In Fig. 8, the time evolution of a laser heated air plasma is shown. Initially, the electron density drops due to recombination and attachment. Later in time, as the electron and vibrational temperature increase, the electron density increases. Later still, molecules begin to dissociate.

Summary: The turboWAVE framework is a flexible foundation on which a diverse set of numerical codes can be built. Two codes that have been deployed

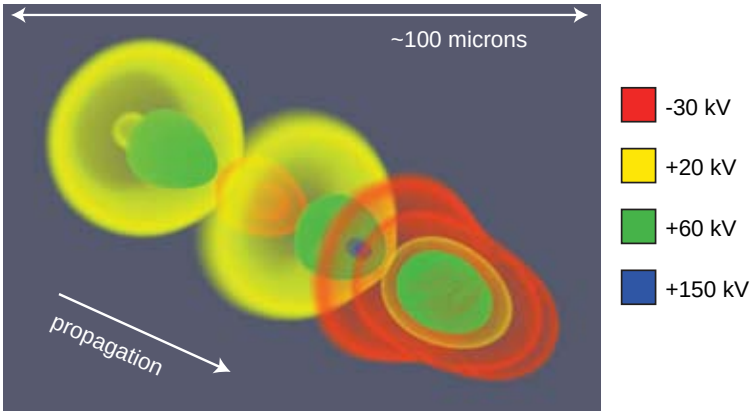

FIGURE 6
The scalar potential in a laser wakefield accelerator as computed by turboWAVE. The structure is in motion at the speed of light. The high potential gradients lead to the rapid acceleration of electrons to high energies.

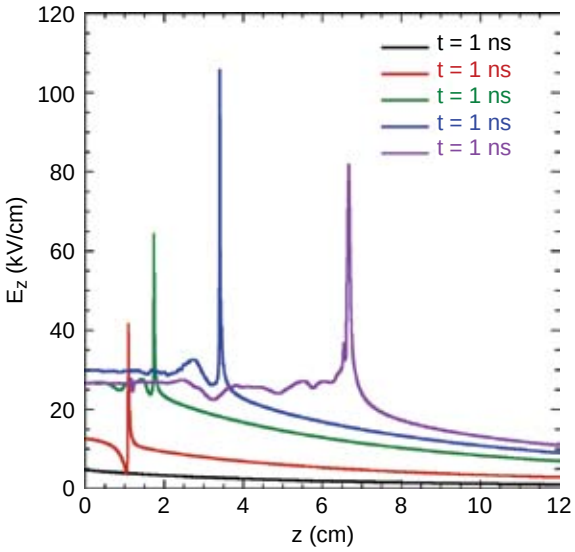

FIGURE 7
Axial electric field associated with a positive streamer driven by a linearly ramped voltage. The electrode is on the left, and the streamer propagates to the right. The large spikes are due to field enhancement at the streamer tip.

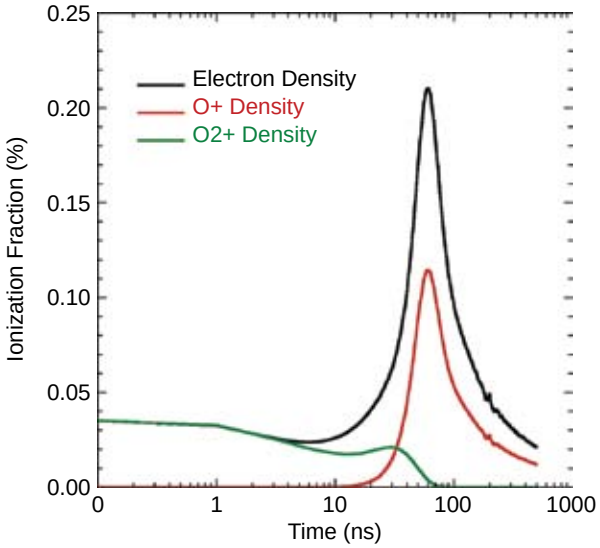

FIGURE 8
Enhancement of an air plasma by a 50-ns, 1-Joule laser pulse. As the air is heated, avalanche ionization overcomes the losses, and the electron density increases. Molecular dissociation can also be seen.

successfully at NRL are the turboWAVE particle-in-cell code for modeling advanced accelerators, and the SPARC hydrodynamics code for modeling laser guided discharges and laser heated air plasmas

[Sponsored by ONR and DOE]

References

[1] D.F. Gordon, "Improved Ponderomotive Guiding Center Algorithm," *IEEE Trans. Plasma Sci.* **35**, 1486–1488 (2007).

[2] A. Ting, D. Kaganovich, D.F. Gordon, R.F. Hubbard, and P. Sprangle, "Generation and Measurements of High Energy Injection Electrons from the High Density Laser Ionization and Ponderomotive Acceleration," *Phys. Plasmas* **12**, 010701-1–010701-4 (2005).

[3] D. Kaganovich, D.F. Gordon, and A. Ting, "Observation of Large-Angle Quasi-Monoenergetic Electrons from a Laser Wakefield," *Phys. Rev. Lett.* **100**, 215002-1–215002-4 (2008).

space research and satellite technology

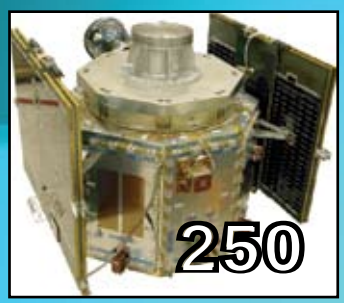

247
Laboratory Investigation of Near-Earth Space Plasma Processes
W.E. Amatucci, D.D. Blackwell, G.R. Gatling, G.I. Ganguli, C.D. Cothran, E.M. Tejero, D.N. Walker, and C.S. Compton

249
A New Class of Radio Halo
W.M. Peters and N.E. Kassim

250
Integration and Testing Challenges of the Operationally Responsive Space (ORS) Phase III Bus Standards Prototype
W.C. Raynor, T.J. Specht, W.R. Braun, E.A. Rossland, S.N. LaCava, M.S. Johnson, P.A. Stadter, C.T. Apland, J.R. Bruzzi, M.T. Marley, B.D. Williams, R.A. Denissen, and D.C. Bentz

Laboratory Investigation of Near-Earth Space Plasma Processes

W.E. Amatucci,[1] D.D. Blackwell,[1] G.R. Gatling,[1]
G.I. Ganguli,[1] C.D. Cothran,[2] E.M. Tejero,[2]
D.N. Walker,[2] and C.S. Compton[2]
[1]*Plasma Physics Division*
[2]*Global Strategies Incorporated*

Introduction: Energetic particles and plasma dynamics in the near-Earth space environment can significantly impact operation of both military and civilian systems. The underlying physical mechanisms relevant to two important space plasma issues, radiation belt dynamics and auroral ionospheric space weather, are under investigation in the NRL Space Physics Simulation Chamber (SPSC). Plasma conditions within this large laboratory device can be scaled to match key dimensionless parameters representative of ionospheric or magnetospheric regions of interest. Under scaled radiation belt conditions, Space Chamber experiments are addressing linear and nonlinear whistler wave propagation characteristics and wave-particle interactions. Under scaled auroral ionospheric conditions, the generation of electromagnetic ion cyclotron waves by sheared plasma flows and their impact on the dynamics and morphology of the geospace environment are being investigated. Additionally, Space Chamber research is directed at development of innovative diagnostic techniques for space and laboratory use.

Background: Both the military and civilian populations are increasingly dependent on space-based assets for uninterrupted operation of critical systems. The reliable operation of space-based assets, in turn, depends on many different physical aspects of the space plasma environment. For example, the operational lifetime of a satellite can be limited by the accumulated dose of high-energy electrons that form the Earth's highly dynamic radiation belts. In the natural environment, populations of high-energy electrons trapped and accelerated in the Earth's dipolar magnetic field can remain in stable, long-lived orbits. Such particles bounce back and forth between the poles, mirroring at altitudes above the Earth's neutral atmosphere. For those particles whose mirror point is at lower altitudes where the density of the neutral atmosphere is sufficiently high, collisions between neutrals and the electrons harmlessly precipitate the energetic particles.

The trapped high-energy electron populations are controlled to some degree by the interactions between naturally generated electromagnetic plasma waves and the energetic electrons. Such interactions scatter the energetic electrons from their stable orbits, which can lower their mirror point, leading to their precipitation into the atmosphere. In addition to natural waves, these particles can also be scattered by waves produced by Navy very low frequency (VLF) transmitters. Field experimental work on such wave-particle interactions has uncovered a wealth of interesting, unexplained phenomena. Among the most interesting are the nonlinear amplification of waves and triggered wave emissions at frequencies different from that of the transmitter. At present, these phenomena are not well understood, but appear to result from nonlinear interactions with the trapped radiation belt population itself.

At lower altitudes, in the auroral zones, ion cyclotron waves triggered by localized plasma flows can have significant impact on the dynamics and morphology of high-latitude ionospheric and magnetospheric plasmas. Broadband extremely low frequency waves are routinely observed by sounding rockets and satellites. These waves are often observed in conjunction with ion energization perpendicular to the magnetic field. The same force that causes mirroring of the energetic radiation belt electrons causes these heated ions to move to higher altitudes, allowing heavy, otherwise gravitationally bound ionospheric ions to become a major constituent of magnetospheric plasma. This chain of events resulting in a redistribution of the mass, energy, and momentum of ionospheric and magnetospheric plasma can affect near-Earth space weather processes. In addition, electromagnetic ion cyclotron waves created in this process can propagate to the magnetosphere, where they are an important secondary source of energetic radiation belt electron scattering and precipitation.

Current Research: The natural phenomena described above share some common space physics themes, namely, the transition from electrostatic to electromagnetic character of waves and the interaction of waves with plasma particles. These themes are being investigated in the SPSC, shown in Fig. 1. The SPSC is a state-of-the-art, large-scale laboratory plasma device dedicated to the study of near-Earth space plasma phenomena. Under conditions scaled to the inner radiation belt, electromagnetic whistler wave propagation and nonlinear wave-particle interactions are being investigated. Under conditions scaled to the auroral ionosphere, ion cyclotron wave generation and particle heating are being investigated. Both investigations are being coordinated with NRL theoretical and computational studies.

To simulate wave propagation in the radiation belt environment, various styles of whistler wave antennas have been developed and tested in order to efficiently produce a narrowband electromagnetic

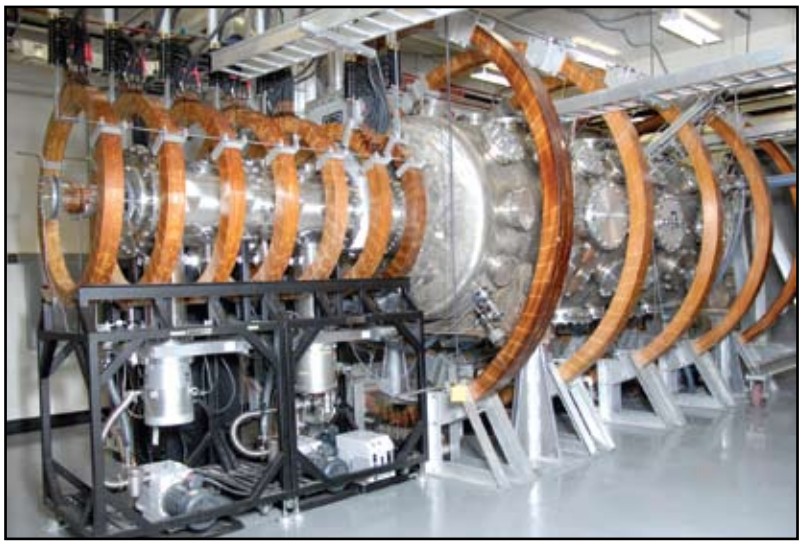

FIGURE 1
NRL Space Physics Simulation Chamber.

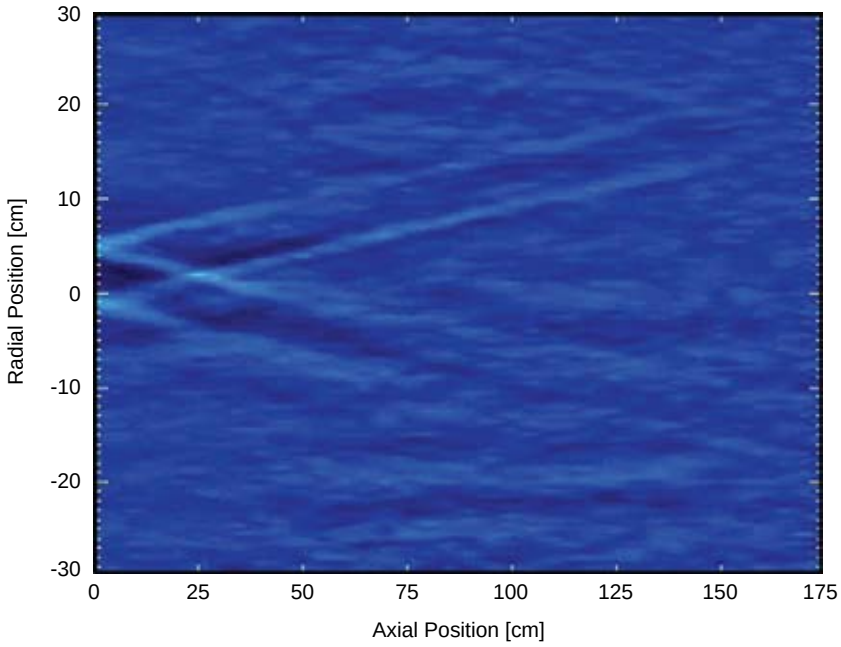

FIGURE 2
Whistler wave propagation in the Space Chamber plasma. A snapshot in time of a planar cut of electric field amplitude of a whistler wave launched from an antenna located at the left of the figure.

whistler wave spectrum, as shown in Fig. 2.[1,2] With the ability to control frequency and wave vector, the linear and nonlinear propagation characteristics have been investigated and compared to the cold-plasma dispersion relation. Transitions between the predominantly electrostatic lower hybrid wave and the predominantly electromagnetic whistler mode have been observed. A nonlinear transition from linear dispersive propagation to nonlinear self-ducted wave propagation, where the wave travels the length of the plasma column without loss, has also been observed. Current research is directed at the development of energetic electron sources and diagnostics. The characteristic residence time of the energetic electrons in a magnetic mirror configuration similar to the Earth's with and without whistler waves will be investigated, followed by studies of nonlinear interactions of the waves with the trapped electrons.

For studies of ionospheric space weather, the generation of electromagnetic ion cyclotron waves by structured quasistatic electric fields that form in the auroral zone are currently under investigation. NRL has led the theoretical and experimental study of ion cyclotron wave destabilization by such fields and has shown that they can lead to plasma energization and transport. In the laboratory, our goal is to investigate the transition from electrostatic to electromagnetic wave propagation, to determine the characteristics of the electromagnetic ion cyclotron waves, to document transverse ion heating and transport produced by such

waves, and to investigate any potential radiation belt electron scattering by these waves.

[Sponsored by ONR]

References

[1] W.E. Amatucci, D.D. Blackwell, D.N. Walker, G. Gatling, and G. Ganguli, "Whistler Wave Propagation and Whistler Wave Antenna Radiation Resistance Measurements," *IEEE Trans. Plasma Sci.* **33**, 637–646 (2005).

[2] D.D. Blackwell, D.N. Walker, S.J. Messer, and W.E. Amatucci, "Antenna Impedance Measurements in a Magnetized Plasma. I. Spherical Antenna," *Phys. Plasmas* **14**, 092105 (2007).

A New Class of Radio Halo

W.M. Peters and N.E. Kassim
Remote Sensing Division

Introduction: Galaxy clusters are the largest gravitationally bound systems in the Universe and their interactions via collisions and mergers are the most energetic events since the Big Bang. The gas in these systems is mixed with magnetic fields and relativistic particles, creating diffuse, megaparsec-scale synchrotron radiation at the cluster center which can be observed at radio wavelengths. Currently detected in only a fraction of known interacting clusters, this emission is called a radio "halo."

A team of scientists, including astronomers from the Naval Research Laboratory, has detected a radio halo at long wavelengths in a colliding, massive galaxy cluster; surprisingly, it is not detected at the shorter wavelengths where these objects are typically seen. The discovery implies that existing radio telescopes have missed a large population of these colliding objects; in fact it suggests a new class of radio halos. These halos could be uniquely studied at long radio wavelengths, using new, more sensitive telescopes currently being built, such as the NRL-conceived Long Wavelength Array (LWA).

Abell 521 Data: Abell 521 is a massive, X-ray luminous cluster involved in multiple ongoing mergers (Fig. 3). We have detected a long-wavelength (λ = 125 cm, 92 cm, 49 cm) radio halo associated with this cluster using the Giant Metrewave Radiotelescope (GMRT) in India. Observations using the National Science Foundation's Very Large Array (VLA) radio telescope at the shorter wavelengths typically used to observe radio halos (λ = 21 cm) were unable to detect it. Observations using the VLA at longer wavelengths (λ = 4 m; a system partly developed at NRL) lacked the sensitivity to detect the halo at its anticipated strength but were able to place a limit on the long-wavelength flux.

Scientific Importance: There are two theories for how the electrons are accelerated to produce radio halos. The turbulent re-acceleration theory posits that older electrons are re-accelerated by merger-induced turbulence to the energies necessary to produce the observed radio-synchrotron emission in the relatively weak cluster magnetic fields. The secondary injection theory generates the necessary energy from collisions between relativistic cluster protons and thermal particles in the intergalactic medium. Previous studies of radio halos have been unable to distinguish which mechanism is correct.

The multi-wavelength observations of Abell 521 (4 m, 125 cm, 92 cm, 49 cm, 21 cm) allow us to reconstruct its radio spectrum. The resulting spectrum has an extremely steep slope, implying a high-frequency (short-wavelength) cutoff in the emission. Such a result is inconsistent with a secondary origin of the relativistic electrons, but instead supports the theory that they were accelerated by turbulent acceleration.

This is the first observational evidence that has enabled us to distinguish between the two theoretical creation mechanisms for radio halos. It represents a step forward in our understanding of interacting galaxy clusters, which in turn play an important role in studies of dark matter and dark energy. If we take Abell 521 as a prototype system, it also suggests that many radio halos in the Universe should emit mainly at long wavelengths.

Importance to NRL Program: In order to properly analyze the radio data, we implemented and improved algorithms for long-wavelength, widefield imaging, radio frequency interference-excision, and ionospheric modeling, all goals of our ongoing 6.1 Advanced Research Initiative, Large Array HF/VHF Imaging. In addition to addressing these technical challenges and refining the software for addressing them, the basic research involved has helped to identify a new class of objects in the Universe that can be uniquely studied with planned instruments such as the LWA.

Acknowledgments: NRL participation on this project centered on reduction and interpretation of the VLA data. Non-NRL collaborators included G. Brunetti, R. Cassano, T. Venturi (INAF–Instituto di Radioastronomia, Italy), S. Giacintucci (INAF; Harvard-Smithsonian Center for Astrophysics), D. Dallacasa (Università di Bologna, Italy), G. Setti (INAF; Università di Bologna), W. D. Cotton (National Radio Astronomy Observatory), and M. Markevitch (Harvard-Smithsonian Center for Astrophysics). Basic research in radio astronomy at NRL is supported by 6.1 base funds.

[Sponsored by NRL and ONR]

FIGURE 3
Superimposed false-color images of the galaxy cluster Abell 521. The blue color represents hot gas typical of many galaxy clusters detected by the Chandra X-ray Observatory. The shape of the X-ray emission indicates that the cluster has undergone a recent collision or "merger event" that could generate turbulent waves. The red represents radio emission at 125 cm wavelength. The bright radio source on the lower left periphery of the X-ray gas is a separate source. The region of radio halo emission generated by turbulent waves is located at the center of the cluster, where the colors overlap.

References
[1] G. Brunetti et al., "A Low-frequency Radio Halo Associated with a Cluster of Galaxies," *Nature* **455**, 944–947, October 16, 2008.

Integration and Testing Challenges of the Operationally Responsive Space (ORS) Phase III Bus Standards Prototype

W.C. Raynor,[1] T.J. Specht,[1] W.R. Braun,[1] E.A. Rossland,[1] S.N. LaCava,[1] M.S. Johnson,[1] P.A. Stadter,[2] C.T. Apland,[2] J.R. Bruzzi,[2] M.T. Marley[2], B.D. Williams,[2] R.A. Denissen,[2] and D.C. Bentz[3]
[1]*Spacecraft Engineering Department*
[2]*The Johns Hopkins University/Applied Physics Laboratory*
[3]*Harris IT Services*

Introduction: On 25 April 2008 the Operationally Responsive Space (ORS) Phase III Bus Prototype spacecraft, being used for the TacSat-4 mission, was successfully bought off by the Director of Defense Research and Engineering (DDR&E), formerly the Office of Force Transformation, the sponsor of this major third phase of the four-phase Standard Bus Initiative. On 30 May 2008 the flight lithium-ion battery was formally delivered. These two events officially marked the completion of the prototype Bus and delivery to the TacSat-4 program. The objective of the Office of the Secretary of Defense's ORS Standard Bus Initiative is to develop and test bus standards and then transition them for acquisition. Ideally, one or two different types of spacecraft buses will support a variety of interchangeable payloads, to achieve the ORS goal of rapid integration, launch, and deployment of satellites in response to emerging needs. To achieve the modularity and responsiveness envisioned for an ORS system, standardized interfaces between, and potentially within, the buses, payloads, and boosters have to be developed and verified. This article presents the challenges of performing spacecraft electrical, mechanical, and system integration and testing (I&T) to develop and mature ORS bus standards in the absence of a payload.

ORS Phase III Bus Prototype Development: The Naval Research Laboratory (NRL) and The Johns Hopkins University/Applied Physics Laboratory (JHU/APL) jointly executed the Bus project, in collaboration with a large industry partnership known as the Integrated Systems Engineering Team (ISET). The main goals of Phase III were to develop ORS bus standards in an open environment, and to produce a prototype for flight experimentation.

TacSat-4 Mission: The prototype Bus and the Office of Naval Research (ONR)-sponsored communication experiment payload, COMMx, together form the key on-orbit space vehicle (SV) elements of the TacSat-4 mission (see Fig. 4). TacSat-4 is a Navy-led joint mission, with NRL as the Program Manager, to provide operationally relevant capabilities and to advance the state of ORS development in spacecraft bus standards, payload standards, long dwell orbits, dynamic tasking, and net-centric operations.

Spacecraft System Testing: For ORS, the basic test flow and philosophy is rapid integration of spacecraft bus to payload, followed by integration of space vehicle

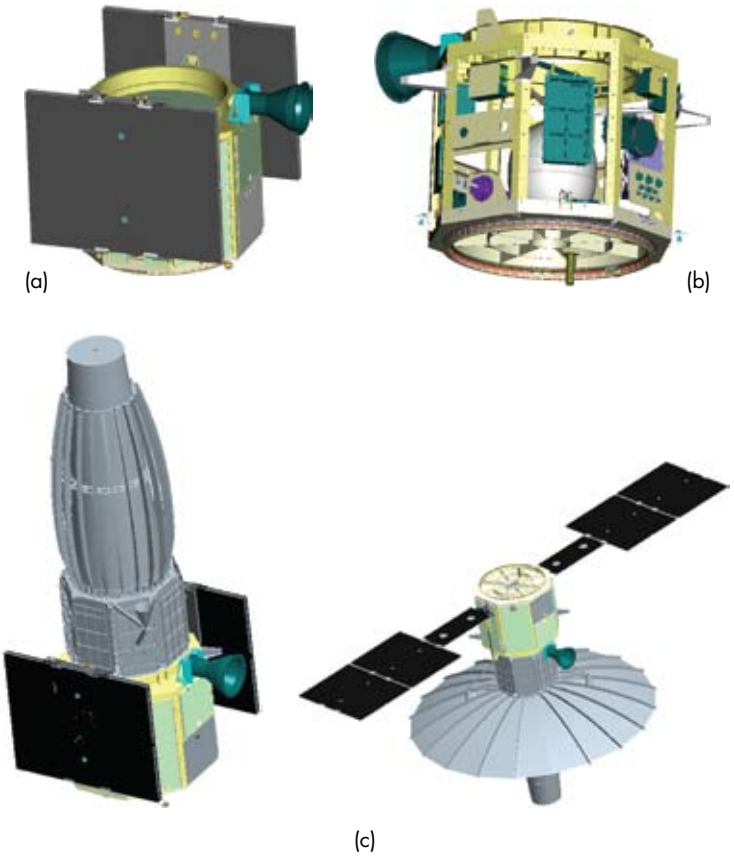

FIGURE 4
Prototype ORS spacecraft configuration: (a) and (b) spacecraft Bus component layout; (c) space vehicle configuration, stowed and deployed.

to launch vehicle (LV). This necessitates high-level "embedded" built-in-test capabilities for the spacecraft bus and payload, as well as standardized interfaces/connectivity to common ground test equipment. The ORS model mandates independent test programs for bus and payload, mandates that bus and payload developers sufficiently test interfaces to ensure minimal risk to mission success, and recommends use of simulators for validation of hardware and software interfaces and performance.

For the prototype Bus, assembly and initial system integration and testing were complete by December 2007. During the subsequent four months, the Bus underwent final system I&T consisting of physical alignments, EMI/EMC, solar array illumination and deployment mechanism release, mass properties, random vibration, and thermal vacuum (TVAC). Functional testing and flight software I&T were performed throughout the system I&T flow. Some of the tests are described here.

Mechanical Subsystem: Static loads and sine vibration testing of the primary bus structure were performed using payload mass simulators to verify the mechanical properties prior to subsystem integration (Fig. 5(a)). The system-level bus vibration test used another payload mass simulator (Fig. 5(b)). The SV-LV interface was also tested. The SV is integrated onto the LV with a motorized Lightband Separation System (LSS) that will deploy TacSat-4 from the LV once on-orbit. TacSat-4 is, to date, the largest-mass, highest center of gravity space vehicle utilizing the LSS. In addition to the standard static loads, random vibration, and TVAC tests, sine-sweep testing of the LSS was performed using a mass simulator representing the TacSat-4 SV (Fig. 5(c)). Specifically, the sine-sweep testing verified LSS stiffness and separation switch electrical performance. The sweeps were conducted bi-directionally (from 5 Hz to 100 Hz and back to 5 Hz) in all three axes to verify the absence of any stiffness non-linearities.

Thermal Subsystem: The ORS philosophy requires that the bus-payload interface be conductively isolated and the radiative effects minimized. Spacers made of G-10 (epoxy-impregnated glass fabric) provide the conductive resistance at the bus-payload interface (Fig. 6). TVAC testing was performed to verify this interface

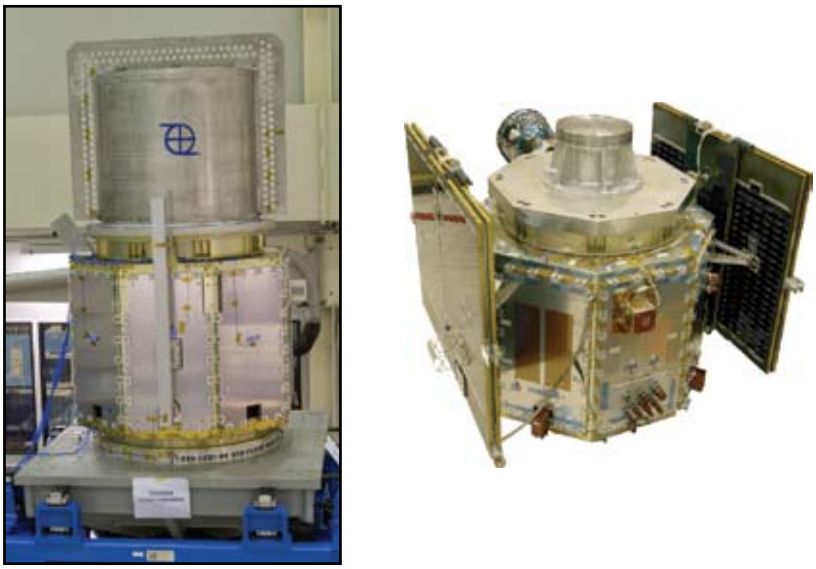

(a) (b)

(c)

FIGURE 5
Vibration test configurations: (a) primary structure with payload mass simulator, (b) Bus system, (c) Lightband Separation System with SV mass simulator.

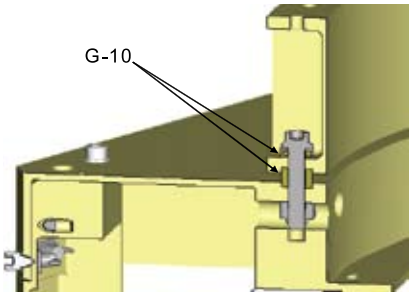

FIGURE 6
G-10 washers for thermal isolation at the bus-payload interface.

and to verify all subsystem performance over mission temperature extremes. A test heater plate simulated the extreme temperatures of the payload, and both sides of the interface were monitored to control the heat transfer between bus and payload and to validate the thermal design and implementation.

Command Telemetry and Data Handling (CT&DH) System: The flight software and CT&DH system underwent extensive integration and subsystem acceptance testing using test beds that stimulated all external command and data electronics (CDE) input interfaces and captured all CDE external output interfaces. The test beds provided flight equivalent electrical simulation of all interfaces, high fidelity simulation of the attitude control system components, medium fidelity simulation of the payload, and a high fidelity attitude and orbit dynamics simulation. At the system level, payload simulators allowed for validation of the bus-payload interface throughout the entire environmental test program. RS-422/HDLC and Spacewire interfaces were connected to payload simulators for all environmental tests. The payload simulator validated electrical characteristics, data protocols, and data transportation envelopes.

Telecommunications System: Standard RF ground support equipment (GSE) was able to support system operability of all RF functions during environmental tests. TacSat-4 mission design required that the second SGLS antenna be placed on the forward end of the COMMx antenna. Without the payload, the second RF path could not be tested in its entirety during Bus I&T. In the absence of this path, hard-wired GSE cables were used to achieve end-to-end telecommunications testing. Portions of the RF telecommunications path that reside on COMMx will undergo testing during SV I&T. The Bus I&T program modified RF power levels to account for the absence of the antenna and associated cables. When cables were unavailable or inappropriate for a given test, RF terminators were used to present a good match to the RF subsystem. See Fig. 7 for the RF block diagram. EMI/EMC testing was conducted on the standalone Bus. Of critical importance was the verification of emissions with specified payload susceptibility. Radiated emission excursions were identified and corrected.

Electrical Power System (EPS): Payload power simulators were used during the Bus test program to validate bus EPS components. A fixed load simulator was installed to validate critical bus feeds to the payload. Variable load simulators were installed to validate high power feeds to the payload. Illumination of the outer solar arrays was performed pre- and post-vibration test to verify function. During component-level testing, a temperature chamber malfunctioned and overheated the lithium-ion battery. The battery

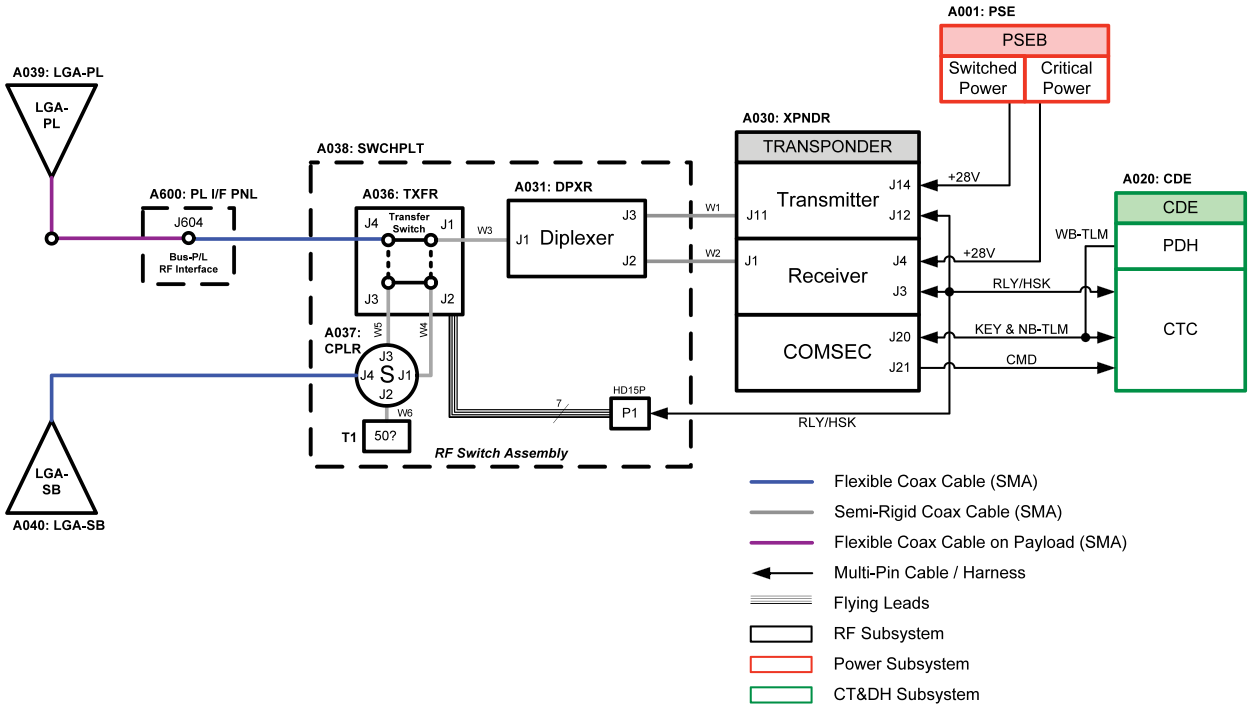

FIGURE 7
RF system block diagram.

had to be replaced, preventing it from entering Bus I&T, and a battery simulator was used in its absence. The standards requirement for the battery to be modular, specifically for rapid integration at the launch site, allowed I&T to be completed despite the malfunction.

Conclusion: The Bus and associated hardware and software underwent an innovative I&T process to verify and validate the critical bus/payload interface standards as defined by the ISET, with only three exceptions: SV-level magnetic dipole, EMI/RF, and command control performance tests. The combined space vehicle will validate these requirements. The Bus program and ISET efforts produced an extensive and well-documented set of standards and interfaces for cost-effective spacecraft systems for TacSat-4 class missions for the ORS initiative. Verification of the standards was a direct result of the Bus I&T process. Validation of these standards proceeded through the development of the Bus in an open manner that has allowed government and industry insight into challenging issues and subsequent successful implementation approaches.

[Sponsored by OSD-DDRE]

programs for professional development

277
Programs for NRL Employees — Graduate Programs, Continuing Education, Professional Development, Equal Employment Opportunity (EEO) Programs, and Other Activities

279
Programs for Non-NRL Employees — Recent Ph.D., Faculty Member, and College Graduate Programs, Professional Appointments, and College and High School Student Programs

PROGRAMS FOR NRL EMPLOYEES

The Human Resources Office supports and provides traditional and alternative methods of training for employees. NRL employees are encouraged to develop their skills and enhance their job performance so they can meet the future needs of NRL and achieve their own goals for growth.

One common study procedure is for employees to work full time at the Laboratory while taking job-related courses at universities and schools local to their job site. The training ranges from a single course to undergraduate, graduate, and postgraduate programs. Tuition for training is paid by NRL. The formal programs offered by NRL are described here.

GRADUATE PROGRAMS

• The **Advanced Graduate Research Program** (formerly the Sabbatical Study Program, which began in 1964) enables selected professional employees to devote full time to research or pursue work in their own or a related field for up to one year at an institution or research facility of their choice without the loss of regular salary, leave, or fringe benefits. NRL pays all travel and moving expenses for the employee. Criteria for eligibility include professional stature consistent with the applicant's opportunities and experience, a satisfactory program of study, and acceptance by the facility selected by the applicant. The program is open to employees who have completed six years of Federal Service, four of which have been at NRL.

• The **Edison Memorial Graduate Training Program** enables employees to pursue graduate studies in their fields at local universities. Participants in this program work 24 hours each workweek and pursue their studies during the other 16 hours. The criteria for eligibility include a minimum of one year of service at NRL, a bachelor's or master's degree in an appropriate field, and professional standing in keeping with the candidate's opportunities and experience.

• To be eligible for the **Select Graduate Training Program**, employees must have a Bachelor's degree in an appropriate field and must have demonstrated ability and aptitude for advanced training. Students accepted into this program devote three academic semesters to graduate study. While attending school, they receive one-half of their salary and benefits, and NRL pays for tuition and travel expenses.

• The **Naval Postgraduate School (NPS)**, located in Monterey, California, provides graduate programs to enhance the technical preparation of Naval officers and civilian employees who serve the Navy in the fields of science, engineering, operations analysis, and management. It awards a master of arts degree in national security affairs and a master of science degree in many technical disciplines. NRL employees desiring to pursue graduate studies at NPS may apply for a maximum of six quarters away from NRL, with thesis work accomplished at NRL. Participants continue to receive full pay and benefits during the period of study.

• In addition to NRL and university offerings, application may be made to a number of noteworthy programs and fellowships. Examples of such opportunities are the **Capitol Hill Workshops**, the **Legislative Fellowship (LEGIS) program**, the **Federal Executive Institute (FEI)**, the **Fellowship in Congressional Operations**, and the **Executive Leadership Program for Mid-Level Employees**. These and other programs are announced from time to time, as schedules are published.

• Research conducted at NRL may be used as **thesis material for an advanced degree**. This original research is supervised by a qualified employee of NRL who is approved by the graduate school. The candidate should have completed the required course work and should have satisfied the language, residence, and other requirements of the graduate school from which the degree is sought. NRL provides space, research facilities, and supervision but leaves decisions on academic policy to the cooperating schools.

CONTINUING EDUCATION

• **Undergraduate and graduate courses** offered at local colleges and universities may be subsidized by NRL for employees interested in improving their skills and keeping abreast of current developments in their fields.

• NRL offers **short courses** to all employees in a number of fields of interest including technical and administrative subjects, and supervisory and management techniques. Laboratory employees may also attend these courses at nongovernment facilities.

For further information on any of the above Graduate and Continuing Education programs, contact the Employee Relations and Development Branch (Code 1850) at (202) 767-6737 or via email at Training@hro.nrl.navy.mil.

• The **Scientist-to-Sea Program (STSP)** provides opportunities for Navy R&D laboratory/center personnel to go to sea to gain first-hand insight into operational factors affecting system design, performance, and operations on a variety of ships. NRL is a participant of this Office of Naval Research (ONR) program. Contact (202) 404-7635.

PROFESSIONAL DEVELOPMENT

NRL has several programs, professional society chapters, and informal clubs that enhance the professional growth of employees. Some of these are listed below.

• The **Counseling & Referral Service (C/RS)** helps employees to achieve optimal job performance through counseling and to resolve problems such as family and work-related stress and relationship difficulties, and behavioral, emotional, and substance use problems that may adversely impact job performance. C/RS provides confidential assessments and short-term counseling, training workshops, and referrals to additional resources in the community. Contact (202) 767-6857.

• The NRL **Women in Science and Engineering (WISE) Network** was formed in 1997 through the merger of the NRL chapter of WISE and the Women in Science and Technology Network. Luncheon meetings and seminars are held to discuss scientific research areas, career opportunities, and career-building strategies. The group also sponsors projects to promote the professional success of the NRL S&T community and improve the NRL working environment. Membership is open to all S&T professionals. Contact (202) 404-4389 or (202) 767-4697.

• **Sigma Xi**, The Scientific Research Society, encourages and acknowledges original investigation in pure and applied science. It is an honor society for research scientists. Individuals who have demonstrated the ability to perform original research are elected to membership in local chapters. The NRL Edison Chapter, comprising approximately 400 members, recognizes original research by presenting awards annually in pure and applied science to outstanding NRL staff members. The chapter also sponsors lectures at NRL on a wide range of scientific topics for the entire NRL community. These lectures are delivered by scientists from all over the nation and the world. The highlight of the Sigma Xi lecture series is the Edison Memorial Lecture, traditionally featuring a distinguished scientist. Contact (202) 404-8626.

• The **NRL Mentor Program** was established to provide an innovative approach to professional and career training and an environment for personal and professional growth. It is open to permanent NRL employees in all job series and at all sites. Mentorees are matched with successful, experienced colleagues having more technical and/or managerial experience who can provide them with the knowledge and skills needed to maximize their contribution to the success of their immediate organization, to NRL, to the Navy, and to their chosen career fields. The ultimate goal of the program is to increase job productivity, creativity, and satisfaction through better communication, understanding, and training. NRL Instruction 12400.1A provides policy and procedures for the program. Contact (202) 767-6737.

• Employees interested in developing effective self-expression, listening, thinking, and leadership potential are invited to join the Forum Club, a chapter of **Toastmasters International**. Members of this club possess diverse career backgrounds and talents and to learn to communicate not by rules but by practice in an atmosphere of understanding and helpful fellowship. NRL's Commanding Officer and Director of Research endorse Toastmasters. Contact (202) 404-4670.

EQUAL EMPLOYMENT OPPORTUNITY (EEO) PROGRAMS

Equal employment opportunity (EEO) is a fundamental NRL policy for all employees regardless of race, color, national origin, sex, religion, age, or disability. The NRL EEO Office is a service organization whose major functions include counseling employees in an effort to resolve employee/management conflicts, processing formal discrimination complaints, providing EEO training, and managing NRL's affirmative employment recruitment program. The NRL EEO Office is also responsible for sponsoring special-emphasis programs to promote awareness and increase sensitivity and appreciation of the issues or the history relating to females, individuals with disabilities, and minorities. Contact the NRL Deputy EEO Officer at (202) 767-2486 for additional information on any of their programs or services.

OTHER ACTIVITIES

• The award-winning **Community Outreach Program** directed by the NRL Public Affairs Office fosters programs that benefit students and other community citizens. Volunteer employees assist with and judge science fairs, give lectures, provide science demonstrations and student tours of NRL, and serve as tutors, mentors, coaches, and classroom resource teachers. The program sponsors African American History Month art and essay contests for local schools, student tours of NRL, and an annual holiday party for neighborhood children in December. Through the program, NRL has active partnerships with three District of Columbia public schools. Contact (202) 767-2541.

• Other programs that enhance the development of NRL employees include sports and theater groups and the **Amateur Radio Club**. The **NRL Recreation Club** encourages wide interest in sports for employees with its many facilities and programs, such as a heated indoor pool, hot tub, table tennis, basketball courts, recreation room, free weight room, new selectorized weight equipment, and volleyball courts. Sportswear and NRL and seasonal paraphernalia are available at the Recreation Club. The NRL Showboaters Theatre, organized in 1974, is "in the dark." Visit www.nrl.navy.mil/showboaters/Past_Productions.php for pictures from past productions such as Annie Get Your Gun, Gigi, and Hello Dolly. Contact (202) 404-4998 for Play Reader's meetings at NRL.

PROGRAMS FOR NON-NRL EMPLOYEES

Several programs have been established for non-NRL professionals. These programs encourage and support the participation of visiting scientists and engineers in research of interest to the Laboratory. Some of the programs may serve as stepping-stones to federal careers in science and technology. Their objective is to enhance the quality of the Laboratory's research activities through working associations and interchanges with highly capable scientists and engineers and to provide opportunities for outside scientists and engineers to work in the Navy laboratory environment. Along with enhancing the Laboratory's research, these programs acquaint participants with Navy capabilities and concerns and provide a path to full-time employment.

RECENT PH.D., FACULTY MEMBER, AND COLLEGE GRADUATE PROGRAMS

• The **National Research Council (NRC) Cooperative Research Associateship Program** selects associates who conduct research at NRL in their chosen fields in collaboration with NRL scientists and engineers. The tenure period is two years (renewable for a possible third year).

• The **NRL/ASEE Postdoctoral Fellowship Program**, administered by the American Society for Engineering Education (ASEE), aims to increase the involvement of highly trained scientists and engineers in disciplines necessary to meet the evolving needs of naval technology. Appointments are for one year (renewable for a second and possible third year).

• The **Naval Research Enterprise Intern Program (NREIP)** is a ten-week program involving NROTC colleges/universities and their affiliates. The Office of Naval Research (ONR) offers summer appointments at Navy laboratories to current sophomores, juniors, seniors, and graduate students from participating schools. Application is online at www.asee.org/nreip through the American Society for Engineering Education. Electronic applications are sent for evaluation to the point of contact at the Navy laboratory identified by the applicant. Students are provided a stipend of $5,500 (undergraduates) or $6,500 (graduate students).

• The American Society for Engineering Education also administers the **Navy/ASEE Summer Faculty Research and Sabbatical Leave Program** for university faculty members to work for ten weeks (or longer, for those eligible for sabbatical leave) with professional peers in participating Navy laboratories on research of mutual interest.

• The **NRL/United States Naval Academy (USNA) Cooperative Program for Scientific Interchange** allows faculty members of the U.S. Naval Academy to participate in NRL research. This collaboration benefits the Academy by providing the opportunity for USNA faculty members to work on research of a more practical or applied nature. In turn, NRL's research program is strengthened by the available scientific and engineering expertise of the USNA faculty.

• The **National Defense Science and Engineering Graduate Fellowship Program** helps U.S. citizens obtain advanced training in disciplines of science and engineering critical to the U.S. Navy. The three-year program awards fellowships to recent outstanding graduates to support their study and research lead-

ing to doctoral degrees in specified disciplines such as electrical engineering, computer sciences, material sciences, applied physics, and ocean engineering. Award recipients are encouraged to continue their study and research in a Navy laboratory during the summer.

For further information about the above six programs, contact (202) 404-7450.

PROFESSIONAL APPOINTMENTS

• **Faculty Member Appointments** use the special skills and abilities of faculty members for short periods to fill positions of a scientific, engineering, professional, or analytical nature at NRL.

• **Consultants and experts** are employed because they are outstanding in their fields of specialization or because they possess ability of a rare nature and could not normally be employed as regular civil servants.

• **Intergovernmental Personnel Act Appointments** temporarily assign personnel from state or local governments or educational institutions to the Federal Government (or vice versa) to improve public services rendered by all levels of government.

COLLEGE AND HIGH SCHOOL STUDENT PROGRAMS

The student programs are tailored to high school, undergraduate, and graduate students to provide employment opportunities and work experience in naval research. These programs are designed to attract applicants for student and full professional employment in fields such as engineering, physics, mathematics, and computer sciences. The student employment programs are designed to help students and educational institutions gain a better understanding of NRL's research, its challenges, and its opportunities.

Employment programs for college students include the following:

• The **Student Career Experience Program** (formerly known as the Cooperative Education Program) employs students in study-related occupations. The program is conducted in accordance with a planned schedule and a working agreement among NRL, the educational institution, and the student. Primary focus is on the pursuit of bachelor's degrees in engineering, computer science, or the physical sciences.

• The **Student Temporary Employment Program (STEP)** enables students to earn a salary while continuing their studies and offers them valuable work experience.

• The **Summer Employment Program** employs students for the summer in paraprofessional and technician positions in engineering, physical sciences, computer sciences, and mathematics.

• The **Student Volunteer Program** helps students gain valuable experience by allowing them to voluntarily perform educationally related work at NRL.

For additional information on these student programs, contact (202) 767-8313.

For high school students, the **DoD Science & Engineering Apprentice Program (SEAP)** offers students grades 9 to 12 the opportunity to serve for eight weeks as junior research associates in a DoD laboratory. Under the direction of a mentor, students gain a better understanding of the challenges and opportunities of research through participation in scientific programs. Criteria for eligibility are based on science and mathematics courses completed and grades achieved; scientific motivation, curiosity, and capacity for sustained hard work; a desire for a technical career; teacher recommendations; and achievement test scores. For additional information, contact (202) 767-2957.

general information

283
Technical Output

284
Key Personnel

285
Contributions by Divisions, Laboratories, and Departments

288
Subject Index

292
Author Index

293
Employment Opportunities

TECHNICAL OUTPUT

The Navy continues to be a pioneer in initiating new developments and a leader in applying these advancements to military requirements. The primary method of informing the scientific and engineering community of the advances made at NRL is through the Laboratory's technical output—reports, articles in scientific journals, contributions to books, papers presented to scientific societies and topical conferences, patents, and inventions.

The figures for calendar year 2008 presented below represent the output of NRL facilities in Washington, D.C.; Bay St. Louis, Mississippi; and Monterey, California.

In addition to the output listed, NRL scientists made more than 1529 oral presentations during 2008.

Type of Contribution	Unclassified	Classified	Total
Articles in periodicals, chapters in books, and papers in published proceedings	1261*	0	1261*
NRL Formal Reports	11	0	11
NRL Memorandum Reports	65	4	69
Books	2	0	2
Patents granted	58		58
Statutory Invention Registrations (SIRs)	3		3

*This is a provisional total based on information available to the Ruth H. Hooker Research Library on April 10, 2009. Additional publications carrying a 2008 publication date are anticipated. Total includes refereed and non-refereed publications.

KEY PERSONNEL

Area Code (202) unless otherwise listed
Personnel Locator - 767-3200
DSN-297 or 754

Code	Office	Phone Number
	EXECUTIVE DIRECTORATE	
1000	Commanding Officer	767-3403
1000.1	Inspector General	767-3621
1001	Director of Research	767-3301
1001.1	Executive Assistant	767-2445
1002	Chief Staff Officer	767-3621
1004	Head, Technology Transfer	767-3083
1006	Head, Office of Program Administration and Policy Development	767-3091
1008	Office of Counsel	767-2244
1030	Public Affairs Officer	767-2541
1100	Director, Institute for Nanoscience	767-3261
1200	Head, Command Support Division	767-3621
1220	Head, Security	767-0793
1400	Head, Military Support Division	767-2273
1600	Commanding Officer, Scientific Development Squadron One	301-342-3751
1800	Director, Human Resources Office	767-3421
1830	Deputy EEO Officer	767-5264
3005	Deputy for Small Business	767-6263
3540	Head, Safety Branch	767-2232
	BUSINESS OPERATIONS DIRECTORATE	
3000	Comptroller/Associate Director of Research	767-2371
3200	Head, Contracting Division	767-5227
3300	Head, Financial Management Division	767-3405
3400	Head, Supply and Information Services Division	767-3446
3500	Director, Research and Development Services Division	404-4054
	SYSTEMS DIRECTORATE	
5000	Associate Director of Research	767-3425
5300	Superintendent, Radar Division	404-2700
5500	Superintendent, Information Technology Division/ NRL Chief Information Officer*	767-2903
5600	Superintendent, Optical Sciences Division	767-7375
5700	Superintendent, Tactical Electronic Warfare Division	767-6278
	MATERIALS SCIENCE AND COMPONENT TECHNOLOGY DIRECTORATE	
6000	Associate Director of Research	767-3566
6100	Superintendent, Chemistry Division	767-3026
6300	Superintendent, Materials Science and Technology Division	767-2926
6400	Director, Laboratory for Computational Physics and Fluid Dynamics	767-3055
6700	Superintendent, Plasma Physics Division	767-2723
6800	Superintendent, Electronics Science and Technology Division	767-3693
6900	Director, Center for Bio/Molecular Science and Engineering	404-6000
	OCEAN AND ATMOSPHERIC SCIENCE AND TECHNOLOGY DIRECTORATE	
7000	Associate Director of Research	404-8690
7100	Superintendent, Acoustics Division	767-3482
7200	Superintendent, Remote Sensing Division	767-3391
7300	Superintendent, Oceanography Division	228-688-4670
7400	Superintendent, Marine Geosciences Division	228-688-4650
7500	Superintendent, Marine Meteorology Division	831-656-4721
7600	Superintendent, Space Science Division	767-6343
	NAVAL CENTER FOR SPACE TECHNOLOGY	
8000	Director	767-6547
8100	Superintendent, Space Systems Development Department	767-0410
8200	Superintendent, Spacecraft Engineering Department	404-3727

*Additional Duty

CONTRIBUTIONS BY DIVISIONS, LABORATORIES, AND DEPARTMENTS

Institute for Nanoscience

192 Making the Most of a Scarce Metal
C.N. Chervin, A.M. Lubers, J.W. Long, and D.R. Rolison

Radar Division

157 The Multifunction Electronic Warfare (MFEW) Advanced Development Model (ADM)
G.C. Tavik and N.M. Thomas III

221 Polarimetric Radar Imaging of the Ocean Surface
M.A. Sletten and K. Scheff

228 Impulsive Noise Suppression via Adaptive Filtering
G.S. San Antonio

Information Technology Division

59 A Novel User Interface Controller for Dismounted Infantry Training
J.N. Templeman, L.E. Sibert, R.C. Page, and P.S. Denbrook

235 The DIME/PMESII Model Suite Requirements Project
R. Hillson

Optical Sciences Division

167 Free-Space Optical Link to an Explosive Ordnance Disposal (EOD) Robot
W.S. Rabinovich, J.L. Murphy, M. Suite, M.F. Ferraro, R. Mahon, and P.G. Goetz

189 Charge Transfer Between Quantum Dots and Peptide-Coupled Redox Complexes
I.L. Medintz, T. Pons, S.A. Trammell, and H. Mattoussi

213 Project CHLOE: High Altitude Defense Against Anti-Aircraft Missiles
R.M. Mabe, K.A. Sarkady, and B.A. Nichols

215 Transparent Spinel Ceramic
J.S. Sanghera, G.Villalobos, W. Kim, S. Bayya, and I.D. Aggarwal

217 Lightning Strike Sensing System for the Space Shuttle Launch Pad
A. Davis, J. McVicker, P. Karatsinides, A. Dandridge, and C. Kirkendall

Tactical Electronic Warfare Division

160 Transportable Electronic Warfare Module (TEWM)
D.E. Tremper, R.S. Cortesi, J. Heyer, J. Geib, and D. Bay

162 Laser Decoy System for Small Ground Platforms
R. Evans and S. Moroz

Chemistry Division

67 High Expansion Foam for Protecting Large Volume Mission Critical Shipboard Spaces
J.P. Farley and F.W. Williams

87 Chemically Modified Graphene for Sensing and Nanomechanical Applications
J.T. Robinson, F.K. Perkins, E.S. Snow, M. Zalalutidinov, B.H. Houston, J.W. Baldwin, Z. Wei, and P.E. Sheehan

149 Innovative Foldamers: Engineering Heterochiral Peptides
T.D. Clark and J.L. Kulp III

192 Making the Most of a Scarce Metal
C.N. Chervin, A.M. Lubers, J.W. Long, and D.R. Rolison

Materials Science and Technology Division

75 Sensor Systems for Measuring Helmet-Head-Brain Response to Blast
K.E. Simmonds, A. Bagchi, A.C. Leung, W.R. Pogue III, P. Matic, J.M. Byers, G.K. Hubler, D.R. Mott, D.A. Schwer, R.D. Corsaro, and B.H. Houston

180 Risk Mitigation for High Temperature Superconducting Generators
R.L. Holtz

185 Multifunctional Structure-Battery Composites for Marine Applications
J.P. Thomas, M.A. Qidwai, W.R. Pogue III, and A. Rohatgi

Laboratory for Computational Physics and Fluid Dynamics

75 Sensor Systems for Measuring Helmet-Head-Brain Response to Blast
K.E. Simmonds, A. Bagchi, A.C. Leung, W.R. Pogue III, P. Matic, J.M. Byers, G.K. Hubler, D.R. Mott, D.A. Schwer, R.D. Corsaro, and B.H. Houston

182 CT-Analyst Integration in Chemical/Biological/Radiological (CBR) Analysis Applications
A. Moses

239 Simulation of Supersonic Military Aircraft Jet Noise
K. Kailasanath, J. Liu, and R. Ramamurti

Plasma Physics Division

241 Numerical Modeling of Plasmas Using the Turbo-WAVE Framework
D.F. Gordon, P. Sprangle, A.C. Ting, R. Fernsler, M. Lampe, S. Slinker, and B. Hafizi

247 Laboratory Investigation of Near-Earth Space Plasma Processes
W.E. Amatucci, D.D. Blackwell, G.R. Gatling, G.I. Ganguli, C.D. Cothran, E.M. Tejero, D.N. Walker, and C.S. Compton

Electronics Science and Technology Division

87 Chemically Modified Graphene for Sensing and Nanomechanical Applications
J.T. Robinson, F.K. Perkins, E.S. Snow, M. Zalalutidinov, B.H. Houston, J.W. Baldwin, Z. Wei, and P.E. Sheehan

147 Guided Terahertz Waves for Characterizing Explosives
J.S. Melinger and D. Grischkowsky

177 Tunable Filter and Multiplexer for Improved Transmitter Electromagnetic Compatibility
D.R. Jachowski, C. Rauscher, S.W. Kirchoefer, W. Kruppa, A.C. Guyette, and J.M. Pond

194 Optical Pulse Control of Electron and Nuclear Spins in Quatum Dots
S. Carter, S. Economou, A. Shabaev, T. Kennedy, A. Bracker, and T. Reinecke

Center for Bio/Molecular Science and Engineering

152 A Multiwavelength Microflow Cytometer
F.S. Ligler, J.S. Erickson, J.P. Golden, J.S. Kim, M. Nasir, P.J. Howell, A.L. Thangawng, L.R. Hilliard, L.C. Shriver-Lake, and G.P. Anderson

189 Charge Transfer Between Quantum Dots and Peptide-Coupled Redox Complexes
I.L. Medintz, T. Pons, S.A. Trammell, and H. Mattoussi

Acoustics Division

75 Sensor Systems for Measuring Helmet-Head-Brain Response to Blast
K.E. Simmonds, A. Bagchi, A.C. Leung, W.R. Pogue III, P. Matic, J.M. Byers, G.K. Hubler, D.R. Mott, D.A. Schwer, R.D. Corsaro, and B.H. Houston

87 Chemically Modified Graphene for Sensing and Nanomechanical Applications
J.T. Robinson, F.K. Perkins, E.S. Snow, M. Zalalutidinov, B.H. Houston, J.W. Baldwin, Z. Wei, and P.E. Sheehan

97 Investigating Acoustic Causality in Highly Dispersive Bubbly Liquids
G.J. Orris, M. Nicholas, and D.K. Dacol

127 Reconstruction of Acoustic Exposure on Orcas in Haro Strait
D.M. Fromm

130 Operational Acoustic Transmission Loss Uncertainty Characterization
R.A. Zingarelli and J.P. Fabre

Remote Sensing Division

221 Polarimetric Radar Imaging of the Ocean Surface
M.A. Sletten and K. Scheff

223 Airborne Remote Sensing of Trafficability in the Coastal Zone
C.M. Bachmann, C.R. Nichols, M.J. Montes, R.-R. Li, P. Woodward, R.A. Fusina, W. Chen, V. Mishra, W. Kim, J. Monty, K. McIlhany, K. Kessler, D. Korwan, D. Miller, E. Bennert,

G. Smith, D. Gillis, J. Sellars, C. Parrish, A. Weidemann, W. Goode, A. Schwarzschild, and B. Truitt

249 A New Class of Radio Halo
W.M. Peters and N.E. Kassim

Oceanography Division

199 A Thinning Arctic Ice Cap as Simulated by the Polar Ice Prediction System (PIPS): 2000–2008
P.G. Posey, R.H. Preller, L.F. Smedstad, and C.N. Barron

202 Predicting "Ocean Weather" Using the HYbrid Coordinate Ocean Model (HYCOM)
E.J. Metzger, H.E. Hurlburt, A.J. Wallcraft, O.M. Smedstad, J.A. Cummings, and E.P. Chassignet

223 Airborne Remote Sensing of Trafficability in the Coastal Zone
C.M. Bachmann, C.R. Nichols, M.J. Montes, R.-R. Li, P. Woodward, R.A. Fusina, W. Chen, V. Mishra, W. Kim, J. Monty, K. McIlhany, K. Kessler, D. Korwan, D. Miller, E. Bennert, G. Smith, D. Gillis, J. Sellars, C. Parrish, A. Weidemann, W. Goode, A. Schwarzschild, and B. Truitt

Marine Geosciences Division

171 Tiled Image Archival and Distribution for Seafloor and Terrestrial Imagery
E. Ioup, J. Sample, and F. McCreedy

206 Littoral Battlespace Characterization Using Small Unmanned Aerial Systems
K.T. Holland, D. Lalejini, and K. Plavnick

208 The Environmental Post-Mission Analysis System: Through-the-Sensor to the Warfighter
B.Y. Lin, S.A. Myrick, W.E. Avera, and M.M. Harris

Marine Meteorology Division

135 Operational Radar Performance Surfaces for RIMPAC 2008
T. Haack and J. Hansen

142 Observing Guidance for Tropical Cyclones
C.A. Reynolds, J.D. Doyle, C. Amerault, and H. Jin

Space Science Division

105 Opening a New Window on the High Energy Space Environment
J.E. Grove and W.N. Johnson

138 The Atmospheric Neutral Density Experiment (ANDE)
A. Nicholas, T. Finne, I. Galysh, M. Davis, and L. Healy

Space Systems Development Department

138 The Atmospheric Neutral Density Experiment (ANDE)
A. Nicholas, T. Finne, I. Galysh, M. Davis, and L. Healy

169 A Maritime Information Exchange Model (MIEM) for Sharing Actionable Intelligence
C. Dwyer, R. Hayes-Roth, D. Reading, and G. Small

172 Cross-Domain Payload Migration
C.M. Huffine

Spacecraft Engineering Department

113 Design and Analysis of the Thermal Control System for the TacSat-4 Spacecraft COMMx Payload
R.W. Baldauff, W.J. Armiger, and T.T. Hoang

138 The Atmospheric Neutral Density Experiment (ANDE)
A. Nicholas, T. Finne, I. Galysh, M. Davis, and L. Healy

250 Integration and Testing Challenges of the Operationally Responsive Space (ORS) Phase III Bus Standards Prototype
W.C. Raynor, T.J. Specht, W.R. Braun, E.A. Rossland, S.N. LaCava, M.S. Johnson, P.A. Stadter, C.T. Apland, J.R. Bruzzi, M.T. Marley, B.D. Williams, R.A. Denissen, and D.C. Bentz

SUBJECT INDEX

3-MV Tandem Pelletron Accelerator Facility, 41
3D Virtual and Mixed Environments Laboratory (3DVMEL), 37
Abell 521, 249
Acoustic propagation, 127
Acoustic Seafloor Characterization System, 49
Acoustic simulation, 130
Acoustics Division, 44
Acoustics, 97
Active sonar, 127
Adaptive filtering, 228
Administrative Services Branch, 52
Advanced Graduate Research Program, 277
Advanced Multifunction Radio Frequency Concept (AMRFC), 36
Advanced Silicon Carbide Epitaxial Research Laboratory (ASCERL), 43
Afghanistan integrated airborne geospatial study, 33
Airborne Polarimetric Microwave Imaging Radiometer (APMIR), 47
Amateur Radio Club, 279
Amphibious operations, 206
Anti-ship missile defense, 160
Application Programmer's Interface (API), 208
Atmospheric Prediction System Development Laboratory, 50, 54
Atomic resolution transmission electron microscopy (ARTEM), 42
Audio Laboratory, 37
Autonomous Systems Research Laboratory, 55
β helices, 149
Behavioral Detection Laboratory, 37
Biodefense, 152
Blast, 75
Blunt trauma, 75
Bubbles, 97
C-12 Beech King Air research aircraft, 54
Capitol Hill Workshops, 277
Catalysis, 192
Causality, 97
Center for Bio/Molecular Science and Engineering, 44
Center for Higher Learning, 53
Central Thermal Bus (CTB) concept, 113
Charge transfer, 189
Chemical Vapor and Plasma Deposition Facility, 40
Chemically modified graphene (CMG) films, 32
Chemically modified graphene, 87
Chemistry Division, 39
Chesapeake Bay Detachment (CBD), 36, 53, 54
Civic affairs, 235
COAMPS-TC, 33
Coastal Ocean Imaging Spectrometer (COIS), 46
College and high school student programs, 280
Combat Development Command, 54
Community Outreach Program, 35, 279
COMMx electronic payload, 113
COMMx Thermal Control System (TCS), 113
Compact Airborne Spectrographic Imager (CASI-1500), 46
Compact Antenna Range, 36
Composite laminate, 185
Compound Semiconductor Processing Facility, (CSPF), 43
Comprehensive maritime awareness (CMA), 169
Computational Electromagnetics (CEM) Facility, 36
Conductive nanoscale coating, 192
Continuing education, 277
Continuous-wave (CW) fiber lasers, 42
Cooperative Aircraft Identification system, 37
Cooperative Research and Development Agreements (CRADAs), 51
Coronal Physics Explorer (CPEX), 51
Corporate Facilities Investment Plan (CFIP), 55
Counseling Referral Service (C/RS), 278
Countermeasures, 162
Countersurveillance, 160
Cryogenic materials, 180
Cryptographic Technology Laboratory, 37
CT-Analyst, 182
Cyber Defense Development Laboratory, 37
Cyclic voltammogram (CV), 189
DDG-1000, 215
Deep-Towed Acoustics/Geophysics System, 49
Defense Research and Engineering Network (DREN), 37
Department of Defense Operationally Responsive Space (ORS), 113
Digital Holographic Imaging System, 45
Digital Library, 52
Digital publishing technology, 52
Digital radio frequency memory (DRFM), 160
Diplexer, 177
Diplomatic, Information, Military, and Economic (DIME), 235
Dismounted infantry tactics, 59
DoD Science & Engineering Apprentice Program (SEAP), 280
Drag, 138
Ducting, 135
Edison Memorial Graduate Training Program, 277
Electra, 42
Electric discharge machining (EDM) tool, 43
Electrical, Magnetic, and Optical Measurement Facility, 41
Electro-osmotic flow (EOF)-based micropump, 29
Electrode structure, 192
Electrolytic deposition, 41
Electromagnetic compatibility, 177
Electromagnetic propagation, 135
Electron energy loss spectroscopy (EELS), 42
Electron spins, 194
Electronic support measures, 157
Electronics Research Laboratory, 55
Electronics Science and Technology Division, 43
Environmental Chemistry Laboratory, 53
Environmental effects and variability, 135
Environmental Post-Mission Analysis (EPMA) system, 208
Environmental Protection Agency's Gulf of Mexico Program, 53
Epicenter, 43
Equal Employment Opportunity (EEO) programs, 278
Ex-USS Shadwell (LSD 15), 40, 54
Executive Leadership Program for Mid-Level Employees, 277
Expeditionary fighting vehicle (EFV), 162
Extensible Markup Language (XML), 169
Far-infrared, 147
Fatigue, 180
Federal Executive and Professional Association, 35
Federal Executive Institute (FEI), 277
Fellowship in Congressional Operations, 277
Fermi gamma-ray space telescope, 28
Fermi Large Area Telescope (LAT), 105
Fire I, 40
Fire suppression, 68
Fleet Numerical Meteorology and Oceanography Center (FNMOC), 53
Flight Support Detachment, 35
Flow Cytometer, 152
Focal Plane Array Evaluation Facility, 38

Foldamers, 149
Force protection/homeland defense (FP/HD), 40
Forecasts, 142
Forms and Reports Management Programs, 52
Free space optical (FSO) communication, 167
Free-Surface Hydrodynamics Laboratory (FSHL), 46
Freespace Laser Communications Laboratory, 37
Frequency-agile, 177
Front-end Robotic Enabling Near-term Demonstration (FREND), 33
Fuel cell, 192
Funding, Recruitment, Information, and Support (FRIS), 235
Gamble II, 43
Gamma ray imaging, 105
Gamma Ray Large Area Telescope (GLAST), 105
Geoacoustic Model Fabrication Laboratory, 45
Geospatial Information Data Base, 49
Giant Metrewave Radiotelescope (GMRT), 249
Global Assimilation of Ionospheric Measurements (GAIM), 51
Global Information Grid Evaluation Facility (GIG-EF), 37
Government Purpose Licenses, 51
Graduate programs, 277
Graphene, 87
Graphics support, 52
Helium Resonant Scattering in the Corona and HELiosphere (HERSCHEL), 51
Heterochiral peptides, 149
High altitude missile warning, 213
High Energy Laser Laboratory, 42
High energy lasers, 215
High expansion foam, 68
High frequency over-the-horizon radar (HF-OTHR), 228
High Performance Computing Facilities, 37
High performance computing, 182
High temperature superconductor, 180
High-power fiber lasers, 32
Human machine interface (HMI), 157
Human Resources Office, 277
Humanitarian Aid, 235
Hybrid Coordinate Ocean Model (HYCOM), 202
Hyperspectral Imager for Coastal Ocean (HICO), 30, 46
Immersive Simulation Laboratory, 37
Impulsive noise, 228
In Situ Sediment Acoustic Measurement System, 49
Information Technology Division (ITD), 37
Infrared photothermal imaging, 32
Inside air (HotFoam), 68
Institute for Nanoscience, 36, 40
Integrated Systems Engineering Team (ISET), 250
Interferometer, 157, 217
Inverse synthetic aperture radar (ISAR), 36
IR Missile-Seeker Evaluation Facility, 38
Irregular warfare, 235
JEOL 2010F transmission electron microscope, 42
John C. Stennis Space Center (SSC), 53
Joint Capabilities Technology Demonstration (JCTD), 169
Kilowatt-scale radiation-balanced laser, 31
Krypton fluoride (KrF) lasers, 42
Laboratory for Advanced Materials Synthesis (LAMS), 43
Laboratory for Computational Physics and Fluid Dynamics, 42
Laboratory for Large Data, 37
Laboratory for the Structure of Matter, 39
Laboratory plasma, 247
Large Area Plasma Processing Systems (LAPPS), 43
Laser guided weapon, 162
Legislative Fellowship (LEGIS) program, 277
Leo scanning electron microscope, 42
Lightning strike sensor system, 217
Liquid chromatograph-mass spectrometer (LCMS), 44
Lithium-ion battery, 185
Long Wavelength Demonstrator Array (LWDA), 47
Loop Heat Pipe (LHP) technology, 113
Low frequency broadband mine hunting, 30
Magnetic field gradient sensing system, 217
Magnetic Resonance Facility, 40
Magnetoelectronics Fabrication Facility, 40
Major Shared Resource Center (MSRC), 53
Manned Portable Air Defense Systems (MANPADS), 213
Marine Corrosion and Marine Coatings Facility, 40
Marine Corrosion Facility, 54
Marine Geosciences Division, 49
Marine mammal, 127
Marine Meteorology Center, 55
Marine Meteorology Division (NRL-MRY), 49, 53
Maritime Automated Supertrack Enhanced Reporting (MASTER) Joint Capability Technology Demonstration (JCTD), 34
Maritime Information Exchange Model (MIEM), 169
Materials Processing Facility, 41
Materials Science and Technology Division, 40
Materials Synthesis/Property Measurement Facility, 40
Mechanical Characterization Facility, 41
Mercury, 43
Meteorological and oceanographic conditions (METOC), 206
Micro/Nanostructure Characterization Facility, 42
Microfluidics, 152
MicroSTAR-H X-ray generator, 44
Microwave Microscope (MWM), 37
Midway Research Center (MRC), 54
Millimeter-Wave Vacuum Electronics Synthesis Facility (MWVESF), 43
Missile Defense Agency (MDA), 54
Mobile Ad Hoc Networking (MANET) technology, 37
Mobile Atmospheric Aerosol and Radiation Characterization Observatory (MAARCO), 49
Mobile Imaging and Spectroscopic Threat Identification (MISTI), 51
Modeling and computing, 130
Moderate Resolution Imaging Spectroradiometer (MODIS), 49
Modulating retroreflector (MRR), 167
Molecular beam epitaxy (MBE), 43
Monotonically integrated large eddy simulations (MILES), 31, 239
Motion imagery, 206
Motor propulsion, 180
Moving Map Composer Facility, 49
Multifunction Electronic Warfare (MFEW) Advanced Development Model (ADM), 29
Nanomechanical, 87
Nanometer Characterization/Manipulation Facility, 40
NASA Small Explorer Mission, 51
National Coastal Data Development Center, 53
National Data Buoy Center, 53
National Defense Science and Engineering Graduate Fellowship Program, 279
National Radio Astronomy Observatory's (NRAO) Very Large Array (VLA), 47
National Research Council (NRC) Cooperative Research Associateship Program, 279
NATO Undersea Research Center (NURC), 48
Naval Center Space Technology (NCST), 51
Naval Key Management Laboratory, 37
Naval Meteorology and Oceanographic Command, 53
Naval Oceanographic Office, 53
Naval Postgraduate School (NPS), 53, 277
Naval Research Enterprise Intern Program (NREIP), 279
Navy Fleet Numerical Meteorology and Oceanography Center (FNMOC), 47
Navy Fuel Research Facility, 40
Navy Prototype Optical Interferometer (NPOI), 47
Navy Small Craft Instruction and Training Center, 53
Navy/ASEE Summer Faculty Research and Sabbatical Leave Program, 279
Nearfield scanning optical microscope (NSOM), 45
Network for Detection of Atmospheric Change (NDAC), 47
Nike, 42
Non-blinking semiconductor nanocrystals, 30
Non-combatant evacuation, 235
NP-3D EW flying laboratory, 39

NP-3D Orion aircraft, 54
NRL Federal Credit Union (NRLFCU), 35
NRL Focused Phased Array Imaging Radar (NRL FOPAIR), 46, 221
NRL Global Ocean Nowcast/Forecast System v2.6, 34
NRL Interferometric Synthetic Aperture Radar (NRL INSAR), 46
NRL Mentor Program, 278
NRL Online Bibliography, 53
NRL Recreation Club, 279
NRL/ASEE Postdoctoral Fellowship Program, 279
NRL/United States Naval Academy (USNA) Cooperative Program for Scientific Interchange, 279
Nuclear magnetic resonance (NMR) sensors, 149
Nuclear magnetic resonance (NMR) spectroscopy, 40
Nuclear spins, 194
Numerical ocean modeling, 202
Ocean Dynamics and Prediction Computational Network Facility, 48
Ocean nowcast/forecast, 202
Ocean weather, 202
Oceanography Division, 48
Operation Rampant Lion II, 54
Operation Rampant Lion III, 54
Operational Responsive Space (ORS), 250
Optical Calibration Facility, 46
Optical Sciences Division, 38
Optimal manning, 68
Orbit determination, 138
Packbot, 167
Peptide coupled redox complexes, 189
Personal protective equipment, 75
Phillips CM30 transmission electron microscope, 42
Photographic services, 52
Photoinduced electron transfer, 30
Photonic mast, 215
Plasma Physics Division, 42
Plasma waves, 247
Plasmas, 241
Platinum-group metals, 192
Plume modeling, 182
Point-of-care, 152
Polar Ozone and Aerosol Measurement (POAM II and III), 47
Political, Military, Economic, Social, Information, and Infrastructure (PMESII), 235
Portable Hyperspectral Imager for Low-Light Spectroscopy (PHILLS), 46
Portable power, 192
Predictability, 142
Professional appointments, 280
Profiling Optics Package, 46
Programmable Embedded INFOSEC Product–Phase II (PEIP-II), 31
Project CHLOE, 213
Publications services, 52
Pulsed laser deposition (PLD), 41
Quantum dots, 189
Quantum dots, 194
Radar Division, 36
Radar Imaging Facility, 36
Radar ocean backscatter, 221
Radar performance, 135
Radar remote sensing, 221
Radar Signature Calculation Facility, 36
Radar Testbed Facility, 36
Radar-absorbing materials/radar-absorbing structures (RAM/RAS), 39
Radiation belts, 247
Radio halo, 249
Railgun Materials Testing Facility, 42
Records management services, 52
Recreation Club, 35
Remote Sensing Division, 46
Resonator, 87
Ridge-waveguide multiplexer, 177
Rim of the Pacific (RIMPAC) 2008, 160
Robotics and Autonomous Systems Laboratory, 37
Ruth H. Hooker Research Library, 52
Ruthenium dioxide, 192
Salt Water Tank Facility, 45
Satellite Data Processing Laboratory, 49, 54
Satellites, 138
Scanfish, 48
Scanning laser Doppler vibrometry (LDV), 44
Scanning transmission electron microscopy (STEM), 42
Scientific Development Squadron One (VXS-1), 53
Scientific Development Squadron ONE, 54
Scientist-to-Sea Program (STSP), 278
Sea ice forecasting, 199
Sea ice models, 199
Select Graduate Training Program, 277
Shallow water bathymetry, 223
Ship motion simulator (SMS), 54,157
Sigma Xi, 278
Slocum Gliders, 48
Small Unmanned Aerial Systems (SUAS), 206
Smart materials, 149
Software reprogrammable payloads, 172
Solar Coronagraph Optical Test Chamber (SCOTCH), 50
SOnoMAgnetic LABoratory (SOMALAB), 45
Space payloads, 172
Space Plasma Simulation Chamber (SPSC), 43
Space Science Division, 50
Space Solar Cell Characterization Facility (SSCCF), 43
Space Systems Development Department, 54
Space Systems Technology Laboratory, 55
Space weather, 138, 247
Special Boat Team-Twenty-two, 53
Special Sensor Microwave Imager/Sounder (SSMIS), 47
Spectroscopy, 147
Spinel, 215
Steam generation, 68
Stennis Space Center (NRL-SSC), 53
Streamer Propagation and ARCing (SPARC), 241
Student Career Experience Program, 35, 280
Student Temporary Employment Program (STEP), 280
Student Volunteer Program, 280
Substrate bearing strength, 223
Summer Employment Program, 280
Superconducting Quantum Interference Device (SQUID), 41
Supersonic military aircraft jet noise, 239
Surface Characterization Facility, 38
Surface Electronic Warfare Improvement Program (SEWIP), 157
Surrogates, 75
Synchrotron Radiation Facility, 40
Table-Top Terawatt (T3) laser, 42
TacSat-4 COMMx, 113, 250
Tactical Aircraft Directed Infrared Countermeasure (TADIRCM), 213
Tactical Electronic Warfare (TEW) Division, 39
Target detection ranges, 135
Technical Information Services (TIS) Branch, 51
Technology Transfer Act, 51
Technology Transfer Office (TTO), 51
Terahertz, 147
Thermal technology, 113
Thermoelectric cooler (TEC), 113
Thin-Film Materials Synthesis and Processing Facility, 41
THORPEX Pacific-Asian Regional Campaign (T-PARC), 54
Through-the-sensor plug-in, 208
Ti:Sapphire Femtosecond Laser (TFL), 42
Tile archival and distribution systems, 171
Toastmasters International, 35, 278
TORPEDO Ultra, 53
Trafficability, 223
Training simulators, 59
Transmission electron microscopy (TEM), 42
Transmission Electron Microscopy Facility, 49
Transparent spinel ceramic, 215
Transportable Electronic Warfare Module (TEWM), 160
Traumatic brain injury (TBI), 75
Tropical cyclones, 142
TTCP Anti-ship Missile Project Arrangement (TAPA), 29
Tunable microstrip notch filter, 177
turboWAVE modules, 241
U.S. Geological Survey, 53
Ultrafast Laser Facility (ULF), 43
Ultrafast optical control, 194
Ultralow-loss Infrared (IR) Fiber-Optic Waveguide Facility, 38
Uncertainty, 130
Unmanned underwater vehicle, 185
User avatar, 59

User interface, 59
Vacuum Ultraviolet Solar Instrument Test (SIT) facility, 50
Vertical Microstructure Profilier (VMP), 48
VEry high angular Resolution Imaging Spectrometer (VERIS), 51
Video services, 52
Virtual environments, 59
Voice Communication Laboratory, 37
W-band Advanced Radar for Low Observable Control (WARLOC), 36
Warfighter Human Systems Integration Laboratory, 37
Water Vapor Millimeter-wave Spectrometer (WVMS), 47
Waveguide explosives sensing, 147
Web Map Service (WMS), 171
WindSat, 47
Women in Science and Engineering (WISE) Network, 35, 278
Z-contrast imaging, 42

AUTHOR INDEX

Aggarwal, I.D., 215
Amatucci, W.E., 247
Amerault, C., 142
Anderson, G.P., 152
Apland, C.T., 250
Armiger, W.J., 113
Avera, W.E., 208
Bachmann, C.M., 223
Bagchi, A., 75
Baldauff, R.W., 113
Baldwin, J.W., 87
Barron, C.N., 199
Bay, D., 160
Bayya, S., 215
Bennert, E., 223
Bentz, D.C., 250
Blackwell, D.D., 247
Bracker, A., 194
Braun, W.R., 250
Bruzzi, J.R., 250
Byers, J.M., 75
Carter, S., 194
Chassignet, E.P., 202
Chen, W., 223
Chervin, C.N., 192
Clark, T.D., 149
Compton, C.S., 247
Corsaro, R.D., 75
Cortesi, R.S., 160
Cothran, C.D., 247
Cummings, J.A., 202
Dacol, D.K., 97
Dandridge, A., 217
Davis, A., 217
Davis, M., 138
Denbrook, P.S., 59
Denissen, R.A., 250
Doyle, J.D., 142
Dwyer, C., 169
Economou, S., 194
Erickson, J.S., 152
Evans, R., 162
Fabre, J.P., 130
Farley, J.P., 67
Fernsler, R., 241
Ferraro, M.F., 167
Finne, T., 138
Fromm, D.M., 127
Fusina, R.A., 223
Galysh, I., 138
Ganguli, G.I., 247
Gatling, G.R., 247
Geib, J., 160
Gillis, D., 223
Goetz, P.G., 167
Golden, J.P., 152
Goode, W., 223
Gordon, D.F., 241
Grischkowsky, D., 147
Grove, J.E., 105
Guyette, A.C., 177
Haack, T., 135
Hafizi, B., 241
Hansen, J., 135
Harris, M.M., 208
Hayes-Roth, R., 169
Healy, L., 138
Heyer, J., 160
Hilliard, L.R., 152
Hillson, R., 235
Hoang, T.T., 113
Holland, K.T., 206
Holtz, R.L., 180
Houston, B.H., 75, 87
Howell, P.J., 152
Hubler, G.K., 75
Huffine, C.M., 172
Hurlburt, H.E., 202
Ioup, E., 171
Jachowski, D.R., 177
Jin, H., 142
Johnson, M.S., 250
Johnson, W.N., 105
Kailasanath, K., 239
Karatsinides, P., 217
Kassim, N.E., 249
Kennedy, T., 194
Kessler, K., 223
Kim, J.S., 152
Kim, W., 215, 223
Kirchoefer, S.W., 177
Kirkendall, C., 217
Korwan, D., 223
Kruppa, W., 177
Kulp, J.L., III, 149
LaCava, S.N., 250
Lalejini, D., 206
Lampe, M., 241
Leung, A.C., 75
Li, R.-R., 223
Ligler, F.S., 152
Lin, B.Y., 208
Liu, J., 239
Long, J.W., 192
Lubers, A.M., 192
Mabe, R.M., 213
Mahon, R., 167
Marley, M.T., 250
Matic, P., 75
Mattoussi, H., 189
McCreedy, F., 171
McIlhany, K., 223
McVicker, J., 217
Medintz, I.L., 189
Melinger, J.S., 147
Metzger, E.J., 202
Miller, D., 223
Mishra, V., 223
Montes, M.J., 223
Monty, J., 223
Moroz, S., 162
Moses, A., 182
Mott, D.R., 75
Murphy, J.L., 167
Myrick, S.A., 208
Nasir, M., 152
Nicholas, A., 138
Nicholas, M., 97
Nichols, B.A., 213
Nichols, C.R., 223
Orris, G.J., 97
Page, R.C., 59
Parrish, C., 223
Perkins, F.K., 87
Peters, W.M., 249
Plavnick, K., 206
Pogue, W.R., III, 75, 185
Pond, J.M., 177
Pons, T., 189
Posey, P.G., 199
Preller, R.H., 199
Qidwai, M.A., 185
Rabinovich, W.S., 167
Ramamurti, R., 239
Rauscher, C., 177
Raynor, W.C., 250
Reading, D., 169
Reinecke, T., 194
Reynolds, C.A., 142
Robinson, J.T., 87
Rohatgi, A., 185
Rolison, D.R., 192
Rossland, E.A., 250
Sample, J., 171
San Antonio, G., 228
Sanghera, J.S., 215
Sarkady, K.A., 213
Scheff, K., 221
Schwarzschild, A., 223
Schwer, D.A., 75
Sellars, J., 223
Shabaev, A., 194
Sheehan, P.E., 87
Shriver-Lake, L.C., 152
Sibert, L.E., 59
Simmonds, K.E., 75
Sletten, M.A., 221
Slinker, S., 241
Small, G., 169
Smedstad, L.F., 199
Smedstad, O.M., 202
Smith, G., 223
Snow, E., 87
Specht, T.J., 250
Sprangle, P., 241
Stadter, P.A., 250
Suite, M., 167
Tavik, G.C., 157
Tejero, E.M., 247
Templeman, J.N., 59
Thangawng, A.L., 152
Thomas, N.M., III, 157
Thomas, J.P., 185
Ting, A.C., 241
Trammell, S.A., 189
Tremper, D.E., 160
Truitt, B., 223
Villalobos, G., 215
Walker, D.N., 247
Wallcraft, A.J., 202
Wei, Z., 87
Weidemann, A., 223
Williams, B.D., 250
Williams, F.W., 67
Woodward, P., 223
Zalalutidinov, M., 87
Zingarelli, R.A., 130

NRL EMPLOYMENT OPPORTUNITIES

for Highly Innovative, Motivated, and Creative Professionals

NRL offers a wide variety of challenging S&T positions that involve skills from basic and applied research to equipment development. The nature of the research and development conducted at NRL requires professionals with experience. Typically there is a continuing need for electronics, mechanical, aerospace, and materials engineers, metallurgists, computer scientists, and oceanographers with bachelor's and/or advanced degrees and physical and computer scientists with Ph.D. degrees.

■ Biologists. Biologists conduct research in areas that include biosensor development, tissue engineering, molecular biology, genetic engineering, proteomics, and environmental monitoring.

■ Chemists. Chemists are recruited to work in the areas of combustion, polymer science, bioengineering and molecular engineering, surface science, materials, synthesis, nanostructures, corrosion, fiber optics, electro-optics, microelectronics, electron-device technology, and laser physics.

■ Electronics Engineers and Computer Scientists. These employees may work in the areas of communications systems, electromagnetic scattering, electronics instrumentation, electronic warfare systems, radio frequency/microwave/millimeter-wave/infrared technology, radar systems, laser physics technology, radio-wave propagation, electron device technology, spacecraft design, artificial intelligence, information processing, signal processing, plasma physics, vacuum science, microelectronics, electro-optics, fiber optics, solid state, software engineering, computer design/architecture, ocean acoustics, stress analysis, and expert systems.

■ Materials Scientists/Engineers. These employees are recruited to work on materials, microstructure characterization, electronic ceramics, solid-state physics, fiber optics, electro-optics, microelectronics, fracture mechanics, vacuum science, laser physics and joining technology, and radio frequency/microwave/millimeter-wave/infrared technology.

■ Mechanical and Aerospace Engineers. These employees may work in areas of spacecraft design, remote sensing, propulsion, experimental and computational fluid mechanics, experimental structural mechanics, solid mechanics, elastic/plastic fracture mechanics, materials, finite-element methods, nondestructive evaluation, characterization of fracture resistance of structural alloys, combustion, CAD/CAM, and multi-functional material response.

■ Oceanographers, Meteorologists, and Marine Geophysicists. These employees work in the areas of ocean and atmospheric dynamics, air-sea interaction, upper-ocean dynamics, oceanographic bio-optical modeling, oceanic and atmospheric numerical modeling and prediction, data assimilation and data fusion, retrieval and application of remote sensing data, benthic processes, aerogeophysics, marine sedimentary processes, advanced mapping techniques, atmospheric physics, and remote sensing. Oceanographers and marine geophysicists are located in Washington, DC, and at the Stennis Space Center, Bay St. Louis, Mississippi. Meteorologists are located in Washington, DC, and Monterey, California.

■ Physicists. Physics graduates may concentrate on such fields as materials, solid-state physics, fiber optics, electro-optics, microelectronics, vacuum science, plasma physics, fluid mechanics, signal processing, ocean acoustics, information processing, artificial intelligence, electron-device technology, radio-wave propagation, laser physics, ultraviolet/X-ray/gamma-ray technology, electronic warfare, electromagnetic interaction, communications systems, radio frequency/microwave/millimeter-wave/infrared technology, computational physics, radio and high-energy astronomy, solar physics, and space physics.

For more information and current vacancy listings, visit http://hroffice.nrl.navy.mil/

NAVAL RESEARCH LABORATORY

4555 Overlook Ave., SW • Washington, DC 20375-5320

LOCATION OF NRL IN THE CAPITAL AREA

Quick Reference Telephone Numbers

	NRL Washington	NRL-SSC	NRL-Monterey	NRL CBD	NRL VXS-1 Patuxent River
Hotline	(202) 767-6543	(202) 767-6543	(202) 767-6543	(202) 767-6543	(202) 767-6543
Personnel Locator	(202) 767-3200	(228) 688-3390	(831) 656-4763	(410) 257-4000	(301) 342-3751
DSN	297- or 754-	828	878	—	342
Direct-in-Dialing	767- or 404-	688	656	257	342
Public Affairs	(202) 767-2541	(228) 688-5328	(202) 767-2541	—	(202) 767-2541

Additional telephone numbers are listed on page 284.

ON THE COVERS

FRONT COVER:

(Top, left to right)

1. This high-resolution satellite true-color image of Hurricane Ivan from NASA's Moderate Resolution Imaging Spectroradiometer (MODIS) - Aqua at 18:50 UTC on September 15, 2004 was produced by the Ocean Optics Section at the Naval Research Laboratory, Stennis Space Center, MS.
2. Raven B Small Unmanned Aerial System (SUAS) (shown at launch) is used to develop a collection of motion imagery for estimation of high-resolution shorelines, sand bars, and surf zones, in addition to a bathymetric surface.
3. TacSat-4 "COMMx" Payload in Thermal Vacuum Chamber.
4. Scanning electron microscope images of self-assembled alumina-silica nanostructures.
5. The Navy Center for Applied Research in Artificial Intelligence is exploring fundamental and applied research on how future warfighters will interact with teams of autonomous systems. The Center recently received three MDS (mobile, dexterous, social) robots, which are named Issac, Lucas, and Octavia.

(Bottom, left to right)

6. Atomic force microscope image of single crystal diamond dome resonator with frequency 100 MHz in quality factor of 5000.
7. Room temperature real-color cathodoluminescence (CL) image acquired from a highly defective region of a homoepitaxial 4H-SiC film that incorporated a variety of microscopic defects.
8. .50 cal fragment-simulating projectile shot from a rifle barrel strikes the front side of a steel armor plate coated with an elastomeric coating. The initially rubbery coating transitions to a glassy state due to the high-speed impact of the projectile (which is traveling about 3000 feet per second).
9. The Technical Information Services Branch offers digital still camera coverage for data documentation, both at NRL and in the field. Images are captured with state-of-the-art digital cameras. Photofinishing services provide custom printing and quick-service color prints from digital files.
10. Laboratory facility for development and testing of missile warning systems and sensors including real-time detection, tracking, discrimination algorithms, sensors, focal plane arrays, optics, infrared lasers, pointer trackers, and jammers.

BACK COVER:

(Top left, clockwise)

1. An electron backscatter diffraction (EBSD) map across a Ti-5111 friction stir weld. This image shows the orientation of individual grains within the microstructure (indicated by their color) and illustrates how the coarse parent base plate microstructure is deformed and refined as the material is swept into the friction stir weld.
2. Six Barny moorings containing acoustic Doppler current profilers (ADCPs) and wave/tide gauges are safely lashed to the deck of the *Seward Johnson II.* These moorings survived the wrath of Hurricane Ivan in the Gulf of Mexico. They resemble barnacles and hence are called Barnys. They were deployed by the Naval Research Laboratory on the ocean bottom at depths ranging between 60 and 90 m. The moorings collected the most comprehensive set of current and wave measurements ever made beneath a category 4 storm.
3. RAMPANT LION II 2008, Kandahar, Afghanistan.
4. An x-ray microtomograph isosurface rendering (with transparency) of a live barnacle (*Amphibalanus amphitrite)* showing the junction of the base plate and lateral plates, where cement is released through cement ducts during growth. In the image, approximately one quarter of the barnacle is shown oriented with its baseplate up (essentially upside-down to how it grows).
5. Multiple-beam klystrons (MBKs) are a class of vacuum electronic amplifiers capable of producing coherent, broadband, high-power microwave radiation in a compact form factor, and provide the low-noise, high power transmitter performance required by advanced radar systems to operate in high-clutter environments.
6. Model of layers for a wide stripe distributed feedback (WDFB) laser with scanning electron microscope image of the cross section an actual WDFB laser in the background.
7. Three-dimensional depiction of the forecast sensitivity based on a COAMPS forecast of hurricane Katrina using the adjoint and tangent linear model system.
8. VXS-1's RC-12 conducts airborne scientific research.
9. NRL's Low Frequency Broadband (LFBB) mine hunter after deployment in recent at-sea trials.
10. Scientists at the Center for Bio/Molecular Science and Engineering and the Optical Sciences Division are engineering advanced nanoparticle-protein bioconjugate materials with application in cellular targeting, biosensing, and nanoparticle-mediated drug delivery. This photo shows cells microinjected with semiconductor quantum dot-fluorescent protein conjugates.
11. Learjet with ALE-43 shaped RF electronic pods installed on the wings flying over NRL's Chesapeake Bay Detachment during Multi-Function Electronic Warfare testing.
12. Silicon-on-insulator Fabry-Perot optical microcavity coupled to a micro-electro-mechanical (MEMS) microbridge resonator.
13. Contracting specialists in NRL's Contracting Division are responsible for the acquistion of major research and development materials, services, and facilities in excess of $100K.
14. A computer generated graphic of the Japanese Experiment Module (JEM) attached to the International Space Station (ISS). Also shown is the remote manipulator arm which will be used to capture and attach science payloads to the JEM.
15. Woodworkers in NRL's Supply and Information Services Division prepare custom boxes for packing and shipping of materials and equipment.
16. A compact 5 MeV X-band test accelerator located in NRL's Plasma Physics Division's Magnicon Laboratory. This device, a powerful microwave source that was developed at NRL, will be used to study electron beam acceleration in dielectric-loaded accelerating structures as part of the U.S. High Gradient Collaboration funded by the Department of Energy.
17. Three-dimensional simulation results of equatorial spread F using the NRL code SAMI3/ESF. Electron density isosurfaces and contour maps are shown at times 1933 UT and 2103 UT.
18. NRL's Technical Information Services Branch provides graphic support which includes technical and scientific illustrations, computer graphics, design services, photographic composites, display posters, and framing.
19. Learjet with ALE-43 shaped RF electronic pods installed on the wings while conducting NULKA testing with the USS *Oak Hill* (LSD 51).
20. Employees from several agencies including NRL worked around the clock at the NRL HazMat Reachback Center to evaluate possible threats during the 2009 Presidential Inauguration. NRL's CT-Analyst was identified as the crisis assessment model for the first 30 minutes.

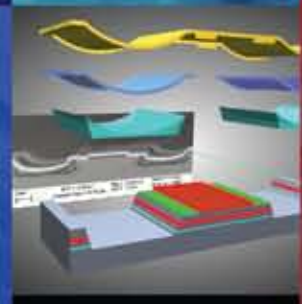

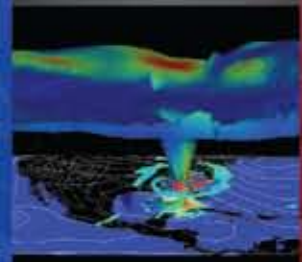

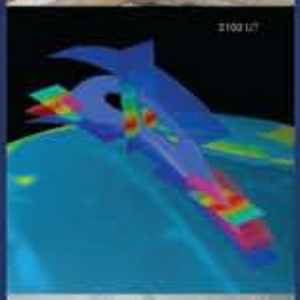

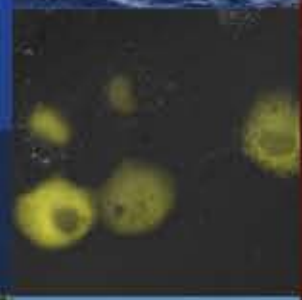

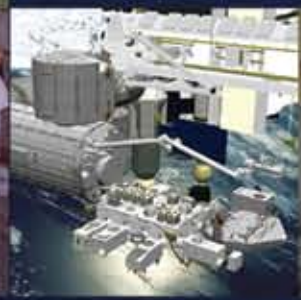

www.nrl.navy.mil